WILEY-VCH

Hans Bisswanger

Enzyme Kinetics

Principles and Methods

Hans Bisswanger

Enzyme Kinetics
Principles and Methods

Enzyme Kinetics: Principles and Methods. Hans Bisswanger

ISBN: 3-527-30343-X

Hans Bisswanger

Enzyme Kinetics

Principles and Methods

Translated by
Leonie Bubenheim

WILEY-VCH

Prof. Dr. Hans Bisswanger
Physiologisch-Chemisches Institut
der Universität Tübingen
Hoppe-Seyler-Straße 4
D-72076 Tübingen
Germany

Library of Congress Card No.: applied for

British Library Cataloguing-in-Publication Data:
A catalogue record for this book
is available from the British Library

Die Deutsche Bibliothek – CIP-Einheitsaufnahme
A catalogue record for this book is available from Die Deutsche Bibliothek
ISBN 3-527-30343-X

Printed on acid free paper

Composition: K+V Fotosatz GmbH, Beerfelden
Printing: betz-druck GmbH, Darmstadt
Bookbinding: Großbuchbinderei J. Schäffer GmbH + Co. KG, Grünstadt
Printed in the Federal Republic of Germany

Dedicated to Anna and Michael

Preface to the Third German Edition

> The time needed for a distinct amount of substrate to be changed, i.e., the degree of acceleration of the reaction by the catalyst primarily depends on its amount. In a great number of cases it is even directly proportional to the efficient amount of the ferment. In other cases more complicated relationships exist. It was attempted to formulate these in the so-called "ferment laws". However, to a large extent, they are very unsatisfactorily founded.
>
> Carl Oppenheimer (1919) *Biochemie*
> Georg-Thieme-Verlag Leipzig

After the first German edition of *Enzymkinetik – Theorie und Methoden* has already established itself as a standard work, the text for the second edition was completely revised, with substantial additions in the theoretical and methods sections, in order to update the material and to cover a wider area of the subject, as the book should also serve as a reference for the expert. Consequently, the regular curriculum even for students of biochemistry was exceeded, but everybody can make his special choice out of the extended material.

Complete re-editing of the third edition seemed, however, not indicated. The addition of a chapter on isotope exchange and isotope effects closed a serious gap. The new edition also gave the opportunity to improve the layout by converting the text into a modern software program and insert required corrections. I would like to thank for all the numerous hints on errors and suggestions for improvements.

A basic change, evident already from the new CD-ROM, was made in the enzyme kinetics program *EK13.exe* by Dmitry Degtiarev, a student of informatics from Moscow, who wrote a completely new concept for the program. Compared with the earlier version, it contains more plots, and the plots can be directly fed into the printer. Compatibility with the former version was, however, largely neglected. Included are sample files of representative mechanisms. The program operates under the system Win95/98/NT. Assuming that PC users will test the program on their own, the attached instructions are rather short. Most functions are self-explanatory. The user may forgive the simple layout, compared with expensive commercial graphics programs, as the program is mainly intended as a companion to the book.

Tübingen, November 1999 Hans Bisswanger

Enzyme Kinetics: Principles and Methods. Hans Bisswanger

ISBN: 3-527-30343-X

Preface to the English Edition

The time about three decades ago may be regarded as the *Golden Age* of enzyme kinetics. Then it became obvious that many biological processes can be forced into terrifying formulas with which experts intimidate their colleagues from other fields. The subject has been treated in several competent textbooks, all published in the English language.

For students with English not being their mother tongue this did not provide a simple language problem, but rather confronted them simultaneously with a difficult matter *and* a foreign language. So the original intention to write a textbook in German was to minimise the fear of the difficult matter. Very difficult derivations were renounced realising the fact that most biochemists will never need or keep in mind every specialised formula. They rather require fundamentals and an understanding of the relationships between theoretical treatments and biological processes explained by such derivations as well as the knowledge which practical approaches are most suited to examine theoretical predictions. Therefore, the book is subdivided into three parts, only the central chapter dealing with classical enzyme kinetics. This is preceded by an introduction into the theory of binding equilibria and followed by a chapter about methods for both binding studies and enzyme kinetics including fast reactions.

Since the German edition is well introduced and the concept broadly accepted, the publication of an English edition appeared justified. This is supported by the fact that new editions in enzyme kinetics are rare, although a thorough understanding of the field as an essential branch of biochemistry is indispensable. The original principle of the former editions to present only fundamentals for a general understanding cannot consequently be maintained, as a specialist book on the subject must exceed the level of general textbooks and should assist the interested reader with comprehensive information to solve kinetic problems. Nevertheless, the main emphasis still is to mediate the understanding of the subject. The text is not limited to the derivation and presentation of formula, but much room is given for explanations of the treatments, their significance, applications, limits, and pitfalls. Special details and derivations turn to experts and may be skipped by students and generally interested readers.

The present English edition is a translation of the Third German edition including revisions to eliminate mistakes.

I would like to acknowledge many valuable suggestions especially from students from my enzyme kinetics courses as well as the support from WILEY-VCH, especially from Mrs. Karin Dembowsky. Her encouraging optimism was a permanent stimulus for this edition.

Tübingen, January 2002 Hans Bisswanger

Contents

Enzyme Kinetics: Principles and Methods. Hans Bisswanger

ISBN: 3-527-30343-X

Symbols and Abbreviations

(units in brackets)
special abbreviations are defined in the text

A, B, C	ligands, substrates
A	absorption measure
c	concentration
D	diffusion coefficient
e	Euler number (e = 2.71828)
E	enzyme, macromolecule
E_a	activation energy
F	relative intensity of fluorescence
ε	molar absorption coefficient
η	viscosity
η_e	efficiency factor
η_{e1}	efficiency factor for first order reactions
Φ	optical rotation
Φ_F	quantum yield
Φ_s	substrate resp. Thiele module
ΔG°	free standard energy
G	electric conductance (S)
ΔH°	standard reaction enthalpy
h	Planck constant ($6.626 \cdot 10^{-34}$ J·s)
h_s	transport coefficient of substrate
I	inhibitor
I	light intensity
J	flow
IU	enzyme unit (international unit, μmol/min)
K	microscopic equilibrium constant
K'	macroscopic equilibrium constant
K_a	association constant
K_{app}	apparent equilibrium constant
K_d	dissociation constant
K_g	equilibrium constant of a reaction
K_i	inhibition constant
K_{ic}	inhibition constant for competitive inhibition
K_{iu}	inhibition constant for uncompetitive inhibition
K_m	Michaelis constant
K_{mA}	Michaelis constant for substrate A
k_1	rate constant of the forward reaction

Enzyme Kinetics: Principles and Methods. Hans Bisswanger

ISBN: 3-527-30343-X

k_{-1}	rate constant of the reverse reaction
k_{cat}	catalytic constant
k_B	Boltzmann constant ($k_B = R/N = 1.38 \cdot 10^{-23}$ J·K^{-1})
kat	Katal, enzyme unit according to the SI system (mol/s, 1 nkat = 0.06 IU, 1 IU = 16.67 nkat)
M_r	relative molecular mass (dimensionless)
m	number of binding classes per macromolecule
n	number of identical binding sites per macromolecule
n_h	Hill coefficient
N_A	Avogadro constant ($6.022 \cdot 10^{23}$ mol^{-1})
Or	ordinate intercept
P, Q, R	products
P	polarisation
R	gas constant (8.314 J·K^{-1} mol^{-1})
r	fraction of ligands bound per macromolecule
ρ	density (kg·m^{-3})
ΔS	standard reaction entropy
Sl	gradient (slope)
T	absolute temperature (K)
t	time (s)
Θ	ellipticity
τ	relaxation time
U	voltage (V)
v	reaction velocity
v_0	initial velocity for $t = 0$
V	maximal velocity for substrate concentrations $\rightarrow \infty$
$\overline{Y}$	fraction of ligands bound per binding site

Introduction

Enzyme reactions are usually formulated as simple processes, e.g., for the case of a single substrate reaction:

$$\mathrm{E} + \mathrm{A} \underset{k_{-1}}{\overset{k_1}{\rightleftharpoons}} \mathrm{EA} \xrightarrow{k_2} \mathrm{E} + \mathrm{P}\,.$$

On closer scrutiny, however, such mechanisms prove much more complex, a process composed of several partial steps:

$$\mathrm{E} + \mathrm{A} \underset{k_{-1}}{\overset{k_1}{\rightleftharpoons}} \mathrm{EA} \underset{k_{-2}}{\overset{k_2}{\rightleftharpoons}} \mathrm{E^*A} \underset{k_{-3}}{\overset{k_3}{\rightleftharpoons}} \mathrm{E^*P} \underset{k_{-4}}{\overset{k_4}{\rightleftharpoons}} \mathrm{EP} \underset{k_{-5}}{\overset{k_5}{\rightleftharpoons}} \mathrm{E} + \mathrm{P}\,.$$

In a rapid equilibrium, an initial loose association complex is formed between enzyme E and substrate A. Subsequently, the enzyme shifts into its active form E* and can then convert substrate into product P. Upon reversion of the enzyme into its original state E, the product molecule dissociates, and the enzyme is ready to interact with another substrate molecule. The complete mechanism consists of a sequence of five partial reactions. For a full extensive characterisation, five equilibrium constants, or ten rate constants, respectively, have to be determined. Enzyme mechanisms become even more complicated when involving two or more substrates, cofactors, and effectors.

Kinetic constants like the Michaelis constant and the maximum velocity, both themselves composed of distinct rate constants, are obtained by enzyme kinetic measurement. A reversible reaction as shown in the second equation can be analysed in both directions and for each a set of kinetic constants will be obtained. Enzyme kinetic studies, however, only consider the process as a whole. In order to fully understand the mechanism in all its individual parts, it must be divided into single steps and each analysed separately.

Both the initial and final step of such a series of reactions is a rapid association equilibrium, preceding the catalytic turnover. Such processes can be studied by special binding methods based on theoretical descriptions summarised under the term *multiple equilibria* (see Chapter 1). It is assumed that a mostly low-molecular compound, the *ligand*, enters into a *specific* interaction with a *macromolecule*, i.e., the macromolecule has a distinct binding site for this specific ligand (contrary to unspecific binding, e.g., to ionic interactions for the compensation of surplus charges on protein surfaces, or hydrophobic associations). Since catalytic turnover is excluded, the laws described in this chapter do not only apply to enzymes but to macromolecules in general, like transporter molecules, receptors or nucleic acids. Ligands may be substrates, products, co-factors, inhibitors, activators, regulators, hormones, neurotransmitters or drugs. In the case of enzyme substrates, however, conversion into

Enzyme Kinetics: Principles and Methods. Hans Bisswanger

ISBN: 3-527-30343-X

product must be assumed. By applying the laws of *multiple equilibria*, equilibrium constants (*association or dissociation constants*) are obtained, and interactions between enzyme and ligands can be analysed in the absence of a catalytic turnover. This procedure simplifies the treatment of complex mechanisms, e.g., of allosteric enzymes. Mechanisms that can entirely be characterized by multiple equilibria will be described in this chapter, although they often are analysed by enzyme kinetic methods, since enzymatic turnover can be followed easier experimentally than binding processes.

Enzyme kinetic methods require only *catalytic quantities* of enzyme material. Because of their extraordinary catalytic potential, minute quantities of enzyme suffice to convert large quantities of substrate into product. Enzyme concentration is always lower by a number of degrees than the concentration of substrate. The product formed is chemically different from the substrate and can be detected by adequate methods. In contrast to this, for the study of reversible equilibria, the ligand and the macromolecule must be present in comparable concentrations. The ligand binding to the macromolecule does not change its chemical nature, and thus, binding is difficult to detect. Due to the fast reversible equilibrium, the association complexes are not stable and cannot be isolated. As changes caused by binding are often rather weak, high concentrations of macromolecules are required. The purity requirements for enzyme kinetic measurements (as long as there are no interfering side effects) are less stringent than for binding measurements, for which the molar concentration of the macromolecules must exactly be known. Sometimes enzyme kinetic data may even be obtained from raw extracts. So we may deduct from this that enzyme kinetics recommend themselves rather by practiced considerations than by theoretical manifestation.

By applying techniques to pursue rapid kinetic reactions with adequate methods it is possible to separate a complete mechanism into different time segments and to determine the rate constants of individual steps of the reaction. Therefore, a detailed analysis of a catalytic reaction of an enzyme requires a combination of various methods. The intention of this book is to demonstrate this way of operation, thereby (especially in the treatment of equilibria) going beyond the limits of enzyme kinetics in a narrow sense, dealing in the Greek meaning of the word, ($\chi\iota\nu\eta\sigma\iota\sigma$ – motion), with time-dependent processes. A standardised nomenclature throughout the book links the individual chapters. For the enzyme in enzyme kinetics, as well as for the non-enzymatic macromolecule in multiple equilibria, “E” is uniformly used. Enzyme substrates and ligands in binding processes are labelled “A”, “B”, and “C”, etc. Different types of ligands are given different denominators, e.g., “P, Q, R”, etc. for products, “I” for inhibitors, etc.

In order to standardise the heterogeneous terms and definitions in the various publications, the terminology used in this book follows as far as possible the NC-IUB recommendations (Nomenclature Committee of the International Union of Biochemistry, 1982) and the IUPAC regulations (International Union of Pure and Applied Chemistry, 1981). Concentrations are indicated by square brackets ([A], etc.). The following reference list comprises important standard text books relevant to the different fields treated in this book.

References

General literature on theory and methods of enzmye kinetics

Ahlers, J., Arnold, A., v. Döhren, F.R. & Peter, H.W. (1982) *Enzymkinetik*, 2. Aufl. Fischer Verlag, Stuttgart.

Cantor, C.R. & Schimmel, P.R. (1980) *Biophysical chemistry.* Freeman & Co., San Francisco.

Cornish-Bowden, A. (1976) *Principles of enzyme kinetics*. Butterworth, London.

Cornish-Bowden, A. & Wharton, C.W. (1988) *Enzyme kinetics*. IRL Press, Oxford.

Cornish-Bowden, A. (1995) *Fundamentals of enzyme kinetics.* Portland Press, London.

Dixon, M. & Webb, E.C. (1979) *Enzymes*. Academic Press, New York.

Edsall, J.T. & Gutfreund, H. (1983) *Biothermodynamics.* J. Wiley & Sons, New York.

Eisenthal, R. & Danson, J.M. (1992) *Enzyme assays.* A practical approach. IRL Press, Oxford.

Engel, P.C. (1977) *Enzyme kinetics.* Chapman & Hall, London.

Fersht, A. (1977) *Enzyme structure and mechanism*. Freeman & Co., San Francisco.

Fromm, H.J. (1975) *Initial rate kinetics*. Springer-Verlag, Berlin.

Klotz, I.M. (1986) *Introduction to biomolecular energetics including ligand-receptor interactions*. Academic Press, Orlando.

Kuby, S.A. (1991) *Enzyme catalysis, kinetics and substrate binding.* CRC Press, Boca Raton.

Laidler, K.J. & Bunting, P.S. (1973) *The chemical kinetics of enzyme action*, 2. edn. Clarendon Press, Oxford.

Lasch, J. (1987) *Enzymkinetik*. Springer-Verlag, Berlin.

Lüthje, J. (1990) *Enzymkinetik.* Urban & Schwarzenberg, München.

Plowman, K.M. (1972) *Enzyme kinetics*. McGraw-Hill, New York.

Price, N.C. & Stevens, L. (1989) *Fundamentals of enzymology.* Oxford University Press, Oxford.

Purich, D.L. *Enzyme kinetics and mechanics. Part A:* Methods in Enzymology, Vol. 63 (1979); *Part B:* Methods in Enzymology, Vol. 64 (1980); *Part C:* Methods in Enzymology, Vol. 87 (1982); *Part D:* Methods in Enzymology, Vol. 249 (1995); *Part E:* Methods in Enzymology, Vol. 308 (1999). Academic Press, New York.

Purich, D.L. (1996) *Contemporary enzyme kinetics and mechanism.* Academic Press, New York.

Purich, D.L. (1999) *Handbook of biochemical kinetics.* Academic Press, New York.

Piszkiewicz, D. (1977) *Kinetics of chemical and enzyme-catalyzed reactions.* Oxford University Press, Oxford.

Roberts, D.V. (1977) *Enzyme kinetics.* Cambridge University Press, Cambridge.

Schellenberger, A. (1989) *Enzym-Katalyse*. Springer-Verlag, Berlin.

Schulz, G.E. & Schirmer, R.H. (1979) *Principles of protein structure*. Springer-Verlag, Berlin.

Segel, I.H. (1975) *Enzyme kinetics*. John Wiley & Sons, New York.

Suelter, C.H. (1990) *Experimentelle Enzymologie*. Fischer-Verlag, Stuttgart.

Wong, J.T.-F. (1975) *Kinetics of enzyme mechanisms*. Academic Press, London.

Nomenclature instruction

Nomenclature Committee of the International Union of Biochemistry (NC-IUB) (1982) Symbolism and terminology in enzyme kinetics. European Journal of Biochemistry 128, 281–291.

International Union of Pure and Applied Chemistry (1981) Symbolism and terminology in chemical kinetics. Pure and Applied Chemistry 53, 753–771.

1 Multiple Equilibria

Contrary to chemical reactions in which two different chemical substances in a solution are either completely inert, or immediately react with each other on contact and are changed into product:

$$A + B \longrightarrow P + Q$$

biologically active macromolecules, e.g., enzymes, have the ability to specifically bind their reaction partner without changing their individual nature:

$$E + A \underset{k_{-1}}{\overset{k_1}{\rightleftharpoons}} EA$$

Specific binding is a precondition for all functional processes, e.g., membrane transportation, hormone effects or substrate modifications. The study of specific binding processes will, therefore, be substantial for understanding biological principles. First, the existence of a specific binding has to be established and unspecific association, e.g., hydrophobic or electrostatic interactions between macromolecule and ligand must be excluded. An indicator is the size of the dissociation constant, which as a rule is lower than 10^{-3} M in specific bindings (although there are exceptions, e.g., the binding of H_2O_2 to catalase, or the binding of glucose to glucose isomerase). Specific binding is governed by a strict stoichiometric relationship to the macromolecule, thus the binding process is saturable. Furthermore, the ligand can be replaced at its binding site by structural analogues. For introduction into the topic an impression will be given how the ligand locates its binding site on the macromolecule and which factors determine its affinity to the binding site. Subsequently, the main types of interaction between ligands and macromolecules are demonstrated.

1.1 Diffusion

For a macromolecule to react with its ligand, the partners have to locate each other first. It can be imagined that a particle moves along an axis with the kinetic energy $k_BT/2$. T is the absolute temperature, k_B the Boltzmann constant. According to the Einstein relation, a particle with the mass m, moving a distinct direction with the velocity v possesses the kinetic energy of $m\ v^2/2$, i.e.

$$v^2 = k_B T/m\ . \tag{1.1}$$

Accordingly, a macromolecule like lactate dehydrogenase (M_r=140 000) would move at a rate of 4 m per second, whereas its substrate, lactic acid (M_r=90.1), would cover

Enzyme Kinetics: Principles and Methods. Hans Bisswanger

ISBN: 3-527-30343-X

170 m at the same time, and a water molecule ($M_r = 18$) would even cover 370 m. Enzyme and substrate would pass each other like rifle balls and would arrive at the cell wall within fractions of a second. In the overcrowded medium of the inner cell, however, the moving particles are permanently hampered by numberless obstacles, e.g., water molecules, ions, metabolites, macromolecules, and cell organelles, so that the movements of the molecules look more like the weavings of a drunkard than a linear progress. This tumbling motion not only slows down the progress of the molecules, it significantly increases the probability of certain molecules colliding with each other.

The distance x, covered by a molecule in solution within time t into one direction is dependent on the diffusion coefficient D according to the equation:

$$x^2 = 2Dt \; . \tag{1.2}$$

The diffusion coefficient is itself a function of the concentration of the diffusing matter. In diluted solutions, however, it may be regarded as constant. It also depends on particle size, the kind of medium and temperature. For small particles in water, the coefficient is $D = 10^{-5}$ cm^2/s. In order to pass through a cell of 1 μm, the molecule needs 0.5 ms, for 1 mm 8.33 min, i.e., for a thousandfold distance a millionfold time is required. This demonstrates that there exists no "diffusion velocity". The movement of molecules in medium is not proportional to time, but to its square root. A diffusing molecule does not recall its earlier position, i.e., it searches a certain area at random (in undirected movement) and is not inclined to look for new spaces. As an example, a 10 cm high sucrose gradient, which is used for the separation and the size determination of macromolecules and particles, has a life-span of about four months, based on the diffusion coefficient of $D = 5 \cdot 10^{-6}$ cm^2/s for saccharose.

Equation (1.2) describes the one-dimensional diffusion of a molecule. For the three-dimensional space over a distance r follows, since diffusion into the three space directions x, y and z are independent of each other:

$$r^2 = x^2 + y^2 + z^2 = 6Dt \; . \tag{1.3}$$

For a specific binding to succeed it is not sufficient for the ligand to meet the macromolecule, but it has to locate its proper binding site. This is done by translocation of its volume $4\pi R^3/3$ by the relevant distance of its own radius R. After a time t_x the molecule has searched (according to Eq. (1.3) for $r = R$) a volume of:

$$\frac{6Dt_x}{R^2} \cdot \frac{4\pi R^3}{3} = 8\pi DRt_x \; . \tag{1.4}$$

The volume searched per time unit is $8\pi DR$, the probability of a collision for a certain particle in solution is proportional to the diffusion coefficient and to the particle radius.

At the start of a reaction

$$\mathrm{A} + \mathrm{B} \quad \rightarrow \quad \mathrm{P}$$

both participants are equally distributed in solution. Within a short time molecules of one type (e.g., B) are depleted in the vicinity of the molecules of the other type (A) not yet converted so that a concentration gradient is formed. Consequently, a net flow ϕ of B-molecules forms in the direction of the A-molecules located at distance r,

$$\Phi = \frac{\mathrm{d}n}{\mathrm{d}t} = DF\frac{\mathrm{d}c}{\mathrm{d}r} \ , \tag{1.5}$$

n being the net surplus of molecules passing within time t through an area F, and c the concentration of B-molecules located at distance r from the A-molecules. This relation in its general form is known as *Fick's First Law of Diffusion*. In our example of a reaction of two reactants, F has the dimension of a spherical surface with a radius r. Equation (1.5) then changes into:

$$\left(\frac{\mathrm{d}c}{\mathrm{d}r}\right)_r = \frac{\Phi}{4\pi r^2 D'} \tag{1.6}$$

D' is the diffusion coefficient for the relative diffusion of the reactive molecules. Integration of Eq. (1.6) yields:

$$c_\mathrm{r} = c_\infty - \frac{\Phi}{4\pi r D'} \tag{1.7}$$

c_r is the concentration of B-molecules at distance r and c_∞ the concentration at infinite distance from the A-molecules. The last corresponds approximately to the average concentration of B-molecules. The net flow Φ is proportional to the reaction rate and that is again proportional to the average concentration c of those B-molecules just in collision with the A-molecules, $r_{\mathrm{A+B}}$ being the sum of the radii of an A- and a B-molecule:

$$\Phi = kc_{r_{\mathrm{A+B}}} \ . \tag{1.8}$$

k is the rate constant of the reaction in the steady state, where c_r becomes equal to $c_{r_{\mathrm{A+B}}}$, and r equal to $r_{\mathrm{A+B}}$. Inserted into Eq. (1.7), this becomes

$$c_{r_{\mathrm{A+B}}} = \frac{c_\infty}{1 + \dfrac{k}{4\pi r_{\mathrm{A+B}} D'}} \ . \tag{1.9}$$

The net flow under steady-state conditions is

$$\Phi = k_\mathrm{a} c_\infty \ . \tag{1.10}$$

k_a is the relevant association rate constant. Equations (1.8–1.10) may thus be reformed:

$$\frac{1}{k_a} = \frac{1}{4\pi r_{A+B} D'} + \frac{1}{k} \ . \tag{1.11}$$

This relation can be shown in linear form in a graph, if $1/k_a$ is plotted against the viscosity η of the solution, as according to the *Einstein-Sutherland Equation* the diffusion coefficient at infinite dilution D_0 is conversely proportional to the friction coefficient f and that again is directly proportional to the viscosity η:

$$D_0 = \frac{k_B T}{f} = \frac{k_B T}{6\pi\eta r} \ . \tag{1.12}$$

$1/k$ is the ordinate intercept. In the case of $k \gg 4\pi r_{A+B} D'$ the intercept is placed near the coordinate base, it becomes

$$k_a = 4\pi r_{A+B} D' \ . \tag{1.13}$$

This borderline relationship is known as the *Smoluchowski limit* for translating diffusions, the reaction is *diffusion-controlled*. In *reaction-controlled* reactions, however, the step following the diffusion, i.e., the substrate turnover, determines the rate. A depletion zone emerges around the enzyme molecule, as substrate molecules are not replaced fast enough. A *diffusion-limited dissociation* occurs, if the dissociation of product limits the reaction. Viewing two equally reactive spheres with the radii r_A and r_B and the diffusion coefficient D_A and D_B, we obtain for Eq. (1.13):

$$k_a = 4\pi r_{A+B} D' = 4\pi (r_A + r_B)(D_A + D_B) \ . \tag{1.14}$$

By inserting Eq. (1.12) and with the approximation $r_A = r_B$ and with $D_0 = D_A = D_B$ we obtain:

$$k_a = \frac{8 k_B T}{3\eta} \ . \tag{1.15}$$

Thus we obtain the association rate constants for diffusion-controlled reactions in the size range of 10^9–$10^{10}\ M^{-1}\ s^{-1}$.

If the rate constants were exclusively determined by diffusion uniform values should be found. In reality, however, the values of rate constants of diffusion-controlled reactions of macromolecules vary within a range of more than five orders of magnitude. Responsible for this variety is the fact that for successful binding of the ligand, random collision with the macromolecule is not sufficient. Both molecules must be in a favourable position to each other. This causes a considerable retardation of the whole binding process. On the other hand, attracting forces could facilitate interaction and direct the ligand towards its correct orientation. Thus rate constants may even surpass the values of mere diffusion control. Quantitative recording of such influences is difficult, as they depend on the specific structures of both the macromolecule and the ligand. There are efforts to establish general rules for ligand binding with the assistance of various theories.

A ligand approaches a macromolecule at a rate to be calculated according to Eq. (1.13), but only the part meeting the correct site with the right orientation will react. If we regard the binding site as a circular area on the macromolecule forming an angle α with the centre of the macromolecule (Figure 1.1), the association rate constant of Eq. (1.13) will be reduced by the sine of that angle:

$$k_a = 4\pi r_{A+B} D' \sin \alpha \, . \tag{1.16}$$

The necessity of adequate orientation between binding site and ligand should be considered by the introduction of a further factor, which depends on the nature of the reactive groups involved. It is also suggested that the ligand may associate unspecifically to the surface of the macromolecule and tries to locate the binding site by two-dimensional diffusion on the molecule surface and dissociates if the search was not successful (*sliding model*; Berg, 1985). Such unspecific binding, however, is not able to distinguish between the specific ligand and other metabolites, which may also bind unspecifically and impede the two-dimensional diffusion. The *gating model* assumes the binding site to be opened and closed like a gate by changing the conformation of the protein, thus modulating the accessibility for the ligand (McCammon and Northrup, 1981).

A basic limit for the association rate constants for the enzyme substrate is the quotient from the catalytic constant k_{cat} and Michaelis constant K_m (see Section 2.2)

$$\frac{k_{cat}}{K_m} = \frac{k_{cat} k_1}{k_{-1} + k_2} \tag{1.17}$$

ranging frequently in the area of $10^8\ M^{-1}\ s^{-1}$ of a diffusion-controlled reaction. It is mostly the non-covalent steps during substrate binding and product dissociation rather than the splitting of bindings that determine the reaction rate for a majority of enzyme reactions.

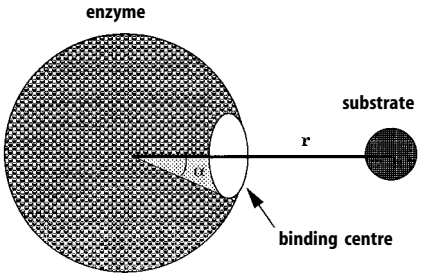

Figure 1.1. Schematic illustration of the interaction of a substrate molecule with its enzyme binding site.

1.2 Interaction of Ligands and Macromolecules

1.2.1 Binding Constants

Binding of a ligand A to a macromolecule E

$$\mathrm{E} + \mathrm{A} \underset{k_{-1}}{\overset{k_1}{\rightleftharpoons}} \mathrm{EA} \tag{1.18}$$

can be described with the law of mass action by the association constant K_a or its reciprocal value, the dissociation constant K_d:

$$K_a = \frac{k_1}{k_{-1}} = \frac{[\mathrm{EA}]}{[\mathrm{A}][\mathrm{E}]} \tag{1.19 a}$$

$$K_d = \frac{k_{-1}}{k_1} = \frac{[\mathrm{A}][\mathrm{E}]}{[\mathrm{EA}]} \tag{1.19 b}$$

Both notations are used. The association constant is more frequently used for the treatment of equilibria, whereas enzyme kinetic constants like the Michaelis constant derive from dissociation constants. To demonstrate the analogy between the two areas, here the dissociation constant will be employed throughout. It has the dimension of a concentration (M), the association constant the dimension of a reciprocal concentration (M^{-1}). Equations (1.19 a, b) are not quite correct, in place of the concentrations [c] the activities $a = f$ [c] should be used. Since the activity coefficients f of the components, however, tend towards one in very diluted solutions normally used in enzyme reactions, they may be disregarded.

If one reaction component is in such an excess to the other ones that its concentration will not be altered measurably by the reaction, it may be included in the constant. This applies especially for the reaction component water, e.g., in hydrolytic processes:

$$\mathrm{A} + \mathrm{H_2O} \underset{}{\overset{\text{enzyme}}{\rightleftharpoons}} \mathrm{P} + \mathrm{Q}\ .$$

As a solvent with a concentration of 55.56 mol/l, water exceeds by far the micro- or millimolar quantities of the other components of the enzyme reaction. A change of the water concentration caused by the reaction is practically impossible to detect. Therefore, binding constants for water to enzymes cannot be given. It is also difficult to identify specific binding sites for water. The reaction is treated as if water was not involved:

$$K'_d = \frac{[\mathrm{A}][\mathrm{H_2O}]}{[\mathrm{P}][\mathrm{Q}]} = K_d[\mathrm{H_2O}]\,; \quad K_d = \frac{[\mathrm{A}]}{[\mathrm{P}][\mathrm{Q}]}\ .$$

Hydrogen ions, frequently involved in enzyme reactions, are treated in a similar way. An apparent equilibrium constant is defined here:

$$K_{app} = K_d[H^+] \ .$$

Contrary to genuine equilibrium constants, this constant is dependent on the pH value of the solution. This must be considered by the study of such processes.

1.2.2 Derivation of the Binding Equation

For the calculation of the dissociation constants for the reaction (1.18) according to the law of mass action (1.19) the concentration of the free macromolecule [E], the free ligand [A], and of the macromolecule-ligand complex [EA] under equilibrium conditions must be known. At first, however, only the total quantities used for the experiment $[E]_0$ and $[A]_0$ are known. They separate into the free and bound components according to the mass conservation equations:

$$[E]_0 = [E] + [EA] \tag{1.20}$$

$$[A]_0 = [A] + [EA] \ . \tag{1.21}$$

The portion of the bound ligand $[A]_{bound}$ can be determined by specified experiments (see Chapter 3). In the simple reaction equilibrium (1.18) with only one binding site per macromolecule $[A]_{bound}$ is equal to [EA]. By inserting Eq. (1.20) into (1.19b) [E] is eliminated.

$$K_d = \frac{([E]_0 - [EA])[A]}{[EA]}$$

$$[A]_{geb} = [EA] = \frac{[E]_0[A]}{K_d + [A]} \ . \tag{1.22}$$

Equation (1.22) describes the binding of a ligand to a macromolecule with one binding site. It will be discussed in detail together the analogue Eq. (1.23) for macromolecules with several identical binding sites.

1.3 Macromolecules with Identical Independent Binding Sites

1.3.1 General Binding Equation

Most proteins and enzymes are composed of several, mostly identical subunits. For reasons of symmetry it can be taken that each of these subunits possesses an identical binding site for the respective ligand, so that the number n of binding sites may be equated with that of the subunits. In general this is correct, but it should be pointed out that here identity in the sense of binding only means equality of the binding

constants. Structurally different binding sites should also differ in their affinities. If the values of dissociation constants for different binding sites are equal by chance they cannot be differentiated by binding measurements only. On the other hand also single protein subunits might possess two or more identical binding sites, e.g., due to a gene duplication. In such, however rare, cases the number n of identical binding sites differs from the number of identical subunits per macromolecule.

If binding of the ligand molecules to the individual binding centres occurs independently, i.e., without mutual influence, it should be irrespective whether the binding, as assumed in Eq. (1.22) takes place at isolated units or at subunits associated with each other. The enzyme would be saturated stepwise by the ligand, and for each binding site [U] Eq. (1.22) holds, so this would result in a sum of n identical terms:

$$[U_1A] + [U_2A] + [U_3A] + \ldots [U_nA] = [A]_{geb} = \frac{n[E]_0[A]}{K_d + [A]} \ . \tag{1.23}$$

This equation differs from Eq. (1.22) for the binding to a macromolecule with only one binding site by the factor n for the number of identical binding sites per macromolecule. Furthermore, $[A]_{bound}$ can no longer be equated with [EA], but comprises the sum of all forms of ligand-bound macromolecules.

Although the derivation of Eq. (1.23) is simplified and not quite accurate, the correct result is achieved. The fact that not a single equilibrium, but n equilibria with n dissociation constants are manifested, is disregarded.

$$\begin{aligned}
E + A &\rightleftharpoons EA & K'_1 &= \frac{[E][A]}{[EA]} \\
EA + A &\rightleftharpoons EA_2 & K'_2 &= \frac{[EA][A]}{[EA_2]} \\
EA_2 + A &\rightleftharpoons EA_3 & K'_3 &= \frac{[EA_2][A]}{[EA_3]} \\
\vdots & \quad \vdots & & \\
EA_{n-1} + A &\rightleftharpoons EA_n & K'_n &= \frac{[EA_{n-1}][A]}{[EA_n]} \ .
\end{aligned}$$

The existence of these equilibria requires a more complicated derivation. Although, we will finally arrive at the same Eq. (1.23) the complete procedure will be demonstrated here, as it is of importance especially for the treatment of more complex mechanisms. The hurried reader may confidently proceed to Section 1.3.2.

The constants K' of the individual states are denominated as *macroscopic* dissociation constants. The difference to the *microscopic* (or *intrinsic*) dissociation constants can be demonstrated by a simple example. Assuming a macromolecule has three binding sites, called 1–3 in the sequence $2E_3^1$ (see Scheme 1.1). The first ligand binding to the macromolecule can choose freely between these three binding sites. For the singly occupied macromolecule-ligand complex three possible forms with three microscopic dissociation constants are available. The second ligand may still choose

between two binding sites. Six binding constants result, while three equilibria lead to the fully saturated stage. The three macroscopic binding constants of the complete binding process are thus opposed by 12 microscopic dissociation constants.

macroscopic binding constants

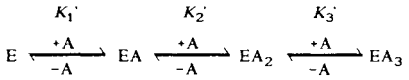

microscopic binding constants

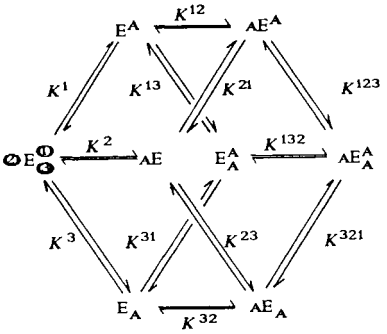

Scheme 1.1. Macroscopic and microscopic binding constants of a macromolecule with three identical binding sites. The E-form at the left in the lower plot shows the relative orientation and the denomination of the binding sites. The denomination of the constants refers to the sequence of occupation, the last figure, respectively, defines the actual occupation.

The macroscopic binding constant of the first step is:

$$K_1' = \frac{[\mathrm{E}][\mathrm{A}]}{[\mathrm{EA}]} = \frac{[\mathrm{E}][\mathrm{A}]}{[\mathrm{E^A}] + [{}_\mathrm{A}\mathrm{E}] + [\mathrm{E_A}]} \ .$$

The individual forms of the enzymes are replaced by the microscopic binding constants:

$$K^1 = \frac{[\mathrm{E}][\mathrm{A}]}{[\mathrm{E^A}]} \ ; \quad [\mathrm{E^A}] = \frac{[\mathrm{E}][\mathrm{A}]}{K^1}$$

$$K^2 = \frac{[\mathrm{E}][\mathrm{A}]}{[{}_\mathrm{A}\mathrm{E}]} \ ; \quad [{}_\mathrm{A}\mathrm{E}] = \frac{[\mathrm{E}][\mathrm{A}]}{K^2}$$

$$K^3 = \frac{[\mathrm{E}][\mathrm{A}]}{[\mathrm{E_A}]} \ ; \quad [\mathrm{E_A}] = \frac{[\mathrm{E}][\mathrm{A}]}{K^3}$$

$$K_1' = \frac{1}{\frac{1}{K^1} + \frac{1}{K^2} + \frac{1}{K^3}} \ .$$

If the binding sites 1–3 are identical, then $K^1 = K^2 = K^3 = K$ applies and

$$K_1' = \frac{K}{3} \ .$$

Correspondingly, the second binding step is:

$$K_2' = \frac{[EA][A]}{[EA_2]} = \frac{([E^A] + [{}_AE] + [E_A])[A]}{[{}_AE^A] + [E_A^A] + [{}_AE_A]}$$

$$K^{12} = \frac{[E^A][A]}{[{}_AE^A]} \ ; \quad [{}_AE^A] = \frac{[E^A][A]}{K^{12}} \quad \text{etc., hence}$$

$$K_2' = \frac{K^{13}K^{21}K^{23} + K^{12}K^{13}K^{23} + K^{13}K^{21}K^{32}}{K^{13}K^{23} + K^{12}K^{23} + K^{13}K^{21}} \ .$$

For $K^{12} = K^{13} = \ldots K$ results $K_2' = K$.

The third binding step is:

$$K_3' = \frac{[EA_2][A]}{[EA_3]} = \frac{([{}_AE^A] + [E_A^A] + [{}_AE_A])[A]}{[{}_AE_A^A]} \ ,$$

$$K^{123} = \frac{[{}_AE^A][A]}{[{}_AE_A^A]} \ ; \quad [{}_AE^A] = \frac{K^{123}[{}_AE_A^A]}{[A]} \text{ etc.}$$

For $K^{123} = K^{132} = \ldots K^{321} = K$ results $K_3' = K^{123} + K^{132} + K^{321} = 3K$.

It becomes evident that even with identical microscopic constants the macroscopic constants differ from the microscopic ones and also from each other in each single step of the process. For n binding sites the general relationship between macroscopic and microscopic binding constants applies:

$$K_d' = K_d \frac{i}{n - i + 1} \ , \tag{1.24}$$

whereby i represents the respective binding step. The number of orientation possibilities Ω of the ligand on the macromolecule is also dependent on *i:*

$$\Omega = \frac{n!}{(n-i)!i!} \tag{1.25}$$

To simplify the derivation of the general binding equation, a saturation function r is defined as a quotient from the portion of the bound ligand $[A]_{bound}$ and the total amount of the macromolecule $[E]_0$:

$$r = \frac{[A]_{geb}}{[E]_0} = \frac{[EA] + 2[EA_2] + 3[EA_3] + \ldots n[EA_n]}{[E] + [EA] + [EA_2] + [EA_3] + \ldots [EA_n]} \ . \tag{1.26}$$

The concentrations of the individual forms of the macromolecule not accessible by experiment are replaced by the macroscopic binding constants:

$$
\begin{aligned}
K_1' &= \frac{[\mathrm{E}][\mathrm{A}]}{[\mathrm{EA}]}\ ; & [\mathrm{EA}] &= \frac{[\mathrm{E}][\mathrm{A}]}{K_1'} \\
K_2' &= \frac{[\mathrm{EA}][\mathrm{A}]}{[\mathrm{EA_2}]}\ ; & [\mathrm{EA_2}] &= \frac{[\mathrm{EA}][\mathrm{A}]}{K_2'} = \frac{[\mathrm{E}][\mathrm{A}]^2}{K_1' K_2'} \\
K_3' &= \frac{[\mathrm{EA_2}][\mathrm{A}]}{[\mathrm{EA_3}]}\ ; & [\mathrm{EA_3}] &= \frac{[\mathrm{EA_2}][\mathrm{A}]}{K_3'} = \frac{[\mathrm{E}][\mathrm{A}]^3}{K_1' K_2' K_3'} \\
&\vdots & &\vdots \quad \vdots \\
K_\mathrm{n}' &= \frac{[\mathrm{EA_{n-1}}][\mathrm{A}]}{[\mathrm{EA}]_\mathrm{n}}\ ; & [\mathrm{EA_n}] &= \frac{[\mathrm{EA_{n-1}}][\mathrm{A}]}{K_\mathrm{n}'} = \frac{[\mathrm{E}][\mathrm{A}]^\mathrm{n}}{K_1' K_2' K_3' \cdots K_\mathrm{n}'}\ .
\end{aligned}
$$

Thus evolves:

$$
\begin{aligned}
r &= \frac{\dfrac{[\mathrm{A}]}{K'} + \dfrac{2[\mathrm{A}]^2}{K_1' K_2'} + \dfrac{3[\mathrm{A}]^3}{K_1' K_2' K_3'} + \cdots \dfrac{n[\mathrm{A}]^\mathrm{n}}{K_1' K_2' K_3' \ldots K_\mathrm{n}'}}{1 + \dfrac{[\mathrm{A}]}{K_1'} + \dfrac{[\mathrm{A}]^2}{K_1' K_2'} + \dfrac{[\mathrm{A}]^3}{K_1' K_2' K_3'} + \cdots \dfrac{[\mathrm{A}]^\mathrm{n}}{K_1' K_2' K_3' \ldots K_\mathrm{n}'}} \\
&= \frac{\displaystyle\sum_{i=1}^{n} \frac{i[\mathrm{A}]^i}{\left(\displaystyle\prod_{j=1}^{i} K_j'\right)}}{1 + \displaystyle\sum_{i=1}^{n} \frac{[\mathrm{A}]^i}{\displaystyle\prod_{j=1}^{i} K_j'}}\ .
\end{aligned}
\tag{1.27}
$$

In the case of independent identical binding sites the macroscopic binding constants of the individual steps according to Eq. (1.24) can be replaced by a uniform microscopic constant K_d:

$$
r = \frac{\displaystyle\sum_{i=1}^{n} i \left(\prod_{j=1}^{i} \frac{n-j+1}{j}\right) \left(\frac{[\mathrm{A}]}{K_\mathrm{d}}\right)^i}{1 + \displaystyle\sum_{i=1}^{n} \left(\prod_{j=1}^{i} \frac{n-j+1}{j}\right) \left(\frac{[\mathrm{A}]}{K_\mathrm{d}}\right)^i}\ .
\tag{1.28}
$$

The product terms of numerator and denominator are binomial coefficients which may be converted as follows:

$$\binom{n}{i} = \left(\frac{n!}{i!(n-i)!}\right),$$

so that Eq. (1.28) may be written in the form of:

$$r = \frac{\sum_{i=1}^{n} i\binom{n}{i}\left(\frac{[A]}{K_d}\right)^i}{1 + \sum_{i=1}^{n}\binom{n}{i}\left(\frac{[A]}{K_d}\right)^i}.$$

By applying the binomial rule, the denominator can be converted as $(1+[A]/K_d)^n$, for the numerator the derived binomial rule applies:

$$r = \frac{n\left(\frac{[A]}{K_d}\right)\left(1+\frac{[A]}{K_d}\right)^{n-1}}{\left(1+\frac{[A]}{K_d}\right)^{n}}.$$

By reducing we achieve the already known form of the binding equation:

$$r = \frac{[A]_{geb}}{[E]_0} = \frac{n[A]}{K_d + [A]}. \tag{1.23}$$

An equation of this kind was established in 1916 by Irvin Langmuir for the adsorption of gases to solid surfaces. The discovery of this equation is, therefore, mostly ascribed to him, although in 1900 A.J. Brown and V. Henri developed a similar equation, which was described in detail by L. Michaelis and M. Menten in 1913. Known as the "Michaelis-Menten equation", it is of central importance to enzyme kinetics (see Section 2.2).

Equation (1.23) establishes a simple correlation between the concentrations of free and bound ligand. By altering the first, we obtain the curve shown in Figure 1.2A for the increase of the bound ligand, which, as explained in Section 2.2, follows the function of a right-angle hyperbola. From this plot the dissociation constant K_d as well as the number of binding sites n can be determined. For very high ligand concentrations, i.e., $[A] \rightarrow \infty$, one may apply $r \rightarrow n$, as in this case K_d in the denominator may be ignored. The curve approach is in an asymptotic manner towards the saturation value, with all binding sites occupied. At half of the saturation value, $n/2$, the free ligand concentration adopts the value of the dissociation constants: $[A] = K_d$.

In the graphic analysis of binding experiments the portion of the bound ligand $[A]_{bound}$ may be entered either directly, or in the form of the saturation function r, reduced by the macromolecule concentration $[E]_0$. In both cases the curves are identical. In the first case, saturation has the value $n[E]_0$, in the second n, i.e., the macromolecule concentration chosen at random does not affect the result, and differing experiments can be compared more easily. If the molar concentration of the macromolecule is not known, the saturation function $\overline{Y}$, reduced by n, can be applied:

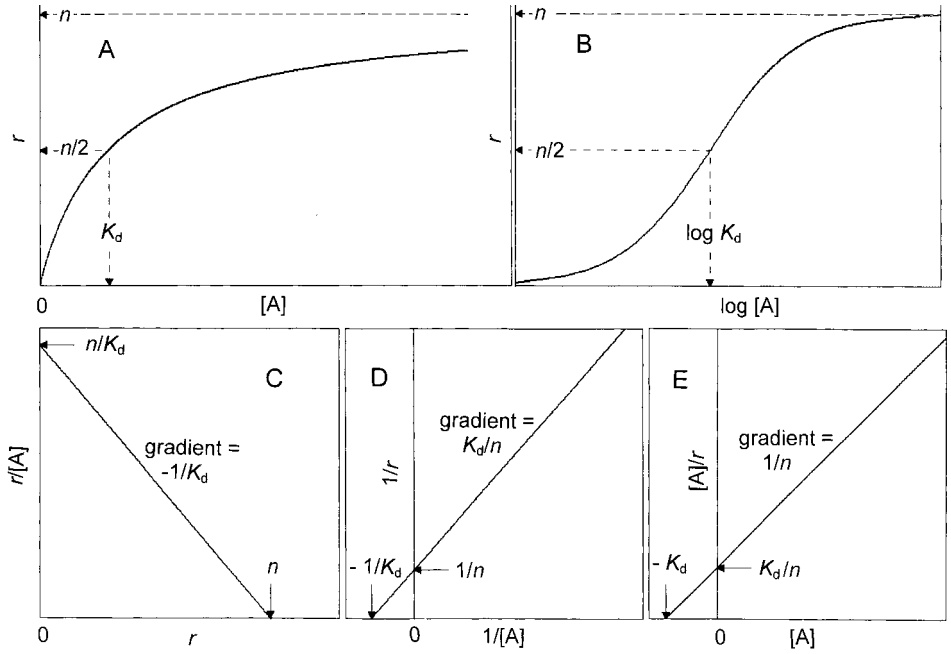

Figure 1.2. Methods of representation for the evaluation of binding data. (A) Direct plot, (B) semi-logarithmic plot, (C) Scatchard plot, (D) double-reciprocal plot, (E) Hanes plot.

$$\overline{Y} = \frac{[\mathrm{A}]_{\mathrm{geb}}}{n[\mathrm{E}]_0} = \frac{[\mathrm{A}]}{K_\mathrm{d} + [\mathrm{A}]} \ . \tag{1.23 a}$$

$\overline{Y}$, the portion of the ligand bound per binding site, always adopts the value 1 at saturation, i.e., random marcomolecule concentrations can be standardised by it. $\overline{Y}$ is applied in experiments where the portion of bound ligands cannot be obtained directly, but as relative values as in spectroscopic titrations (see Section 1.3.2.1). It is also used in theoretical treatments, as the curve, independent of the actual number of binding sites, always tends towards the same saturation level. The number of binding sites, however, will not be obtained with this function.

1.3.2 Graphic Representation of the General Binding Equation

1.3.2.1 Direct Analysis

Figure 1.2A shows the direct representation of data from binding measurements and the determination of the constants according to Eq. (1.23). Principally this direct representation of experimental data is to be recommended, as no distortions caused by recalculation factors occur. Nevertheless, the plot keeps some problems. If the free li-

gand is varied within a broad concentration range, then the front part of the curve will touch the ordinate so closely that K_d can be determined only with difficulty. However, if only the front part is presented, saturation is not discernible. In such cases one may enter the ligand concentration on the abscissa in a logarithmic manner (Figure 1.2B). This way of presentation shows the lower values that are important for the determination of K_d much more clearly. The curve assumes a sigmoidal shape. At half saturation, the curve has a turning point with an abscissa value of log K_d.

Non-linear plots have the following disadvantages:

1. From experimental, i.e., scattering data the course of the hyperbolic function is not always definite. Sometimes quite differing runs of a curve can be fitted with comparable reliability to a given distribution of points (see Figure 2.5, Section 2.3.1.1).
2. The determination of the constants depends on the adaptation of asymptotes, which are frequently underestimated.
3. Deviations from the hyperbolic run of the curve due to artificial influences (systematic errors) or the occurrence of other mechanisms are difficult to detect in non-linear functions.

At least the problems, mentioned in point 2, can be circumvented by applying non-linear regression procedures, and mostly reliable values for the constants can be obtained. Such procedures, however, cannot guarantee the avoidance of the other disadvantages. On the contrary, they often give the impression of exact and objective interpretation of the data. Here, linearised representations based on the conversion of Eq. (1.23) into linear equations, are better suited to show characteristic deviations from the linear run, if the supposed equation is not fulfilled. From the nature of the deviation conclusions may be drawn on the type of an attractive mechanism. Furthermore, such plots allow for the determination of the constants by simple extrapolation to the co-ordinate axes. Three simple conversions of Eq. (1.23) into linear equations are possible. Each of these has some disadvantages, so it may be advisable using several procedures for analysis, especially when a curve is atypical.

The double-reciprocal plot according to I. Klotz (1946) is based on the reciprocal form of Eq. (1.23):

$$\frac{1}{r} = \frac{1}{n} + \frac{K_d}{n[A]} . \tag{1.29}$$

By entering $1/r$ versus $1/[A]$, an even gradient K_d/n is obtained, crossing the ordinate at $1/n$ and the abscissa at $-1/K_d$ (Figure 1.2D). This plot corresponds to the Lineweaver-Burk plot of enzyme kinetics (see Section 2.3.1.3). Its disadvantages are discussed in detail there. They are even more serious with binding measurements, as with the strong compression of values in areas of high concentration the exact determination of n is difficult because of the reciprocal entry. Furthermore, the reciprocal entry of data causes a rather high distortion of the error limits so that the application of simple linear regression procedures may not be applied without considering suitable weighting factors.

The plot described by G. Scatchard (1949) (corresponding to the Eadie-Hofstee plot of enzyme kinetics) is much more suitable. Multiplying Eq. (1.29) with rn/K_d results in:

$$\frac{r}{[A]} = \frac{n}{K_d} - \frac{r}{K_d} \ , \tag{1.30}$$

r is entered versus $r/[A]$ (Figure 1.2C). In this plot n is to be read directly from the abscissa intercept. The ordinate intercept has the value n/K_d, the gradient is $-1/K_d$. The error limits increase towards lower as well as towards high ligand concentrations. This relatively symmetrical error distortion makes the application of simple linear regressions possible, although with reservations.

Multiplying Eq. (1.29) by [A] results in the presentation known in enzyme kinetics as the Hanes plot:

$$\frac{[A]}{r} = \frac{[A]}{n} + \frac{K_d}{n} \ , \tag{1.31}$$

Here [A] is entered against $[A]/r$ (Figure 1.2E). This plot is rarely used for binding measurements, as n can only be obtained from the gradient $(1/n)$ or, together with K_d, from the ordinate intercept point (K_d/n), so that an error in the determination of one constant is also transferred to the other one. Error distortion, however, is smaller in this plot than in the other two. This plot has the disadvantage (same as in the Scatchard plot) that the two variables are not separated by the axes.

1.3.2.2 Analysis of Binding Curves from Spectroscopic Titration Procedures

The evaluation procedures discussed so far are based on the assumption that the amount of free ligand [A] within the equilibrium results from the experiment. In various binding methods, especially spectroscopic titrations (see Section 3.4.1.5), [A] is not directly obtained from the measurements. The same applies to enzyme kinetic measurements. There the problem is circumvented by using the simplification $[A]_0 = [A]$. This is permissible as long as the condition $[E] \ll [A]$ holds. Thus the portion of bound ligands becomes small compared with the total amount $[A]_{bound} \ll [A]_0$, and nearly all of the added ligand remains free. With binding measurements, conditions are completely different. Macromolecules and ligands as equal participants are employed in comparable quantities. The total amount of the ligand becomes noticeably reduced by the binding process. $[A]_0$ can no longer be equalled to [A]. Therefore, the saturation functions obtained from spectroscopic titrations no longer follow the hyperbolic curve described by Eq. (1.23) (Figure 1.3A) and may no longer be evaluated by the procedures discussed so far. Furthermore, the portion of $[A]_{bound}$ is obtained only as a measurement signal proportional to the saturation degree of the macromolecule, and not in molar units.

For the evaluation of spectroscopic titrations an asymptote is attached to the curve in the saturation area (Figure 1.3A). Compared with a hyperbolic saturation function, the titration curve nears saturation earlier, the asymptotic approach is, therefore, more reliable. The intercept of the ordinate is $x \cdot n[E]_0$, x being a proportional factor dependent on the measurement signal. The saturation value $x \cdot n[E]_0$ is arbitrarily set at 1

and all ordinate values refer to this. Thus they correlate to the saturation function $\overline{Y}$ defined in Eq. (1.23a). A tangent is laid through the ordinate base to the almost linearily rising values in the start area at low ligand concentrations. Both lines intersect at the abscissa value $[A]_0 = n[E]_0$. From this n is obtained. Now the proportional factor x can be calculated, and the ordinate values can be converted into $[A]_{bound}$. The values for [A] are obtained by deducting the ordinate values from the abscissa values. The data displayed in the plot of Figure 1.2 can now be analysed with these values. [A] also visually evolves from the titration curve as shown in Figure 1.3A. While the total distance from the ordinate to a certain measuring point is $[A]_0$, the abscissa section up to the source tangent is $[A]_{bound}$, and from there to the measuring point [A]. This tangent corresponds to a binding behaviour at infinitely high affinity ($K_d \to 0$), the ligand fully binding to the macromolecule ($[A]_0 = [A]_{bound}$), no free ligand remaining in the solution. If all binding sites are saturated, further ligand can only be present in free form ($[A]_0 = [A]$), the binding curve merging with the saturation asymptote. The experimental curve will deviate from the ideal form to such an extent as free ligands will appear already, before full saturation is reached, as in real systems with finite affinity. The deviation directly shows the free ligand as the overall shape of the curve indicates the strength of affinity: high-affinity curves keep closer to the two asymptotes compared with low-affinity curves. In the latter case the actual position of the straight line is more difficult to detect. Especially the source tangent is laid out too low, causing serious deviations in the analysis. A similar effect is caused by too low concentrations of the macromolecule.

A method of A. Stockell (1959) allows direct linearisation of binding curves obtained from spectroscopic titrations, if in Eq. (1.29) $r = n\overline{Y} = n[EA]/[E]_0$ is inserted, and $[A]_{bound} = n[EA]$:

$$\frac{1}{\overline{Y}} = 1 + \frac{K_d}{[A]_0 - n[EA]} = 1 + \frac{K_d}{[A]_0 - n\overline{Y}[E]_0} .$$

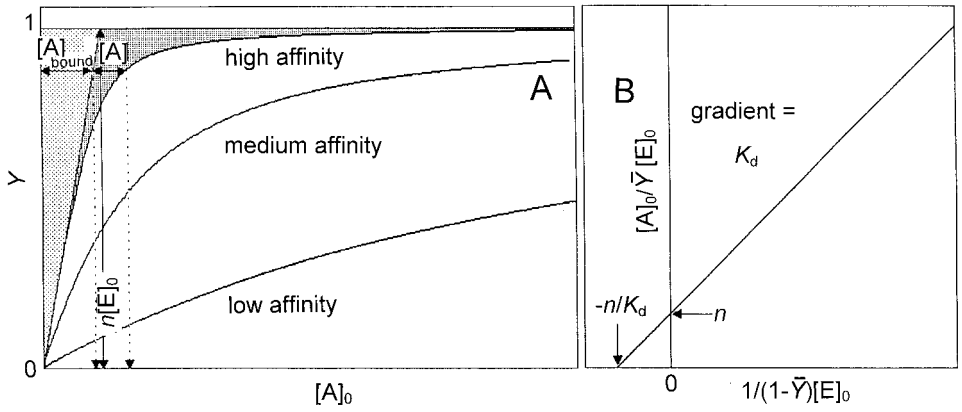

Figure 1.3. Evaluation of spectroscopic titrations. (A) Direct plot, (B) Stockell plot.

From transformation to

$$\frac{[A]_0}{\overline{Y}} - [A]_0 = n[E]_0(1 - \overline{Y}) + K_d$$

results:

$$\frac{[A]_0}{[E]_0\overline{Y}} = \frac{K_d}{[E]_0(1 - \overline{Y})} + n \; . \tag{1.32}$$

This equation now contains only known or directly detectable terms. When entering $[A]_0/[E]_0\overline{Y}$ against $1/[E]_0(1-\overline{Y})$ a straight line with the gradient K_d evolves, the ordinate intercept n and the abscissa intercept $-n/K_d$ (Figure 1.3B). In contrast to the linearisation procedures of Eq. (1.23) the saturation value cannot be obtained by extrapolation, but still has to be taken from the asymptote of the saturation curve ($\overline{Y}=1$) to define $\overline{Y}$ (Figure 1.3A). Therefore, measurements have to be carried out far into the saturation area. The Stockell plot is very sensitive to deviations from the normal behaviour, e.g., due to erroneous or artificial influences, so that a reliable evaluation can only be made with minimal error scattering. This plot is also more difficult to interpret than the direct linearisation methods, if other mechanisms are involved.

In the evaluation procedure of P. Job (1928) the total concentration of ligand and macromolecule is kept constant and only the molar proportion of both components is altered. X is the mol fraction of the macromolecule and Y that of the ligand, $X+Y=1$. This is entered versus a parameter of the complex, e.g., $[A]_{bound}$, an optical signal, or the enzyme activity. Figure 1.4 demonstrates this curve. Tangents are laid at the points $X=0$ and $Y=0$. Their joint intercept has the value

$$\frac{Y_i}{X_i} = \frac{K_d + nc_0}{K_d + c_0} \; . \tag{1.33}$$

X_i and Y_i are the mol fractions of enzyme and ligand at the intercept, $c_0=[E]_0+[A]_0$ is the constant total concentration of macromolecule and ligand. For $c_0 \gg K_d$ becomes $Y_i/X_i=n$. Here the stoichiometry of the binding can be taken from the ratio of the mol fractions at the tangent intercept. For $c_0 \ll K_d$ becomes $Y_i/X_i = 1$, the curve takes a symmetrical shape and the intercept always has the value 1, irrespective of the actual number of binding sites. This is a disadvantage of the Job plot. It can be circumvented as long as the sum of macromolecule and ligand concentration is higher than the value of the dissociation constant. If n is known, K_d can be calculated from Eq. (1.33), whereby the condition $c_0 \sim K_d$ should be regarded. K_d can also be obtained from the maximum of the curve in Figure 1.4 according to

$$K_d = \frac{(an + a - n)^2 c_0}{4an} \; . \tag{1.34}$$

Here a represents the ratio of the measurement value at the maximum M_m to the saturation value M_∞.

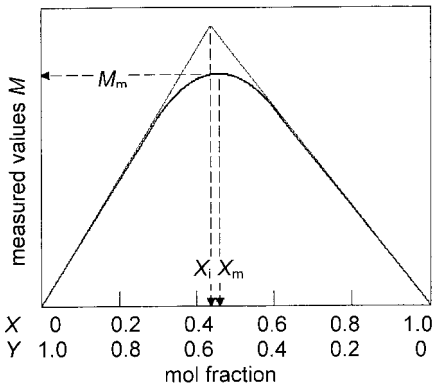

Figure 1.4. Evaluation of binding data after P. Job.

Further methods for the analysis of binding data from spectroscopic titrations are described in Section 2.3.1.1.

1.3.3 Binding of Various Ligands, Competition

Due to the high binding specificity of proteins, especially of enzymes, normally only the ligand designated by nature, e.g., the enzyme substrate, is bound and all other bindings are rejected. This selection can, however, not be absolute. Depending on the specific nature of the binding sites and their binding affinity, structurally analogous compounds to the native ligand are more or less well accepted, according to their degree of homology. Certain analogues even bind considerably stronger than the native ligand, due to special interactions with the binding centres. Analogues sometimes develop similar effects as the ligand, but mostly they remain inactive but block the binding site for the native ligand and thus have an antagonistic effect. This competition for a distinct binding site serve to as a proof for specific binding of a ligand. The efficiency of many (antagonistic) medicines and drugs (e.g., β-receptor blockers) is based on this competition. The mechanism of competition can be expressed as shown below:

$$\begin{array}{ccc} \mathrm{E} & + \mathrm{A} \underset{}{\overset{K_A}{\rightleftharpoons}} & \mathrm{EA} \\ + & & \\ \mathrm{B} & & \\ \Big\| K_B & & \\ \mathrm{EB} & & \end{array}$$

The binding affinities are expressed by the dissociation constants

$$K_A = \frac{[E][A]}{[EA]} \quad \text{and} \quad K_B = \frac{[E][B]}{[EB]} \tag{1.35 a}$$

The total amount of the macromolecule is

$$[E]_0 = [EB] + [EA] + [EB] \quad .$$

(E) and (EB) may be replaced by K_A and K_B in Eq. (1.35a):

$$[E]_0 = \frac{K_A[EA]}{[A]}\left(\frac{1+[B]}{K_B}\right) + [EA]\,.$$

By conversion

$$[EA] = \frac{[E]_0[A]}{[A] + K_A\left(1+\frac{[B]}{K_B}\right)}$$

is obtained.

For a macromolecule with n binding sites the following equation results, as discussed for Eq. (1.23):

$$r = \frac{n[A]}{[A] + K_A\left(1+\frac{[B]}{K_B}\right)}\,. \tag{1.36}$$

The double-reciprocal formula is:

$$\frac{1}{r} = \frac{1}{n} + \frac{K_A}{n[A]}\left(1+\frac{[B]}{K_B}\right) \tag{1.37}$$

and the Scatchard equation:

$$\frac{r}{[A]} = \frac{n}{K_A\left(1+\frac{[B]}{K_B}\right)} - \frac{r}{K_A\left(1+\frac{[B]}{K_B}\right)}\,. \tag{1.38}$$

There are now two variable concentration terms compared to the general binding equation, but this relationship is still applicable as long as one component, e.g. B, may be regarded constant while the other one (A) is altered. Thus, the bracket term remains constant, however, K_A is apparently increased by this term. The resulting curve still retains the hyperbolic shape. A second test series with an altered concentration $[B]_2$ (remaining, however, also constant during the test series) also results in a hyperbolic curve but with an altered steepness, as the apparent K_A changes correspondingly (Figure 1.5A). Under the same condition ([B] = constant) the double-reciprocal and the Scatchard plot yield straight lines, but also here K_A is modified by the bracket term. The saturation n, however, remains unchanged. Thus all straight lines in the double-reciprocal plot have a joint ordinate intercept (Figure 1.5 B), in the

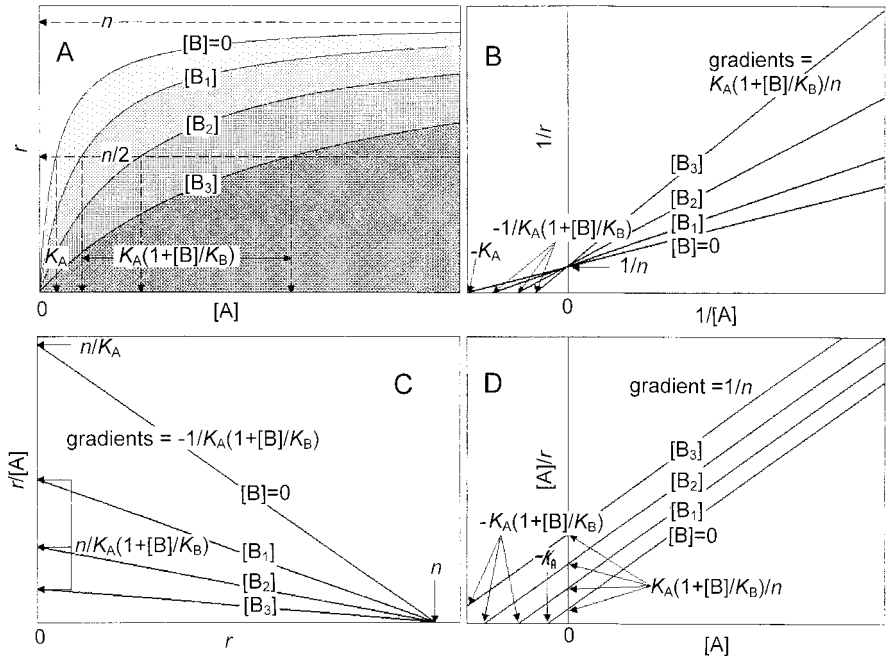

Figure 1.5. Competition of two ligands for a binding site. The concentration of A is altered with B at various, but respectively constant quantities. (A) Direct plot, (B) double-reciprocal plot, (C) Scatchard plot, (D) Hanes plot.

Scatchard plot they meet on the abscissa (Figure 1.5 C). Such straight line-patterns are characteristic for the competition of two ligands for the same binding site. In the case of $[A] \rightarrow \infty$, B will be displaced from all binding sites (and *vice versa*).

To identify the dissociation constants for A and B, K_A can at first be determined in the absence of B, e.g., from the abscissa intercept in the double-reciprocal plot (Figure 1.2D) – as described for the single Eq. (1.23). K_B can be obtained in the presence of B in the same way, if the term $K_A(1+[B]/K_B)$ is inserted in place of K_A, as [B] is known and K_A has already been identified.

Further methods for the analysis of competition data are described in Section 2.5.1.3.

If B influences the binding of A to the macromolecule but cannot completely displace this ligand (e.g., by binding in the vicinity of A, or by induction of a modification of the conformation of the macromolecule influencing the A binding site), the following mechanism applies:

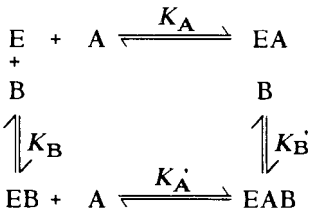

In contrast to the competitive mechanism, in addition to Eq. (1.35a), two further dissociation constants are obtained:

$$K'_A = \frac{[EB][A]}{[EAB]} \quad \text{and} \quad K'_B = \frac{[EA][B]}{[EAB]} , \tag{1.35 b}$$

that are linked according to Eqs. (1.35a) and (1.35b):

$$\frac{K_A}{K_B} = \frac{K'_A}{K'_B} . \tag{1.39}$$

Based on the relationship for the total amount of the macromolecule:

$$[E]_0 = [E] + [EA] + [EB] + [EAB]$$

the individual forms of enzymes can be replaced by constants:

$$[E]_0 = [E] + \frac{[E][A]}{K_A} + \frac{[E][B]}{K_B} + \frac{[E][A][B]}{K_A K'_B} ,$$

$$[E] = \frac{[E]_0}{1 + \frac{[A]}{K_A} + \frac{[B]}{K_B} + \frac{[A][B]}{K_A K'_B}} .$$

The portion of the bound ligand $[A]_{bound}$ is:

$$[A]_{bound} = [EA] + [EAB] = \frac{[E][A]}{K_A} + \frac{[E][A][B]}{K_A K'_B} ,$$

$$[A]_{bond} = \frac{\frac{[E]_0[A]}{K_A}\left(1 + \frac{[B]}{K'_B}\right)}{1 + \frac{[A]}{K_A} + \frac{[B]}{K_B} + \frac{[A][B]}{K_A K'_B}} .$$

Replacing $[A]_{bound}$ by $r = [A]_{bound}/[E]_0$, assuming n binding sites, and multiplying with K_A, the following equation results:

$$r = \frac{n[A]\left(1 + \frac{[B]}{K'_B}\right)}{K_A\left(1 + \frac{[B]}{K_B}\right) + [A]\left(1 + \frac{[B]}{K'_B}\right)} . \tag{1.40}$$

A mutual influence or impediment of the binding of both ligands occurs only in the case of $K_A \neq K'_A$, and $K_B \neq K'_B$, whereas Eq. (1.40) is reduced to the normal binding Eq. (1.23) for $K_A = K'_A$, $K_B = K'_B$. Each ligand then binds idependently from the other. In the linearised plots, i.e., the double-reciprocal plot

$$\frac{1}{r} = \frac{1}{n} + \frac{K_A\left(1 + \frac{[B]}{K_B}\right)}{n[A]\left(1 + \frac{[B]}{K'_B}\right)'} \tag{1.41}$$

and the Scatchard plot

$$\frac{r}{[A]} = n\frac{\left(1 + \frac{[B]}{K'_B}\right)}{K_A\left(1 + \frac{[B]}{K_B}\right)} - r\frac{\left(1 + \frac{[B]}{K'_B}\right)}{K_A\left(1 + \frac{[B]}{K_B}\right)}, \tag{1.42}$$

bundles of straight lines with joint intercepts, located identically to the competition plots, are obtained (Figure 1.5), so that both mechanisms are indistinguishable. Here lies a danger of misinterpretation of competition experiments. Both mechanisms may be distinguished from each other by secondary plots commonly used in enzyme kinetics (see Section 2.5.1.2), where the gradients of the straight line resp. the positive reciprocal gradients in the Scatchard plot are entered against the constant ligand concentration B. In the competitive mechanism a straight line with the abscissa intercept $-K_B$ is obtained. For separate ligand bindings the secondary plot will show bended curves.

The interaction of different ligands with the macromolecule correlates with the reversible enzyme inhibition (Section 2.5.1), *competition* correlating with competitive inhibition, the last of the above mechanisms correlating with a partially competitive inhibition. This analogy results from $[A]_{bound}$ being composed of [EA] *and* [EAB], in the same way as both the enzyme-substrate complex and the enzyme-substrate inhibitor complex are equally active in partially competitive inhibition.

1.4 Macromolecules with Non-Identical, Independent Binding Sites

Various macromolecules, e.g., enzymes or membrane receptors, possess different binding sites for the same ligand. These may be located on the same subunit. More often different binding sites are an indicator for the presence of non-identical subunits, e.g., trytophan synthase with two α- and β-type subunits, each of which is able to bind indol. A macromolecule may thus possess several binding classes each with several identical binding sites (n_1, n_2, n_3).

Obviously, ligands will occupy the site with the highest affinity first, and the binding sites with low affinity only with rising concentrations. For independent binding of ligands to the different binding centres the general binding Eq. (1.23) applies for all centres, the total process being the sum of the individual processes:

$$r = \frac{n_1[A]}{K_{d1} + [A]} + \frac{n_2[A]}{K_{d2} + [A]} + \ldots \frac{n_m[A]}{K_{dm} + [A]}. \tag{1.43}$$

K_{d1}, K_{d2}, etc., are the dissociation constants of the individual binding classes. Each individual process follows a normal hyperbolic saturation function. The total function results in a superimposition of several hyperbolae (Figure 1.6A). There is an initial steep gradient in the zone of low ligand concentration due to the occupation of the high affinity sites. When this function tends to saturation, the occupation of sites with low affinity starts and causes the curve to rise further. Compared with a normal hyperbolic function, the initial steep gradient and the extended sloping towards saturation stand out. This depends on the relative ratio of the binding constants and the number of identical binding sites within the different binding classes. This kind of deviation from a normal hyperbola is not easy to detect, and thus an analysis of the constants from this curve seems hardly advisable. The advantage of linearised plots is clearly demonstrated here. They will show a deviation from the linear gradient, which is characteristic for this mechanism. The respective forms of the curve result from the superimposition of two or more straight lines, as shown in Figure 1.6B–D. In the double-reciprocal plot (Figure 1.6B) and in the Hanes plot (Figure 1.6D) the curve deviates from the linear run towards the right lower edge, in the Scatchard plot (Figure 1.6C) the curve appears as a transition from a steep to a flattened gradient.

The analysis of such curves is rather difficult. The total number of ligand binding sites of the macromolecule can be obtained by extrapolating them to the ordinate in case of the double-reciprocal diagram, and to the abscissa for the Scatchard plot. The num-

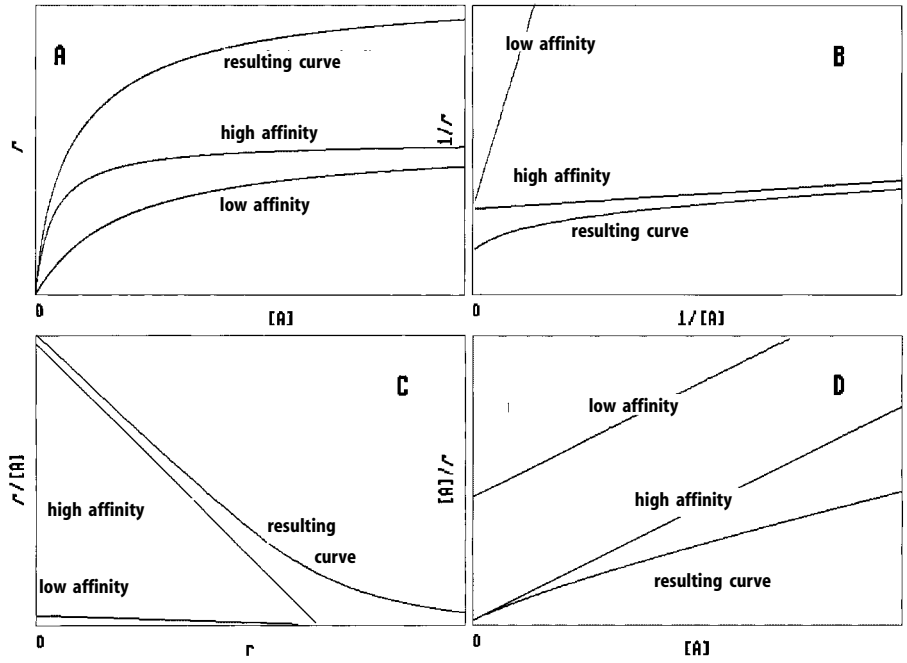

Figure 1.6. Binding of a ligand to two binding sites of different affinity. Shown are the curves for the separate binding to sites of high and low affinity and the curves resulting from the two parts. (A) Direct plot, (B) double-reciprocal plot, (C) Scatchard plot, (D) Hanes plot.

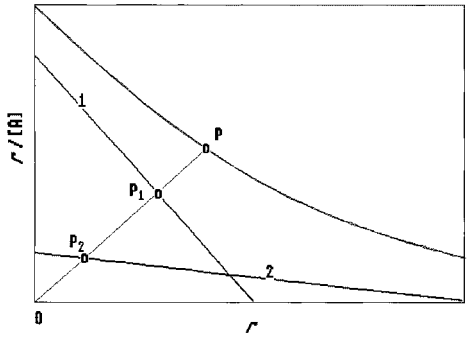

Figure 1.7. Graphic method for the analysis of a binding curve with two binding classes according to Rosenthal (1967). 1 and 2 are the straight lines of the separate binding classes, the original straight line has the gradient 1/[A]. Its intercept point P with the measurement curve with its co-ordinates $[A]_{bound}//[A]_{bound}/[A]$ is the sum of the binding co-ordinates of the intercepts P_1 and P_2 with the straight lines of the separate binding classes.

ber of binding categories, of identical binding sites per binding classes, and the relevant binding constants cannot be directly determined. If there are, as in the majority of cases, only two binding classes, it may be assumed that there is only one binding class predominating in both extreme areas of ligand concentration. In the low substrate range preferentially the high affinity sites will be occupied, in the saturation range the low affinity sites. It would, however, be incorrect to conclude that the respective ends of the curve represent the separate binding classes and constants could be directly obtained by attaching tangents to these regions, as seen in Figure 1.6B–D. In the Scatchard plot these tangents may be moved in a parallel manner, so that the sum of their ordinate intercepts correlates with the ordinate intercepts of the experimental curve. With a graphic method according to Rosenthal (1967) the resulting binding curve can be obtained from two such straight lines by way of the original straight line. The sum of the distances from the co-ordinate source to each of the lines correlates to a point on the resulting binding curve (Figure 1.7). An analysis of such curves can be successfully performed with suitable computer program by numeric adaptation of the parameters or with the least-error squares-method (Weder et al., 1974). Such methods can also be applied for the analysis of curves with more than two binding classes. It remains, however, difficult to analyse such cases by binding curves alone, as the curves for three and more binding classes are not much different from the ones for two binding classes. Furthermore, similar curves are found for isoenzymes with negative cooperativity and half-of-the-sites reactivity (see Section 1.5.6).

1.5 Macromolecules with Identical, Interacting Binding Sites, Cooperativity

1.5.1 The Hill Equation

It has been common knowledge for a hundred years that the binding of oxygen to haemoglobin does not follow a normal hyperbolic function, but has a characteristic, s- or *sigmoidal* shape, whereas the binding to the closely related myoglobin is completely normal (Figure 1.8). Since then this remarkable fact has initiated a large number of the-

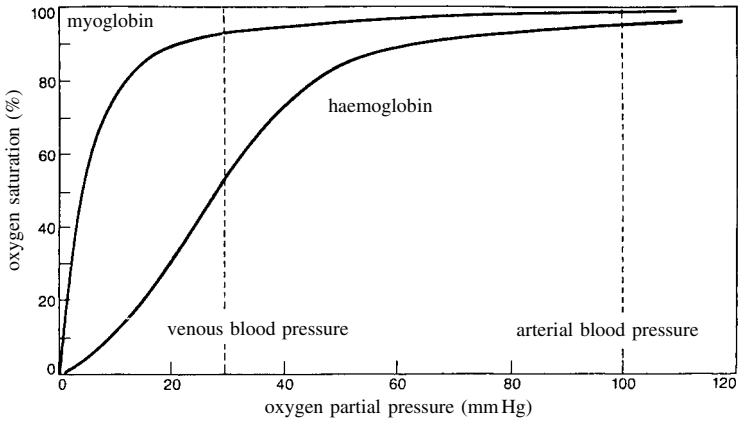

Figure 1.8. Oxygen saturation curves for myoglobin and haemoglobin (according to M.F. Perutz, 1978, Scientific American 239 (6), 68–86).

oretical and methodical studies. This phenomenon became even more interesting when comparable saturation curves were found in enzymes occupying key positions in metabolism. Obviously an important regulatory principle of the cell was hidden here.

A first attempt to interpret this phenomenon was undertaken by A.V. Hill in 1910. He postulated that several (n) oxygen molecules bind simultaneously to a haemoglobin molecule:

$$\mathrm{E} + n\mathrm{A} \rightleftharpoons \mathrm{EA_n} \; . \tag{1.44}$$

The law of mass action for this reaction equilibrium is:

$$K_\mathrm{d} = \frac{[\mathrm{E}][\mathrm{A}]^\mathrm{n}}{[\mathrm{EA_n}]} \; . \tag{1.45}$$

A binding equation analogous to Eq. (1.23) can be established by replacing [A] by $[\mathrm{A}]^\mathrm{n}$:

$$r = \frac{n[\mathrm{A}]^\mathrm{n}}{K_\mathrm{d} + [\mathrm{A}]^\mathrm{n}} \; . \tag{1.46}$$

This *Hill equation* describes sigmoidal binding curves as found for hemoglobin. In order to determine n, the number of ligand molecules bound per haemoglobin molecule, Hill converted Eq. (1.46) into a linear form by transformation into logarithms, r was replaced by $\overline{Y} = r/n$:

$$\frac{\overline{Y}}{1-\overline{Y}} = \frac{[\mathrm{A}]^\mathrm{n}}{K_\mathrm{d}} \; ,$$

$$\log \frac{\overline{Y}}{1-\overline{Y}} = n \cdot \log[\mathrm{A}] - \log K_\mathrm{d} \; . \tag{1.47}$$

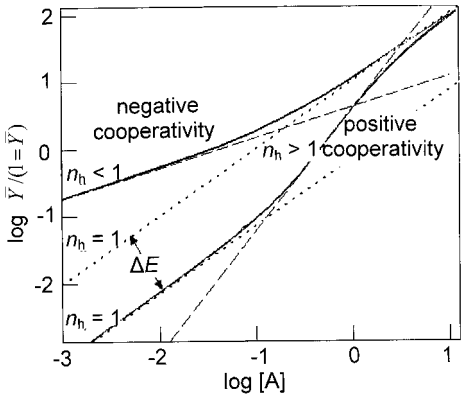

Figure 1.9. Hill plot for positive and negative cooperativity. The dotted tangents to the curves in the lower and upper ligand region have a gradient of 1 and correspond to a normal hyperbolic binding curve. The Hill coefficient is the gradient of the dashed tangents to the areas of maximum deviation.

Logarithmic entry of $\overline{Y}/(1-\overline{Y})$ against the ligand concentration results in a straight line with the gradient n (Figure 1.9). The number of oxygen molecules bound per haemoglobin molecule could thus be read from the gradient. However, the sigmoidal binding curves obtained from haemoglobin and also from various enzymes cannot be linearised in a Hill plot, nor does the gradient show the expected value of 4 for the number of binding sites. Actually, all sigmoidal curves obtained from experiments show in this plot a characteristic three-phase behaviour. At low substrate concentrations the curve runs linear with a gradient of 1, rising to a maximum value in the medium saturation range to 2.8 for haemoglobin, returning to a straight gradient of 1 in the saturation range (Figure 1.9). Hyperbolic curves, which follow the general binding equation always yield in the Hill diagram a straight gradient of 1, regardless of the number of binding sites of the macromolecule. Thus, this plot could be regarded as a further possibility of linear presentation of the simple binding equation, but it does not offer any special advantages compared to the methods already described. The constants are even more difficult to work out. K_d equals the abscissa value at the location $\log \overline{Y}/(1-\overline{Y}) = 0$ (half-saturation).

1.5.2 The Adair Equation

G.S. Adair proved that haemoglobin is actually composed of four subunits, and he could show that neither the number of binding sites can be obtained from the Hill plot gradient, nor does the Hill equation sufficiently describe the binding relationships. It does not consider that the different binding sites of the macromolecule are occupied successively in a series of individual reaction steps, as already formulated in the general binding equation in Section 1.3.1. Rather, the mechanism described by the Hill equation (1.44) is derived on the basis of the sum of all individual steps, the interim forms EA to EA_{n-1} being eliminated and thus regarded as non-existent. To conform to such a mechanism, all ligand molecules would have to bind to the macromolecules simultaneously and reach saturation in a single step. Partial saturation should not occur. Such a

mechanism is hardly conceivable, as the ligands cannot communicate with each other, and a single ligand molecule could not be prevented from occupying a free binding site on its own. Similar processes are to be found in the crystallisation and polymerisation from over-saturated solutions. Here the limiting process is the formation of a crystallisation nucleus which in some cases may take even days or weeks. Once this formation occurs, however, crystallisation of the whole solution sets in almost immediately. Applied to a macromolecule with a limited number of binding sites, it would require these binding sites to possess almost no affinity to the ligand. Should a ligand interact with a binding site after all, the affinity of the still unoccupied binding sites of the macromolecule would increase so sharply that they would be occupied directly. The first ligand acts as a door opener and assists the following ligands in binding to the site. This binding mode is termed *cooperativity.*

Adair developed an equation to describe the sigmoidal binding curve of the oxygen of haemoglobin, including all individual reaction steps. The procedure correlates in principle with the one for the general binding equation, only the constants for the single steps are taken as different and can, therefore, not be replaced by a single constant. The different enzyme units in the saturation function r defined according to Eq. (1.26) are replaced by the macroscopic dissociation constants of the individual binding steps resulting in the *Adair equation* already defined in Section 1.3.1:

$$r = \frac{\dfrac{[\mathrm{A}]}{K_1'} + \dfrac{2[\mathrm{A}]^2}{K_1'K_2'} + \dfrac{3[\mathrm{A}]^3}{K_1'K_2'K_3'} + \ldots \dfrac{n[\mathrm{A}]^n}{K_1'K_2'K_3' \ldots K_n'}}{1 + \dfrac{[\mathrm{A}]}{K_1'} + \dfrac{[\mathrm{A}]^2}{K_1'K_2'} + \dfrac{[\mathrm{A}]^3}{K_1'K_2'K_3'} + \ldots \dfrac{[\mathrm{A}]^n}{K_1'K_2'K_3' \ldots K_n'}} \tag{1.27}$$

This equation is not very suitable for the analysis of experimental data, as the different constants cannot be directly determined. On the other hand, distinct curves can be simulated by setting arbitrary constants and fit them to the data obtained from experiments. Sigmoidal saturation curves result when the constants decrease from the first to the last binding step, so that the affinity of the binding sites increases with the degree of occupation. These curves now also show the three-phase behaviour in the Hill plot, the value of the maximum gradient being lower than the actual number of binding sites, as observed in real systems like haemoglobin. The gradient is dependent on the relative ratio of the constants to each other. It becomes steeper and approaches to the number of binding sites, the more the single step constants diverge in the way described above, i.e., the stronger the cooperativity becomes. In no case, however, the gradient value may exceed the number of identical binding sites. On the other hand, the gradient tends towards 1 in the same degree as the constants converge. The Adair model is, therefore, more sophisticated than the vision of Hill: Instead of the simultaneous occupation of all binding sites, a sequential binding with increasing affinity is assumed.

Although the Adair equation, in contrast to the Hill equation, is able to describe experimental binding curves completely, it remains nevertheless unsatisfactory as it is not based on a plausible binding mechanism. The Adair mechanism assumes that the binding steps and not the binding sites of the molecule differ in their affinity. Pri-

marily, all binding sites are equal, but each binding step causes a defined alteration of the affinities of all still unoccupied binding sites. Thus in haemoglobin with four identical binding sites, the site occupied last must change its affinity four times, from K'_1 to K'_4. It is a theoretical mechanism, revealing nothing about the way in which the macromolecule realises these changes of affinity.

1.5.3 The Pauling Model

In 1935 Linus Pauling proposed the first plausible description of cooperative phenomena. He also considered the macromolecule to consist of identical binding sites with an uniform binding constant K_d. He further assumed that the subunit occupied with a ligand convey a stabilising effect on the still free subunits of the macromolecule. This is expressed by an interaction factor α that enhances the binding affinities. Considering the statistical factors of Eq. (1.24) the following binding constants result for each individual step:

$$K'_{d1} = \frac{K_d}{4} \; ; \; K'_{d2} = \frac{2K_d}{3\alpha} \; ; \; K'_{d3} = \frac{3K_d}{2\alpha^2} \; ; \; K'_{d4} = \frac{4K_d}{\alpha^3} \; .$$

When inserting these constants into the Adair equation, the follwing binding function results:

$$r = \frac{\dfrac{4[A]}{K_d} + \dfrac{12\alpha[A]^2}{K_d^2} + \dfrac{12\alpha^3[A]^3}{K_d^3} + \dfrac{4\alpha^6[A]^4}{K_d^4}}{1 + \dfrac{4[A]}{K_d} + \dfrac{6\alpha[A]^2}{K_d^2} + \dfrac{4\alpha^3[A]^3}{K_d^3} + \dfrac{\alpha^6[A]^4}{K_d^4}} \; . \tag{1.48}$$

With this simplified correlation – compared to the Adair equation – a satisfactory description of sigmoidal saturation curves is possible.

1.5.4 Allosteric Enzymes

Subsequently, it became more and more evident that the atypical binding behaviour of this class of macromolecules is not restricted to the sigmoidal shape of the saturation curve of one ligand only (*homotropic effect*), but was additionally influenced – either positively or negatively – by distinct ligands (activators or inhibitors, respectively) (*heterotopic effects*). These effectors do not act by direct interaction with the original ligand, e.g., by displacement from its binding site (competition), rather they occupy a spatially separated binding site, an *allosteric center* (Greek: $\alpha\lambda\lambda o\varsigma$ different; $\sigma\tau\varepsilon\rho\varepsilon o\varsigma$ rigid). It permits the regulation of the interaction of an active centre with its ligand by a second, completely different metabolite. A typical example is the *feedback inhibition* where the final product of a metabolic chain controls its first catalytic step. Generally, heterotropic effectors act on the sigmoidal saturation function of the ligand in a

manner that activators decrease the sigmoidal deviation, i.e., the strength of cooperative interaction, while inhibitors exert an intensifying effect. The sigmoidal saturation behaviour of enzymes can usually be observed measuring the reaction rate in dependence on the substrate concentration. Effectors change the enzyme activity as described above. This class of regulatory enzymes has been termed *allosteric enzymes*. It should be emphasised that cooperativity, expressed in modified binding curves, and allostery, the influence on an active centre by a second, separately binding ligand, basically are phenomena independent of each other which may also occur separately. However, they usually occur jointly – as will be demonstrated later – and only develop their full efficacy in conjunction. The correlation between allosteric properties and cooperativity has not been considered in the models described so far.

1.5.5 The Symmetry Model

In 1965 Jacques Monod, Jeffries Wyman and Jean-Pierre Changeux presented the first comprehensive model for the description of allosteric enzymes in their publication *On the Nature of Allosteric Transition: A Plausible Model*. It became a guideline for the improved understanding of regulatory mechanisms on enzymes. The model, also designated as the *concerted model* is based on certain conditions (see Figure 1.10) that were observed with several enzymes, and also with haemoglobin:

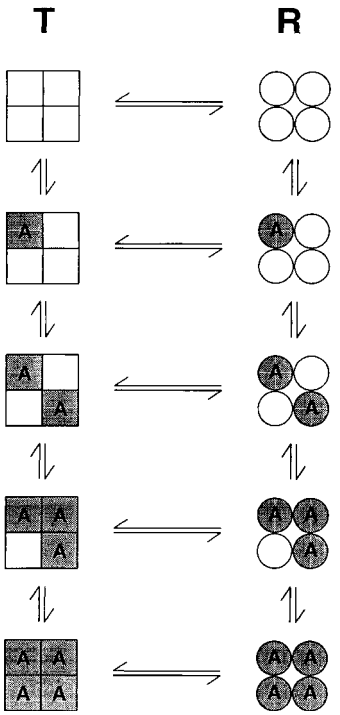

Figure 1.10. Schematic display of the states of conformation and fractional saturation of a tetramer macromolecule according to the symmetry model.

1) An allosteric system is an oligomer composed of a limited number n of identical units (protomers). The protomer itself may either be a subunit (polypeptide chain) or be composed of several non-identical subunits.
2) Protomers occupy equal positions in the enzyme molecule which thus has at least one symmetry axis.
3) The enzyme may exist in at least two states of conformation which are termed T (*tense*) and R (*relaxed*) and differ in their energy potential. In the absence of ligand both enzyme forms exist in an equilibrium characterised by the constant L:

$$L = \frac{[\mathrm{T}]}{[\mathrm{R}]} \; . \tag{1.49}$$

4) The molecular symmetry is preserved during the transition from one enzyme form into the other. All subunits of an enzyme molecule exist at the same time either only in the T or the R state. Intermediate forms with protomers in differing conformations are excluded.
5) Both enzyme forms differ in their ligand affinity. T is the low-affinity (or less active) and R the high-affinity (or fully active) enzyme form, i.e., the ratio c of the dissociation constant is:

$$c = \frac{K_\mathrm{R}}{K_\mathrm{T}} < 1 \; . \tag{1.50}$$

6) In the absence of ligand the equilibrium L is in favour of the low-affinity form T, i.e., L >1.

The following equilibria describe the binding of the ligand to the two enzyme forms:

$$\mathrm{T} \rightleftharpoons \mathrm{R}$$

$$\begin{array}{lll}
\mathrm{T} + \mathrm{A} \rightleftharpoons \mathrm{TA} & & \mathrm{R} + \mathrm{A} \rightleftharpoons \mathrm{RA} \\
\mathrm{TA} + \mathrm{A} \rightleftharpoons \mathrm{TA_2} & & \mathrm{RA} + \mathrm{A} \rightleftharpoons \mathrm{RA_2} \\
\mathrm{TA_2} + \mathrm{A} \rightleftharpoons \mathrm{TA_3} & & \mathrm{RA_2} + \mathrm{A} \rightleftharpoons \mathrm{RA_3} \\
\vdots & & \vdots \\
\mathrm{TA_{n-1}} + \mathrm{A} \rightleftharpoons \mathrm{TA_n} & & \mathrm{RA_{n-1}} + \mathrm{A} \rightleftharpoons \mathrm{RA_n} \; .
\end{array}$$

Assuming identical microscopic binding constants for binding sites on identical subunits, the individual enzyme forms can be characterised by the constants:

$$[\mathrm{TA}] = [\mathrm{T}]n\frac{[\mathrm{A}]}{K_\mathrm{T}} \qquad [\mathrm{RA}] = [\mathrm{R}]n\frac{[\mathrm{A}]}{K_\mathrm{R}}$$

$$[\mathrm{TA}]_2 = [\mathrm{TA}]\frac{(n-1)[\mathrm{A}]}{2K_\mathrm{T}} \qquad [\mathrm{RA}]_2 = [\mathrm{RA}]\frac{(n-1)[\mathrm{A}]}{2K_\mathrm{R}}$$

$$\vdots \qquad\qquad \vdots$$

$$[\mathrm{TA}]_\mathrm{n} = [\mathrm{TA}_{\mathrm{n}-1}]\frac{[\mathrm{A}]}{nK_\mathrm{T}} \qquad [\mathrm{RA}]_\mathrm{n} = [\mathrm{RA}_{\mathrm{n}-1}]\frac{[\mathrm{A}]}{nK_\mathrm{R}} \ .$$

From the fraction of the binding sites occupied by ligand

$$\overline{Y} = \frac{1}{n}\cdot\frac{([\mathrm{TA}] + 2[\mathrm{TA}_2] + \ldots n[\mathrm{TA}_\mathrm{n}]) + ([\mathrm{RA}] + 2[\mathrm{RA}_2] + \ldots n[\mathrm{RA}_\mathrm{n}])}{([\mathrm{TA}] + [\mathrm{TA}_2] + \ldots [\mathrm{TA}_\mathrm{n}]) + ([\mathrm{RA}] + [\mathrm{RA}_2] + \ldots [\mathrm{RA}_\mathrm{n}])} \tag{1.51}$$

the general saturation function for the symmetry model is obtained by replacement of $[\mathrm{A}]/K_\mathrm{R} = \alpha$.

$$\overline{Y} = \frac{Lc\alpha(1+c\alpha)^{\mathrm{n}-1} + \alpha(1+\alpha)^{\mathrm{n}-1}}{L(1+c\alpha)^\mathrm{n} + (1+\alpha)^\mathrm{n}} \ . \tag{1.52}$$

Sigmoidal saturation curves are always obtained when all three conditions are fulfilled simultaneously: $L>1$, $c<1$ and $n>1$. If only one of these preconditions fails and c or $n=1$ or L becomes very small, Eq. (1.52) reduces to the normal binding equation:

$$\overline{Y} = \frac{\alpha}{1+\alpha} = \frac{[\mathrm{A}]}{K_\mathrm{R} + [\mathrm{A}]} \ . \tag{1.23}$$

The degree of curvature, i.e., the sigmoidicity or intensity of cooperativity becomes more evident, the more the preconditions are valid, i.e., the larger L and n become and the smaller c. Such changes in the shape of the curve are less well detectable in the direct non-linear plot (Figure 1.11A), while the linear plots show characteristic deviations from the straight line, in case of the double reciprocal plot (Figure 1.11B) towards the top right, in the Hanes plot (Figure 1.11D) to the top left. In the Scatchard plot (Figure 1.11D) a maximum is passed through. The Hill plot is best suited for the analysis of cooperative systems (Figure 1.9) as two characteristic factors can be identified with it. As already mentioned the curve runs from a straight line with a gradient of 1 at low ligand concentration through a steeper middle section and returns to a straight line with a gradient of 1 in the saturation range. Both straight lines represent simple binding characteristics to distinct states, the T state in the very low and the R state in the high saturation areas. The distance between the two straight lines is a measure of the energy difference between the R and T states. In the middle area the cooperative effect comes into action, the system switches from the low-affinity T state to the high-affinity R state. The maximum gradient is termed the Hill coefficient (n_h) and indicates the strength of cooperativity (see below).

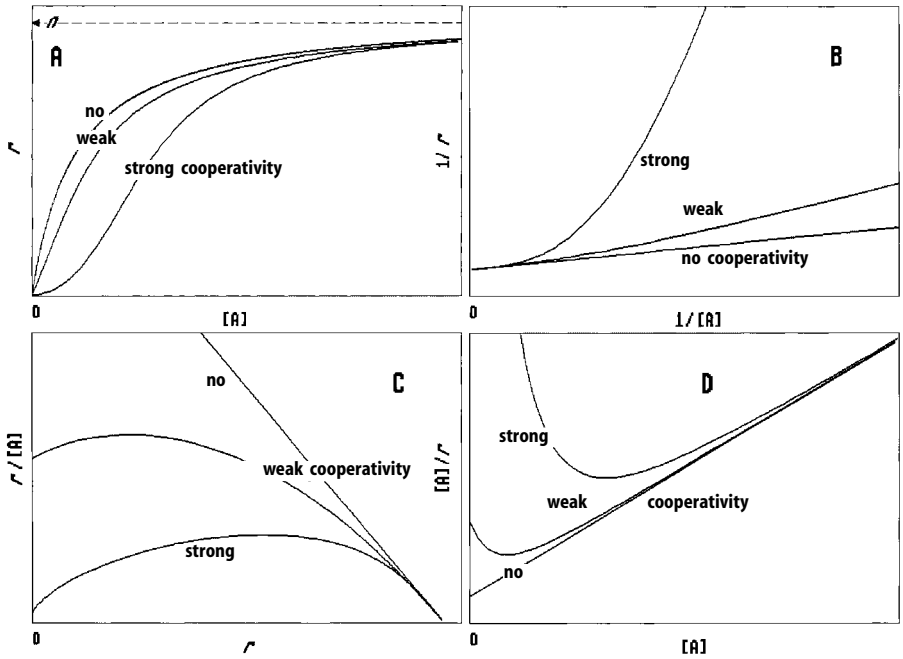

Figure 1.11. Binding curves in various representations of cooperative systems according to the symmetry model. Constants L and c stand for weak cooperativity (5, respectively 0.1), for high cooperativity (100, respectively 0.01), and for non-cooperative behaviour (1). (A) Direct plot, (B) double-reciprocal plot, (C) Scatchard plot, (D) Hanes plot.

The cooperative effect can be interpreted in such a way that the first ligand will find only very few molecules with affinity in the R state as they are in the minority. However, ligand binding stabilises the R state and removes it from equilibrium. To restore the original equilibrium, a macromolecule has to be taken from the surplus of the T fraction and transformed into the R state. The next ligand will find both, binding sites conforming to the original equilibrium as well as still free binding sites in the partially occupied R form removed from equilibrium. The number of available binding sites thus increases faster than the ligand concentration. With four protomers, each binding ligand will provide three additional binding sites apart from its own. If the pool of T-form molecules is exhausted and the whole macromolecule population has shifted to the R form, binding obeys a normal function resulting in a gradient of $n_h = 1$.

The Hill coefficient ranges within the limits of $1 \leq n_h \leq n$. Its relative size is determined by L and c: the better the conditions $L \gg 1$ and $c \ll 1$ are fulfilled, the more n_h will approach the number of protomers n. In no case, however, n can be surpassed by n_h. Reversely, n_h cannot fall below 1 with any combination of L and c. The Hill coefficient thus proves to be a measure for the strength of cooperativity. The more it adapts to the number of protomers, the more pronounced cooperativity becomes. In the extreme case of $n_h = n$ the mechanism defined by the Hill equation (1.46) applies.

Table 1.1. Relationship between the number of protomers n and the Hill coefficient n_h with haem proteins from different organisms (after Wyman, 1967)

Protein	Source	n	n_h
Myoglobin	Mammalian	1	1
Myoglobin	Molluscs	2	1.5
Haemoglobin	Mammalian	4	2.8
Haemocyanin	Lobster	24	4
Chlorocruorin	*Spirographis*	~80	5
Erythrocruorin	*Arenicola*	>100	6

This shows the significance of the Hill coefficient reflecting the reaction order with respect to the varied ligand. According to Eq. (1.44), n should only be an integer, but due to the interactions of subunits also fractioned reaction sequences are possible. The highest possible reaction order, i.e., maximal cooperativity, is achieved when all binding sites are occupied simultaneously. Thus the Hill coefficient is not a direct measure for the number of subunits (or protomers), rather the actual number of protomers is equal to the Hill coefficient or larger (as long as no other mechanism is responsible for the sigmoidal curve). There also exists no direct proportionality between n_h and n (even at identical values for L and n). Table 1.1 demonstrates that several oxygen-binding proteins show a far weaker increase of n_h than the number of protomers. While n increases from 1 to 100 the Hill coefficient only rises to 6. This is confirmed by theoretical calculations.

In the concerted model *heterotopic effectors* influence the equilibrium of R and T states via the allosteric centres. Activators act in the same way as the cooperative ligand, they bind with higher affinity to the R form and shift the equilibrium into this direction. L is thus diminished, cooperativity is weakened, the Hill coefficient becomes smaller. In the presence of the activator, the ligand finds a larger quantity of the macromolecule already in the R state, so that total activity is enhanced. Conversely, the inhibitor will bind and stabilise the T form. L and subsequently n_h increase, cooperativity is intensified. Larger quantities of ligand are now necessary to compensate the shift of equilibrium towards the T form, and an inhibition results.

Heterotopic effectors are considered in Eq. (1.52) by modification of the equilibrium constants from L to L':

$$L' = L\left(\frac{1+d\beta}{1+\beta}\right)^{n} \cdot \left(\frac{1+e\gamma}{1+\gamma}\right)^{n} . \tag{1.53}$$

β and γ are the inhibitor and activator concentrations, respectively, reduced by their respective binding constants to the R form (K_{Ri} and K_{Ra}); $d = K_{Ri}/K_{Ti} > 1$ and $e = K_{Ra}/K_{Ta} < 1$ are the ratios of the binding constants for the R and T states of inhibitor and activator, respectively.

1.5.6 The Sequential Model and Negative Cooperativity

One year after the postulation of the concerted model D.E. Koshland, G. Nemethy and D. Filmer (1966) published an alternative model for allosteric enzymes which describes the cooperative phenomena and heterotopic effects equally well. This model also assumes the macromolecule to be composed of several identical subunits and the existence of at least two conformations of different affinity. The low-affinity or inactive T state (for uniformity the terms from the concerted model are also applied here) prevails in the absence of ligand, the high-affinity or fully active R state prevails in the presence of ligand. K_t is the equilibrium constant of both enzyme forms in the absence of ligand:

$$K_t = \frac{[T]}{[R]} \gg 1 \ . \tag{1.54}$$

There are two substantial differences from the concerted model. Before postulating the sequential model Koshland developed the *induced-fit hypothesis*. In contrast to the *lock-and-key model* of Emil Fischer (1894), it assumes that the substrate specificity of an enzyme is not based on preformed rigid binding regions where only the original substrate molecule can lock into like a key, but that the fitting binding site is created interactively by enzyme and substrate. Only the genuine substrate can induce this adaptation. This hypothesis is a fundamental prerequisite for the sequential model. Unlike the concerted model, where the ligand is not actively involved in the shift from T to R state but only selects the form with higher affinity, in the sequential model ligand induces the conformation transition by binding. The second difference from the concerted model is the sequential transition. Only those subunits the ligand binds to change into the R form, all others remain in the T state. The conformation transition is performed step-by-step with the saturation of the enzyme (Figure 1.12).

Cooperativity originates from the interaction between the subunits. The intensity of this mutual interaction is dependent on the state of conformation of the immediate neighbour subunits and is defined by interaction constants. They indicate the ratio of interacting (e.g., TT) to non-interacting subunits (T, T). As these are relative factors, the constant K_{TT} for TT-interactions is taken as a reference value and set at 1:

$$K_{TT} = \frac{[T][T][TT]}{[TT][T][T]} = 1 \tag{1.55}$$

$$K_{RT} = \frac{[T][R][TT]}{[RT][T][T]} = \frac{[R][TT]}{[RT][T]} \tag{1.56}$$

$$K_{RR} = \frac{[R][R][TT]}{[RR][T][T]} \ . \tag{1.57}$$

Interactions of the subunits at the transition from the T to the R state can thus either be stabilising (K_{RT} and $K_{RR} < 1$) or destabilising K_{RT} and $K_{RR} > 1$.

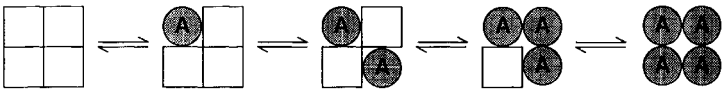

Figure 1.12. Schematic representation of the conformation states and the fractional saturation of a tetrameric macromolecule according to the sequential model.

Table 1.2 Conformation states and definition of the Θ-values for a trimer linear macromolecule according to the sequential model

Enzyme conformation	Interaction constants	Θ values
Free enzyme		
TTT	$K_{TT}K_{TT}=1$	$\Theta_0=1$
1st Binding step		
TRT	$K_{RT}K_{RT} = K_{RT}^2$	$\Theta_1=(K_{RT}^2 + 2K_{RT})K_RK_t$
TTR+RTT	$K_{TT}K_{RT} + K_{RT}K_{TT} = 2K_{RT}$	
2nd Binding step		
RTR	$K_{RT}K_{RT} = K_{RT}^2$	$\Theta_2=(K_{RT}^2+2K_{RT}K_{RR})K_R^2K_t^2$
RRT+TRR	$K_{RT}K_{RR}+K_{RR}K_{RT} = 2K_{RT}K_{RR}$	
3rd Binding step		
RRR	$K_{RR}K_{RR}=2K_{RR}^2$	$\Theta_3=K_{RR}^2K_R^3K_t^3$

The saturation function for the sequential model is derived from the general form of the Adair equation (1.23):

$$\overline{Y} = \frac{1}{n} \cdot \frac{\dfrac{[A]}{\Theta_1} + \dfrac{2[A]^2}{\Theta_2} + \dfrac{3[A]^3}{\Theta_3} + \cdots \dfrac{n[A]^n}{\Theta_n}}{\Theta_0 + \dfrac{[A]}{\Theta_1} + \dfrac{[A]^2}{\Theta_2} + \dfrac{[A]^3}{\Theta_3} + \cdots \dfrac{[A]^n}{\Theta_n}} \; . \tag{1.58}$$

The terms Θ_0, Θ_1 etc. are composed from all constants relevant for the respective binding step. The constant K_R for binding of the ligand to the R state (binding to the T state with low affinity is neglected), the constant K_t for the equilibrium between the two macromolecule forms, and the substrate concentration [A] are inserted into the equation with the power of the respective binding step i. The interaction constants follow the actual occurrence of the respective interactions. Table 1.2 shows the definition of the Θ terms on a macromolecule with three linear-oriented subunits. By inserting the Θ links into Eq. (1.58) the following equation results:

$$\overline{Y} = \frac{1}{3} \cdot \frac{\dfrac{[A]}{(K_{RT}^2 + 2K_{RT})K_RK_t} + \dfrac{2[A]^2}{(K_{RT}^2 + 2K_{RT}K_{RR})K_R^2K_t^2} + \dfrac{3[A]^3}{2K_{RR}^2K_R^3K_t^3}}{1 + \dfrac{[A]}{(K_{RT}^2 + 2K_{RT})K_RK_t} + \dfrac{[A]^2}{(K_{RT}^2 + 2K_{RT}K_{RR})K_R^2K_t^2} + \dfrac{[A]^3}{2K_{RR}^2K_R^3K_t^3}} \; . \tag{1.59}$$

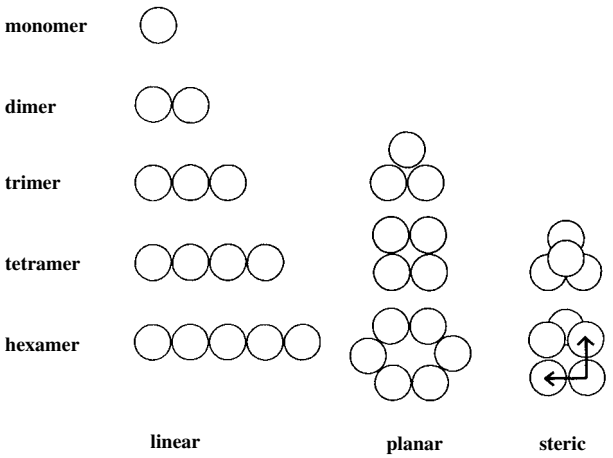

Figure 1.13. Possible arrangements of subunits of differently aggregated macromolecules. The different horizontal and vertical contacts of the subunits for the hexameter are indicated at bottom right.

This equation is valid only for the respective enzyme form for which it was derived. The improbable linear form of the trimer was chosen as it is the simplest oligomer structure to clearly demonstrate the different combinations of interaction constants. Even for a triangular trimer (Figure 1.13) an individual equation must be deduced. For a tetramer, three symmetric orientations are possible: linear, square and tetrahedral. The number of possible arrangements increase for higher oligomers. For the deduction of an equation according to this model both the number of subunits and the respective arrangement must be known. Furthermore, only uniform interactions among subunits are assumed here, requiring identical contact sites between the subunits. Especially in higher aggregates identical subunits can be connected by different contact sites, as demonstrated in Figure 1.13 for a hexamer consisting of two superposed trimers. The subunits within the trimers are connected by one type of contact site while a second type mediates the cohesion of the two trimers. For each type of contact sites individual interaction constants must be defined.

These complications make the model problematic for real systems, as the actual arrangement of the subunits can only be obtained by structure analysis. It may be assumed that certain orientations are preferred such as a tetrahedral form for four subunits. The interaction constants cannot easily be determined by experiments. The importance of the sequential and also of the symmetry model does not rest in the determination of constants but in recovering a better understanding of regulatory mechanisms for which both models provide a clear conceptional basis. More exact information on the existence of a specific model requires detailed structural and conformational studies which are presently available only for few macromolecules. An indication for the occurrence of one of the two models may be the relative position of the cooperative range (i.e., the maximum gradient in the Hill plot) within the saturation function. In the sequential model it coincides exactly with the area of half-saturation, in the concerted model it depends on the number n of protomers. With increasing n the cooperative range shifts to the lower saturation range. With more than 10 protomers, the shift is so pronounced that it is easily detectable.

In the sequential model heterotropic effects are defined in a similar way as in the concerted model. Activators support the effect of the cooperative ligand by inducing the transition from the inactive to the active state, while allosteric inhibitors stabilize the T state rendering the transition more difficult.

As already mentioned, interactions may also be destabilizing if K_{TR} and K_{RR} become larger than K_{TT}. The deviation from the normal hyperbolic saturation function is reversed, instead of a sigmoidal curve, a curve develops similar to that described in Section 1.4 for the case of non-identical independent binding centres. Consistently, the deviations in the linearised plots also correspond to this mechanism (see Figure 1.6). In the Hill plot the gradient falls below 1. This anti-cooperative behaviour, which is in contrast to normal cooperativity (also termed *positive cooperativity*), is defined as *negative cooperativity*. It is often found in enzymes. The binding of NAD to glyceraldehyde-3-phosphate dehydrogenase shows such behaviour and served as the first evidence of the sequential model (Convay and Koshland, 1968).

Many examples of negative cooperativity obey the mechanism of *half-of-the-sites reactivity* in a strict sense. A ligand bound to one site interferes with the occupation of the second, identical site with steric or electrostatic effects or by covalent reactions (phosphorylation). Thus only half of the original binding sites are saturated, the other half remains unsaturated or reaches saturation only at very high ligand concentrations. It is not a genuine negative cooperativity mediated by interaction of subunits, although the binding behaviour and consequently the plot curves are rather indistinguishable. Half-of-the-sites reactivity was observed in alcohol dehydrogenase, malate dehydrogenase and alkaline phosphatase (Levitzki and Koshland, 1976).

Establishing a certain mechanism, e.g., negative cooperativity, for a distinct system is hampered by the fact that various mechanisms, e.g., negative cooperativity, half-of-the-sites reactivity, non-identical and asymmetrical binding centres, different enzyme forms or isoenzymes all show similar saturation patterns. Structural studies are quite helpful, as negative cooperativity and half-of-the-sites reactivity both require identical subunits. In contrast, non-identical binding sites are mostly located on non-identical subunits. Many enzymes, such as glyceraldehyde-3-phosphate dehydrogenase, CTP-synthetase, deoxythymidine kinase, and also receptors and even binding of tRNA to ribosomes show a negative cooperative mechanism. The physiological advantage of negative cooperativity may lie in the greater insensitivity against changes in the metabolite concentration (substrates, effectors). Because of the high affinity of the first binding step these systems are already considerably active at low substrate levels and are able to maintain a basic metabolic turnover. An increase to high substrate levels causes only a small further rise in activity, but the system is able to follow substrate variations over a wide range in a damped mode without reaching early saturation.

1.5.7 Physiological Aspects of Cooperativity

A large number of biological regulatory processes rely on cooperativity. Besides haemoglobin, it occurs in many key enzymes of metabolic pathways and also in membrane-bound enzymes, where it is influenced by membrane fluidity. Cooperativity also appears in transport systems and ATPases, in receptor-ligand binding (e.g., the

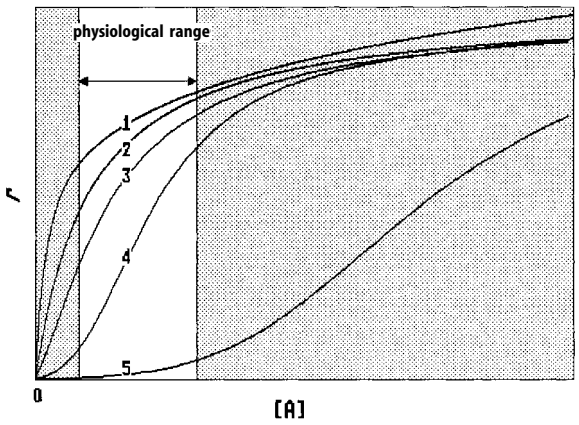

Figure 1.14. Regulatory significance of allosteric enzymes. The physiological ligand area is highlighted. (1) Negative cooperativity, (2) normal binding, (3) positive cooperativity with activator, (4) without effector, and (5) with inhibitor.

estrogen receptor), in acetylcholine esterase involved in synaptic transmission, and in thrombin activity. The advantage of cooperative saturation behaviour lies in the overproportional reaction of the system upon ligand fluctuations and in the allosteric regulation frequently connected with this process. Allosteric influences on active centres through conformational changes induced by spatially separated regulatory centres may also operate on normal binding systems. The advantage of cooperativity, however, lies in the steep rise of the sigmoidal saturation curves, especially in the middle saturation range, that usually correlates with the physiological range of ligand variation (Figure 1.14). A minimal concentration shift causes a much bigger change in activity. The system reacts much more sensitively to concentration changes than hyperbolic systems. Effectors do not only inhibit or activate, they render the system less sensitive against substrate variations. The activator elevates the system to full activity, the inhibitor brings it down to a minimal level.

Recently many allosteric enzymes were described, but still remains the question of the relevance of the models presented. The following examples of thoroughly investigated allosteric enzymes will demonstrate that essential predictions concerning these models have proved correct, e.g., identical subunits, distinct conformations of different affinity, and allosteric regulatory centres for effectors. Sometimes features of both models are found in the same system, as in haemoglobin, where oxygen binding induces a conformational change while the conformation transition of the subunits proceeds in a concerted manner.

As shown in Figure 1.15, both models occupy extreme positions among all conceivable combinations of conformation transitions. The concerted model permits only the uniform conformations bordered in the outer bands, the sequential model permits only the diagonal states of direct linkage of ligand binding and conformation transition. States not considered by the two models can also play a role and can be included in other models. It is, however, obvious that high cooperativity is only to be achieved in extreme positions, so that all other possible variants, based solely on the combination of ligand binding and conformation transition, are already reasonably covered by the models described. Additional models should have to be more comprehensive and include additional aspects.

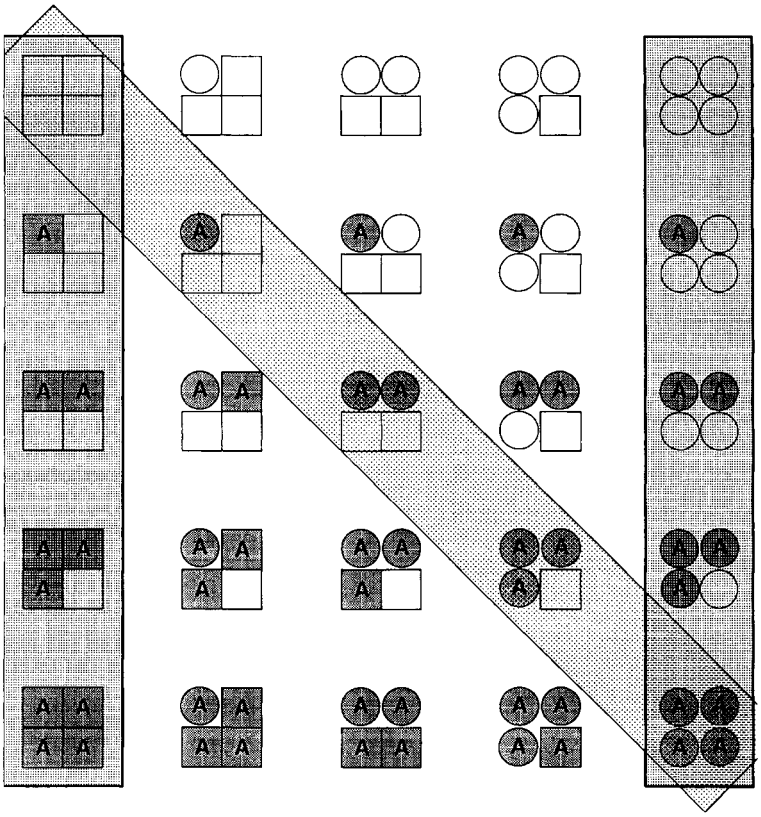

Figure 1.15. Possible conformation and binding states of a tetrameric macromolecule. Inactive T forms are square, active R forms are displayed as circles. The two vertical bars enclose the states permitted in the concerted model, the diagonal bar the possible states in the sequential model.

An important criterion for their validity is the assembly from identical subunits postulated by both models. Cooperative effects in monomer macromolecules cannot be explained by these models. This is established by the observation that monomeric myoglobin, although largely homologous to haemoglobin, shows hyperbolic oxygen binding. Cooperative behaviour of monomers, however, can be described by the models when the transition from the T to the R state is accompanied by aggregation to an oligomer. Ribonuclease was the first example of an exclusively monomeric enzyme with sigmoidal saturation behaviour, whose cooperativity could not have been caused by the interaction of subunits. This mechanism is termed *kinetic cooperativity* as it requires the combination of a fast catalytic turnover with a slow conformation transition between an inactive and an active enzyme form (*slow transition model*, Section 2.8.2). This model is based on a time-dependent process while the models presented so far rely on time-independent equilibria. Kinetic cooperativity is relatively easy to detect, as sigmoidal saturation behaviour can only be found in the substrate turnover and not in binding.

1.5.8 Analysis of Cooperativity

Cooperative effects are first recognised in the atypical saturation behaviour of the ligand. Since the main mechanisms are based on equilibrium assumptions they should preferably be analysed by binding measurements, although enzyme activity, which is easier to determine, usually also shows sigmoidal dependencies, as influences on the substrate affinity are transmitted to the enzyme reaction via the K_m value (K systems). Alternatively, the two enzyme conformations can differ in their catalytic activity instead of their affinity (V systems). Also the action of the effectors is frequently targeted directly on the turnover rate. For the analysis of sigmoidal curves, linearised plots are preferable to direct (non-linear) plots, as deviations from the linear progression are easily detectable. To establish a cooperative mechanism a larger number of measurements are required than for hyperbolic systems and a broader concentration range of the ligand has to be covered.

Deviations from normal behaviour may have other, also artificial reasons. Sigmoidal saturation curves are found in multiple-substrate reactions, with high enzyme concentrations ($[A]_0=[A]$ being no longer valid here, as usually assumed in enzyme kinetics), with instability of the enzyme in diluted solution, or in case of false determination of the initial velocity (see Section 2.3.2).

The strength of cooperativity may be estimated from the relationship between the Hill coefficient and the number of binding sites, with positive cooperativity n_h ranging between 1 and n, and with negative cooperativity tending below 1. The asymptotes of the saturation curve in the low- and high-ligand area in the Hill plot may be regarded as representative of the two enzyme states, and the respective dissociation constants can be yielded from their ordinate values at $\log [A]=0$. The distance of both asymptotes, multiplied by $RT\sqrt{2}$ yields the difference between the free energies for the binding interaction of the first and the last ligand (see Figure 1.9).

Another measure of cooperativity is the R_S value. It is defined as the ratio of ligand concentration at 90% and 10% saturation and always has the value of 81 for a normal hyperbolic saturation curve. With positive cooperativity, the curve becomes steeper, the R_S value decreases with the strength of cooperativity and increases with negative cooperativity (Table 1.3). The Hill coefficient and the R_S value are not directly related. The Hill coefficient records cooperativity at a certain point, i.e., at maximum deviation, while the R_S value covers a wider ligand range, but the relation to the number of protomers is lost. The determination of the R_S value is shown in Figure 1.16 in a semi-logarithmic plot. This diagram is particularly suited for plotting broad ligand ranges in cooperative systems. However, in this plot also normal binding curves assume a sigmoidal shape, so that a distinction can only be made by the steepness of the curve. The curve shows a turning point at half-saturation, its abscissa value at normal behaviour is equal to the K_d value. Such a K_d value defined at half-saturation has no theoretical value for cooperative systems. As the ligand concentration at half-saturation is, nevertheless, a specific and constant value for a given system, a $S_{0.5}$ value is defined as a characteristic factor for the macromolecule, although it has not the significance of a genuine binding constant.

As demonstrated in Figure 1.11, allosteric enzymes show characteristic deviations in linear plots. These curves, however, can be linearised by entering $[A]^n$ instead of

Table 1.3. Comparison of the Hill coefficient n_h and the R_s value (Taketa and Pogell, 1965)

n_h	R_s
0.5	6570
1.0	81
2.0	9
4.0	3

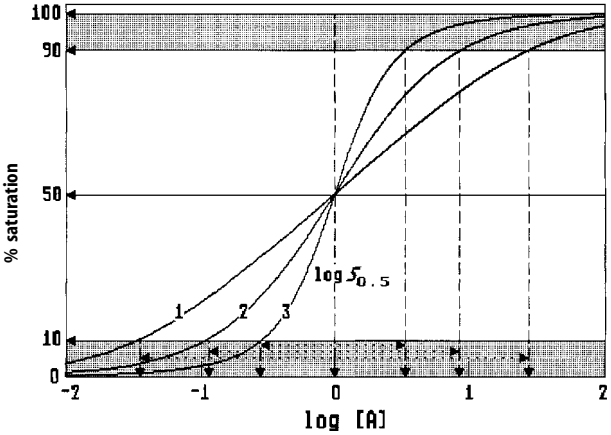

Figure 1.16. Half-logarithmic plot of saturation curves for the definition of the R_s-value from the ratio of ligand concentration at 90% and 10% saturation for (1) negative cooperative, (2) normal and (3) positive cooperative behaviour. The $S_{0.5}$ value, the ligand concentration at half-saturation, is assumed to be 1.

[A]. Following the Hill equation, n defines the reaction order for [A] and, therefore, equals the Hill coefficient n_h and not the number of binding sites.

1.5.9 Examples of Allosteric Enzymes

1.5.9.1 Haemoglobin

Although not an enzyme, haemoglobin has given important impulses for numerous theoretical studies, such as the cooperative models. It inspired the advancement of such significant methods as the X-ray structural analysis and of fast kinetic techniques. Comparison of the sigmoidal oxygen binding characteristics of tetrameric haemoglobin with the hyperbolic saturation behaviour of the closely related monomeric myoglobin clearly demonstrates the significance of the interaction of subunits for cooperativity. There is an apparent contradiction to the postulates of the cooperative models because haemoglobin actually consists of two pairs of non-identical subunits, i.e., two protomers. Accordingly, the Hill coefficient should not be higher than 2, but a value of about 3 is found. The α- and β-subunits are, however, comparable in their affinity to ligand and thus may be regarded as identical. X-ray crystallo-

graphic studies by Max Perutz (1970, 1990) provide detailed insight into the allosteric and cooperative machinery of haemoglobin. In the absence of oxygen (*deoxyhaemoglobin*) haemoglobin is in a T state of low affinity that is stabilized against the R state of the oxygen-rich *oxyhaemoglobin* by eight additional salt bridges between the subunits.

The iron ion in deoxyhaemoglobin is present in a high-spin state and emerges 0.06 nm out of the plane of the porphyrine ring where it is held by a histidine residue on its fifth coordination site. The remaining four coordination sites are occupied by porphyrine nitrogen atoms. By binding of an oxygen molecule to the sixth coordination site, the iron shifts into the low-spin state and moves into the plane of the porphyrine ring, dragging along the histidine and inducing a conformational change into the R state by cleaving the eight salt bridges between the subunits. The R state is stabilised by the bound oxygen molecule.

The significance of the sigmoidal saturation behaviour for the regulation of the oxygen binding is demonstrated by its dependence on the concentration of protons (*Bohr effect*). The protons released from hydrogen carbonate in the blood capillaries bind to the terminal amino acids of haemoglobin and stabilize the T state. The sigmoidicity of the saturation function becomes more pronounced, the binding capacity decreases and oxygen is released into the tissue. In contrast, higher oxygen binding caused by the elevated oxygen pressure in the lungs releases protons from haemoglobin, the pH value is lowered and the sigmoidicity decreases, induced by the stabilized R state. The low pH value in turn induces the release of CO_2 from hydrogen carbonate in the lungs. Stabilisation of the T state by connecting the β-subunits and thus causing a decrease of the oxygen binding capacity produces 2,3-bisphosphoglycerate which is also involved in the regulation of oxygen binding.

1.5.9.2 Aspartate Transcarbamoylase

This enzyme from *Escherichia coli* evidently demonstrates the spatial separation of catalytic and regulatory centres on distinct polypeptide chains. The native enzyme molecule consists of six catalytic subunits (C, $M_r = 33\,000$), joined in two trimers and six regulatory subunits (R, $M_r = 17\,000$) that form three dimers, resulting in a $(C_3)_2(R_2)_3$ structure. Catalytic and regulatory centres are 6 nm apart from one another. The allosteric activator ATP and the inhibitor CTP bind both to the same region at the R subunit. CTP stabilises the T state and enhances the sigmoidal character of the substrate saturation function. ATP preferably binds to the R form and weakens the cooperativity of the substrate aspartate. This also preferably binds to the R form. At the transition from the T into the R state the two catalytic trimers move apart by 1.1 nm and rotate by 12° in relation to each other, while the regulatory dimers rotate by 15° around the two-fold molecule axis. Because of this transition several amino acid residues important for the binding of aspartate move towards the active centre and increase the affinity for the substrate. Removal of the regulatory subunits results in the loss of cooperativity and regulation by ATP and CTP, while the catalytic activity is retained. With this enzyme it was also possible to demonstrate

the concerted transition from the T state to the R state according to the symmetry model. The occupation of half of all binding sites by the transition state analogue PALA (N-phosphoacetyl-L-aspartate) is sufficient to transfer the entire enzyme molecule into the R state.

Aspartate transcarbamoylase is a good example for feedback inhibition. The enzyme catalyses the initial reaction of the pyrimidine nucleotide biosynthesis pathway and is inhibited by CTP, the end product of the pathway. The activator ATP is the end product of the purine biosynthesis pathway. As for nucleic acid biosynthesis both nucleotides are required in an equal ratio, a surplus of purine nucleotides stimulates pyrimidine synthesis, which in turn is inhibited by a surplus of pyrimidine nucleotides (Kantrowitz and Lipscomp, 1990).

1.5.9.3 Aspartokinase

Aspartokinase I : homoserine dehydrogenase I from *Escherichia coli* catalyses the first and the third step of the threonine biosynthesis pathway. Methionine biosynthesis controlled by an aspartokinase II : homoserine dehydrogenase II and lysine biosynthesis regulated by an aspartokinase III both branch off from this pathway. Aspartokinase I : homoserine dehydrogenase I consists of four identical subunits ($M_r = 86\,000$). Each subunit has catalytic centres for both enzyme activities on two separate domains (*multifunctional enzyme*). The separate domains with their respective enzyme activities could be obtained by partial proteolysis or mutations. The aspartokinase domains retain their tetramer structure while homoserine dehydrogenase dissociates into dimers. In the native enzyme both activities are subject to feedback inhibition by threonine that shows a sigmoidal saturation pattern. This is more pronounced in aspartokinase activity ($n_h = 4$) than in homoserine dehydrogenase activity ($n_h = 3$). While the separate aspartokinase domain is still inhibited by threonine, the homoserine dehydrogenase domain becomes insensitive against this inhibition. Thus in the native enzyme both activities are regulated by one single regulatory binding site located on the aspartokinase domain. This was demonstrated by a one-step mutation where cooperativity for both activities was reduced by a comparable amount, i.e., to $n_h = 1.65$ for aspartokinase and $n_h = 1.45$ for homoserine dehydrogenase. From this it may be concluded that the native enzyme was formed by fusion of the genes of two originally separate enzymes, an allosteric aspartokinase inhibited by threonine and an originally unregulated homoserine dehydrogenase which by fusion was forced to adopt allosteric properties.

1.5.9.4 Other Examples

Phosphofructokinase is the most important regulatory enzyme of glycolysis. The corresponding reverse reaction step in gluconeogenesis is catalysed by another enzyme, *fructose-1,6-bisphosphatase*. This necessitates a close regulatory linkage in order to avoid depletion of ATP by a *futile cycle* of the two counteracting reactions, the forward reaction consuming one ATP which cannot be regained in the reverse reaction.

AMP is an activator of phosphofructokinase and an inhibitor of fructose-1,6-bisphosphatase. Phosphofructokinase, a tetrameric enzyme, is inhibited by phosphoenolpyruvate, which stabilises the T state. The substrate fructose-6-phosphate exhibits a cooperative effect. The transition from the T to the R state is effected by a counterrotation of 7° of each two dimers, respectively. The binding of the inhibitor AMP to the tetramer fructose-1,6-bisphosphatase causes a re-orientation of two dimers by 19°. In mammals both enzymes are additionally regulated by fructose-2,6-bisphosphate. Phosphofructokinase is allosterically activated and fructose-1,6-bisphosphatase is inhibited by negative cooperativity. Thus, both enzymes are subject to a reverse regulatory principle preventing a simultaneous parallel run of both reactions.

Biosynthesis and cleavage of glycogen is also regulated by two allosteric enzymes. Here allosteric control is overlaid by a regulation via covalent modification: a phosphorylation governed by a cyclic cascade mechanism. *Glygogen synthase* is activated by glucose-6-phosphate and is inhibited by AMP, while *glycogen phosphorylase* is activated by AMP and is inhibited by glucose-6-phosphate and ATP. The transition of glycogen phosphorylase from the T to the R state is accompanied by a relative rotation of 10° of the subunits against each other. The quaternary structure of the enzyme is modified towards a more favourable folding, the catalytic centre moving into the vicinity of the allosteric AMP binding centre and the phosphorylation site. This enzymatic active R state is stabilised by AMP at the one hand and by phosphate residues covalently bound at the phosphorylation site at the other.

1.6 Non-Identical, Interacting Binding Sites

The description of the binding of ligands to identical, to non-identical independent, and to identical interacting binding sites should consequently be completed by the treatment of ligand binding to non-identical, interacting binding sites. However, such cases could not be convincingly identified so far. Haemoglobin may be such an example due to its α- and β-subunits, but because of their similar binding constants they behave like identical subunits. Differing independent binding sites cause – as shown in Section 1.4 – a deviation from the normal binding pattern (see Figure 1.6) contrary to that observed with identical interacting binding sites as in the case of positive cooperativity (see Figure 1.9). This can easily be understood from the double reciprocal plot (see Figures 1.6B and 1.11B). The curve of positive cooperativity deviates to the upper right, the one for differing binding sites to the lower right. At comparable intensity, both effects compensate each other and a straight line will result as in a normal binding pattern. Even at a different intensity of both effects partial compensation results and only the predominant mechanism can manifest itself in a weakened form. The same applies for the simultaneous existence of positive and negative cooperativity, as the latter shows a similar curvature as binding to non-identical sites. The significance of such superpositions in the sense of counter-regulation or fine tuning may be discussed. Incomplete compensation of counteracting effects might be responsible for inhomogeneities sometimes observed in saturation curves.

In the absence of convincing examples it has to remain open how far contrary mechanisms in the same system in fact are realized.

Superposition congeneric effects such as negative cooperativity and binding to non-identical subunits will result in an amplification, but also there are no convincing examples.

1.7 References

Diffusion

Berg, H.C. (1983) *Random walks in biology.* Princetown University Press, Princetown, New Jersey.

Berg, O.G. (1985) *Orientation constraints in diffusion-limited macromolecular association*. Biophysical Journal 47, 1–14.

McCammon, J.A. & Northrup, S.H. (1981) *Gated binding of ligands to protein*. Nature 293, 316–317.

Noyes, R.M. (1961) *Effects of diffusion rates in chemical kinetics*. Progress in Reaction Kinetics 1, 129–160.

Binding Equilibria

Adair, G.S. (1925) *The hemoglobin system. The oxygen dissociation curve of hemoglobin*. The Journal of Biological Chemistry 63, 529–545.

Klotz, I.M. (1985*) Ligand-rezeptor interactions: facts and fantasies*. Quarterly Reviews of Biophysics 18, 227–259.

Langmuir, I. (1916) *The constitution and fundamental properties of solids and liquids*. Journal of the American Chemical Society 38, 2221–2295.

Graphic Methods

Huang, C.Y. (1982) *Determination of binding stoichiometry by the continuous variation method: The Job plot*. Methods in Enzymology 87, 509–525.

Job, P. (1928) *Recherches sur la Formation de Complexes Minéraux en Solution, et sur leur Stabilité*. Annales de Chimie (Paris) 9, 113–203.

Klotz, I.M. (1946) *The application of the law of mass action to binding by proteins. Interaction with calcium*. Archives of Biochemistry 9, 109–117.

Rosenthal, H.R. (1967) *A graphic method for determination and presentation of binding parameters in a complex system*. Analytical Biochemistry 20, 515–532.

Scatchard, G. (1949) *Attractions of proteins for small molecules and ions*. Annals of the New York Academy of Sciences 51, 660–672.

Stockell, A. (1959) *The binding of diphosphopyridine nucleotide by yeast glyceraldehyde-3-phosphate dehydrogenase*. The Journal of Biological Chemistry 234, 1286–1292.

Weder, H.G., Schildknecht, J., Lutz, L.A. & Kesselring, P. (1974) *Determination of binding parameters from Scatchard plots. Theoretical and practical considerations*. European Journal of Biochemistry 42, 475–481.

Allosteric Enzymes, Cooperativity

Convay, A. & Koshland, D.E. (1968) *Negative cooperativity in enzyme action*. Biochemistry 7, 4011–4023.

Hill, A.V. (1910) *The possible effects of the aggregation of molecules of hemoglobin on its dissociation curves*. The Journal of Physiology 40, 4–7.

Janin, J. (1973) *The study of allosteric proteins*. Progress in Biophysics and Molecular Biology 27, 77–120.

Kantrowitz, E.R. & Lipscomp, W.N. (1990) *Aspartate transcarbamoylase: The molecular basis for a concerted allosteric transition*. Trends in Biochemical Sciences 15, 53–59.

Koshland, D.E., Nemethy, G. & Filmer, D. (1966) *Comparison of experimental binding data and theoretical models in proteins containing subunits*. Biochemistry 5, 365–385.
Levitzki, A. & Koshland, D.E. (1976) *The role of negative cooperativity and half-of-the-sites reactivity in enzyme regulation*. Current Topics in Cellular Regulation 10, 1–40.
Lipscomp, W.N. (1991) *Structure and function of allosteric enzymes*. Chemtracts-Biochemistry and Molecular Biology 2, 1–15.
Monod, J., Wyman, J. & Changeux, J.-P. (1965) *On the nature of allosteric transition: A plausible model*. Journal of Molecular Biology 12, 88–118.
Neet, K.E. (1980) *Cooperativity in enzyme function: Equilibrium and kinetic aspects*. Methods in Enzymology 64, 139–192.
Pauling, L. (1935) *The oxygen equilibrium of hemoglobin and its structural interpretation.* Proceedings of the National Academy of Sciences, USA 21, 186–191.
Perutz, M. (1970) *Stereochemistry of cooperative effects in haemoglobin*. Nature 228, 726–739.
Perutz, M. (1990) *Mechanisms of cooperativity and allosteric regulation in proteins*. Cambridge University Press, Cambridge.
Perutz, M., Wilkinson, A.J, Paoli, G. & Dodson, G. (1998) Annual Reviews of Biophysics and Biomolecular Structure 27, 1–34.
Taketa, K. & Pogell, B.N. (1965) *Allosteric inhibition of rat liver fructose 1,6-diphosphatase by adenosine 5′-monophosphate*. The Journal of Biological Chemistry 240, 651–662.
Wyman, J. (1967) *Allosteric linkage*. Journal of the American Chemical Society 89, 2202–2218.
Wyman, J. & Gill, S.J. (1990) *Binding and linkage*. University Science Books, Mill Valley, California.

2 Enzyme Kinetics

Enzyme kinetics, in contrast to time-independent *multiple equilibria*, deals with time-dependent enzyme reactions which serve to elucidate mechanisms of enzyme catalysis and regulation. Both fields are supplementary: the study of equilibria covers partial areas of enzyme kinetics, e.g., substrate binding or cooperative phenomena, which have been treated in the preceding chapter and will not be repeated here. While the laws of multiple equilibria are applicable to all binding processes, with a few exceptions (e.g., transport systems) enzyme kinetics deals with enzymes only. The most important and thus most extensively studied ligand is the substrate which is converted into product by the enzyme. This conversion can be influenced by other ligands, such as cofactors, inhibitors or activators. A prerequisite for the treatment of enzyme kinetic laws is the chemical reaction order which will explained first.

2.1 Reaction Order

The order of a chemical reaction with respect to the individual components is defined as the power of the component concentration included into the rate equation. The overall reaction order is the sum of all component orders. A reaction

$$2\mathrm{A} + \mathrm{B} \rightleftharpoons \mathrm{P}$$

is third order in the forward reaction, second order for reactant A and first order for both reactant B and the reverse reaction.

2.1.1 First Order Reactions

The simplest chemical reaction is the spontaneous conversion of an educt A into a product P as in radioactive decay:

$$\mathrm{A} \xrightarrow{k_1} \mathrm{P}\,.$$

The reaction rate v can either be determined from the time-dependent decrease of A or from the increase of P and is directly proportional to the quantity of A:

$$v = -\frac{\mathrm{d}[\mathrm{A}]}{\mathrm{d}t} = \frac{\mathrm{d}[\mathrm{P}]}{\mathrm{d}t} = k_1[A]\,; \tag{2.1}$$

Enzyme Kinetics: Principles and Methods. Hans Bisswanger

ISBN: 3-527-30343-X

k_1, the first order rate constant has the dimension s^{-1}. It is concentration-independent. Integration of Eq. (2.1) from 0 to time t yields:

$$-\int_{A_0}^{A_1} \frac{d[A]}{[A]} = \int_{t_0}^{t} k_1 dt \ .$$

$$\ln[A] = \ln[A]_0 - k_1 t \ , \tag{2.2}$$

$$[A] = [A_0]e^{-k_1 t} \ . \tag{2.3}$$

Decrease of substrate or increase of product proceed exponentially with time (Figure 2.1A). Such curves can be linearised according to Eq. (2.2) by semi-logarithmic entry of substrate or product concentrations. The rate constant can be derived from the gradient (Figure 2.1B) or the half life $t_{1/2}$ at which half of the substrate is converted. [A] becomes $[A]_0/2$ and $\ln([A]_0/[A]) = \ln 2$:

$$k_1 = \frac{\ln 2}{t_{1/2}} = \frac{0.69}{t_{1/2}} \ . \tag{2.4}$$

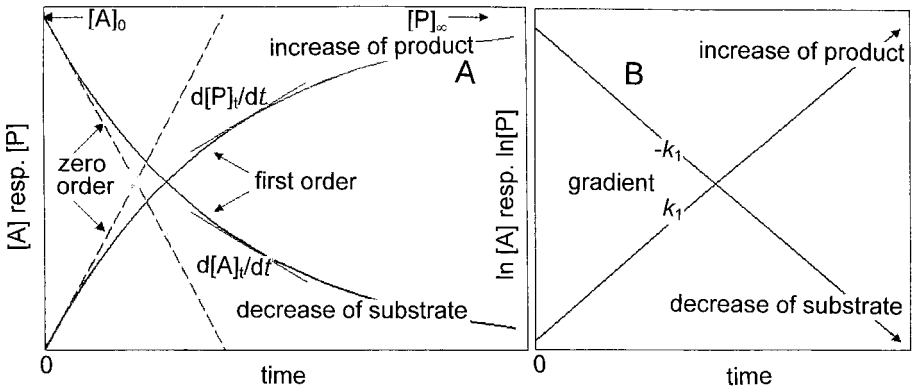

Figure 2.1. Progress curves of zero and first order for the formation of product and consumption of substrate in direct (A) and semi-logarithmic (B) presentation. The evaluation of turnover rates by tangents at the curves is shown in (A).

2.1.2 Second Order Reactions

$$A + B \xrightarrow{k_1} P .$$

The turnover rate in this reaction is proportional to the decrease of both A and B and to the increase of P:

$$v = -\frac{d[A]}{dt} = -\frac{d[B]}{dt} = \frac{d[P]}{dt} = k_1[A][B] . \tag{2.5}$$

The second order rate constant k_1 ($s^{-1} M^{-1}$) also includes a concentration term. Integration of Eq. (2.5) gives:

$$k_1 t = \frac{1}{[A]_0 - [B]_0} \ln \frac{[B]_0[A]}{[A]_0[B]} ; \tag{2.6}$$

t is now dependent on two variables, A and B. The equation can no longer be linearised in semi-logarithmic presentation. To solve Eq. (2.6) one of the variables must be regarded as constant. This can be done when one reactant predominates in a large surplus, so that its concentration will change only insignificantly during the reaction. Then the reaction is of *pseudo-first order*:

$$v = k_1[A][B]_0 = k_1'[A] . \tag{2.7}$$

The concentration $[B]_0$ regarded as constant is included into the pseudo-first order rate constant $k_1' = k_1 [B]_0$. Regarding this precondition as valid, the reaction can be treated as a first order reaction and linearised in a semi-logarithmic plot as in Figure 2.1B. The gradient, divided by the concentration of the constant reaction participant, gives the second order rate constant. By changing the initial concentration of the constant reaction partner pseudo- and true first order can be differentiated in this plot. For pseudo-first order the gradient must change accordingly, whereas it is concentration-independent in a first order reaction. In this way it can, e.g., be distinguished whether a change of conformation of an enzyme occurs spontaneously or is induced by ligand binding.

If pseudo-first order conditions, i.e., very high concentrations of one reactant, cannot be established, Eq. (2.5) may be simplified when both reactants are present in the same concentrations, $[A]_0 = [B]_0$:

$$v = -\frac{d[A]}{dt} = k_1[A]^2 . \tag{2.8}$$

Integration to t

$$-\int_{A_0}^{A_1} \frac{d[A]}{[A]^2} = \int_{t_0}^{t} k_1 dt$$

gives

$$\frac{1}{[A]} = \frac{1}{[A]_0} + k_1 t \ , \tag{2.9}$$

In a diagram 1/[A] versus t a linear function with the gradient k_1 will be obtained. The second order rate constant k_1 can also be determined using the half life:

$$k_1 = \frac{1}{t_{1/2}[A]_0} \ . \tag{2.10}$$

2.1.3 Zero Order Reactions

Zero order reactions are independent of reactant concentrations:

$$v = -\frac{d[A]}{dt} = \frac{d[P]}{dt} = k \ . \tag{2.11}$$

Integration with respect to time gives a linear relation:

$$[A] = [A]_0 - kt \ . \tag{2.12}$$

Reactions obeying this order can easily be recognised from the linear time dependence of substrate decay or product formation (Figure 2.1 A). Reactions are of zero order if driven by a catalyst present in very low concentrations compared with the reactants, so that the turnover rate is only dependent on the invariant catalyst concentration. In this case it is irrespective how many reactants are involved and which order the reaction would follow in the absence of the catalyst.

2.2 Steady-State Kinetics and the Michaelis-Menten Equation

2.2.1 Derivation of the Michaelis-Menten Equation

The simplest case of an enzyme-catalysed reaction is the conversion of a single substrate into a product, as for isomerisations and cleavage reactions (peptidases, proteases, nucleases, etc.). For simplicity an irreversible reaction is assumed and so it is irrespective whether only a single product or two or more cleavage products are formed:

$$\mathrm{A} + \mathrm{E} \underset{k_{-1}}{\overset{k_1}{\rightleftharpoons}} \mathrm{EA} \xrightarrow{k_2} \mathrm{E} + \mathrm{P}\,.$$

The time-dependent variation of the individual reactants is expressed in the following differential equations:

$$\frac{\mathrm{d[A]}}{\mathrm{d}t} = -k_1[\mathrm{A}][\mathrm{E}] + k_{-1}[\mathrm{EA}] \tag{2.13}$$

$$\frac{\mathrm{d[E]}}{\mathrm{d}t} = -k_1[\mathrm{A}][\mathrm{E}] + (k_{-1} + k_2)[\mathrm{EA}]\,, \tag{2.14}$$

$$\frac{\mathrm{d[EA]}}{\mathrm{d}t} = k_1[A][E] - (k_{-1} + k_2)[\mathrm{EA}]\,, \tag{2.15}$$

$$\frac{\mathrm{d[P]}}{\mathrm{d}t} = k_2[\mathrm{EA}] = v\,. \tag{2.16}$$

The *turnover rate* v is defined as the increase in product, which is directly proportional to the concentration of the enzyme-substrate complex EA, according to Eq (2.16). [EA] itself depends on the amount of reactants. To solve the differential equations (2.13–2.16) the time-dependent concentration changes must be known which is hardly to realize, especially for [E] and [EA]. For Figure 2.2 the changes in all reactants have been calculated under the specification of the respective constants. Three phases can be differentiated: 1. Within a short initial phase the [EA] complex is formed while, in turn, the free enzyme decreases. The turnover rate is low in this phase. 2. In a medium phase the turnover rate reaches its maximum. The concentration of the [EA] complex remains nearly constant. 3. The last phase is determined by the decay of the [EA] complex due to depletion of the substrate surplus and a decrease of the turnover rate, finally to zero.

Variation of the rate constants alters the relative duration of the three phases. If all three constants are of comparable size, the medium phase becomes relatively short and the concentration of [EA] will not be constant at any point. If the preceding equilibrium is fast compared with the enzyme catalysis (a plausible hypothesis), i.e., $k_1 \approx k_{-1} > k_2$, the medium phase becomes considerably longer. The concentration of

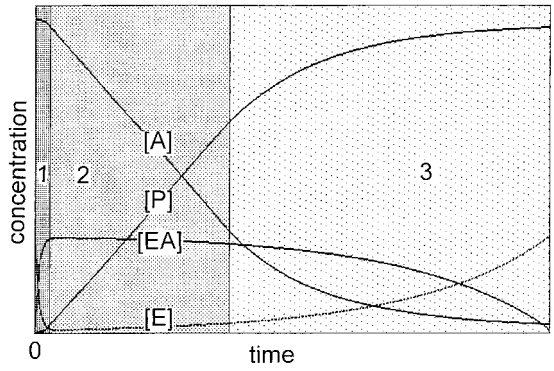

Figure 2.2. Time-related changes of the reactants of an enzyme-catalised reaction. (1) Pre-steady-state phase, (2) steady-state phase, (3) substrate depletion.

the [EA] complex remains nearly constant for a considerable time. In this phase formation and decay of the [EA] complex keep just in balance. There is a quasi-equilibrium state which is maintained, however, only for a limited period of time. In contrast to a true *equilibrium* this state is designated as *steady-state.* As a consequence of the constant state of the [EA] complex, substrate decomposition and product formation occur in a linear, zero order reaction. Since in the steady-state range the time-dependent concentration changes of [EA] and [E] can be assumed to be zero, $d[EA]/dt = d[E]/dt = 0$, Eqs. (2.14) and (2.15) simplify to

$$k_1[A][E] = (k_{-1} + k_2)[EA] ,$$

and by substituting [E] according to the principle of mass conservation $[E]_0 = [E] + [EA]$, the term

$$[EA] = \frac{k_1[A][E]_0}{k_1[A] + k_{-1} + k_2}$$

evolves, which is entered into Eq. (2.16) in order to obtain a relationship between turnover rate and substrate amount:

$$v = \frac{d[P]}{dt} = k_2[EA] = \frac{k_2[E]_0[A]}{\frac{k_{-1} + k_2}{k_1} + [A]} . \tag{2.17}$$

The expression of the three rate constants $(k_{-1} + k_2)/k_1$ is combined in a common constant K_m; $k_2[E]_0 = V$ is the maximum velocity as the total amount of enzyme participates in the reaction. Equation (2.17) becomes:

$$v = \frac{V[A]}{K_m + [A]} . \tag{2.18}$$

This equation presented in 1925 by Briggs and Haldane is of fundamental importance for enzyme kinetics. Although derived only for the simple case of an irreversible one-substrate reaction, it remains also valid, under certain conditions and modifications, for more complex mechanisms. Similar formulae for the description of the invertase reaction were already presented in 1902 by Adrian J. Brown in Birmingham and by Victor Henri in Paris. In 1913 in Berlin Leonor Michaelis together with the Canadian Maud Menten studied the validity of the Henri equation with the enzyme invertase. Their main merit was their perception that for the documentation of enzyme reactions strictly standardised conditions for temperature, pH value and ionic strength have to be maintained. In contrast to the steady-state theory, all these early studies were based on the equilibrium assumption. The balance of equilibrium between free components and the enzyme-substrate complex (*Michaelis complex*) was assumed to happen so quickly, compared with catalytic turnover, that the concentration of the enzyme-substrate complex would be dependent only on k_1 and k_{-1}, but not on k_2. According to Eq. (2.16) v is a direct measure for [EA] or $[A]_{bound}$ in binding equilibria. Thus the velocity equation could be derived analogous to the binding equation (1.23, see Section 1.3.1) and would result in:

$$v = \frac{V[A]}{K_d + [A]} = \frac{V[A]}{\frac{k_{-1}}{k_1} + [A]} \quad , \tag{2.19}$$

K_m being substituted by the dissociation constant K_d. Equation (2.19) is further away from real conditions than Eq. (2.18), as in many cases the catalytic constant k_2 cannot be neglected over the adjustment of equilibrium, and [EA] is effectively determined by both the attainment of equilibrium and the catalytic rate. Correspondingly, the constant K_m, determined by kinetic measurements, frequently deviates from the dissociation constant K_d obtained from binding measurements. Thus the steady-state assumption is the more general and far reaching. Nevertheless, the term *Michaelis-Menten equation* has been kept for the formula developed by Briggs and Haldane, as well as the term *Michaelis constant* for K_m.

Due to the principal analogy between the Michaelis-Menten equation and the general binding equation (1.23), the rules of deriving constants discussed are also applicable here. The *saturation function* $[A]_{bound}$ (resp. $r=[A]_{bound}/[E]_0$) corresponds to the reaction rate v. Saturation is reached at $n[E]_0$ (resp. n) there, and here at V. K_d is substituted by the Michaelis constant K_m. A principal difference, however, exists in the experimental procedure. While for binding measurements the concentration of the free ligand [A] must be determined, in kinetic measurements the total amount of substrate added $[A]_0=[A]+[EA]$ is taken. This is not quite correct, but as for kinetic measurements only catalytic, i.e., minimum quantities of enzyme are required, $[E]_0 \ll [A]$ and thus the portion of [EA] can be neglected and $[A]_0 \sim [A]$.

The Michaelis-Menten equation is characterised by two constants: the Michaelis constant is related to the dissociation constant and gives an indication for the affinity of the substrate, low K_m values indicating high affinities. The *catalytic constant* k_{cat} is the measure of the turnover rate of the enzyme. In contrast to K_m, k_{cat} is not di-

rectly obtained from the equation, but only as $V = k_{cat}/[E]_0$, i.e., the molar amount of the enzyme applied must be known. The ratio $k_{cat}/K_m = k_{cat}\ k_1/(k_{-1} + k_2)$ is defined as *catalytic efficiency*. It has the dimension of a second order rate constant (see Eq. (1.17)). It can be taken as measure of substrate specificity, large values indicating high specificity.

As the Michaelis-Menten equation is of fundamental significance for enzyme kinetics, the analysis and presentation of data is important and numerous publications deal with this matter. Only the most frequently applied methods will be discussed here.

2.3 Analysis of Enzyme Kinetic Data

2.3.1 Graphical Representations of the Michaelis-Menten Equation

2.3.1.1 Non-Linear Representations

Both the Michaelis-Menten and the general binding euqation (1.23) have the shape of a right-angle hyperbola if v (resp. r) is directly plotted against [A]. As the relation of this equation to the hyperbola function is not quite obvious, it is explained below (see Figure 2.3). The general hyperbola equation is:

$$\frac{X^2}{A^2} - \frac{Y^2}{B^2} = 1 \ . \tag{2.20}$$

For a right-angle hyperbola: $A = B$ (Figure 2.3A)

$$X^2 - Y^2 = A^2 \ . \tag{2.21}$$

Rotation of the coordinates by 45°: $X = X' \cos \alpha - Y' \sin \alpha$; $Y = X' \sin \alpha + Y' \cos \alpha$ yields, considering $\sin 45^\circ = \cos 45^\circ = 0{,}7071$ (Figure 2.3 B):

$$(X' - Y')^2 - (X' + Y')^2 = 2A^2 \ ,$$

$$-2X'Y' = A^2 \ .$$

Shifting of the axes by the increments a and b: $X' = X'' + a$; $Y' = Y'' - b$ (Figure 2.3 C):

$$-2(X'' + a)(Y'' - b) = A^2$$

$$Y'' = \frac{-A^2/2 + ab + bX''}{X'' + a} \ .$$

If $ab = A^2/2$ is chosen, the equation simplifies into:

$$Y'' = \frac{bX''}{a + X''} \ , \tag{2.22}$$

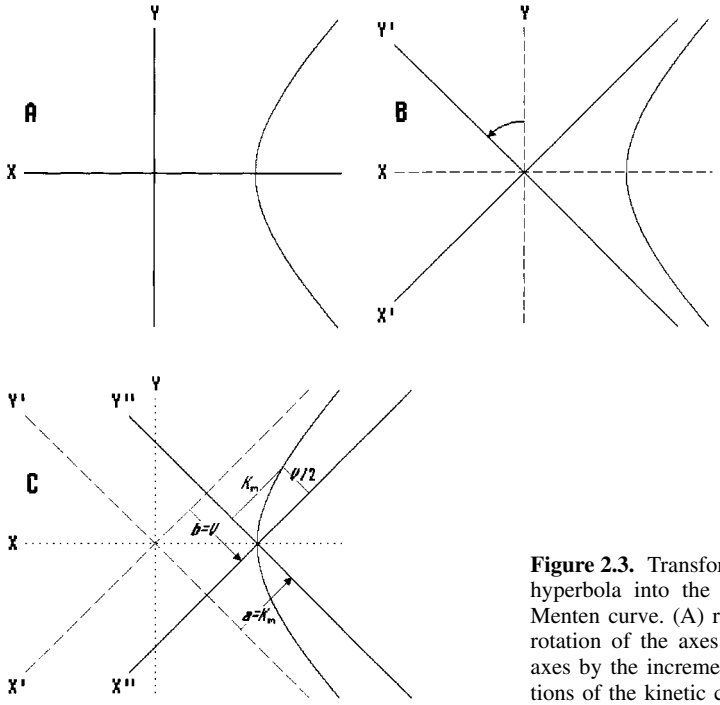

Figure 2.3. Transformation of a right-angle hyperbola into the shape of the Michaelis-Menten curve. (A) right-angle hyperbola, (B) rotation of the axes by 45°, (C) shift of the axes by the increments *a* and *b*. The correlations of the kinetic constants are indicated.

from which the analogy to the Michaelis-Menten equation becomes obvious, if: $Y'' \approx v$, $X'' \approx [A]$, $a \approx K_m$, $b \approx V$.

For very large or infinite substrate concentrations ($K_m \ll [A]$), K_m in Eq. (2.18) may be neglected. The equation reduces to $v = V$, an asymptote to the curve for $[A] \to \infty$ has the ordinate value of V. At the position of $V/2$, the substrate concentration is equal to the Michaelis constant, $[A] = K_m$ (Figure 2.4A). The kinetic constants may be obtained from the plot in this way. This approach is, however, not unproblematic. The condition $[A] \to \infty$ cannot at all be reached experimentally, as substrate in high concentrations, if soluble at all, frequently has a negative effect on enzyme activity (even if there is no specific substrate inhibition). If the substrate concentration is chosen several times higher than the K_m value it could be wrongly assumed that saturation had "practically" been reached. Table 2.1 demonstrates how underestimated saturation causes errors which will be transferred to the determination of K_m.

Another problem is the adaptation of the curve to the experimental data which are inevitably prone to error scattering. For a given set of data to adjust a hyperbolic curve there may exist several apparently equivalent modes (Figure 2.5). Such situation occurs especially if too few data exist or the measurements do not cover the complete saturation range. If only low concentrations were recorded, the determination of V (and thus of K_m) will become unreliable. If the data preferentially lie in the high-saturation range, the determination of K_m becomes inaccurate. To optimally cover the whole curve, an even distribution of substrate concentrations within an area

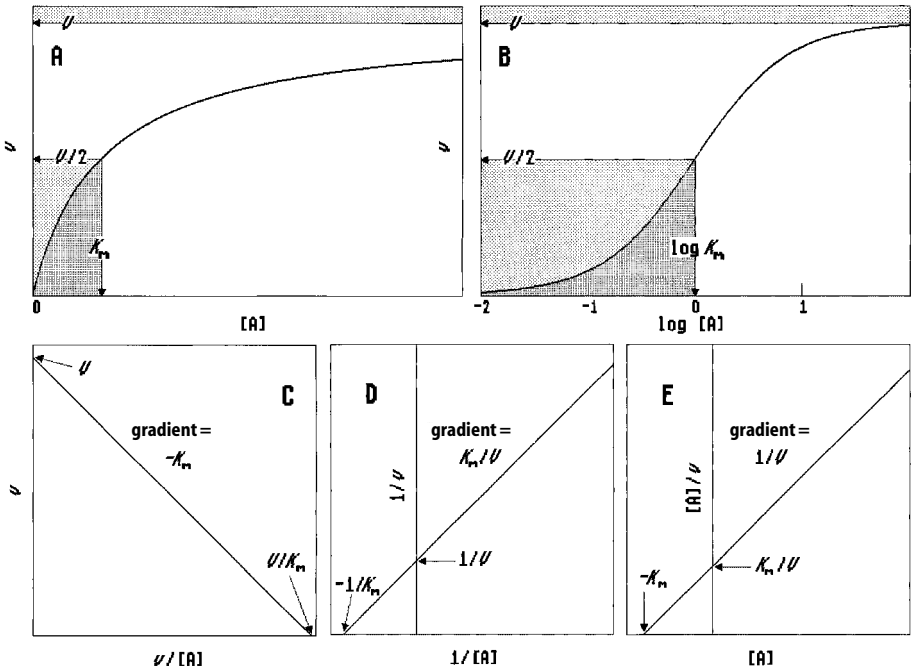

Figure 2.4. Non-linear and linear representations of the Michaelis-Menten equation. (A) direct diagram, (B) semi-logarithmic diagram, (C) Eadie-Hofstee diagram, (D) double reciprocal (Lineweaver-Burk) diagram, (E) Hanes plot. Modes for determination of K_m and V are indicated.

Table 2.1. Enzyme turnover rates expressed in % of the real maximum velocity V at an x-fold surplus of substrate compared with K_m (taken as 1). The right column shows the apparent K_m values determined at $V/2$, when taking the turnover rate determined at the respective substrate surplus for V instead of the real maximum velocity

Substrate surplus (x-fold K_m)	Turnover rate (% V)	K_m from turnover rate
2	66.7	0.50
5	83.3	0.71
10	90.9	0.83
20	95.2	0.91
30	96.8	0.94
40	97.6	0.95
50	98.0	0.96
100	99.0	0.98
∞	100	1

each a power of ten lower and higher than the K_m value is to be recommended. A curve should comprise at least ten concentration values (preferably secured by multiple measurements).

Non-linear representations have the disadvantage that deviations from the hyperbola, caused by alternative mechanisms, artificial influences or systematic errors, are

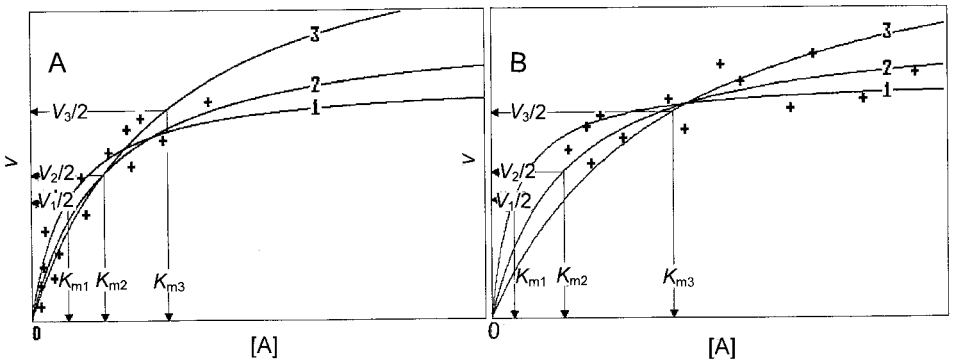

Figure 2.5. Uncertainties in the determination of the kinetic constants of the Michaelis-Menten relationship at inadequate coverage of the measurement range and high error dispersion. In (A) the area of saturation and in (B) the area of low concentration are not considered. Each three curves within the error fluctuation range have been entered.

difficult to recognise and to evaluate. Negative cooperativity or different binding centres yield curves very similar to a hyperbolic curve. Also other deviations, e.g., sigmoidal shapes, may easily be overlooked if weakly pronounced or in the case of broad error scattering.

Non-linear regression methods give some protection against the problems described above. A simple method for the adjustment of the Michaelis-Menten curve according to the least squares method was described by Cornish-Bowden (1984). Regression methods should, however, be critically evaluated, especially in view of the detection of deviations from the hyperbolic curve. The reliability of non-linear regression methods and thus of the constants derived from such treatments is frequently higher than that of linearisation methods. Direct plotting has the further advantage to present the data and also the error scattering without calculatory distortions which can be judged directly.

A variant of direct plotting is the *semi-logarithmic* plot. The logarithmic entry of substrate concentrations on the abscissa permits the inclusion of all values in a single plot even for a wide concentration range and to equally show both the low- and the high-saturation range (Figure 2.4 B). The hyperbolic curve gets an S- (sigmoidal) shape similar to the one already displayed by allosteric enzymes in direct plots. It makes the detection of such deviations more difficult.

A method proposed for the determination of the Michaelis constant by Dixon in 1965 considers a fact mostly neglected in enzyme kinetics: the indicated substrate concentration actually represents the total amount $[A]_0 = [A] + [EA]$ and not, as requested in the Michaelis-Menten equation, the free substrate concentration [A], from which it may deviate considerably at higher enzyme concentrations or stronger binding. This method is also applicable for the analysis of binding measurements by spectroscopic titration (Section 1.3.2.2). A disadvantage is that the saturation value (V) must be known and has to be determined by separate methods. At first a tangent is laid to the curve at the coordinate origin (Figure 2.6 A). A second straight line connects the coordinate origin and the point in the curve at $v = V/2$. The intercepts of

both straight lines with the saturation asymptote V correlate with the substrate concentrations $[A]_0'$ and $[A]_0''$ at the abscissa. The difference between both values is K_m (or K_d). Subtracting this difference from the asymptote leftward, the remaining distance from this point to the ordinate correlates with the total enzyme amount $[E]_0$. With the aid of a connecting line between this point on the asymptote and the coordinate origin, the distribution of components in the solution can be determined at each point of the saturation curve. Imagining a horizontal line through any point of the saturation curve, the distance on this line between the ordinate and the connecting line correlates with the amount of the [EA] complex at this particular saturation level. The distance from there to the saturation curve equals the free substrate [A], while the distance from the same point to the perpendicular on $[E]_0$ indicates the free enzyme [E] (Figure 2.6 A).

To avoid uncertainties in the formation of tangents, Kilroe-Smith (1966) modified this method (Figure 2.6B). Connecting lines are drawn between the ordinate origin and the points $V/2$ or $3V/4$ of the saturation curve. K_m results from the distance of the intercepts of a horizontal line for $V/2$ with these two connecting lines. By extending the connection lines to the asymptote V, this distance equals 2 K_m. Dixon (1972) modified this method further. Straight lines are drawn from the origin through the points $v=(n\text{-}1)V/n$ (for $n=0$, 1, 2, 3, etc.), i.e., $V/2$, $2V/3$, $3V/4$, $4V/5$, etc., intersecting the asymptote V at distances of each K_m (Figure 2.6C). The line for $n=1$ is the tangent of the original method to the origin of the saturation curve (Figure 2.6A). If the section for K_m is again subtracted towards the left, the connecting line for $n=0$ is obtained, the distance to the ordinate indicating, as mentioned above, $[E]_0$. This method is also applicable for the determination of inhibition constants (see Section 2.5.1.2).

For the calculation of this method the concentrations of free substrate or ligand [A] and enzyme [E] are substituted by total quantities minus the part bound as enzyme complex. For the dissociation constant K_d the term:

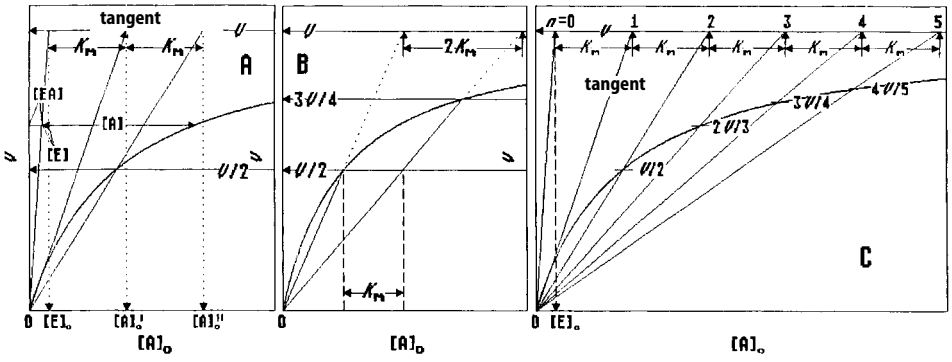

Figure 2.6. Determination of kinetic constants (A) after Dixon (1965), (B) after Kilroe-Smith (1966), and (C) after Dixon (1972).

$$K_d = \frac{[A][E]}{[EA]} = \frac{([A]_0 - [EA])([E)_0 - [EA])}{[EA]}$$
$$K_d = \left(\frac{[A]_0}{[EA]} - 1\right)([E]_0 - [EA]) \tag{2.23}$$

is obtained.

For the equation of the curve tangent in the coordinate origin it may be assumed that $[A]_0$ is small and [EA] may be neglected for $[E]_0$:

$$K_d = \frac{[A]_0}{[EA]}[E]_0 - [E]_0 \ .$$

The equation of the tangent for enzyme kinetic conditions under consideration of $v = k_{cat}[EA]$ and $V = k_{cat}[E]_0$ assuming a rapid equilibrium and setting $K_m \sim K_d$ is:

$$\frac{[A]_0}{v} = \frac{K_m}{V} + \frac{1}{k_{cat}} \ . \tag{2.24}$$

The tangent intersects the saturation asymptote at $v = V$, substrate concentration at this point is $[A]_0' = K_m + V/k_{cat}$. At half saturation $v = V/2$ is $[EA] = [E]_0/2$ or $[E]_0 - [EA] = [E]_0/2$. Following Eq. (2.23) the substrate concentration $[A]_0'$ at this point is:

$$K_m = [A]_0'' - \frac{V}{2k_{cat}} = [A]_0' - \frac{V}{k_{cat}} \tag{2.25}$$
$$\frac{V}{k_{cat}} = 2([A]_0' - [A]_0'')$$
$$K_m = [A]_0' - 2([A]_0' - [A]_0'') = 2[A]_0'' - [A]_0' \ .$$

According to Eq. (2.25) this gives:

$$K_m[A]_0' - [E]_0$$
$$[E]_0 = [A]_0' - K_m \ .$$

From this equation $k_{cat} = V/[E]_0$ or the absorption coefficient for the [EA] complex for spectroscopic titrations can be obtained.

For the conversion after Kilroe-Smith (1966) concentration $[EA]^{\#} = v/k = 3V/4k$ is inserted at $v = 3V/4$:

$$[E]_0 - [EA]^{\#} = \frac{V}{k} - \frac{3V}{4k} = \frac{V}{4k} \ .$$

Inserting this term in Eq. (2.23), considering substrate concentration $[A]_0^{\#}$ at $v = 3V/4$, gives:

$$K_m = \left([A]_0^{\#} \frac{4k}{3V} - 1 \right) \frac{V}{4k} = \frac{[A]_0^{\#}}{3} - \frac{V}{4k} .$$

Finally, by inserting Eq. (2.25) we obtain:

$$K_m = \frac{2[A]_0^{\#}}{3} - [A]_0'' .$$

2.3.1.2 Direct Linear Plots

The direct linear plot of Eisenthal and Cornish-Bowden (1974) represents a completely different plotting method. The Michaelis-Menten equation is modified into a linear equation with the (imaginary) variables V as ordinate and K_m as abscissa:

$$V = K_m \frac{v}{[A]} + v . \tag{2.26}$$

The corresponding straight line intersects the ordinate at v and the abscissa at –[A].

If, conversely, the values for [A] are plotted on the abscissa (with negative signs), the corresponding values for v on the ordinate and each pair of values is connected by a straight line, a bundle of straight lines is obtained with a common intercept to the right of the ordinate with the X and Y coordinates K_m and V, respectively (Figure 2.7 A). Because of error scattering actually no common intercept point will be obtained, rather there will be a cloud of various straight line intercepts. In this case the

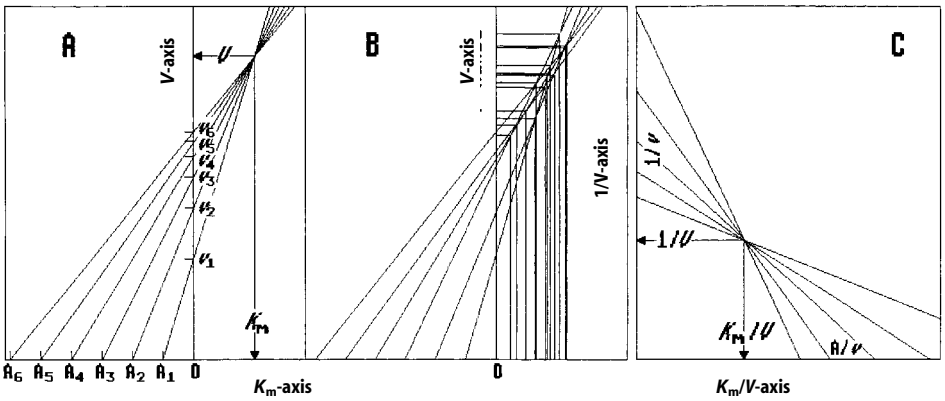

Figure 2.7. Direct linear plot. In (A) substrate concentrations are plotted on the negative branch of the abscissa and v values on the ordinate. In (C) $[A]/v$ is plotted on the abscissa and $1/v$ on the ordinate. In (B) the same diagram is shown as in (A), but with high errror scattering.

constants are obtained from the average value (*median*, see Section 2.11) of all X and Y coordinates of the individual intercepts (Figure 2.7 B).

There is the disadvantage that some of the intercepts can fall far outside the plot, so that it must be drawn in various dimensions. An improvement offers the reciprocal form of Eq. (2.26) (Cornish-Bowden and Eisenthal, 1978):

$$\frac{1}{V} = \frac{1}{v} - \frac{K_m}{V[A]} , \tag{2.27}$$

$1/v$ is plotted on the ordinate and $[A]/v$ on the abscissa (Figure 2.7 C). The joint section of the straight lines, which is now located inside the plot, has the X and Y coordinates K_m/V and $1/V$.

A third transformtion gives the equation:

$$\frac{1}{K_m} = \frac{V}{K_m v} - \frac{1}{[A]} . \tag{2.28}$$

By entering $-1[A]$ against $v/[A]$, a common intercept results with the coordinates $1/K_m$ and V/K_m. This has, however, the disadvantage of reciprocal entry with a scale distortion, same as in the previous plot.

Direct linear plots do not require regression methods, but deviations from normal behaviour are difficult to be detected. They result in a more or less characteristic distortion of the intercept cloud. This holds also for the analyses of enzyme inhibitions and multiple substrate reactions, which cause characteristic shifts of the common intercepts. The large number of single intercepts due to error scattering, however, makes an exact evaluation difficult (see Section 2.5.1.2).

2.3.1.3 Linearisation Methods

Most of the disadvantages mentioned for non-linear plots can be ruled out by linearisation methods. Constants can be calculated easily from axis intercepts or straight line gradients. Deviations of the data from the Michaelis-Menten law result in characteristic deviations from the linear run and give indications for alternative mechanisms (e.g., cooperativity) or artificial influences. A further important advantage of linearisation methods is the analysis of enzyme kinetic methods when two or more ligands are varied as in enzyme inhibitions or multiple substrate reactions. The respective mechanisms can be recognised from the resulting straight line pattern. Principally, however, even these analysis methods are not able to provide informations that are not included in the data. This may be demonstrated by the example of the enzyme catalase, where it was impossible to determine the K_m value of the substrate H_2O_2 with simple measuring methods, as high substrate concentrations damage the enzyme. Saturation could not be reached, and, consequently, also half saturation for K_m determination was not accessible. But the lower part of the saturation curve could be linearised in the double reciprocal plot (which will be discussed later), and in this diagram K_m can be obtained by extrapolation of the straight line to the abscissa, so that the missing saturation range should be not

required for this procedure. However, the data gather far in the upper right of the plot, so that the straight lines practically extrapolate to the coordinate origin and an exact ordinate or abscissa intercept cannot be given.

There exist three possible linear transformations of the Michaelis-Menten equation. All three were first proposed by Woolf and mentiond in the book *Enzyme Chemistry* of Haldane and Stern (1932) without finding particular resonance. Later, other authors described individual linearisation methods in extensive publications. Contrary to the generally accepted rule that the name of a method should be dedicated to the first author, these methods are mostly named after later authors. Although this is not quite just, it is practicable, as not all three diagrams must be called "Woolf plot" and can easily be distinguished. The situation becomes more complicate as the same plots have been described by several authors so that there are numerous combinations of names, some considering the authorship of Woolf (e.g., Scatchard, Eadie, Eadie-Scatchard, Eadie-Hofstee, Woolf-Hofstee plot). As the linear transformation of the Michaelis-Menten equation is hardly to be regarded as an important mathematical discovery, for better understanding the mostly applied names will be preferred here and Woolf's merit may be honoured by this remark.

The *double reciprocal* or *Lineweaver–Burk plot* is based, as expressed in its denomination, on the reciprocal form of the Michaelis-Menten equation:

$$\frac{1}{v} = \frac{1}{V} + \frac{K_\mathrm{m}}{V} \cdot \frac{1}{[\mathrm{A}]} \ . \tag{2.29}$$

Plotting of the reciprocal velocity $1/v$ against the reciprocal substrate concentration $1/[\mathrm{A}]$ results in a straight line intersecting the ordinate at $1/V$, the abscissa at $1/K_\mathrm{m}$ (Figure 2.4D). This linearisation method for the Michaelis-Menten equation is the most frequently used, but the least suitable one (see Markus et al., 1976). The essential disadvantage is the uneven distribution of data. Due to the reciprocal transformation equidisant substrate concentrations will be compressed towards the coordinates and stretched in the opposite direction. If substrate concentrations are chosen to yield equal distances in this plot, they do not cover the saturation curve satisfactorily. A more serious disadvantage is the fact that also the dependent variable v and thus the error limits suffer the same uneven distribution. Assuming an absolute, constant error throughout, the error limits in the double reciprocal plot are compressed towards the ordinate, but extended towards the upper right. A linear regression method cannot recognise this distortion and will evaluate the strong scattering in the right area of the plot in the same way as the compressed ones near the ordinate. Already faint error deviations at low substrate concentrations can greatly influence the adaptation of a regression line. Therefore, suitable weighting factors must be considered (Wilkinson, 1961). Surprisingly, just this unequal distribution in the plot is the reason for its frequent use. The compression of the error limits at high substrate concentrations gives the impression of minor error scattering and presents the data as more reliable. A true advantage of this plot compared with other linearisation methods is the individual display of the variables v and [A], separated by the coordinates. Alternative mechanisms to the Michaelis-Menten equation show characteristic deviations from straight lines and inhibition and multiple substrate mechanisms can easily be evaluated.

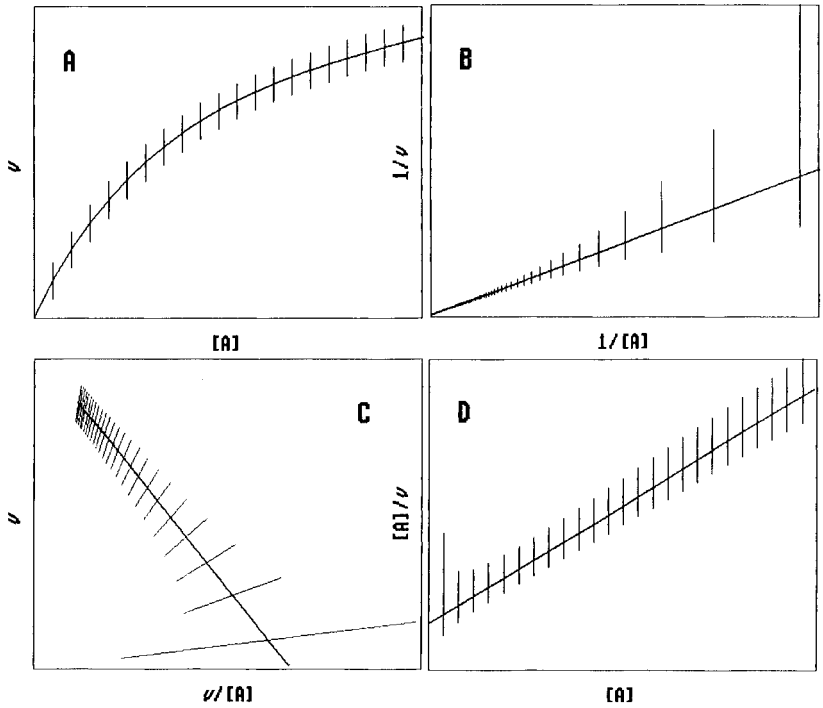

Figure 2.8. Error limits in different plots of the Michaelis-Menten equation assuming an absolute constant error. (A) Direct plot, (B) double reciprocal plot, (C) Eadie-Hofstee plot, (D) Hanes plot.

The equation for the *Hanes plot* derives from multiplication of the reciprocal Michaelis-Menten equation (2.29) by [A]:

$$\frac{[A]}{v} = \frac{[A]}{V} + \frac{K_m}{V}, \tag{2.30}$$

[A]/v is plotted against [A] (Figures 2.4E and 2.8D). The gradient of the straight line is 1/V, intersection with the abscissa is $-K_m$ and with the ordinate K_m/V. Error limits are only slightly distorted, so that a simple linear regression can be applied. Variables, however, are not separated, substrate concentration is entered in both axes.

Multiplication of Eq. (2.29) by vV and conversion gives the equation for the *Eadie-Hofstee plot*:

$$v = V - K_m \cdot \frac{v}{[A]}. \tag{2.31}$$

Plotting v against v/[A] gives V from the ordinate intercept and $-K_m$ from the gradient (Figures 2.4C and 2.8C). Compared with the Scatchard plot mostly used for binding measurements, only the axes have been exchanged (see Section 1.3.2.1). Apart from the disadvantage that variables are not separated there is a distortion of error limits, however, not quite as drastic as in the double reciprocal plot. The error

limits extend from the plot center towards the lower and higher substrate concentrations.

2.3.1.4 Graphic Evaluation of Progress Curves

Evaluation methods described so far are based on the assumption that turnover rates v are measured in separate assays at different substrate concentrations and data are transferred into plots. In fact, all substrate concentrations are run through already during a single enzyme reaction, starting from the initial value $[A]_0$ until the end or equilibrium of the reaction $[A]_\infty$. Registration of such a time run (e.g., in a photometric enzyme test) yields a *progress curve*. Its ordinate values (e.g., via absorption) show the actual substrate or product concentrations, the gradients, as the tangents at the respective points, the corresponding reaction rates $v = d[P]/dt$ (Figure 2.1). A single progress curve thus contains the full information of Michaelis-Menten kinetics and only $[A]_0$ must be chosen large enough to run through the complete saturation region. By this a single progress curve could provide all [A] and v values for a complete evaluation of the Michaelis-Menten equation. However, apart from the inaccuracy in applying a tangent on various points of a curve, this simple method has the disadvantage that interfering effects, e.g., inhibition of the enzyme by the emerging product and its back reaction to the substrate, cannot be easily recognised and could lead to erroneous results. Balcolm and Fitch (1945) modified this method with a computer programme to include also complicated mechanisms, such as product inhibition. For this the progress curve is divided into equal time segments (e.g., 12 s), at which the respective substrate concentration (e.g., via absorption) is determined. The corresponding rate is obtained from the gradient of a connection line of the two neighbouring points.

2.3.1.5 Integrated Michaelis-Menten Equation

Direct evaluation of progress curves can be improved by linearisation, similar to the analysis of hyperbolic saturation curves. A special progress curve, e.g., the print from a photometer, can be recalculated point by point and transferred to a corresponding plot following the method given hereafter, but the true advantage is the online recording of the progress curve in a computer and the immediate analysis after each measurement.

The Michaelis-Menten equation

$$v = -\frac{\mathrm{d[A]}}{\mathrm{d}t} = \frac{V[\mathrm{A}]}{K_\mathrm{m} + [\mathrm{A}]} \tag{2.18}$$

is modified

$$-\frac{K_\mathrm{m} + [\mathrm{A}]}{[\mathrm{A}]}\mathrm{d[A]} = -\frac{K_\mathrm{m}}{[\mathrm{A}]}\mathrm{d[A]} - \mathrm{d[A]} = V\mathrm{d}t$$

and integrated from $[A]_0$ to time $t=0$ until [A] to time t:

$$-K_m \int_{[A]_0}^{[A]} \frac{d[A]}{[A]} - \int_{[A]_0}^{[A]} d[A] = V \int_0^t dt \; .$$

Thus the *integrated Michaelis-Menten equation* reads:

$$K_m \ln \frac{[A]_0}{[A]} + [A]_0 - [A] = Vt \; . \tag{2.33}$$

In this form the Michaelis-Menten equation was first derived by Victor Henri in 1902. Further conversion gives a linear equation (Walker and Schmidt, 1944; Jenning and Niemann, 1953):

$$\frac{[A]_0 - [A]}{t} = V - K_m \frac{\ln \frac{[A]_0}{[A]}}{t} \; . \tag{2.34 a}$$

or in logarithms of ten:

$$\frac{[A]_0 - [A]}{t} = V - K_m \frac{2.3 \cdot \log \frac{[A]_0}{[A]}}{t} \tag{2.34 b}$$

If formation of product is measured instead of substrate consumption one may set: $[P]=[A]_0-[A]$, assuming an irreversible reaction. $[P]_\infty$ is the product concentration at the end of the reaction:

$$\frac{[P]}{t} = V - K_m \frac{\ln \frac{[P]_\infty}{[P]_\infty - [P]}}{t} \; , \tag{2.35 a}$$

$$\frac{[P]}{t} = V - K_m \frac{2.3 \cdot \log \frac{[P]_\infty}{[P]_\infty - [P]}}{t} \; . \tag{2.35 b}$$

$([A]_0-[A])t$ against $\ln([A]_0/[A])t$ or $[P]/t$ against $1n([P]_\infty/([P]_\infty-[P]))/t$ (plotted as ln or log) yields a straight line with a gradient of $-K_m$ and the ordinate intercept V (Figure 2.9 A). This is the most common representation of the integrated Michaelis-Menten equation. In addition there exist two further linearisation methods. $-1/K_m$ from the abscissa section and $1/V$ from the ordinate intercept are obtained from a plot based on the equation:

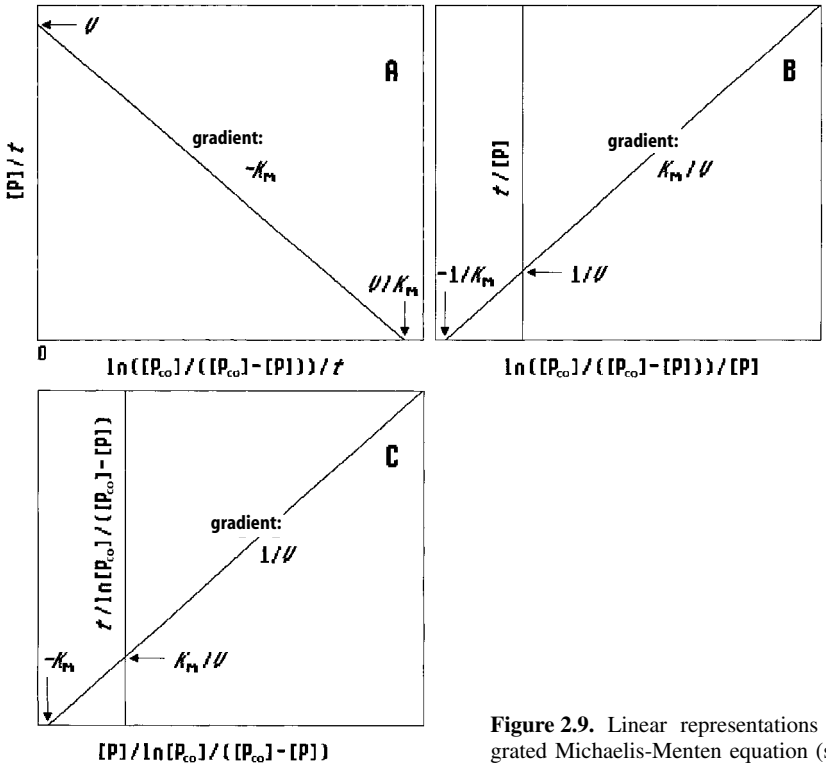

Figure 2.9. Linear representations of the integrated Michaelis-Menten equation (see text).

$$\frac{t}{[\mathrm{P}]} = \frac{2.3 \cdot \log \dfrac{[\mathrm{P}]_\infty}{[\mathrm{P}]_\infty - [\mathrm{P}]}}{[\mathrm{P}]} \cdot \frac{K_\mathrm{m}}{V} + \frac{1}{V} \tag{2.36}$$

(Figure 2.9 B). A third linearisation method is based on the formula:

$$\frac{t}{2.3 \cdot \log \dfrac{[\mathrm{P}]_\infty}{[\mathrm{P}]_\infty - [\mathrm{P}]}} = \frac{[\mathrm{P}]}{V \cdot 2.3 \cdot \log \dfrac{[\mathrm{P}]_\infty}{[\mathrm{P}]_\infty - [\mathrm{P}]}} + \frac{K_\mathrm{m}}{V} \tag{2.37}$$

$1/V$ as gradient, K_m/V as ordinate intercept and $-K_\mathrm{m}$ as abscissa intercept are obtained (Figure 2.9 C).

Similar to the evaluation methods for the simple Michaelis-Menten equation, the representations of its integrated form can also display more complex mechanisms, such as enzyme inhibition or multiple substrate reactions, detectable from the line patterns or from deviations from the straight line.

2.3.2 Determination of the Reaction Rate

2.3.2.1 Experimental Analysis

For the previously discussed evaluation methods the reaction rate must be known. Since enzyme kinetics is widely based on such methods, some principal aspects should be discussed. As shown in Figure 2.2, the time progression of enzyme-catalysed reactions can be divided into three phases, a pre-steady-state phase, the steady-state phase and finally the phase of substrate depletion. For the enzyme kinetic measurements based on the validity of the steady-state equation, only the middle linear phase is of importance, excepting the previously discussed direct analysis of progress curves.

Recording of the steady-state phase requires the continual registration of progress curves, e.g., by optical measurements. In many enzyme reactions, however, substrate or product alterations cannot be followed by a directly detectable signal during the reaction, rather the turnover has to be determined by stopping the enzyme reaction and subsequent analysis of the reaction products, e.g., by colour reaction, separation by HPLC, or radioactive labelling (*stopped test*). By stopping the tests at varying times, progress curves may be composed from different time values, but this is a laborious procedure, and the initial linear phase cannot be clearly defined with few time values. To simplify such tests, frequently only a single time value is taken (*single point measurement*). This method is completely inadequate for enzyme kinetic studies. Another principle to make hardly detectable enzyme reactions accessible, is that they are connected to continually detectable reactions, like NADH-dependent dehydrogenases, whereby the product of the one reaction serves as substrate for the other one (*coupled assay*). This is equally problematic. Under no conditions the indicator reaction should become time limiting. This cannot always be guaranteed considering the broad variations of parameter necessary for enzyme kinetic studies.

The linear steady-state region is decisive for enzyme kinetic studies, as the Michaelis-Menten equation was derived for $d[EA]/dt = 0$ and is valid only for this region. The better the condition $[E]_0 \ll [A]_0$ is fulfilled, the more pronounced the linear region becomes. On the other hand, the steady-state phase is short and difficult to detect when the substrate falls below the K_m value (Figure 2.10 A). As this phase should begin directly at the start of the reaction, usually a tangent is laid to the curve at $t = 0$ to determine an "initial rate" (*tangent method*). The advantage of this procedure is that influences of the product such as product inhibition and reverse reaction, may be disregarded. However, apart from the uncertainty whether the steady-state equation is valid for the non-linear initial region, there is the problem that the reaction has already progressed between reaction start at the mixing of reactants and the onset of the registration and there is no longer an initial reaction rate. The reaction rate is mostly underestimated, all the more if the initial substrate concentration is low. The analysis of such data may result in sigmoidal instead of hyperbolic curves (Figure 2.10 B).

In such cases, the amount of enzyme should be reduced. This improves steady-state conditions, time progression and thus the linear region is extended. In parallel

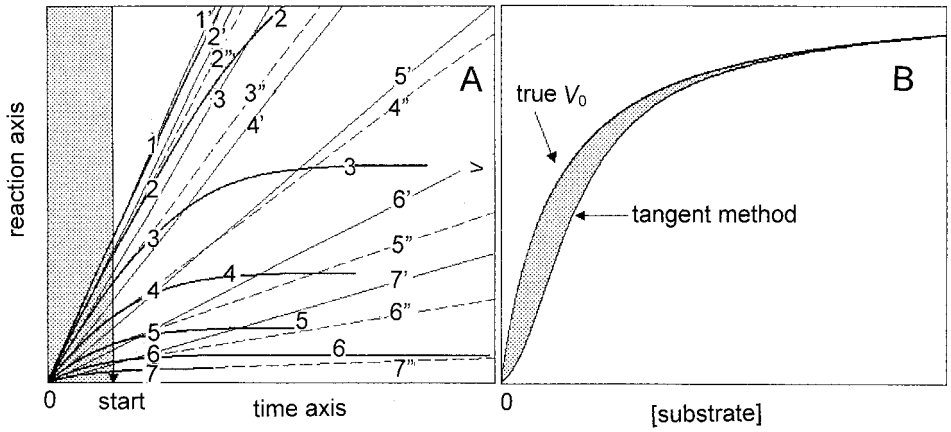

Figure 2.10. Determination of the initial velocities by the tangent method. (A) The curves show real progress curves (1, 2, 3…), and the straight lines the actual initial rates (1′, 2′, 3′…). The shaded area is the period between mixing (0) and start of the reaction. The dotted lines correlate to the tangents attached to the progress curves at the starting point (1″, 2″, 3″…). (B) Direct plotting of the true initial velocities and the values yielded from the tangent method against substrate concentration.

the sensitivity of the measuring method has to be increased as far as possible. If all methodical possibilities have been exhausted, there are graphic methods for the determination of the initial reaction rate. Before going into this, an apparent contradiction should be mentioned. The derivation of the Michaelis-Menten equation was performed exclusively under the steady-state condition $d[EA]/dt = 0$, independent from substrate concentration, as long as $[E]_0 \ll [A]_0$ is valid. This often leads to the misunderstanding that the enzyme should be saturated because of the large surplus of substrate and the linearity of progress curves could only be expected at substrate saturation. It is overlooked that surplus of substrate does not automatically mean enzyme saturation. This solely depends on the equilibrium constant. For example, setting a substrate concentration of a tenth of the K_m value, e.g., 10^{-6} M at $K_m = 10^{-5}$ M, and an enzyme concentration of $[E]_0 = 10^{-9}$ M, the quantity of the enzyme-substrate complex according to $K_d = [A][E]/[EA]$ is $[EA] = 10^{-10}$. In spite of a thousand-fold substrate surplus the enzyme is only saturated by 10%.

2.3.2.2 Graphic Methods

An improvement of the tangent method was described by Lee and Wilson (1971). Two random points on the progress curve (e.g., 0 and 30% reaction turnover) are connected by a straight line. Its gradient correlates with the reaction rate at the substrate concentration of the average value of both points (here 15%). A further improvement is the *secant method* by Waley (1981). Here also a connecting line is drawn between two points of a progress curve $[A]_1$, t_1, and $[A]_2$, t_2 (Figure 2.11A). Its gradient $([A]_1 - [A]_2)/(t_1 - t_2)$ correlates to the gradient of a tangent to the curve and thus to the rate for a third substrate concentration $[A]_3$ with the value

$$[A]_3 = \frac{[A]_1 - [A]_2}{\ln \dfrac{[A]_1}{[A]_2}} \tag{2.38 a}$$

or

$$[P]_3 = [A]_0 - \frac{[P]_2 - [P]_1}{\ln \dfrac{[A]_0 - [P]_1}{[A]_0 - [P]_2}} \ , \tag{2.38 b}$$

if the formation of product is recorded. The concentration of $[A]_3$ can be obtained from the absorption values A at corresponding times with photometric measurements, A_0 and A_∞ being the absorption values at the start and the end of the reaction:

$$[A]_3 = \frac{[A]_0}{A_0 - A_\infty} \cdot \frac{A_1 - A_2}{\ln \dfrac{A_1 - A_\infty}{A_2 - A_\infty}} \ . \tag{2.38c}$$

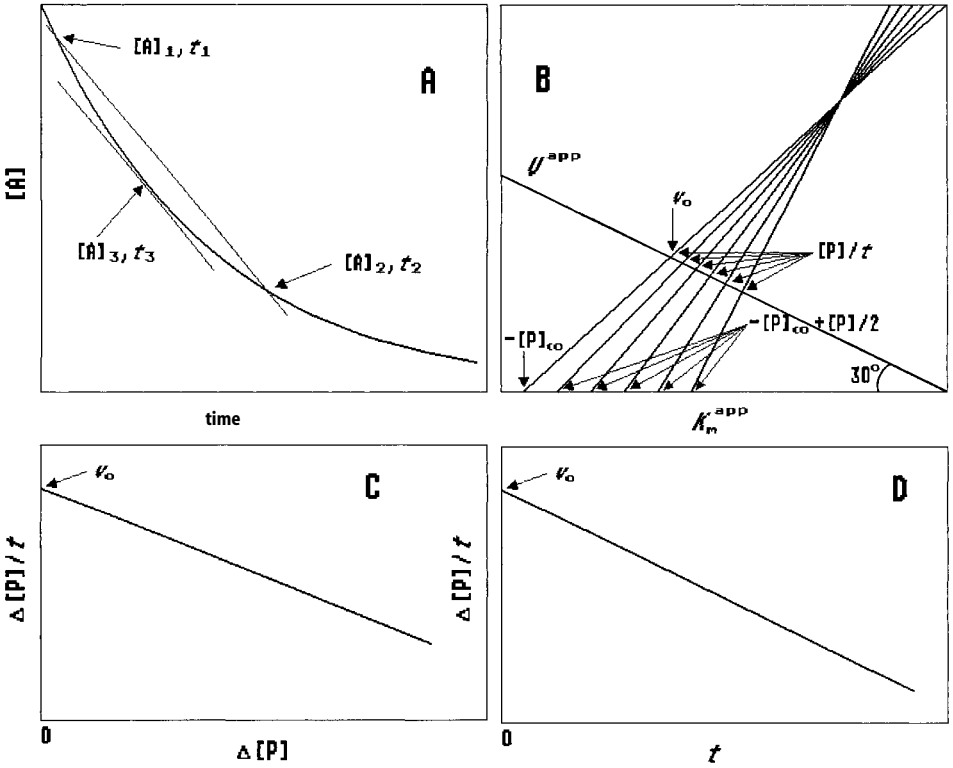

Figure 2.11. Methods for the determination of the actual and the true initial reaction rate. (A) Secant method (Waley, 1981), (B) direct linear plot (Cornish-Bowden, 1975), (C) method of Boeker (1982), and (D) method of Alberty and Koerber (1957).

v can be determined with the secant method even with single point measurement, the gradient of the connecting line between start and measuring point of the reaction being determined. The method requires the absence of product inhibition, but even in its presence v can be obtained by a simple modification, as long as this inhibition is competitive, which mostly applies. In this case two secants are drawn, one e.g. from 0–20%, the other from 0–40%. Both gradients correlate to two rates v_1 and v_2 with two corresponding substrate concentrations $[A]_1$ and $[A]_2$. The actual initial rate is obtained from the equation:

$$v = \frac{[A]_0([A]_1 - [A]_2)}{[A]_1[A]_2\left(\frac{1}{v_2} - \frac{1}{v_2}\right) + [A]_0\left(\frac{[A]_1}{v_1} - \frac{[A]_2}{v_2}\right)} \quad . \tag{2.39}$$

Conversely the existence of product inhibition can be detected by comparing the gradients of the two secants. The ratio v/v' lies between 1 and 1.145 for an uninhibited reaction, with product inhibition it is higher (up to maximal 2.2).

While the methods discussed so far serve to objectify the determination of turnover rate with the aid of tangents, the method of Cornish-Bowden (1975) based on the integrated Michaelis-Menten equation permits the determination of the true initial rate v_0 at $t=0$. The constants K_m and V in the integrated Michaelis-Menten equation (2.33) are only identical with those of the original Michaelis-Menten equation (2.18) if this equation is valid for the complete progress curve. This holds, however, only for irreversible one-substrate reactions. With more complex mechanisms, such as product inhibition, reversibility of reactions or tow or more substrates K_m and V remain not constant and are termed apparent constants (K_m^{app}, V^{app}). Equation (2.33) then is

$$V^{app} = \frac{[P]}{t} + \frac{K_m^{app}}{t} \ln \frac{[P]_\infty}{[P]_\infty - [P]} \quad , \tag{2.40}$$

[P] being the product concentration at time t and $[P]_\infty$ at equilibrium. In a plot of V^{app} against K_m^{app}, straight lines with ordinate intercepts $[P]/t$ and abscissa intercepts $-[P]/\ln [P]_\infty/([P]_\infty - [P])$ are obtained. Actually the procedure is reversed. The axis intercept values are obtained from the progress curve and entered onto the corresponding axes. Without severe loss of accuracy the abscissa value may be simplified into to $-[P]_\infty + 1/2[P]$. The corresponding axis sections are connected by straight lines in a direct linear plot and meet in a point to the right of the ordinate (Figure 2.11 B). The connecting straight line between this point and the abscissa value $[P]_\infty$ intercepts the ordinate at $V^{app}[P]_\infty/(K_m^{app} + [P]_\infty)$, the true initial rate v_0 of the reaction. As gradients of straight lines taken from a progress curve do not significantly differ, the joint intercept is frequently difficult to detect. It becomes more visible if the ordinate is inclined towards the abscissa to an angle of 20° to 30°, which does not affect the result. For a determination of v_0 five straight lines are sufficient. Under experimental conditions frequently an intercept cloud results instead of the expected joint intercept. The connecting straight line may then be drawn through the

cloud center, still giving sufficient accuracy. For complete accuracy, connecting lines must be drawn from $[P]_\infty$ to each individual intercept and the median of all ordinate intercepts should be calculated.

The method of Boeker (1982) is also based on the integrated Michaelis-Menten equation. Here $\Delta[P]/t$ is plotted against $\Delta[P]$. $\Delta[P]=[P]-[P]_0$ is the product formed during reaction ($[P]_0$ not necessarily being zero). The plot gives a linear relationship, v_0 being obtained by extrapolation to $\Delta[P]_0$ (Figure 2.11 C). $[P]_\infty$ must not necessarily be known. In the similar method of Alberty and Koerber (1957) $\Delta[P]/t$ is plotted against t and v_0 is obtained by extrapolation to $t=0$ (Figure 2.11 D).

The general problem of the analysis of progress curves with the integrated Michaelis-Menten equation in the presence of product inhibition will be discussed in Section 2.4.3.

2.4 Reversible Enzyme Reactions

2.4.1 Rate Equation for Reversible Enzyme Reactions

The derivation of the Michaelis-Menten equation is based on an irreversible enzyme reaction like phosphatases or peptidases. Most enzyme reactions, however, e.g. isomerases, dehydrogenases or transaminases tend towards an equilibrium which will be attained both from the site of the substrate as well as the product:

$$A + E \underset{k_{-1}}{\overset{k_1}{\rightleftharpoons}} EA \underset{k_{-2}}{\overset{k_2}{\rightleftharpoons}} E + P\,. \tag{2.41}$$

In the differential equations for [E] and [EA] the reverse reaction must be considered, also the expression for the velocity v is modified:

$$\frac{d[E]}{dt} = (k_{-1} + k_2)[EA] - (k_1[A]+k_{-2}[P])[E]\,, \tag{2.42}$$

$$\frac{d[EA]}{dt} = -(k_{-1} + k_2)[EA] + (k_1[A]+k_{-2}[P])[E]\,, \tag{2.43}$$

$$\frac{d[P]}{dt} = k_2[EA] - k_{-2}[E][P] = v\,. \tag{2.44}$$

[E] and [EA] can be calculated from Eqs. (2.42) and (2.43) applying the relationship for the total enzyme amount $[E]_0=[E]+[EA]$:

$$[E] = \frac{(k_{-1} + k_2)[E]_0}{k_1[A]+k_{-2}[P]+(k_{-1} + k_2)}\,, \tag{2.45}$$

$$[EA] = \frac{(k_1[A] + k_{-2}[P])[E]_0}{k_1[A]+k_{-2}[P]+(k_{-1} + k_2)} \tag{2.46}$$

Insertion into Eq. (2.44) gives the rate equation in the form of the rate constants:

$$v = \frac{(k_1 k_2[\mathrm{A}] + k_{-1}k_{-2}[\mathrm{P}])[\mathrm{E}]_0}{k_1[\mathrm{A}] + k_{-2}[\mathrm{P}] + (k_{-1} + k_2)} \ . \tag{2.47}$$

Since rate constants are difficult to determine, Eq. (2.47) is converted into the form of the kinetic constants. For this, numerator and denominator are multiplied by $(k_{-1} + k_2)/k_1 k_{-2}$. K_{mA} and V_1 representing the Michaelis constant and the maximum velocity for the forward reaction, K_{mP} and V_2 the respective constants for the reverse reaction:

$$K_{\mathrm{mA}} = \frac{k_{-1} + k_2}{k_1} \ ; \quad K_{\mathrm{mP}} = \frac{k_{-1} + k_2}{k_{-2}} \ ;$$

$$V_1 = k_2[\mathrm{E}]_0 \ ; \quad V_2 = k_{-1}[\mathrm{E}]_0 \ ;$$

$$v = v_1 - v_2 = \frac{K_{\mathrm{mP}} V_1[\mathrm{A}] - K_{\mathrm{mA}} V_2[\mathrm{P}]}{K_{\mathrm{mA}} K_{\mathrm{mP}} + K_{\mathrm{mP}}[\mathrm{A}] + K_{\mathrm{mA}}[\mathrm{P}]} \tag{2.48}$$

Equation (2.48) includes the Michaelis-Menten equations for both the forward and the reverse reaction. If [P] or [A]=0 the equations for the separate reactions are obtained:

$$v_1 = \frac{V_1[\mathrm{A}]}{K_{\mathrm{mA}} + [\mathrm{A}]} \ ; \quad v_2 = \frac{V_2[\mathrm{P}]}{K_{\mathrm{mP}} + [P]} \ . \tag{2.18}$$

Thus the Michaelis-Menten equation is valid even in the presence of a reverse reaction, as long as product is negligible. If, however, the product concentration rises considerably during the reaction, the commencing reverse reaction will increasingly affect the reaction rate and lower rate values would be obtained than with the original Michaelis-Menten equation. On the one hand, this demonstrates the universality of the Michaelis-Menten equation, being applicable even for reverse reactions, on the other hand its validity range is restricted to a more narrow time period, the initial range of the progress curve at time t_0, and thus enzyme kinetic studies must concentrate strictly on initial rates.

Following Eq. (2.48), a reverse reaction may be analysed with the simple Michaelis-Menten equation (2.18) from both the substrate and the product side. By this way all four kinetic constants, K_{mA}, K_{mP}, V_1, and V_2 become determinable and with their knowledge also the four rate constants can be calculated:

$$k_1 = \frac{V_1 + V_2}{K_{\mathrm{mA}}[\mathrm{E}]_0} \ ; \quad k_{-1} = \frac{V_2}{[\mathrm{E}]_0} \ ; \quad k_2 = \frac{V_1}{[\mathrm{E}]_0} \ ; \quad k_{-2} = \frac{V_1 + V_2}{K_{\mathrm{mP}}[\mathrm{E}]_0} \ .$$

Obviously from the initial rates of the forward and reverse reaction a lot of information can be obtained. However, the increase of the reverse reaction will alter the initial phase of the progress curves. The linearisation methods derived from the inte-

grated Michaelis-Menten equation (Eqs. (2.34)–(2.36)) do no longer yield straight lines. Integration of Eq. (2.48), however, includes the reverse reaction and a linear relationship is obtained also for this case:

$$\frac{[A]_0 - [A]}{t} = \frac{K_{mP}V_1 + K_{mA}V_2}{K_{mP} - K_{mA}} - \frac{K_m K_{mP}}{K_{mP} - K_{mA}} \times \left(1 + \frac{(V_1 + V_2)[A]_0}{K_{mP}V_1 + K_{mA}V_2}\right) \frac{\ln\left(1 - \frac{[A]_0 - [A]}{[P]_e}\right)}{t} \tag{2.49}$$

$([A]_0-[A])/t$ is plotted against $\ln(1-([A]_0-[A])/[P]_e)/t$, $[P]_e$ being the product concentration at the equilibrium of the reaction. If $[P]_e$ or V_2 are not known, K_{mA} and V_1 may be obtained from the starting region ($[P]=0$) by plotting $([A]_0-[A])/t$ against $\ln([A]_0/[A])/t$ according to Foster and Niemann (Section 2.4.3) at various $[A]_0$ values. Accordingly K_{mP} and V_2 can be determined from the reverse reaction. This procedure, however, differs hardly from the usual method to determine initial rates at different substrate concentrations.

2.4.2 The Haldane Equation

In reversible reactions, contrary to irreversible reactions, substrate is only consumed until a state of equilibrium is achieved, the turnover rates in both directions compensating each other. The overall reaction rate then is $v=0$. Equations (2.47) and (2.48) may be modified into:

$$k_1 k_2 [A]_g = k_{-1} k_{-2} [P]_e \tag{2.50}$$

$$K_{mP} V_1 [A]_g = K_{mA} V_2 [P]_e \tag{2.51}$$

$[A]_e$ and $[P]_e$ represent the concentrations at equilibrium. The equilibrium constant K_e for the whole reaction is:

$$K_e = \frac{[E]_e[P]_e}{[E]_e[A]_e} = \frac{[P]_e}{[A]_e} = \frac{k_1 k_2}{k_{-1} k_{-2}} = \frac{K_{mP} V_1}{K_{mA} V_2} = \frac{K_p}{K_a} \; . \tag{2.52}$$

K_e is the ratio of dissociation constants of the enzyme-product complex $K_p=k_2/k_{-2}$ and the enzyme-substrate complex $K_a=k_{-1}/k_1$. This relation between the kinetic constants and the thermodynamic equilibrium constants described by J.B.S. Haldane shows that Michaelis constants and maximum reaction rates of forward and reverse reactions are not independent of each other. To guide a reaction into the direction of product ($K_e \gg 1$), conditions must be: $V_1 \gg V_2$, respectively $K_{mA} \ll K_{mP}$.

2.4.3 Product Inhibition

Another consequence of the reversibility of Eq. (2.48) is the inhibition of the enzyme by its own product. While the original derivation of the Michaelis-Menten equation for an irreversible reaction assumes a binding equilibrium only for substrate, for the reaction mechanism (2.41) such an equilibrium must also be assumed for product, even if the reverse reaction is negligible. Thus product inhibition is to be expected for each enzyme, although it may not always be very pronounced (in case of weak product binding). The inhibitory effect is not constant but increases in parallel with product formation. To study this inhibition, product is added in a certain concentration [P] at reaction start where the reverse reaction can be neglected. Thus in Eq. (2.48) $V_2 = k_{-1}[E]_0 = 0$ and, for the same reason the Michaelis constant of product K_{mP} reduces to the binding constant $K_p = k_2/k_{-2}$ which has in this context the significance of an inhibition constant:

$$v = \frac{K_p V_1 [A]}{K_{mA} K_P + [A] K_P + [P] K_{mA}} = \frac{V_1 [A]}{K_{mA}\left(1 + \frac{[P]}{K_P}\right) + [A]} \,. \tag{2.53}$$

In its double reciprocal form the equation is:

$$\frac{1}{v} = \frac{1}{V_1} + \frac{K_{mA}\left(1 + \frac{[P]}{K_P}\right)}{V_1 [A]} \,. \tag{2.54}$$

This is a *competitive product inhibition*, i.e., product competes for the substrate binding site at the active enzyme centre. The substrate converted into product remains at its original binding site and prevents the attachment of a new substrate molecule. In the double reciprocal diagram (Figure 2.12), a group of straight lines is obtained for different product concentrations, with a common ordinate intercept at $1/V$ and the ab-

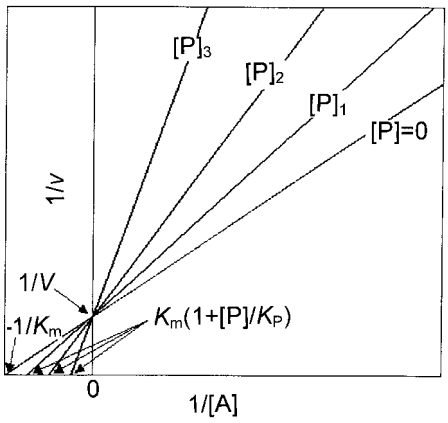

Figure 2.12. Competitive product inhibition in a double reciprocal plot. The determination of the kinetic constants is indicated.

scissa intercepts $-1/K_{mA}(1+[P]/K_P)$. With K_{mA} known (determined in the absence of product), K_p can be calculated.

The most common type of product inhibition is competitive, there are, however, other ways for product to affect enzyme reactions. In multiple substrate reactions, the product from one substrate may displace this substrate and block the reaction, but the cosubstrate is not necessarily displaced. For the cosubstrate, inhibition is *non-competitive*. In rare cases, an *uncompetitive product inhibition* is observed. The same types of inhibition occur with specific inhibitors of the enzyme. They are described in detail in Section 2.5.1. The equations derived there and the evaluation methods are analogously applicable, if inhibitor [I] is substituted by [P], and the inhibition constant K_i is substituted by K_P. This is only valid as long as product concentration [P] can be regarded constant within the measuring range. In fact, the continuously increasing product concentration is the main difference to inhibition of the enzyme by compounds remaining constant during the whole reaction period. This becomes particularly evident if, instead of determining initial rates, complete progress curves are evaluated, applying the integrated Michaelis-Menten equation. The run of these curves is strongly affected by product inhibition.

The integrated Michaelis-Menten equation in the presence of product inhibition reads (Foster and Niemann, 1953):

$$\frac{[A]_0 - [A]}{t} = \frac{VK_P}{K_p - K_A} - \frac{K_{mA}(K_P + [A]_0)}{K_P - K_{mA}} \cdot \frac{\ln \frac{[A]_0}{[A]}}{t} \,. \tag{2.55}$$

In a plot $([A]_0-[A])/t$ against $\ln([A]_0/[A])/t$, for $K_{mA}<K_P$ straight lines with a negative gradient result (Figure 2.13), for $K_{mA}>K_P$ straight lines with a positive gradient. With $K_{mA}=K_P$ the straight line stands at a right angle to the abscissa. Different initial concentrations of $[A]_0$ yield in this plot a group of straight lines with a common ordinate intercept at $\pm V(1-K_{mA}/K_P)$. Intercepts of these straight lines with source straight lines of the gradient $[A]_0$ have the Y coordinate v_0, the true initial rate at

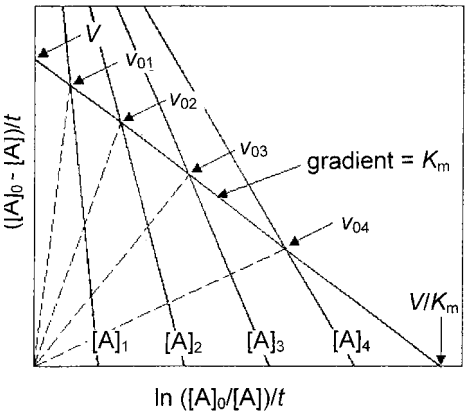

Figure 2.13. Foster and Niemann evaluation method of the integrated Michaelis-Menten equation, considering product inhibition (1953).

$t=0$. The intercepts of several linearised progress curves with their respective source straight lines lie in turn on a straight line correlating to an ideal progress curve in the absence of product inhibition. Its gradient has the value K_m, the ordinate intercept is V and the abscissa intercept V/K_m. With these constants, K_P can be calculated from the gradients of the individual progress curves with has value K_m $(K_P+[A]_0)/(K_P-K_m)$ according to Eq. (2.55). More simple $-K_P$ can be obtained as abscissa intercept by replotting the gradients against $[A]_0$.

Product inhibition may not be confused with *feedback inhibition*, a general regulation principle in metabolic pathways. The end product of the chain inhibits the activity of the initial enzyme and switches off the whole reaction sequence, so that no intermediates can accumulate. Due to the multiple steps of the chain, the end product structurally is so different from the substrate or product of the first enzyme, that it is no longer recognised by its active centre. Therefore, the inhibitor binds to a separate *allosteric* regulatory site, indirectly influencing (e.g., by conformational change) the catalytic center (Section 1.54.). Regarding kinetics end product inhibition is usually a non-competitive inhibition (Section 2.5.1.2). With allosteric enzymes, however, the sigmoidal saturation behaviour has to be considered.

2.5 Enzyme Inhibition

Enzyme inhibition is defined as the negative effect on enzyme activity by ligands (*inhibitors*) specifically binding to defined catalytic or regulatory centres. A reduction of the reaction rate can be caused also by other factors, e.g., temperature, pH value, ionic strength or polarity of the solvent. Such influences happen unspecifically by changes of the enzyme structure through surface effects, interactions with charged groups or disturbance of the hydrate shell. This includes interactions with hydrophobic compounds, detergents or chaotropic substances, e.g., ammonium sulphate. Such effects are not considered as enzyme inhibition and should be excluded as the cause of the observed inhibition. However, this is not always evident as they act in the same way as specific inhibition, i.e., by reduction of the turnover rate. Adding a precooled solution of a supposed inhibitor to the enzyme test will reduce the turnover rate because of temperature decrease. The same holds for modification of the pH value by addition of acid or basic compounds or high salt. All these effects are increased with the amount of added solution and simulate concentration dependency.

The nature of binding of a specific inhibitor is of importance for the treatment of the obtained data. Mostly the inhibitor binds reversibly and can be released or displaced from the enzyme (*reversible inhibition*). Certain inhibitors, however, bind so strong that they cannot not be detached (*irreversible inhibition*). This can be caused by covalent binding, as for *suicide substrates* that initially follow the catalytic process but subsequently form a covalent bond with a functional group of the active center and block the enzyme. *Transition state analogues* mimicking the real transition state bind non-covalently, but extremely powerful, so that it is quite impossible to remove them. Reversible and irreversible enzyme inhibitions create differing dependencies and are described separately.

2.5.1 Reversible Enzyme Inhibition

2.5.1.1 General Rate Equation

An inhibitor binds to an enzyme and affects its reaction rate. The rate constant k_2 for the uninhibited reaction is altered by binding of the inhibitor to the ESI complex to k_6:

$$\begin{array}{ccccccc} \mathrm{E} & + & \mathrm{A} & \underset{k_{-1}}{\overset{k_1}{\rightleftharpoons}} & \mathrm{EA} & \xrightarrow{k_2} & \mathrm{E} + \mathrm{P} \\ + & & & & + & & \\ \mathrm{I} & & & & \mathrm{I} & & \\ k_3 \Big\| \Big\backslash k_{-3} & & & & k_4 \Big\| \Big\backslash k_{-4} & & \\ \mathrm{EI} & + & \mathrm{A} & \underset{k_{-5}}{\overset{k_5}{\rightleftharpoons}} & \mathrm{EAI} & \xrightarrow{k_6} & \mathrm{EI} + \mathrm{P} \end{array} \tag{2.56}$$

This reaction mechanism contains each two dissociation constants for substrate A and for inhibitor I:

$$K_\mathrm{A} = \frac{k_{-1}}{k_1} = \frac{[\mathrm{E}][\mathrm{A}]}{[\mathrm{EA}]}\,; \quad K_\mathrm{Ai} = \frac{k_{-5}}{k_5} = \frac{[\mathrm{EI}][\mathrm{A}]}{[\mathrm{EAI}]}\,;$$

$$K_\mathrm{ic} = \frac{k_{-3}}{k_3} = \frac{[\mathrm{E}][\mathrm{I}]}{[\mathrm{EI}]}\,; \quad K_\mathrm{iu} = \frac{k_{-4}}{k_4} = \frac{[\mathrm{EA}][\mathrm{I}]}{[\mathrm{EAI}]}\,.$$

These terms yield the relation

$$\frac{K_\mathrm{A}}{K_\mathrm{Ai}} = \frac{K_\mathrm{ic}}{K_\mathrm{iu}}\,, \tag{2.57}$$

so that the fourth constant can be calculated when the other three are known.

The differential equations for the free enzyme and the enzyme-substrate complex, assuming steady-state conditions, and for the reaction rate v are:

$$\frac{\mathrm{d}[\mathrm{E}]}{\mathrm{d}t} = (k_{-1} + k_2)[\mathrm{EA}] - (k_1[\mathrm{A}] + k_3[\mathrm{I}])[\mathrm{E}] + k_{-3}[\mathrm{EI}] = 0\,, \tag{2.58}$$

$$\frac{\mathrm{d}[\mathrm{EA}]}{\mathrm{d}t} = -(k_{-1} + k_2 + k_4)[\mathrm{EA}] + k_1[\mathrm{A}][\mathrm{E}] + k_{-4}[\mathrm{EAI}] = 0\,, \tag{2.59}$$

$$\frac{\mathrm{d}[\mathrm{P}]}{\mathrm{d}t} = k_2[\mathrm{EA}] + k_6[\mathrm{EAI}] = v\,. \tag{2.60}$$

The terms for the enzyme-inhibitor complexes are replaced by the inhibitor constants in the equation for the total amount of the enzyme:

$$[\mathrm{E}]_0 = [\mathrm{E}] + [\mathrm{EA}] + [\mathrm{EI}] + [\mathrm{EAI}] = [\mathrm{E}] + [\mathrm{EA}] + \frac{[\mathrm{E}][\mathrm{I}]}{K_\mathrm{ic}} + \frac{[\mathrm{EA}][\mathrm{I}]}{K_\mathrm{iu}}\,. \tag{2.61}$$

This gives:

$$[\mathrm{E}] = \frac{[\mathrm{E}]_0 - [\mathrm{EA}]\left(1 + \dfrac{[\mathrm{I}]}{K_{\mathrm{iu}}}\right)}{1 + \dfrac{[\mathrm{I}]}{K_{\mathrm{ic}}}} \,. \tag{2.62}$$

In Eq. (2.58) [EI] is replaced by $K_{\mathrm{ic}} = k_{-3}/k_3$:

$$-(k_1[\mathrm{A}] + k_3[\mathrm{I}])[\mathrm{E}] + (k_{-1} + k_2)[\mathrm{EA}] + k_3[\mathrm{E}][\mathrm{I}] = 0$$

$$-k_1[\mathrm{A}][\mathrm{E}] + (k_{-1} + k_2)[\mathrm{EA}] = 0 \,.$$

so that [E] is eliminated from Eq. (2.62):

$$\frac{(k_{-1} + k_2)[\mathrm{EA}]}{k_1[\mathrm{A}]} = \frac{[\mathrm{E}]_0 - [\mathrm{EA}]\left(1 + \dfrac{[\mathrm{I}]}{K_{\mathrm{iu}}}\right)}{1 + \dfrac{[\mathrm{I}]}{K_{\mathrm{ic}}}} \,.$$

This gives a term for [EA], setting $K_{\mathrm{m}} = (k_{-1}+k_2)/k_1$:

$$[\mathrm{EA}] = \frac{[\mathrm{E}]_0}{\dfrac{K_{\mathrm{m}}}{[\mathrm{A}]}\left(1 + \dfrac{[\mathrm{I}]}{K_{\mathrm{ic}}}\right) + \left(1 + \dfrac{[\mathrm{I}]}{K_{\mathrm{iu}}}\right)} \,.$$

Inserting this term in the rate equation (2.60), applying $V_1 = k_2[\mathrm{E}]_0$, $V_2 = k_6[\mathrm{E}]_0$ and replacing [EAI] by K_{iu}, follows:

$$v = \left(k_2 + \frac{k_6[\mathrm{I}]}{K_{\mathrm{iu}}}\right)[\mathrm{EA}] \,.$$

$$v = \frac{\left(V_1 + \dfrac{V_2[\mathrm{I}]}{K_{\mathrm{iu}}}\right)[\mathrm{A}]}{K_{\mathrm{m}}\left(1 + \dfrac{[\mathrm{I}]}{K_{\mathrm{ic}}}\right) + \left(1 + \dfrac{[\mathrm{I}]}{K_{\mathrm{iu}}}\right)[\mathrm{A}]} \,. \tag{2.63}$$

The mechanism described in the reaction equation (2.56) and formulated in Eq. (2.63) corresponds to a *partially non-competitive inhibition* (see Section 2.5.1.5). Although a rather rare type of inhibition, its equation was derived to be representative for the following mechanisms. The equation represents the general mechanism of a reversible enzyme inhibition. All other equations for specific mechanisms can be derived from it by simplification.

Figure 2.14 provides a survey over all important reversible types of inhibitions. They are divided into two main groups: In *partial inhibitions*, as for the partially

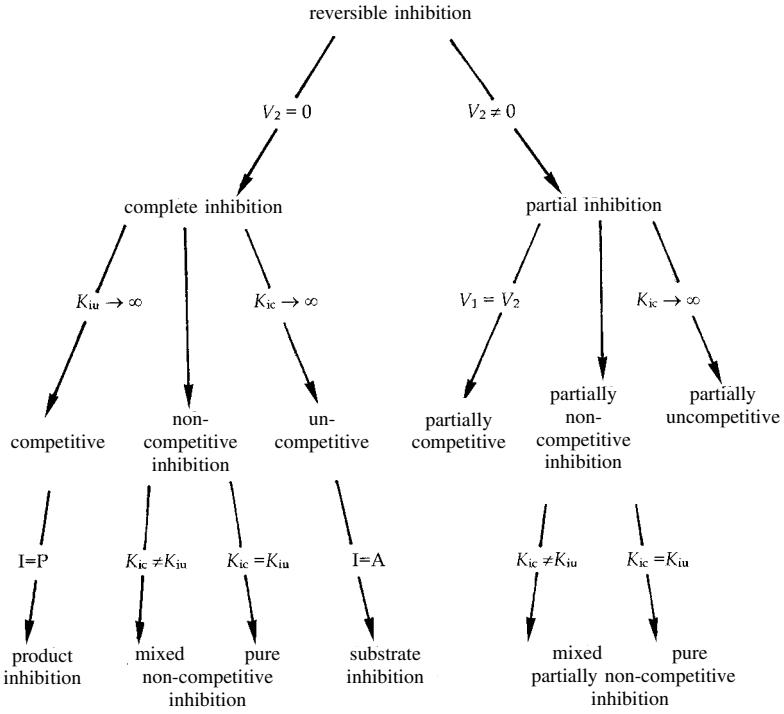

Figure 2.14. Survey of the most essential reversible inhibition mechanisms.

non-competitive inhibition, the enzyme remains active even after binding to the inhibitor, but the activity may be affected by the inhibitor. In complete inhibitions the enzyme forms an inactive *dead-end complex* with the inhibitor.

2.5.1.2 Non-Competitive Inhibition, Graphic Representation of Inhibition Data

Complete inhibition results when the EAI complex is inactive: k_6 resp. $V_2 = 0$

$$\begin{array}{ccccccc} E & + & A & \underset{k_{-1}}{\overset{k_1}{\rightleftharpoons}} & EA & \xrightarrow{k_2} & E + P \\ + & & & & + & & \\ I & & & & I & & \\ k_3 \Big\| \Big\backslash k_{-3} & & & & k_4 \Big\| \Big\backslash k_{-4} & & \\ EI & + & A & \underset{k_{-5}}{\overset{k_5}{\rightleftharpoons}} & EAI & & \end{array} \qquad (2.64)$$

Equation (2.63) is simplified into ($V_1 = V$):

$$v = \frac{V[\mathrm{A}]}{K_\mathrm{m}\left(1 + \frac{[\mathrm{I}]}{K_\mathrm{ic}}\right) + \left(1 + \frac{[\mathrm{I}]}{K_\mathrm{iu}}\right)[\mathrm{A}]} \,. \tag{2.65}$$

The reciprocal form for the Lineweaver-Burk plot is:

$$\frac{1}{v} = \frac{1 + \frac{[\mathrm{I}]}{K_\mathrm{iu}}}{V} + \frac{K_\mathrm{m}\left(1 + \frac{[\mathrm{I}]}{K_\mathrm{ic}}\right)}{V[\mathrm{A}]}. \tag{2.66}$$

Transformation according to the Hanes plot:

$$\frac{[\mathrm{A}]}{v} = \frac{[\mathrm{A}]\left(1 + \frac{[\mathrm{I}]}{K_\mathrm{iu}}\right)}{V} + \frac{K_\mathrm{m}\left(1 + \frac{[\mathrm{I}]}{K_\mathrm{ic}}\right)}{V} \tag{2.67}$$

and the Eadie-Hofstee plot:

$$v = \frac{V}{1 + \frac{[\mathrm{I}]}{K_\mathrm{iu}}} - \frac{K_\mathrm{m}\left(1 + \frac{[\mathrm{I}]}{K_\mathrm{ic}}\right)}{\left(1 + \frac{[\mathrm{I}]}{K_\mathrm{iu}}\right)} \cdot \frac{v}{[\mathrm{A}]} \,. \tag{2.68}$$

This general form of a complete inhibition is termed *non-competitive* (for the notations of inhibition types, see Section 2.5.1.7). The apparent Michaelis constant and the maximum velocity are both affected by the inhibitor. To characterise this inhibition type the turnover rates of several measuring series with varying substrate concentrations are performed, each series containing a constant amount of the inhibitor. One series without inhibitor is tested for control and for the determination of K_m and *V*. Substrate and inhibitor concentrations are varied around their respective Michaelis and inhibition constants (a power of 10 below and above). The direct plot (Figure 2.15 A) yields hyperbolic curves even in the presence of the inhibitor. They flatten with increased inhibitor concentration and move towards lower saturation values. A distinctive criterion of this type of inhibition is that the maximum velocity without inhibitor is no longer reached in the presence of the inhibitor, although this is not always clearly visible in the non-linear plot. Herein the linear diagrams prove to be superior. Linearity is also conserved in the presence of the inhibitor, and the lines from the different measuring series form patterns characteristic for the respective type of inhibition. In the double reciprocal plot all straight lines meet in a joint intercept left of the ordinate, i.e., they differ in gradient and ordinate intercept, because the inhibitor influences both the apparent Michaelis constant and the maximum velocity (Figure 2.15B). The relative position of the common intercept of the lines displays the relation of the two inhibition constants to each other. For $K_\mathrm{ic} < K_\mathrm{iu}$, it is located above the abscissa. In this frequently occurring case the substrate impedes binding of the inhibitor. Consequently, according to Eq. (2.57) the condition $K_\mathrm{A} < K_\mathrm{Ai}$ must hold,

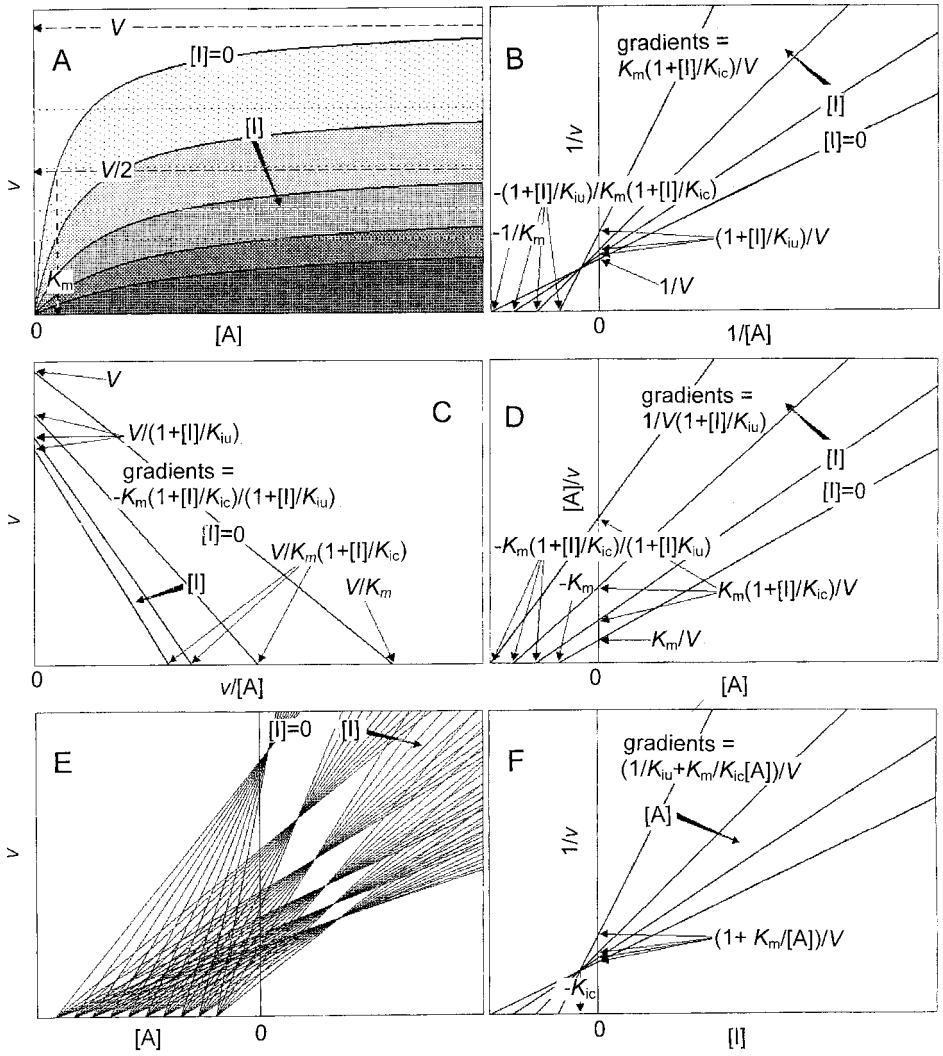

Figure 2.15. Non-competitive inhibition in different representations. (A) Direct plot, (B) double-reciprocal plot, (C) Eadie-Hofstee plot, (D) Hanes plot, (E) direct linear plot, (F) Dixon inhibition plot (1953). The potential determinations of the kinetic constants are indicated.

i.e., the inhibitor also impedes substrate binding. If, on the other side, inhibitor and substrate support each other in their binding to the enzyme, i.e., $K_{ic} > K_{iu}$ and $K_A > K_{Ai}$, the joint straight line intercept is located below the abscissa. For $K_{ic} = K_{iu}$ and $K_A = K_{Ai}$ there is no interaction. Binding of substrate and inhibitor occur completely independent of each other, the intercept is now located on the abscissa. This special case where K_m is not changed is often designated as true non-competitive inhibition in contrast to a so-called *mixed inhibition*. It is assumed that by the shift of the intercept up or

down, away from the abscissa, this type of inhibition increasingly changes into a competitive or uncompetitive inhibition, respectively. This term is not quite adequate, as there is no principal difference in the mechanisms (Eq. 2.64) of non-competitive and "mixed" inhibitions, but there is one very well between mixed inhibition and competitive and uncompetitive inhibition (see Sections 2.5.1.3 and 2.5.1.4).

In the Hanes plot (Figure 2.15D) the straight line pattern is the same as in the double reciprocal plot, only the location of the intercepts above or below the abscissa is reversed. In the Eadie-Hofstee plot (Figure 2.15C) the straight line intercept for $K_{ic} < K_{iu}$ is located in the second, for $K_{ic} > K_{iu}$ in the fourth quadrant, $K_{ic} = K_{iu}$ yields parallels.

The changes in the positions of the lines with increasing inhibitor concentration serve to determine the inhibition constants K_{ic} and K_{iu} according to Eqs. (2.66)–(2.68). From Figure 2.15 it can be seen that in the double reciprocal plot K_{ic} enters the gradient and K_{iu} the ordinate intercept. The abscissa intercept contains both constants and is less useful for determination. As this calculation method is somewhat circumstantial, *secondary plots* (replots) are recommended, giving the advantage of additional control of the type of inhibition. Here parameters altered by inhibition in the primary plot, e.g., gradients and ordinate intercepts, are plotted against the respective inhibitor concentrations. Complete inhibitions with inactive dead-end complexes yield linear secondary plots. Partial inhibitions show non-linear dependencies, so that both main types of reversible inhibition can be distinguished. Secondary plots can be derived from all three linearisation methods. This is demonstrated with the example of the double reciprocal plot. The gradient *Sl* according to Eq. (2.66) is:

$$Sl = \frac{K_m}{V} + \frac{[I]K_m}{K_{ic}V} \ , \tag{2.69}$$

the ordinate intercept *Or*:

$$Or = \frac{1}{V} + \frac{[I]}{K_{iu}V} \ . \tag{2.70}$$

Plotting the gradients or the ordinate intercepts against the inhibitor concentrations results in straight lines with the abscissa intercepts $-K_{ic}$ and $-K_{iu}$, respectively (Figure 2.16).

The direct linear plot yields a group of straight lines with a common intercept already for the variation of substrate. For each measuring series in the presence of inhibitor, a further group of straight lines with a common intercept results. This intercept shifts in a way characteristic for the respective inhibition type, i.e., it moves transversely downwards for the non-competitive inhibition (Figure 2.15E).

Dixon (1953) proposed a plot particularly for the representation of inhibition data in which K_{ic} can be read directly from the x-coordinate of the joint straight line intercept, following the transformation of Eq. (2.66)

$$\frac{1}{v} = \frac{1}{V}\left(1 + \frac{K_m}{[A]}\right) + \frac{[I]}{V}\left(\frac{1}{K_{iu}} + \frac{K_m}{K_{ic}[A]}\right) \ , \tag{2.71}$$

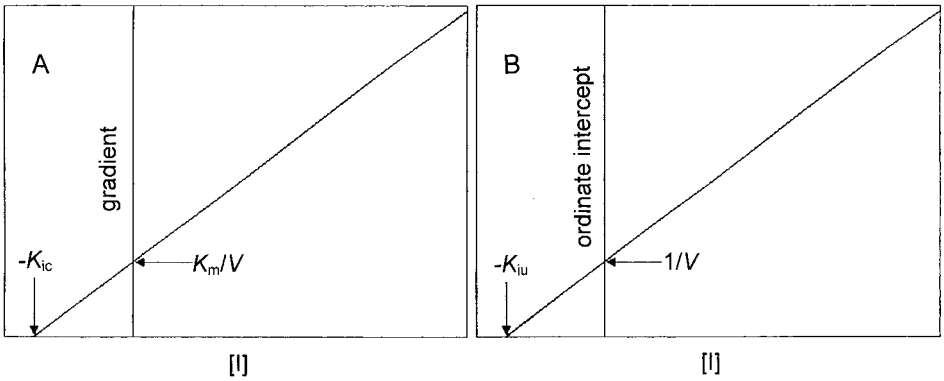

Figure 2.16. Secondary plots of gradients (A) and ordinate intercepts (B) from a double reciprocal plot for non-competitive inhibition.

This results in a linear dependence of $1/v$ from [I]. Compared with the other plots a reverse experimental approach is used. Within a measuring series the amount of inhibitor is changed, the substrate concentration remaining constant. The common intercepts of the lines are located as in the Lineweaver-Burk plot in the second or third quadrant, or on the abscissa according to the ratio of the inhibition constants (Figure 2.15 F). Contrary to the other plots, dependence of the reaction rate on the inhibitor is directly displayed. As in the secondary plots, linearity results only for complete inhibition mechanisms. Partial mechanisms show bended curves. The disadvantage of this plot is that non-competitive (here only the case $K_{ic} < K_{iu}$) and competitive inhibition share a straight line intercept in the second quadrant. Thus these prevalent inhibition types cannot be clearly distinguished here.

Another method of Dixon (1972), suited also for K_m determination only requires the dependence of the turnover rate on the inhibitor concentration at a single (saturating) substrate amount. For this method, the respective inhibition type must be known. V' is the uninhibited turnover rate at [I] = 0 (not identical with the maximum velocity V at infinite substrate concentration) which forms a declining hyperbola in the presence of inhibitor and runs towards the base line at complete inhibition (Figure 2.17 A). Connecting lines are drawn between V' and the points on the curve $v' = V'(n-1)/n$ (for $n = 1$, 2, 3, etc., i.e. $V'/2$, $2V'/3$, $3V'/4$, $4V'/5$, etc.). They cut the base line at equal distances, with the value of K_{ic} in a non-competitive inhibition (referring to the concentration scale of the abscissa). The line for $n = 1$ is equal to the source tangent to the curve. If the distance for K_{ic} is once again entered to the left of its intercept, the line for $n = 0$ is obtained. The distance from there to the ordinate ([I] = 0) corresponds to the applied enzyme concentration. In competitive inhibition the intercept distances of the connecting lines with the base line depend on the substrate concentration. In this case the experiment must be performed at varying substrate concentrations. Plotting the distances against substrate amounts results in a straight line intercepting the ordinate ([A] = 0) at K_{ic} and the abscissa at $-K_m$ (Figure 2.17 B).

The mechanisms of enzyme inhibition can be analysed with the integrated Michaelis-Menten equation. For non-competitive inhibition integration of Eq. (2.65) gives

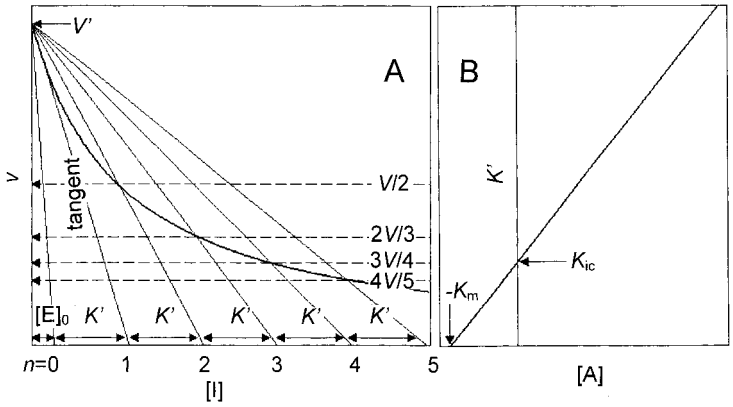

Figure 2.17. Graphic method (A) for the determination of inhibition and Michaelis constants after Dixon (1972). (B) Secondary plot of the apparent constant K' against substrate concentration.

$$\frac{K_m\left(1+\frac{[I]}{K_{ic}}\right)}{1+\frac{[I]}{K_{iu}}}\ln\frac{[A]_0}{[A]}+[A]_0-[A]=\frac{Vt}{1+\frac{[I]}{K_{iu}}}, \tag{2.72}$$

that may be transferred into the three linear forms of Section 2.3.1.5. Only one of these is presented here:

$$\frac{[A]_0-[A]}{t}=\frac{V}{1+\frac{[I]}{K_{iu}}}-\frac{K_m\left(1+\frac{[I]}{K_{ic}}\right)}{\left(1+\frac{[I]}{K_{iu}}\right)}\cdot\frac{\ln\frac{[A]_0}{[A]}}{t}. \tag{2.73}$$

Varying inhibitor concentrations yield groups of straight lines with a joint intercept. The ratio of inhibition constants can be read from its location: in the second quadrant $K_{ic}<K_{iu}$ (Figure 2.18 A), in the fourth quadrant for $K_{ic}>K_{iu}$ (Figure 2.18 C), and parallels for $K_{ic}=K_{iu}$ (Figure 2.18 B). As with the other linearisation methods inhibition constants can be obtained from secondary plots (Figure 2.18 D and E).

Non-competitive inhibition is the most important type of inhibition for the regulation of cell metabolism. Enzyme activity can be affected by metabolites without direct substrate analogy, as in the case of feedback inhibition and with allosteric enzymes (Section 1.5.4). These enzymes often show non-hyperbolic saturation curves due to cooperative effects, which cannot be linearised by simple methods. Non-competitive inhibition mechanisms with cooperative enzymes can be detected by extrapolation on infinite substrate concentration, where reduced maximum velocities must appear for varying inhibitor concentrations. Non-competitive inhibition is frequently observed with product inhibition in multiple substrate reactions. Usually product prevents the binding of the substrate it was formed from (competitive product inhibition, Section 2.4.3). The cosubstrate is not displaced, but without the first substrate the cat-

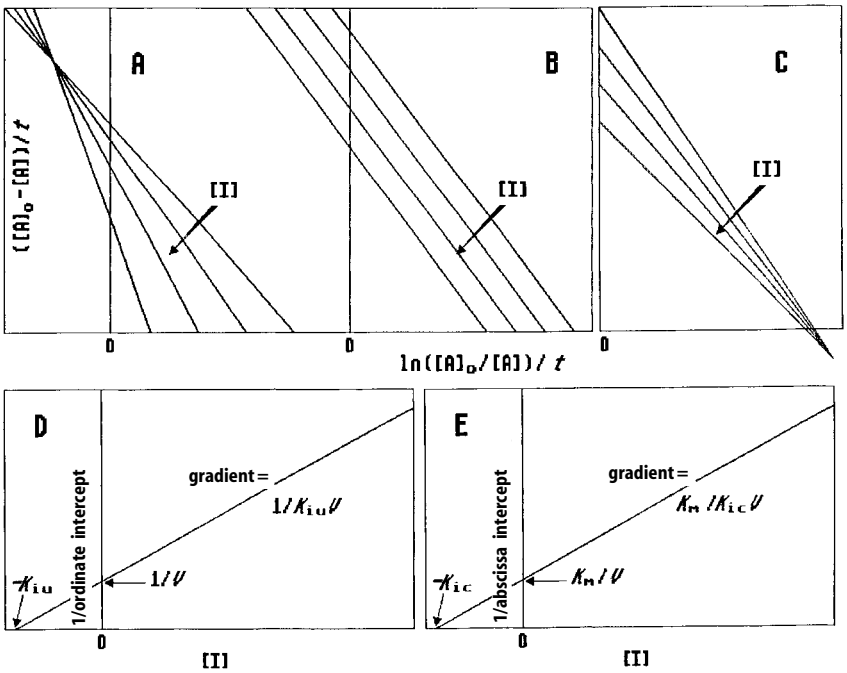

Figure 2.18. Non-competitive inhibition in linearised plots of the integrated Michaelis-Menten equation. (A) $K_{ic} < K_{iu}$, (B) $K_{ic} = K_{iu}$, (C) $K_{ic} > K_{iu}$, (D) secondary plot of reciprocal ordinate intercepts, and (E) reciprocal abscissa intercepts against inhibitor concentration.

alytic reaction cannot proceed. So the product acts as a non-competitive inhibitor towards the cosubstrate. Correspondingly, inactive analogues of the first substrate will also act as non-competitive inhibitors with respect to the cosubstrate (actually the situation is more complicated, dependent on the respective multi-substrate mechanism, see Sections 2.6.2 ff).

2.5.1.3 Competitive Inhibition

In this type of inhibition the inhibitor competes with the enzyme substrate for its binding site at the active enzyme centre. Either substrate or inhibitor can be bound, simultaneous binding is not possible:

$$\begin{array}{ccccccc} E & + & A & \underset{k_{-1}}{\overset{k_1}{\rightleftharpoons}} & EA & \xrightarrow{k_2} & E + P \\ + & & & & & & \\ I & & & & & & \\ k_3 \downarrow\uparrow k_{-3} & & & & & & \\ EI & & & & & & \end{array} \qquad (2.74)$$

The rate equation (2.65) for non-competitive inhibition is simplified by deleting K_{iu} (i.e., $K_{iu} \to \infty$; $[I]/K_{iu} \to 0$), so that only one inhibition constant has to be considered:

$$v = \frac{V[A]}{K_m\left(1 + \frac{[I]}{K_{ic}}\right) + [A]} \ . \tag{2.75}$$

Linearisation after Lineweaver-Burk:

$$\frac{1}{v} = \frac{1}{V} + \frac{K_m\left(1 + \frac{[I]}{K_{ic}}\right)}{V[A]} \ , \tag{2.76}$$

after Hanes:

$$\frac{[A]}{v} = \frac{[A]}{V} + \frac{K_m\left(1 + \frac{[I]}{K_{ic}}\right)}{V} \ , \tag{2.77}$$

after Eadie-Hofstee:

$$v = V - K_m\left(1 + \frac{[I]}{K_{ic}}\right) \cdot \frac{v}{[A]} \tag{2.78}$$

and after Dixon:

$$\frac{1}{v} = \frac{1}{V}\left(1 + \frac{K_m}{[A]}\right) + \frac{[I]K_m}{VK_{ic}[A]} \ . \tag{2.79}$$

V is not changed in this inhibition, as substrate in large surplus ($[A] \to \infty$) displaces the inhibitor (as reversely large quantities of inhibitor displace the substrate). This feature is indicative of this type of inhibition and is noticeable in the double reciprocal plot at a joint ordinate intercept of all straight lines at $1/V$ (Figure 2.19 B). Correspondingly, the hyperbolae in the direct diagram tend towards a common level of saturation. Only the apparent Michaelis constant is affected by the inhibition, so only those parameters containing K_m are altered in the linearised plots, e.g., gradients in the Lineweaver–Burk plot. By this there also exists only one secondary plot for the determination of K_{ic}. This binding constant characteristic for competitive inhibition is also called *competitive inhibition constant*. In the Dixon plot the straight lines meet in a joint intercept in the second quadrant with $-K_{ic}$ as x-coordinate (Figure 2.19 F). In the direct linear plot the joint intercept of the straight lines moves straight towards the right (Figure 2.19 E).

The integrated Michaelis-Menten equation for a competitive inhibition can be deduced from Eq. (2.72) for the non-competitive inhibition disregarding the terms containing K_{iu}:

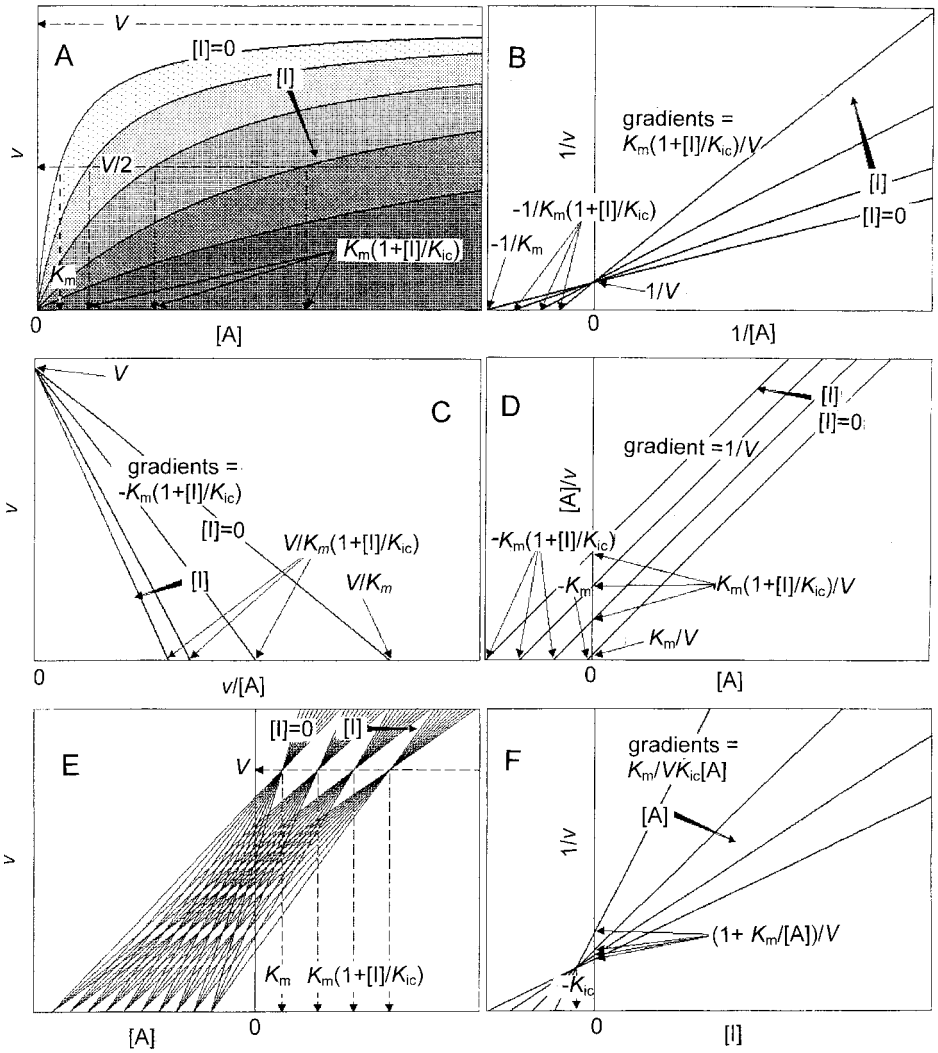

Figure 2.19. Competitive inhibition in various representations. (A) Direct plot, (B) double-reciprocal plot, (C) Eadie-Hofstee plot, (D) Hanes plot, (E) direct linear plot, (F) Dixon inhibition plot (1953). The determination of the kinetic constants from these plots is indicated.

$$K_{\mathrm{m}}\left(1+\frac{[\mathrm{I}]}{K_{\mathrm{ic}}}\right)\ln\frac{[\mathrm{A}]_0}{[\mathrm{A}]}+[\mathrm{A}]_0-[\mathrm{A}]=Vt\ , \tag{2.80}$$

in the form of a linear equation:

$$\frac{[\mathrm{A}]_0-[\mathrm{A}]}{t}=V-K_{\mathrm{m}}\left(1+\frac{[\mathrm{I}]}{K_{\mathrm{ic}}}\right)\cdot\frac{\ln\dfrac{[\mathrm{A}]_0}{[\mathrm{A}]}}{t}\ . \tag{2.81}$$

The straight lines have a common intercept at *V*. Plotting the gradients and the reciprocal abscissa intercepts against the inhibitor concentration in a secondary plot yields $-K_{ic}$ from the abscissa intercept.

Competitive inhibition is very important for the analysis of enzyme specificity by substrate analoga. Competitive inhibitors (antagonists) also serve as targeted blockers of enzyme reactions in therapy. As a natural regulatory principle, this inhibition type mostly appears in the form of product inhibition (Section 2.4.3). Product accumulation in the course of a reaction causes increasing enzyme inhibition so that product can form only in limited quantities, even at a substrate surplus, and does not accumulate in the cell.

Although competitive inhibition is usually regarded to be caused by a structural analogy between substrate and inhibitor, this inhibition type is sometimes found in widely varying compounds. Cibracon dyes, which are structurally different, compete for the NAD binding site in dehydrogenases – a fact that is also used in affinity chromatography. Reversely, a competitive inhibition pattern is not conclusive for competition. O-phenanthrolin is competitive with NAD in alcohol dehydrogenase, but the inhibition actually is based on complex formation with active zinc ions (Bowie and Branden, 1977). Also partially competitive inhibition based on a completely different mechanism shows a similar straight line pattern (Section 2.5.1.7).

2.5.1.4 Uncompetitive Inhibition

This rare type of inhibition binds the inhibitor exclusively to the enzyme-substrate complex. Such a mechanism will be realized when the binding site for the inhibitor is only formed in interaction with substrate:

$$\begin{array}{ccccccccc} \mathrm{E} & + & \mathrm{A} & \underset{k_{-1}}{\overset{k_1}{\rightleftharpoons}} & \mathrm{EA} & \xrightarrow{k_2} & \mathrm{E} & + & \mathrm{P} \\ & & & & + & & & & \\ & & & & \mathrm{I} & & & & \\ & & & & k_4 \Vert \backslash k_{-4} & & & & \\ & & & & \mathrm{EAI} & & & & \end{array} \qquad (2.82)$$

In Eq. (2.65) for the non-competitive inhibitions K_{ic} must be disregarded:

$$v = \frac{V[\mathrm{A}]}{K_m + \left(1 + \frac{[\mathrm{I}]}{K_{iu}}\right)[\mathrm{A}]} \; . \qquad (2.83)$$

Equation after Lineweaver-Burk:

$$\frac{1}{v} = \frac{1 + \frac{[\mathrm{I}]}{K_{iu}}}{V} + \frac{K_m}{V[\mathrm{A}]} \; , \qquad (2.84)$$

Equation after Hanes:

$$\frac{[A]}{v} = \frac{[A]\left(1 + \frac{[I]}{K_{iu}}\right)}{V} + \frac{K_m}{V} \ , \tag{2.85}$$

Equation after Eadie-Hofstee:

$$v = \frac{V}{1 + \frac{[I]}{K_{iu}}} - \frac{K_m}{\left(1 + \frac{[I]}{K_{iu}}\right)} \cdot \frac{v}{[A]} \ , \tag{2.86}$$

and after Dixon:

$$\frac{1}{v} = \frac{1}{V}\left(1 + \frac{K_m}{[A]}\right) + \frac{[I]}{VK_{iu}} \ . \tag{2.87}$$

The steepness of hyperbolae is similar at low substrate concentrations, both in the absence and the presence of the inhibitor, at higher concentrations the curves move towards differing saturation values. The double reciprocal and the Dixon plots both yield parallels (Figures 2.20 B and F). The *uncompetitive inhibition constant* K_{iu} is obtained from a secondary plot of the ordinate sections. In the direct linear plot the intercepts tend straight downwards (Figure 2.20 E). The integrated Michaelis-Menten equation for this type of inhibition is:

$$\frac{K_m}{\left(1 + \frac{[I]}{K_{iu}}\right)} \ln \frac{[A]_0}{[A]} + [A]_0 - [A] = \frac{Vt}{\left(1 + \frac{[I]}{K_{iu}}\right)} \tag{2.88}$$

and linearised:

$$\frac{[A]_0 - [A]}{t} = \frac{V}{1 + \frac{[I]}{K_{iu}}} - \frac{K_m \ln \frac{[A]_0}{[A]}}{\left(1 + \frac{[I]}{K_{iu}}\right)t} \ . \tag{2.89}$$

A joint abscissa intercept is obtained. A secondary plot of the reciprocal ordinate sections against the inhibitor concentrations yields $-K_{iu}$ as an abscissa section.

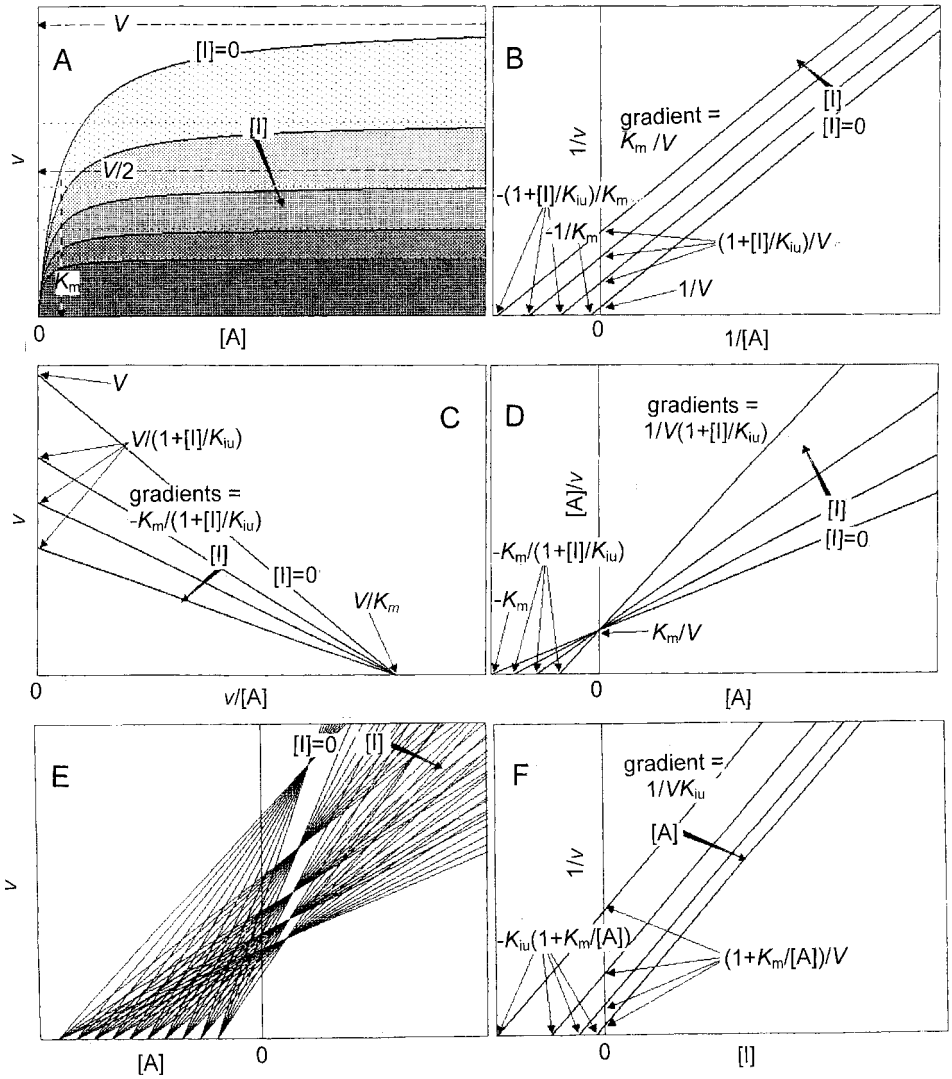

Figure 2.20. Uncompetitive inhibition in different representations. (A) Direct plot, (B) double reciprocal plot, (C) Eadie-Hofstee plot, (D) Hanes plot, (E) direct linear plot, (F) inhibition plot after Dixon (1953). The determination of the kinetic constants from these plots is indicated.

2.5.1.5 Partial Inhibition Mechanisms, Partially Non-Competitive Inhibition

The reaction scheme (2.56) and the rate equation (2.63) for this type of inhibition have already been described representatively for all reversible enzyme inhibitions (Section 2.5.1.1). The double reciprocal form reads:

$$\frac{1}{v} = \frac{K_m\left(1 + \frac{[I]}{K_{ic}}\right)}{\left(V_1 + \frac{V_2[I]}{K_{iu}}\right)[A]} + \frac{1 + \frac{[I]}{K_{iu}}}{V_1 + \frac{V_2[I]}{K_{iu}}}, \tag{2.90}$$

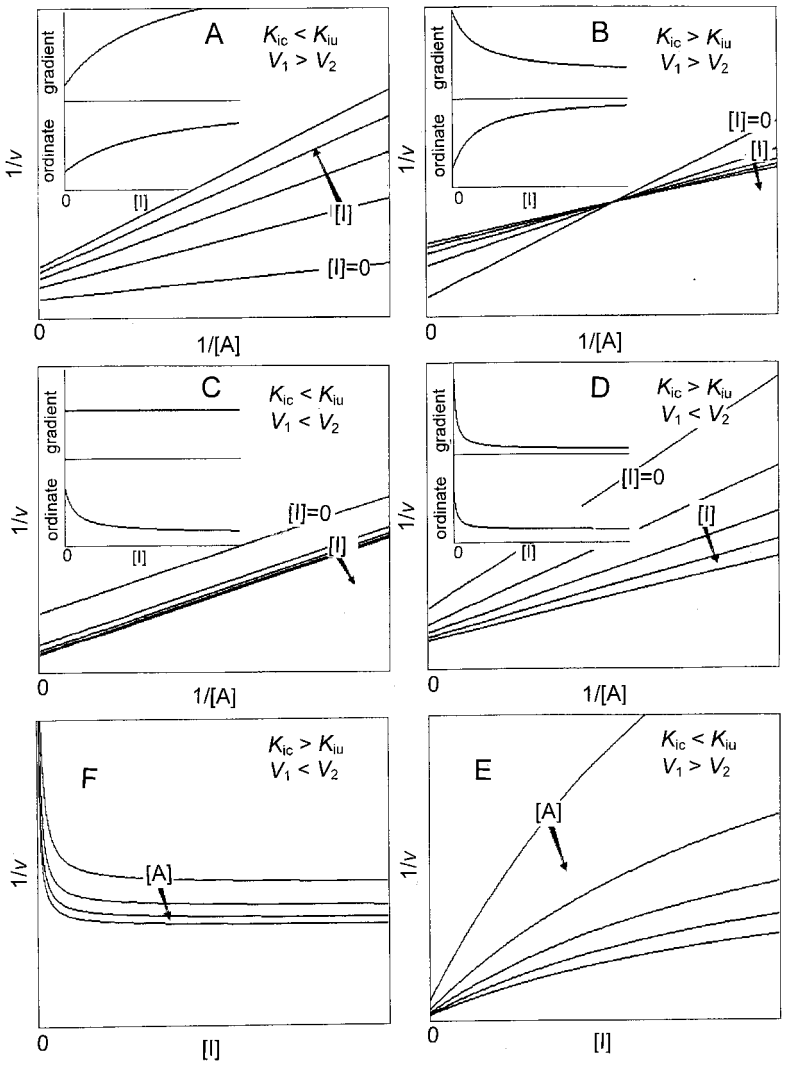

Figure 2.21. Partially non-competitive inhibition in a double-reciprocal plot (A–D) and in the Dixon plot (E, F) in various combinations of inhibition constants and maximum velocities. The inserts show secondary plots of gradients and ordinate intercepts set against inhibitor concentrations.

after Hanes:

$$\frac{[A]}{v} = \frac{K_m\left(1+\frac{[I]}{K_{ic}}\right)}{V_1+\frac{V_2[I]}{K_{iu}}} + \frac{\left(1+\frac{[I]}{K_{iu}}\right)[A]}{V_1+\frac{V_2[I]}{K_{iu}}} \quad , \tag{2.91}$$

after Eadie-Hofstee:

$$v = \frac{V_1+\frac{V_2[I]}{K_{iu}}}{1+\frac{[I]}{K_{iu}}} - \frac{K_m\left(1+\frac{[I]}{K_{ic}}\right)}{\left(1+\frac{[I]}{K_{iu}}\right)} \cdot \frac{v}{[A]} \quad . \tag{2.92}$$

Also partial inhibitions show linear dependencies in all three diagrams and the relative position for the straight lines is often similar to the respective complete inhibition types. However, a larger variety of curve patterns is possible because the additional turnover rate k_6 for the EAI complex can also be varied. This complicates the identification and analysis of this type of inhibition. Figure 2.21 shows some of these combinations. The possible location of a common intercept in the first quadrant of the double reciprocal plot is also remarkable (Figure 2.21B). Characteristic for partial inhibitions and a criterion for discrimination from complete inhibitions is the fact that all plots with the inhibitor are variable, i.e., secondary and Dixon plots do not yield straight lines (Figures 2.21E and F and inserts in A–D). A further peculiarity of partial inhibition mechanisms is that they describe *activations*, even in two different ways. For $k_6 > k_2$ the EAI complex becomes more active than the EA complex. For $K_{ic} > K_{iu} \approx K_A > K_{Ai}$ the equilibrium shifts from the inactive E and EI forms to the active EA and EAI complexes.

2.5.1.6 Partially Uncompetitive Inhibition

This inhibition type is a special form of uncompetitive inhibition when the ternary EAI complex is still active:

$$\begin{array}{ccccccc} E & + & A & \underset{k_{-1}}{\overset{k_1}{\rightleftharpoons}} & EA & \xrightarrow{k_2} & E + P \\ & & & & + & & \\ & & & & I & & \\ & & & & k_4 \downarrow\uparrow k_{-4} & & \\ & & & & EAI & \xrightarrow{k_6} & EI + P \end{array} \tag{2.93}$$

The rate equation for this inhibition type is:

$$v = \frac{\left(V_1+\frac{V_2[I]}{K_{iu}}\right)[A]}{K_m+\left(\frac{1+[I]}{K_{iu}}\right)[A]} \quad , \tag{2.94}$$

in the double reciprocal form:

$$\frac{1}{v} = \frac{K_m}{\left(V_1 + \frac{V_2[I]}{K_{iu}}\right)[A]} + \frac{1 + \frac{[I]}{K_{iu}}}{V_1 + \frac{V_2[I]}{K_{iu}}} , \tag{2.95}$$

after Hanes:

$$\frac{[A]}{v} = \frac{K_m}{V_1 + \frac{V_2[I]}{K_{iu}}} + \frac{\left(1 + \frac{[I]}{K_{iu}}\right)[A]}{V_1 + \frac{V_2[I]}{K_{iu}}} , \tag{2.96}$$

after Eadie–Hofstee:

$$v = \frac{V_1 + \frac{V_2[I]}{K_{iu}}}{1 + \frac{[I]}{K_{iu}}} - \frac{K_m}{\left(1 + \frac{[I]}{K_{iu}}\right)} \cdot \frac{v}{[A]} . \tag{2.97}$$

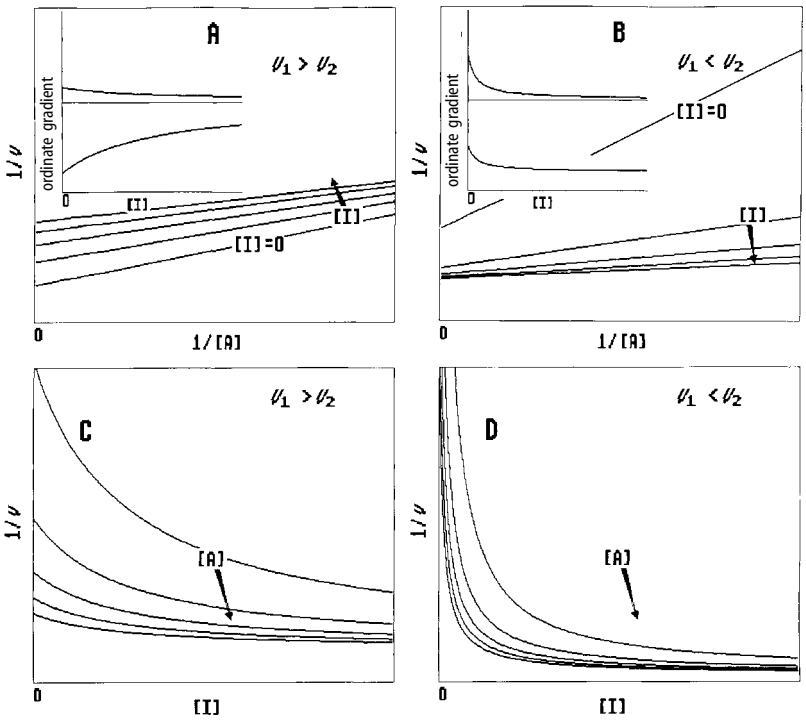

Figure 2.22. Partially uncompetitive inhibition on the double reciprocal plot (A, B) and in the Dixon plot (C, D) in various combinations of maximum velocities. The inserts show secondary plots of gradients and ordinate intercepts set against inhibition concentrations.

The diagrams may deviate from those of complete uncompetitive inhibition, i.e., the lines in the double reciprocal plot must no longer be parallel (Figures 2.22 A, B). Dixon and secondary plots are non-linear (Figures 2.22 A, C), and also activation may occur (Figure 2.22 B, D).

2.5.1.7 Partially Competitive Inhibition

Observing the inhibition mechanisms uncompetitive and non-competitive inhibitions may occur both as complete and partial inhibition types. This should not apply to competitive inhibition as there is no active EAI complex. The conformity of partial and complete competitive inhibition, however, does not rest in the mechanism but in the comparable curve pattern of the various plots. This fact may cause serious misinterpretations, which can, however, easily be prevented, because Dixon and secondary plots are non-linear (Figure 2.23). Properly this is a partially non-competitive inhibition in which the inhibitor does not affect the turnover rate, i.e., $k_2 = k_6$:

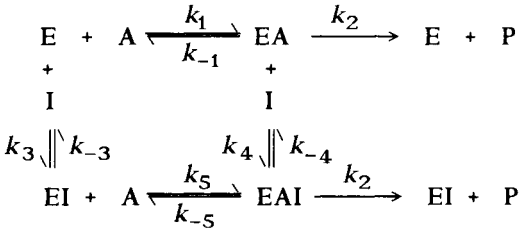

(2.98)

The rate equation for this inhibition type is:

$$v = \frac{V[\mathrm{A}]}{K_\mathrm{m} \cdot \dfrac{\left(1 + \dfrac{[\mathrm{I}]}{K_\mathrm{ic}}\right)}{\left(1 + \dfrac{[\mathrm{I}]}{K_\mathrm{iu}}\right)} + [\mathrm{A}]}\,, \tag{2.99}$$

after Lineweaver-Burk:

$$\frac{1}{v} = \frac{1}{V} + \frac{K_\mathrm{m}\left(1 + \dfrac{[\mathrm{I}]}{K_\mathrm{ic}}\right)}{V\left(1 + \dfrac{[\mathrm{I}]}{K_\mathrm{iu}}\right)} \cdot \frac{1}{[\mathrm{A}]}\,, \tag{2.100}$$

after Hanes:

$$\frac{[\mathrm{A}]}{v} = \frac{[\mathrm{A}]}{V} + \frac{K_\mathrm{m}\left(1 + \dfrac{[\mathrm{I}]}{K_\mathrm{ic}}\right)}{V\left(1 + \dfrac{[\mathrm{I}]}{K_\mathrm{iu}}\right)}\,, \tag{2.101}$$

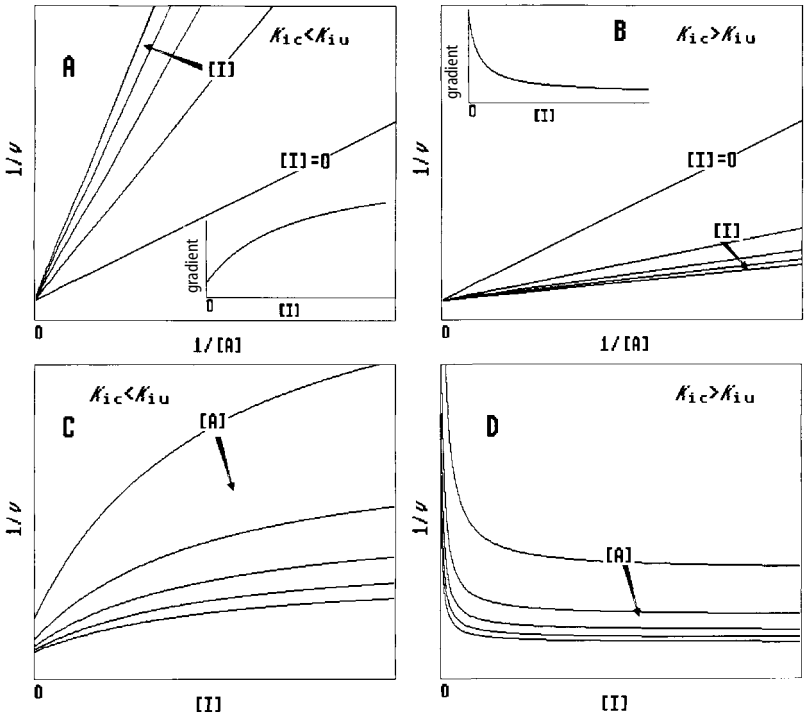

Figure 2.23. Partially competitive inhibition in double reciprocal plots (A, B) and in Dixon plots (C, D) in various combinations of inhibition constants. The inserts show secondary plots of gradients set against inhibition concentrations.

and after Eadie-Hofstee:

$$v = V - \frac{K_m\left(1+\frac{[I]}{K_{ic}}\right)}{\left(1+\frac{[I]}{K_{iu}}\right)} \cdot \frac{v}{[A]} \ . \tag{2.102}$$

It is remarkable that all inhibition types discussed so far contain the term *competitive*, although it applies to only one of these inhibitions. Originally, inhibitions were classified according to the straight line patterns in the linearised diagrams, e.g., the double reciprocal plot. According to this, a distinction is made between a competitive inhibition with a straight line intercept on the ordinate at the one hand, and a non-competitive inhibition with an intercept on the abscissa at the other. If the intercept is located in between, the inhibition was termed *mixed*. Parallel lines were ascribed to a uncompetitive inhibition. How far these terms are away from the actual mechanism becomes evident in the fact that "mixed inhibition" is not a consistent term. For $K_{ic}<K_{iu}$ there would be a mix of competitive and non-competitive inhibitions, for $K_{ic}>K_{iu}$ a mix of uncompetitive and non-competitive inhibitions, and the partially

competitive inhibition is by no means competitive. Competitive inhibition in its strict sense is understood as competition of two ligands (substrate and inhibitor) for the same binding site. This is an exclusive process. If replacement is not complete, both ligands cannot bind to the same site, the inhibition must be non-competitive, although both ligands may perturb one another in their binding.

2.5.1.8 Non- and Uncompetitive Product Inhibition

Competitive product inhibition resulting from reversibility of an enzyme reaction has already been described in Section 2.4.3. Product can also act as a non- or uncompetitive inhibitor, especially in multi-substrate reactions. In the corresponding rate equations, the term for [I] must be substituted by [P], neglecting the reverse reaction. The respective straight line patterns follow the corresponding inhibition type. The inhibition constants are to be taken as product binding constants.

Integration of Eq. (2.65) for the case of non-competitive product inhibition results in the following term, setting $[P]=[A]_0-[A]$:

$$K_m\left(1+\frac{[A]_0}{K_{ic}}\right)\cdot\ln\frac{[A]_0}{[A]}+\left(1-\frac{K_m}{K_{ic}}\right)[P]+\frac{[P]^2}{2K_{iu}}=Vt\ . \tag{2.103}$$

Because of the quadratic term this relationship cannot be converted into a linear equation according to the linearisation method of the integrated Michaelis-Menten equation, as demonstrated for plotting of $([A]_0-[A])/t$ against $1n\,([A]_0/[A])/t$:

$$\frac{[A]_0-[A]}{t}=\frac{V}{1+\dfrac{[A]_0-[A]}{2K_{iu}}-\dfrac{K_m}{K_{ic}}}-\frac{K_m\left(1+\dfrac{[A]_0}{K_{ic}}\right)}{1+\dfrac{[A]_0-[A]}{2K_{iu}}-\dfrac{K_m}{K_{ic}}}\cdot\frac{\ln\dfrac{[A]_0}{[A]}}{t}\ . \tag{2.104}$$

By adding a constant amount of product [P] from the start of the reaction, Eq. (2.104) becomes:

$$\frac{[A]_0-[A]}{t}=\frac{V}{1+\dfrac{[P]_0}{K_{iu}}+\dfrac{[A]_0-[A]}{2K_{iu}}-\dfrac{K_m}{K_{ic}}}-\frac{K_m\left(1+\dfrac{[A]_0}{K_{ic}}\right)}{1+\dfrac{[P]_0}{K_{iu}}+\dfrac{[A]_0-[A]}{2K_{iu}}-\dfrac{K_m}{K_{ic}}}\cdot\frac{\ln\dfrac{[A]_0}{[A]}}{t}\ . \tag{2.105}$$

As non-competitive inhibition also includes competitive and uncompetitive inhibitions, their equations can be obtained by reduction of Eqs. (2.103–2.105), setting

$K_{iu} = \infty$ for competitive, $K_{ic} = \infty$ for uncompetitive inhibition. An evaluation of progress curves for the identification of the type of inhibition can be performed with the Foster and Niemann method described in Section 2.4.3.

2.5.1.9 Substrate Inhibition

This frequent type of inhibition, also called *substrate surplus inhibition*, is identified when at high substrate concentrations the reaction rate declines again, instead of approaching the maximum velocity. This is caused by the fact that apart from the substrate molecule to be converted into product, another substrate molecule binds to the enzyme and inhibits the reaction. Assuming that the first binding substrate molecule will always take part in the catalysis (otherwise the enzyme will not be functional), the second molecule acts as an uncompetitive inhibitor, only binding to the enzyme-substrate complex:

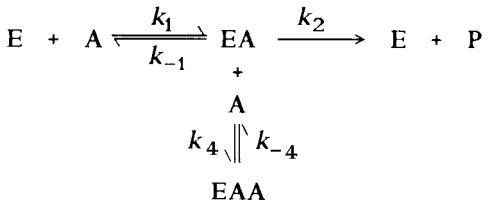

(2.106)

Eqs. (2.83)-(2.87) for uncompetitive inhibition apply by substituting [I] by [A]:

$$v = \frac{V[\mathrm{A}]}{K_m + \left(1 + \frac{[\mathrm{A}]}{K_{iu}}\right)[\mathrm{A}]} \ , \tag{2.107}$$

Lineweaver-Burk equation:

$$\frac{1}{v} = \frac{1 + \frac{[\mathrm{A}]}{K_{iu}}}{V} + \frac{K_m}{V[\mathrm{A}]} \ , \tag{2.108}$$

Hanes equation:

$$\frac{[\mathrm{A}]}{v} = \frac{[\mathrm{A}]\left(1 + \frac{[\mathrm{A}]}{K_{iu}}\right)}{V} + \frac{K_m}{V} \ , \tag{2.109}$$

Eadie-Hofstee equation:

$$v = \frac{V}{1 + \dfrac{[\mathrm{A}]}{K_{\mathrm{iu}}}} - \frac{K_{\mathrm{m}}}{\left(1 + \dfrac{[\mathrm{A}]}{K_{\mathrm{iu}}}\right)} \cdot \frac{v}{[\mathrm{A}]} \ , \tag{2.110}$$

Dixon equation:

$$\frac{1}{v} = \frac{1}{V}\left(1 + \frac{K_{\mathrm{m}}}{[\mathrm{A}]}\right) + \frac{[\mathrm{A}]}{VK_{\mathrm{iu}}} \ . \tag{2.111}$$

As the same compound acts both as substrate and inhibitor at the same time, the two opposing effects cannot be shown separately. The linearised plots do not yield straight lines. The mode of deviation identifies the substrate inhibition, e.g., the reversion of the course of the curve to the ordinate in the double reciprocal plot (Figure 2.24 A), but determining the constants is more difficult, as even the Michaelis constant cannot be determined in the absence of inhibitor. To obtain an approximation, it may be assumed that the inhibitory effect is negligible at minimal substrate concentrations. K_{m} and V can be estimated from an asymptote to the curve in this region, (Figure 2.24A). In a similar way, K_{iu} is obtained from the abscissa intercept with an asymptote of the Dixon plot to the points at high substrate concentrations where the inhibitory effect predominates.

Progress curves also cannot be linearised by integration of Eq. (2.107):

$$\frac{[\mathrm{A}]_0 - [\mathrm{A}]}{t} = V - \frac{[\mathrm{A}]_0^2 - [\mathrm{A}]^2}{2K_{\mathrm{iu}}t} - K_{\mathrm{m}} \frac{\ln \dfrac{[\mathrm{A}]_0}{[\mathrm{A}]}}{t} \ . \tag{2.112}$$

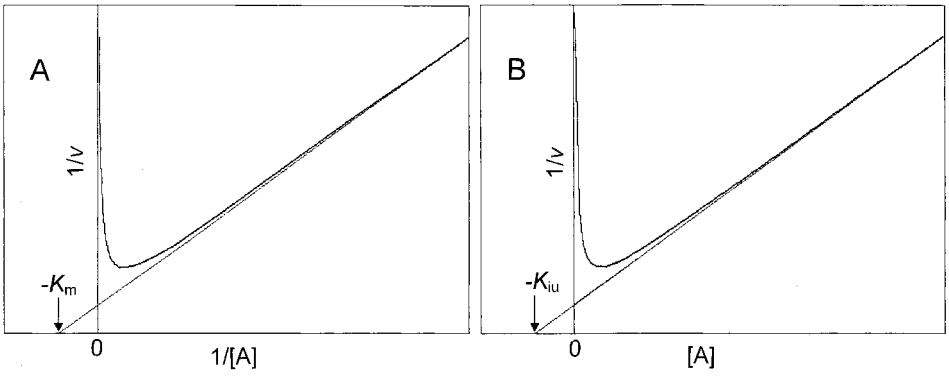

Figure 2.24. Substrate inhibition. (A) Double reciprocal plot, (B) Dixon plot.

2.5.2 Irreversible Enzyme Inhibition

2.5.2.1 Distinction between Reversible and Irreversible Inhibitors

Reversible and irreversible inhibitors have to be discussed separately. Therefore, the nature of inhibition has to be established in advance. In most cases the difference is obvious, i.e., whether covalent interaction of ligand with the enzyme can be excluded by chemical reasons or must be expected because of the presence of reactive groups. Especially in the latter case it cannot always be foreseen whether covalent binding will be actually formed or whether binding only happens by reversible association. For example, the prerequisite of binding of suicide substrates is non-covalent association to the active site because of their substrate analogy, covalent reaction is the succeeding step. Otherwise the analogue will also bind to other reactive sites and be no suicide substrate at all. On the other hand non-covalent binding may lead to (quasi) irreversible inhibitions when they are exceptionally strong ($K_d < 10^{-10}$ M), as is frequently observed in transition state analogues. A distinction between reversible and irreversible inhibition can be established by separating the inhibitor by dialysis, gel filtration, ultrafiltration, etc. In reversible binding total enzyme activity should be restored, while no reactivation may be expected for irreversible binding. Results, however, are not always unequivocal, as the enzyme may suffer from activity loss by the separation procedure, and it will be difficult to distinguish inactivation from inhibition.

A simple, although not always clear-cut method is measuring the enzyme activity of an enzyme-inhibitor mix before and after a defined dilution. If an enzyme solution is, e.g., diluted by a factor of 10, its activity will be reduced by the same factor. If part of the enzyme was inactivated by covalent binding of an inhibitor before dilution, the remaining activity will be equally reduced by dilution. A reversible inhibitor, in contrast, will partly dissociate upon dilution and the resulting enzyme activity will be higher than expected from the dilution effect.

A reliable and simple test is the determination of the time dependence of the inhibition effect. A reversible inhibitor immediately reduces enzyme activity to a constant time-independent value (Figure 2.25 A). An irreversible inhibitor will exponentially reduce enzyme activity (pseudo first order reaction). This effect is due to the concentration dependence of the (actually existing) second order reaction that permits reduction of the inhibitor to such a small amount, which allows to follow up the time course of the reaction. At this low concentration the inhibitory effect may not be detectable at the start, but if the inhibitor has at least the same molar concentration as the enzyme (at stoichiometric binding to the enzyme), it will finally inactivate all enzyme molecules.

The stoichiometry of binding can be determined from the dependence of enzyme activity on inhibitor concentration. In the case of strong binding the enzyme activity declines nearly linear in the lower and middle concentration range of the inhibitor. The share of inhibitor bound per added enzyme is obtained by extrapolation to the abscissa (Figure 2.25 B).

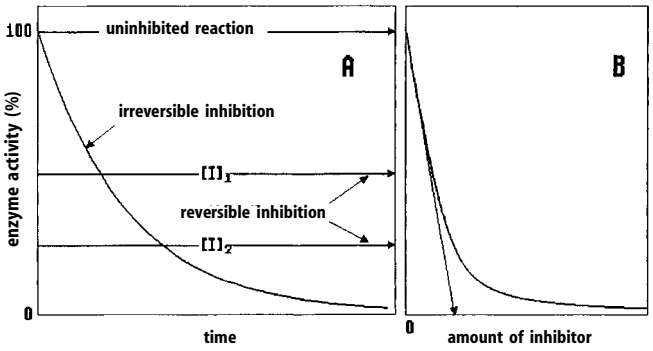

Figure 2.25. Time course of an irreversible and a reversible inhibition (A) and determination of the share of irreversibly bound inhibitor (B).

2.5.2.2 Characterisation of Irreversible Inhibitions

Irreversible binding of inhibitor to an enzyme can be described by the following reaction scheme:

$$E + I \underset{k_{-1}}{\overset{k_1}{\rightleftharpoons}} EI \xrightarrow{k_2} EI_i$$

The inhibitor initially forms an non-covalent association complex EI with the enzyme, which will be transformed by an irreversible process into the inactive complex EI_i. The total enzyme amount $[E]_0$ will be distributed between all enzyme forms:

$$[E]_0 = [E] + [EI] + [EI]_i = [E]_a + [EI]_i \; . \tag{2.114}$$

[E] and [EI] is the share of active enzyme $[E]_a$, as with surplus substrate the inhibitor will be displaced from [EI] in the enzyme test. In analogy to the Michaelis-Menten equation, and assuming $[I] \gg [E]_0$, the time-dependent formation of the inactive enzyme form $[EI]_i$ is directly proportional to the concentration of the reversible [EI] complex:

$$\frac{d[EI]_i}{dt} = \frac{d([E]_0 - [E]_a)}{dt} = k_2[EI] \; .$$

The total amount of enzyme $[E]_0$ remains constant, $d[E]_0/dt = 0$:

$$-\frac{d[E]_a}{dt} = k_2[EI] \; . \tag{2.115}$$

[EI] can be replaced from Eq. (2.114), considering the inhibition constant for the reversible binding of inhibitor $K_i = [E][I]/[EI]$:

$$[E]_a = [EI] + [E] = [EI] + \frac{[EI]K_i}{[I]}$$

thus [EI] is eliminated from Eq. (2.115):

$$\frac{d[E]_a}{dt} = \frac{k_2[E]_a}{1 + \frac{K_i}{[I]}} .$$

Integration from $[E]_0$ at time $t=0$ to $[E]_a$ at time t:

$$-\int_{[E]_0}^{[E]_a} \frac{d[E]_a}{[E]_a} = \int_{t=0}^{t} \frac{k_2 dt}{1 + \frac{K_i}{[I]}}$$

results in:

$$\ln \frac{[E]_a}{[E]_0} = -\frac{k_2 t}{1 + \frac{K_i}{[I]}} \qquad (2.116\,a)$$

or in logarithm of ten:

$$\log \frac{[E]_a}{[E]_0} = -\frac{k_2 t}{2.3\left(1 + \frac{K_i}{[I]}\right)} . \qquad (2.116\,b)$$

Plotting of the residual activities of the enzyme log ($[E]_a/[E]_0$) against the incubation time t yields straight lines for different inhibitor concentrations (Figure 2.26 A) whose gradients Sl have the value:

$$Sl = \frac{k_2}{1 + \frac{K_i}{[I]}} \qquad (2.117)$$

The reciprocal values of the gradients plotted against the reciprocal inhibitor concentrations yield a linear function:

$$\frac{1}{Sl} = \frac{1}{k_2} + \frac{K_i}{k_2[I]} \qquad (2.118)$$

with $1/k_2$ and $-1/K_i$ as ordinate and abscissa intercepts, respectively (Figure 2.26 B).

If a second ligand A (e.g., the substrate) competes for the inhibitor binding site, Eq. (2.116) has to be extended by the term $1+[A]/K_A$ in the denominator:

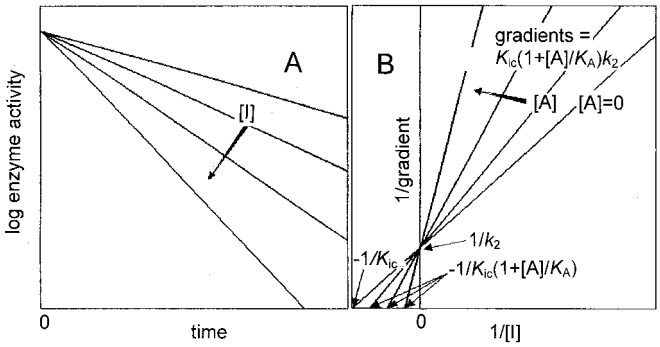

Figure 2.26. Representation of an irreversible inhibition. (A) Semi-logarithmic diagram for different inhibition concentrations, (B) secondary plot of the slopes from plot (A) for several substrate concentrations.

$$\ln\frac{[\mathrm{E}]_a}{[\mathrm{E}]_0} = \frac{k_2 t}{\left(1+\frac{K_i}{[\mathrm{I}]}\right)\left(1+\frac{[\mathrm{A}]}{K_A}\right)} \quad . \tag{2.119}$$

The equation for the gradient has then to be extended correspondingly:

$$\frac{1}{Sl} = \frac{1}{k_2} + \frac{K_i\left(1+\frac{[\mathrm{A}]}{K_A}\right)}{k_2[\mathrm{I}]} \quad . \tag{2.120}$$

Different straight lines are obtained for different concentrations of A, and K_a can be calculated either from their intercept with the abscissa or be taken from a secondary plot of the gradients of this diagram plotted against [A].

2.5.3 Enzyme Reactions with Two Competing Substrates

Because of their strict specificity enzymes preferably react with a certain substrate A_1 to produce product P_1, but often the enzyme also accepts homologous compounds of the substrate (A_2), which may be converted to the respective product (P_2):

$$\begin{array}{rcccc} & \mathrm{A_1} & \underset{k_{-1}}{\overset{k_1}{\rightleftharpoons}} & \mathrm{EA_1} & \xrightarrow{k_2} & \mathrm{E+P_1} \\ \mathrm{E} & + & & & & \\ & \mathrm{A_2} & \underset{k_{-3}}{\overset{k_3}{\rightleftharpoons}} & \mathrm{EA_2} & \xrightarrow{k_4} & \mathrm{E+P_2}\,. \end{array} \tag{2.121}$$

One of the substrates, usually the native one, will be more effective than the other. If both substrates are added simultaneously, the poorer one will impede the better one, the overall turnover rate will decline. The situation becomes more complex as the ef-

ficiency of both substrates as to binding and catalysis may differ and sometimes counteract each other. One substrate may be bound with higher affinity but evolve a slower turnover than the second one.

Assuming steady-state:

$$\frac{\mathrm{d}[\mathrm{EA}_1]}{\mathrm{d}t} = k_1[\mathrm{E}][\mathrm{A}_1] - (k_{-1} + k_2)[\mathrm{EA}_1] = 0 \,, \tag{2.122}$$

$$\frac{\mathrm{d}[\mathrm{EA}_2]}{\mathrm{d}t} = k_3[\mathrm{E}][\mathrm{A}_2] - (k_{-3} + k_4)[\mathrm{EA}_2] = 0 \,, \tag{2.123}$$

$$v = k_2[\mathrm{EA}_1] + k_4[\mathrm{EA}_2] \,, \tag{2.124}$$

$$[\mathrm{E}]_0 = [\mathrm{E}] + [\mathrm{EA}_1] + [\mathrm{EA}_2] \,. \tag{2.125}$$

Replacement of [E] from Eq. (2.125) in Eq. (2.122) and Eq. (2.123) gives:

$$[\mathrm{EA}_2] = [\mathrm{E}]_0 - [\mathrm{EA}_1]\left(1 + \frac{k_{-1} + k_2}{k_1[\mathrm{A}_1]}\right) \tag{2.126}$$

$$[\mathrm{EA}_1] = [\mathrm{E}]_0 - [\mathrm{EA}_2]\left(1 + \frac{k_{-3} + k_4}{k_3[\mathrm{A}_2]}\right) \tag{2.127}$$

and insertion of Eq. (2.126) into Eq. (2.127), considering $K_{\mathrm{m1}} = (k_{-1} + k_2)/k_1$ and $K_{\mathrm{m2}} = (k_{-3} + k_4)/k_3$:

$$[\mathrm{EA}_1] = \frac{K_{\mathrm{m2}}[\mathrm{E}]_0[\mathrm{A}_1]}{K_{\mathrm{m2}}[\mathrm{A}_1] + K_{\mathrm{m1}}[\mathrm{A}_2] + K_{\mathrm{m1}}K_{\mathrm{m2}}} \,, \tag{2.128 a}$$

$$[\mathrm{EA}_2] = \frac{K_{\mathrm{m1}}[\mathrm{E}]_0[\mathrm{A}_2]}{K_{\mathrm{m2}}[\mathrm{A}_1] + K_{\mathrm{m1}}[\mathrm{A}_2] + K_{\mathrm{m1}}K_{\mathrm{m2}}} \,. \tag{2.128 b}$$

Inserting Eq. (2.128 a) and Eq. (2.128 b) into Eq. (2.124) results in the rate equation for a reaction with two alternate substrates, setting $V_1 = k_2\,[\mathrm{E}]_0$ and $V_2 = k_4\,[\mathrm{E}]$:

$$v = \frac{V_1K_{\mathrm{m2}}[\mathrm{A}_1] + V_2K_{\mathrm{m1}}[\mathrm{A}_2]}{K_{\mathrm{m2}}[\mathrm{A}_1] + K_{\mathrm{m1}}[\mathrm{A}_2] + K_{\mathrm{m1}}K_{\mathrm{m2}}} \,. \tag{2.129}$$

Figure 2.27 demonstrates such a mechanism in the double reciprocal plot, varying the more active substrate at constancy of the poorer one. There are obvious deviations from linearity and crossing of the curves in the first quadrant.

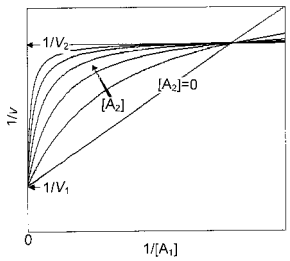

Figure 2.27. Reaction with two alternate substrates in a double reciprocal representation. The maximum velocity V_1 of the varying substrate A_1 is higher than V_2 of the constant substrate A_2. In the reverse case the curves will deviate downward and tend towards the lower value $1/V_1$. The Michaelis constants of both substrates are assumed equal.

2.6 Multi-Substrate Reactions

2.6.1 Nomenclature

For the enzyme reactions discussed so far it was assumed that only one substrate molecule participates in the catalytic turnover. In most enzyme reactions, however, two or even three substrates may take part. This could restrict the relevance of the previous discussions to a large extent. The Michaelis–Menten model proves, however, to be also principally valid for this wider aspect, as long as the dependence of only one substrate is studied and the other substrates and cofactors are kept in a large, practically saturating, surplus. In this way, the kinetic constants of the varied substrate are obtained, but no information is given on the existing multi-substrate mechanism. A comprehensive analysis of such complex reactions requires the mutual variations of all participating substrates. R.A. Alberty (1959), K. Dalziel (1957), and especially W. Wallace Cleland (1963) have described multi-substrate reactions in detail. The following treatment keeps essentially to the concise nomenclature introduced by Cleland.

Substrates are termed in the sequence of their binding to the enzymes as A, B, C, products in the sequence of their release P, Q, R. Different enzyme states are named E, F, G. With substrates and products the enzyme forms *transitory complexes*, EA, EP, etc., that decay in a unimolecular step releasing substrate or product. Catalytic reactions occur from *central complexes* which are set in brackets to distinguish them from transitory complexes, e.g., (EAB). Central complexes cannot bind further substrate or product as all sites are occupied. Rather they release substrate or product in unimolecular steps. As steady-state kinetics gives no information on the catalytic conversion of substrate into product (and *vice versa*) directly on the enzyme molecule, only one central complex for both states before and after catalysis (EAB-EPQ) is defined. The number of substrates participating in the forward, and that of products participating in the reverse reaction will be adhered in the terms *uni, bi, ter* to the name of the respective reaction mechanisms. Two substrates being converted into one single product is called a *bi-uni* mechanism. Mechanisms where all substrates must bind before product can be released are called *sequential* mechanisms. The binding of substrates may either be *random* or *ordered*. In a *ping-pong* mechanism, product is already released before all substrates are bound. The enzyme exists in two or more forms, modified by groups of the substrate. In the *iso mechanism* the enzyme isomerises into two or more stable conformations.

The reaction equations are presented in a schematic form. Reaction progress is symbolised by a horizontal base line. The various enzyme states are indicated below this line. Substrate binding is indicated by vertical arrows on to the base line, dissociation of product by vertical arrows from the base line. Rate constants are inscribed beside these arrows, at left for the forward, at right for the reverse reaction. The reaction scheme for an *ordered bi-bi mechanism* in conventional mode is:

$$E + A \underset{k_{-1}}{\overset{k_1}{\rightleftharpoons}} EA$$

$$EA + B \underset{k_{-2}}{\overset{k_2}{\rightleftharpoons}} EAB\text{-}EPQ \underset{k_{-3}}{\overset{k_3}{\rightleftharpoons}} EQ + P$$

$$EQ \underset{k_{-4}}{\overset{k_4}{\rightleftharpoons}} E + Q$$

takes the following form:

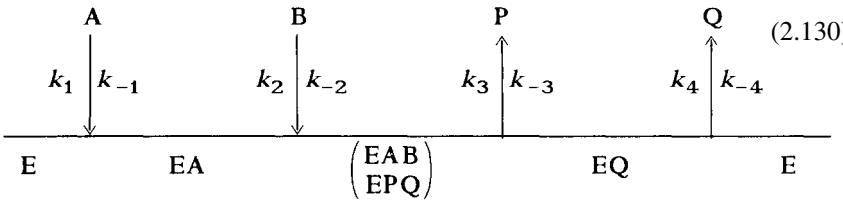

(2.130)

First the most relevant multi-substrate mechanisms are presented, followed by a description of methods to derive complex rate equations.

2.6.2 Random Mechanism

This general multi-substrate mechanism to be found in, e.g., kinases or phosphorylase B, assumes binding of substrates and products in random sequence. In the simplest case, binding is completely independent; there are no mutual interactions. The reaction scheme for a *random bi-bi* mechanism with two substrates and two products is:

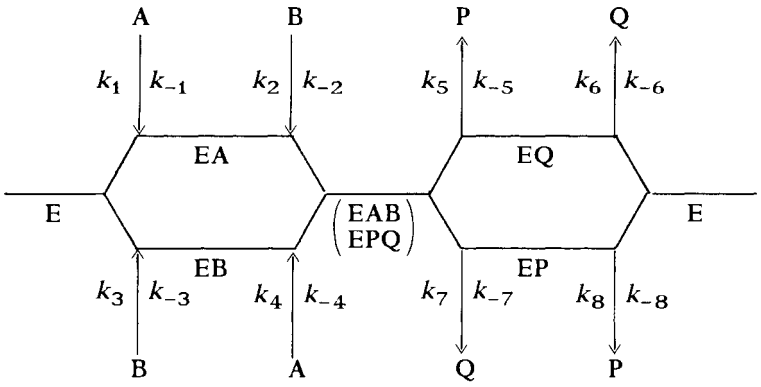

(2.131)

Compared to a reversible one-substrate mechanism with two maximum velocities (V_1 for the forward reaction and V_2 for the reverse reaction) and two Michaelis constants (K_{mA} for substrate and K_{mP} for product) a variety of new constants is created. Each substrate and each product has its own Michaelis constant (K_{mA}, K_{mP}, etc.) for the interaction with the central complex. Each ligand has an additional constant for binding to the free enzyme while forming transitory complexes. These are binding constants termed *inhibition constants* K_i, as in reverse reactions they are identical to the product inhibition constants (see Section 2.5.1.8). For the random bi-bi mechanism there are 10 kinetic constants: two maximum velocities and four inhibition and Michaelis constants each for substrates and products. These constants are not obtainable by simple kinetic analysis as described above. Inhibition and Michaelis constants also are interrelated, similar to the non-competitive inhibition mechanism (Section 2.5.1.2) to which the random bi-bi mechanism shows some parallels: $K_{iA}/K_{iB} = K_{mA}/K_{mB}$ and $K_{iP}/K_{iQ} = K_{mP}/K_{mQ}$. Inhibition and Michaelis constants for the same substrate or product are also equal when their binding is not affected by the cosubstrate or coproduct, e.g., $K_{iA} = K_{mA}$ and $K_{iB} = K_{mB}$.

Because of its alternate reaction pathways the random mechanism in its general form results in a complex rate reaction, and as long as substrate is not available at saturating level, no hyperbolic curves (or linear curves in the respective diagrams) are yielded in dependence of the substrate concentration. A significant simplification is achieved by the assumption of a rapid equilibrium compared with relatively slow conversion of the central ternary complexes (EAB) and (EPQ) (*rapid equilibrium-random mechanism*). The rate equation for the random *bi-bi* mechanism then is:

$$v = \frac{V_1 V_2 \left([A][B] - \frac{[P][Q]}{K_e} \right)}{K_{iA} K_{mB} V_2 + K_{mB} V_2 [A] + K_{mA} V_2 [B] + \frac{K_{mQ} V_1 [P]}{K_e} + \frac{K_{mP} V_1 [Q]}{K_e} + V_2 [A][B] + \frac{V_1 [P][Q]}{K_e}} . \tag{2.132}$$

K_e is the equilibrium constant of the overall reaction. For the determination of initial velocities in the forward reaction, i.e., $[P] = [Q] = 0$, Eq. (2.132) is reduced to:

$$v = \frac{V_1 [A][B]}{K_{iA} K_{mB} + K_{mB} [A] + K_{mA} [B] + [A][B]} . \tag{2.133}$$

If one of the two substrates is kept constant, it can be seen that the Michaelis-Menten equation attains its original form, and hyperbolic dependencies can be expected. Linearisation methods as the Lineweaver-Burk plot can be applied:

$$\frac{1}{v} = \frac{K_{iA} K_{mB}}{V_1 [A][B]} + \frac{K_{mA}}{V_1 [A]} + \frac{K_{mB}}{V_1 [B]} + \frac{1}{V_1} . \tag{2.134}$$

If one substrate, e.g., [A], is varied in one measurement series, while [B] is kept constant within the same series, but changed in the following series, this results in

straight lines with an intercept left to the ordinate in the double reciprocal plot (Figure 2.28 B). Again, in analogy to the non-competitive inhibition, the relative position of the intercept depends on the ratio of the constants and thus on the interactions of the two substrates. Without any interaction, i.e., for $K_{iA} = K_{mA}$ and $K_{iB} = K_{mB}$, the intercept is directly on the abscissa and has the value $-1/K_{mA}$ or $-1/K_{mB}$ if the cosubstrate is varied. In reversible reactions, the Michaelis constants for the reverse reaction can be obtained correspondingly. Thus all kinetic constants are easily accessible for this uncomplicated case. For $K_{iA} < K_{mA}$, $K_{iB} < K_{mB}$ the common intercept lies above the abscissa and for $K_{iA} > K_{mA}$, $K_{iB} > K_{mB}$ below the abscissa and has the coordinates shown in Figure 2.28 B. Regardless whether [A] or [B] is the variable within a measurement series, a similar straight line pattern is obtained. For determination of the Michaelis and inhibition constants the secondary plot method discussed above in inhibition kinetics can be recommended. Linearity in these plots is an additional test for the assumed mechanism (Table 2.1). Following Eq. (2.134), the gradient Sl_A of the straight line in the primary plot is:

$$Sl_A = \frac{K_{iA} K_{mB}}{V_1 [B]} + \frac{K_{mA}}{V_1} \ , \tag{2.135}$$

Plotting the gradient against 1/[B] gives a straight line with an abscissa intercept $-K_{mA}/K_{iA}K_{mB}$ (or $-1/K_{mB}$ for $K_{mA} = K_{iA}$). The ordinate intercepts Or_A of the primary plot

$$Or_A = \frac{K_{mB}}{V_1 [B]} + \frac{1}{V_1} \tag{2.136}$$

also plotted against 1/[B], result in a straight line with the abscissa intercept $-1/K_{mB}$. Variations of [B] in the primary plot result in a straight line in a secondary plot from gradients Sl_B plotted against 1/[A]

$$Sl_B = \frac{K_{iA} K_{mB}}{V_1 [A]} + \frac{K_{mB}}{V_1} \tag{2.137}$$

intercepting the abscissa at $-1/K_{iA}$. An abscissa intercept of $-1/K_{mA}$ is yielded from plotting the ordinate intercepts Or_B against 1/[A]:

$$Or_B = \frac{K_{mA}}{V_1 [A]} + \frac{1}{V_1} \ . \tag{2.138}$$

Plotting after Hanes [A]/v against [A], or [B]/v against [B], respectively

$$\frac{[A]}{v} = \frac{1}{V_1} \left(K_{mA} + \frac{K_{iA} K_{mB}}{[B]} \right) + \frac{[A]}{V_1} \left(\frac{1 + K_{mB}}{[B]} \right) \tag{2.139}$$

$$\frac{[B]}{v} = \frac{K_{mB}}{V_1} \left(1 + \frac{K_{iA}}{[A]} \right) + \frac{[B]}{V_1} \left(1 + \frac{K_{mA}}{[A]} \right) \tag{2.140}$$

results in a common intercept left of the ordinate (Figure 2.28 C). Kinetic constants can be obtained from secondary plots, plotting the gradients or the ordinate intercepts against the reciprocal cosubstrate concentration (Table 2.1).

The equations after Eadie-Hofstee, plotting v/[A], respectively v/[B], against v are:

$$v = \frac{V_1}{1 + \frac{K_{mB}}{[B]}} + \frac{v}{[A]} \cdot \frac{K_{mA} + \frac{K_{iA} K_{mB}}{[B]}}{1 + \frac{K_{mB}}{[B]}} \tag{2.141}$$

$$v = \frac{V_1}{1 + \frac{K_{mA}}{[A]}} + \frac{v}{[B]} \cdot \frac{K_{mB}\left(1 + \frac{K_{iA}}{[A]}\right)}{1 + \frac{K_{mA}}{[A]}} \; . \tag{2.142}$$

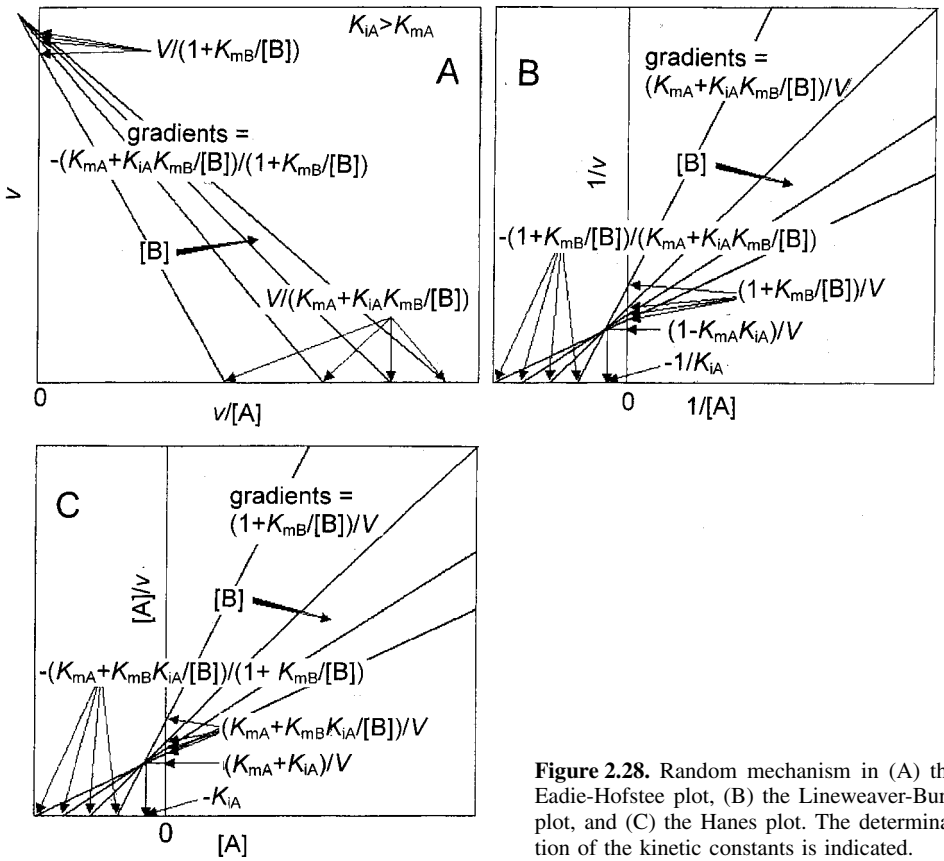

Figure 2.28. Random mechanism in (A) the Eadie-Hofstee plot, (B) the Lineweaver-Burk plot, and (C) the Hanes plot. The determination of the kinetic constants is indicated.

Table 2.2. Abscissa and ordinate intercepts of secondary plots for bisubstrate reactions Sl_A, Sl_B are the gradients, Or_A, Or_B the ordinate intercepts, and Ab_A, Ab_B the abscissa intercepts from the primary plots, with varying [A] or [B], respectively

Primary plot		Secondary plot					
Designation of axis		Designation of axis		Intercepts			
Y	X	Y	X	Random/ordered mechanism		Ping-pong mechanism	
				Ordinate	Ascissa	Ordinate	Abscissa
$1/v$	1/[A]	Sl_A	1/[B]	K_{mA}/V	$-K_{mA}/K_{iA}K_{mB}$		
		Ab_A	1/[B]			$1/K_{mA}$	$-1/K_{mB}$
		Or_A	1/[B]	$1/V$	$-1/K_{mB}$	$1/V$	$-1/K_{mB}$
$1/v$	1/[B]	Sl_B	1/[A]	K_{mB}/V	$-1/K_{iA}$		
		Ab_B	1/[A]			$1/K_{mB}$	$-1/K_{mA}$
		Or_B	1/[A]	$1/V$	$-1/K_{mA}$	$1/V$	$-1/K_{mA}$
[A]/v	[A]	Sl_A	1/[B]	$1/V$	$-1/K_{mB}$	$1/V$	$-1/K_{mB}$
		$1/Ab_A$	1/[B]			K_{mA}	$-1/K_{mB}$
		Or_A	1/[B]	K_{mA}/V	$-K_{mA}/K_{iA}K_{mB}$		
[B]/v	[B]	Sl_B	1/[A]	$1/V$	$-1/K_{mA}$	$1/V$	$-1/K_{mA}$
		$1/Ab_B$	1/[A]			K_{mB}	$-1/K_{mA}$
		Or_B	1/[A]	K_{mB}/V	$-1/K_{iA}$		
v/[A]	v	Sl_A	1/[B]			$-1/K_{mA}$	$-1/K_{mB}$
		$1/Ab_A$	1/[B]	$1/V$	$-1/K_{mB}$	$1/V$	$-1/K_{mB}$
		Or_A	1/[B]	K_{mA}/V	$-K_{mA}/K_{iA}K_{mB}$		
v/[B]	v	Sl_B	1/[A]			$-1/K_{mB}$	$-1/K_{mA}$
		$1/Ab_B$	1/[A]	$1/V$	$-1/K_{mA}$	$1/V$	$-1/K_{mA}$
		Or_B	1/[A]	K_{mB}/V	$1/K_{iA}$		

The joint intercept of the straight lines is located left of the ordinate for $K_{iA} > K_{mA}$ (Figure 2.28 A), for $K_{iA} < K_{mA}$ at the right below the abscissa, and for $K_{iA} = K_{mA}$ parallels are obtained. In the secondary plots the reciprocal abscissa or ordinate intercepts are plotted against the corresponding cosubstrate concentrations (Table 2.2).

2.6.3 Ordered Mechanism

This mechanism, already presented in the reaction scheme (2.130) presumes a strict sequence of substrate binding. The detailed rate equation of an ordered *bi-bi* mechanism is derived in the following paragraph (Eq. (2.168)). Its reduction for the forward reaction is the same Eq. (2.133) already introduced for the rapid equilibrium *random bi-bi* mechanism. This reveals the ordered mechanism to be a special form of the general random mechanism, with maximum substrate interaction, so that the plots described there also apply here. Both mechanisms can only be distinguished from a

Table 2.3. Product inhibition pattern in bisubstrate mechanisms (after Cleland, 1963). C: competitive, NC: non-competitive, UC: uncompetitive, nI: no inhibition

Mechanism	Inhibiting product	Variable substrate			
		A		B	
		Not saturated	Saturated with B	Not saturated	Saturated with A
Ordered *bi-bi*	P	NC	UC	NC	NC
	Q	C	C	NC	nI
Teorell Chance	P	NC	nI	C	C
	Q	C	C	NC	nI
Iso ordered *bi-bi*	P	NC	UC	NC	NC
	Q	NC	NC	NC	UC
Random *bi-bi* Rapid equilibrium	P or Q	C	nI	C	nI
Ping-pong *bi-bi*	P	NC	nI	C	C
	Q	C	C	NC	nI
Iso ping-pong *bi-bi* (isomerisation of the enzyme)	P	NC	nI	C	C
	Q	NC	NC	NC	NC

"pure" random mechanism without any influence on substrate binding and with identical inhibition and Michaelis constants, resulting in a common abscissa intercept in the double reciprocal plot.

Both mechanisms can be distinguished by analysis of product inhibition. The reaction is inhibited in the presence of product. Preferably a product will competitively inhibit the reaction in dependence of the substrate it originated from (e.g., acetaldehyde from ethanol in the case of alcohol dehydrogenase). It will inhibit non-competitively against the cosubstrate (e.g., NAD), as it cannot displace it but will prevent the turnover reaction. The actual conditions within a multi-substrate reaction are more complex and depend on the respective mechanism and saturation with the cosubstrate. The product inhibition pattern is indicative for a special multi-substrate mechanism and besides graphic methods a further criterion for the analysis of such mechanisms (Table 2.3).

Ordered mechanisms are frequently observed in dehydrogenases. In alcohol dehydrogenase there is the exceptional case of the *Teorell-Chance mechanism*, in which the central complex decomposes so rapidly that its stationary concentration is negligible and can be disregarded in the rate equation:

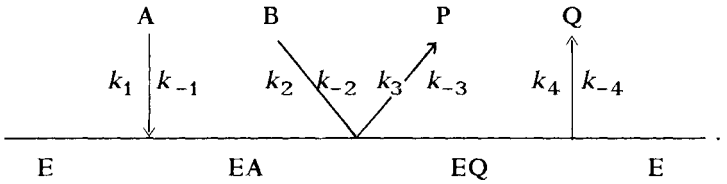

(2.143)

The reduced rate equation of the forward reaction (2.133) holds for this and also for the normal ordered mechanisms, so that no distinction can be made in graphic representations. Because of the absence of the central complex, however, an altered product inhibition occurs (Table 2.3).

If the enzyme isomerises in the central complex from EAB to FPQ

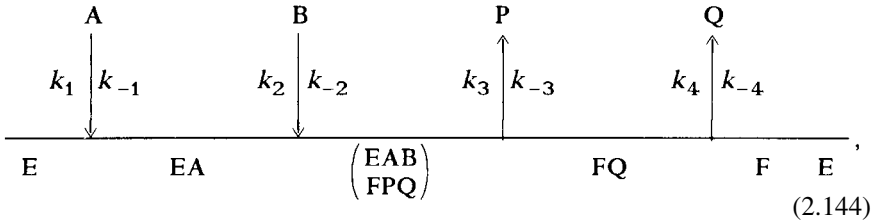

(2.144)

an *iso-ordered mechanism* is created, expressing itself in additional links of the rate equation influencing product inhibition (Table 2.3), but being irrelevant for the forward reaction, so that Eq. (2.133) can be regarded as also valid for this mechanism.

2.6.4 Ping-Pong Mechanism

The name illustrates alternate binding of substrates and release of products characteristic for this mechanism:

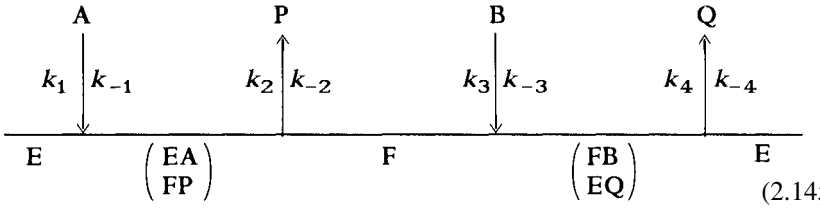

(2.145)

After release of the first product the enzyme retains an intermediary form, usually by taking over a reactive group from the first substrate that is subsequently transferred to the second substrate, forming a second product. The aminotransferase reaction is a typical example. From an amino acid, e.g., aspartate, the amino group is transferred to the pyridoxalphosphate cofactor of the enzyme and is itself released as α-oxo acid (oxalacetate). A second α-oxo acid (α-oxoglutarate) takes over the amino group, forming glutamate. A *multisite ping-pong mechanism* is found in fatty acid synthase. The substrate is passed on by the growing fatty acid chain bound to the central pantetheine residue over 7 catalytic centres.

The general rate equation for the *ping-pong bi-bi mechanism* is derived in Section 2.73. The reduced equation for the forward reaction is:

$$v = \frac{V_1[\mathrm{A}][\mathrm{B}]}{K_{\mathrm{mB}}[\mathrm{A}] + K_{\mathrm{mA}}[\mathrm{B}] + [\mathrm{A}][\mathrm{B}]} \ . \tag{2.146}$$

Differing from the other bisubstrate mechanisms, parallels appear in the double reciprocal plot (Figure 2.29B):

$$\frac{1}{v} = \frac{K_{\mathrm{mA}}}{V_1[\mathrm{A}]} + \frac{K_{\mathrm{mB}}}{V_1[\mathrm{B}]} + \frac{1}{V_1} \ . \tag{2.147}$$

Secondary plots of the ordinate and abscissa intercepts, plotted against the reciprocal cosubstrate concentrations can be drawn (Table 2.2).

In the Hanes plot

$$\frac{[\mathrm{A}]}{v} = \frac{K_{\mathrm{mA}}}{V_1} + \frac{[\mathrm{A}]}{V_1}\left(1 + \frac{K_{\mathrm{mB}}}{[\mathrm{B}]}\right) \tag{2.148}$$

$$\frac{[\mathrm{B}]}{v} = \frac{K_{\mathrm{mB}}}{V_1} + \frac{[\mathrm{B}]}{V_1}\left(1 + \frac{K_{\mathrm{mA}}}{[\mathrm{A}]}\right) \tag{2.149}$$

the straight lines have a joint intercept at K_{mA}/V_1 and K_{mB}/V_1 (Figure 2.29C). Secondary plots can be obtained by plotting the gradients or the abscissa intercepts, respectively, against the reciprocal cosubstrate quantities (Table 2.2).

The Eadie-Hofstee plot also yields a joint straight line intercept on the abscissa (Figure 2.29A):

$$v = \frac{V_1}{1 + \dfrac{K_{\mathrm{mB}}}{[\mathrm{B}]}} - \frac{v}{[\mathrm{A}]} \cdot \frac{K_{\mathrm{mA}}}{1 + \dfrac{K_{\mathrm{mB}}}{[\mathrm{B}]}} \tag{2.150}$$

$$v = \frac{V_1}{1 + \dfrac{K_{\mathrm{mA}}}{[\mathrm{A}]}} \cdot \frac{v}{[\mathrm{B}]} \cdot \frac{K_{\mathrm{mB}}}{1 + \dfrac{K_{\mathrm{mA}}}{[\mathrm{A}]}} \ . \tag{2.151}$$

The secondary plots can be obtained from the gradients and the reciprocal abscissa sections (Table 2.2).

In an *iso-ping-pong mechanism,* the enzyme form F isomerises further into form G:

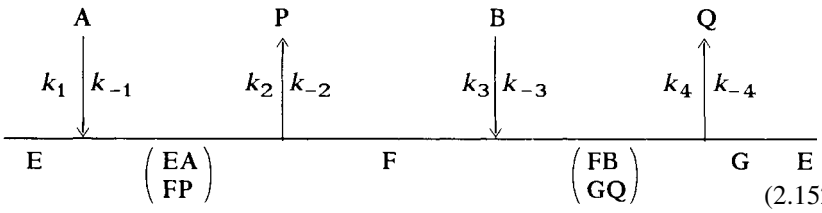

(2.152)

This mechanism can be detected in the product inhibition pattern (Table 2.3).

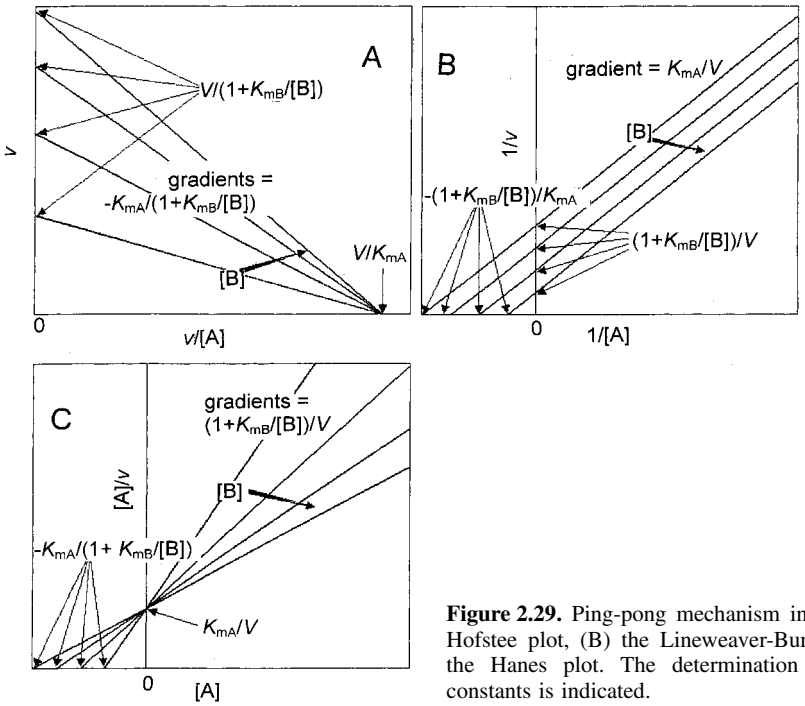

Figure 2.29. Ping-pong mechanism in (A) the Eadie-Hofstee plot, (B) the Lineweaver-Burk plot, and (C) the Hanes plot. The determination of the kinetic constants is indicated.

2.6.5 Haldane Relationships in Multi-Substrate Reactions

As already demonstrated for a one-substrate reaction (Section 2.4.2), one or more Haldane relationships can also be derived for other kinetic mechanisms, the equilibrium constant K_e of the overall reaction correlating with the kinetic constants. A Haldane relationship can be expressed in a general form:

$$K_e = \left(\frac{V_1}{V_2}\right)^n \frac{K_P K_Q K_R}{K_A K_B K_C} \quad . \tag{2.153}$$

The nominator contains the maximum velocity of the forward reaction and constants of the products, the denominator the maximum velocity of the reverse reaction and constants of the substrates. The constants are, depending on the respective mechanism, either Michaelis or inhibition constants. The exponent n mostly has the value 0, 1, or 2, but there always exists at least one Haldane relationship for $n=1$ which serves to eliminate K_e from the rate equation. This can be derived from the constant term in the denominator of the respective rate reaction (e.g., $K_{iA}K_{mB}V_2$ in Eq. (2.132)). For this, the equation must be transformed into the form of rate constants, anticipating the derivation of rate equations to be discussed in Section 2.7.1. Nominator and denominator of Eq. (2.132) are extended by K_e/V_1, the constant term is then $K_{iA}K_{mB}V_2K_e/V_1$. Expressed in the form of the coefficients and combining the rate constants (as shown in Eq. (2.166)), this term is:

$$K_{iA}K_{mB}V_2K_e\left(\frac{1}{V_1}\right) = \frac{Ko}{KoA}\cdot\frac{KoA}{KoAB}\cdot\frac{Z_2}{KoPQ}\cdot\frac{Z_1}{Z_2}\cdot\frac{KoAB}{Z_1}\ .$$

After reduction and extension with KoQ, the remaining coefficients can be reverted into kinetic constants:

$$\frac{K_{iA}K_{mB}V_2K_e}{V_1} = \frac{Ko}{KoQ}\cdot\frac{KoQ}{KoPQ} = K_{iQ}K_{mP}\ .$$

This results in the Haldane relationship:

$$K_e = \frac{V_1K_{iQ}K_{mP}}{V_2K_{iA}K_{mB}}\ . \tag{2.154}$$

Other Haldane relationships can be derived with the coefficient form of the rate equation and with K_e from denominator terms in a similar way.

2.6.6 Mechanisms with More than Two Substrates

Principally all multi-substrate reactions, including the ones with three or four substrates, can be reduced to the three main mechanisms already discussed. There are, however, combinations of different mechanisms, e.g., hybrid *ping-pong ordered* and *ping-pong random* mechanisms. An *ordered ter-ter* mechanism

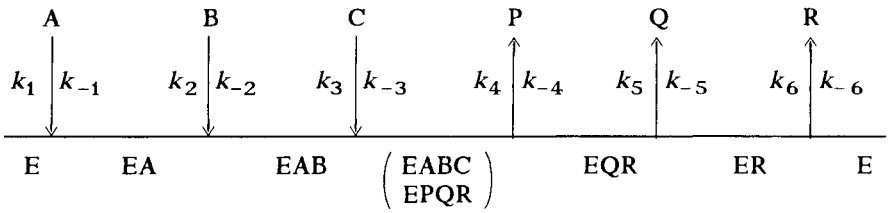

(2.155)

obeys the equation given below in the forward reaction:

$$v = \frac{V_1[A][B][C]}{K_{iA}K_{iB}K_{mC} + K_{iB}K_{mC}[A] + K_{iA}K_{mB}[C] + K_{mC}[A][B] + K_{mB}[A][C] \\ \frac{V_1[A][B][C]}{+K_{mA}[B][C] + [A][B][C]}} \tag{2.156}$$

The procedure corresponds the one for bisubstrate reactions. Each respective substrate is varied at different fixed concentrations of a cosubstrate. The third substrate remains constant during the whole process. The double reciprocal plot yields intercepts left of the ordinate and corresponding secondary plots can be derived from Eq. (2.156).

Altogether five *ping-pong* mechanisms with three participating substrates are possible. In the *hexa-uni-ping-pong* mechanism, all substrates and products bind alternately and there are three central complexes:

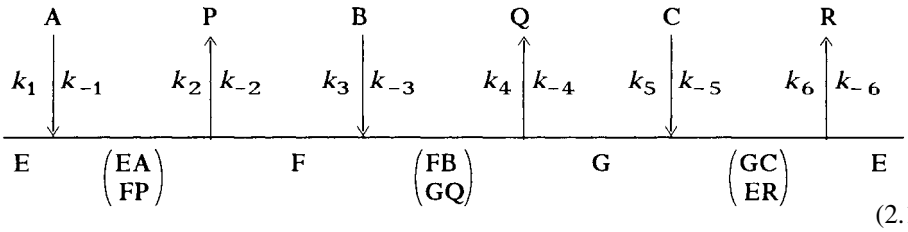

(2.157)

The rate reaction for the forward reaction is:

$$v = \frac{V_1[\mathrm{A}][\mathrm{B}][\mathrm{C}]}{K_{\mathrm{mC}}[\mathrm{A}][\mathrm{B}] + K_{\mathrm{mB}}[\mathrm{A}][\mathrm{C}] + K_{\mathrm{mA}}[\mathrm{B}][\mathrm{C}] + [\mathrm{A}][\mathrm{B}][\mathrm{C}]} \,. \tag{2.158}$$

Parallels are obtained in the double reciprocal plot at variation of each of the three substrates against each one cosubstrate, respectively.

Four ping-pong mechanisms with two central complexes each may occur, with each two ligands binding or detaching in ordered sequence, i.e., the *bi-uni-uni-bi-ping-pong* mechanism,

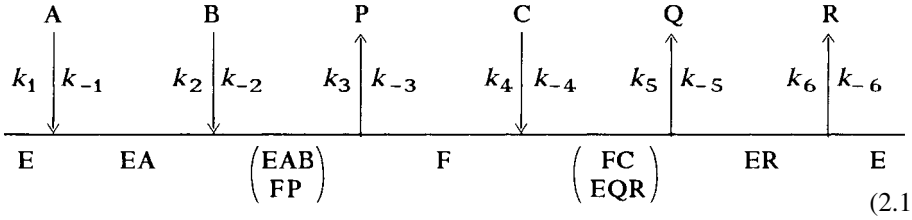

(2.159)

the *uni-bi-bi-uni*, the *bi-bi-uni-uni*, and the *uni-uni-bi-bi* mechanism. The latter two have the same reverse reaction. All four mechanisms have the same rate equattion for the forward reaction

$$v = \frac{V_1[\mathrm{A}][\mathrm{B}][\mathrm{C}]}{K_{\mathrm{iA}}K_{\mathrm{mB}}[\mathrm{C}] + K_{\mathrm{mC}}[\mathrm{A}][\mathrm{B}] + K_{\mathrm{mB}}[\mathrm{A}][\mathrm{C}] + K_{\mathrm{mA}}[\mathrm{B}][\mathrm{C}] + [\mathrm{A}][\mathrm{B}][\mathrm{C}]} \tag{2.160}$$

and thus cannot be distinguished by graphic representations, but only by analysing product inhibition. The double reciprocal plot yields parallels. Only when varying [A] against different amounts of [B], or, *vice versa*, varying [B] against several concentrations of [A], all straight lines will join in a point left of the ordinate.

There are some rare examples for *quad mechanisms* with four participating substrates, as in carbamoylphosphate synthetase.

2.6.7 Other Notations for Multi-Substrate Reactions

Cleland's nomenclature is most widely used for multi-substrate reactions, but notations of other authors are still applied. The one by Dalziel (1957) deviates farthest, as V is inserted into other kinetic constants. The rate reactions can be converted into the Dalziel notation by multiplying nominator and denominator by the reciprocal catalytic constants $\Phi_0 = 1/k_{cat}$. Equation (2.133) takes the following form (substrates are designated S_1, S_2):

$$v = \frac{[E]_0[S_1][S_2]}{\Phi_{12} + \Phi_2[S_1] + \Phi_1[S_2] + \Phi_0[S_1][S_2]} \ .$$

The Dalziel coefficients then are: $\Phi_1 = K_{mA}/k_{cat}$ and $\Phi_2 = K_{mB}/k_{cat.}$ Φ_{12}/Φ_2 equals K_{iA}. The notation of Alberty (1953) is largely identical with the Cleland nomenclature ($K_A = K_{mA}$, etc.), but for product $K_{iA}K_{mB}$ in Eq. (2.133) a common constant K_{AB} is set and $K_{iA} = K_{AB}/K_{mB}$.

2.7 Derivation of Rate Equations of Complex Enzyme Mechanisms

2.7.1 King-Altman Method

It is evident that the derivation of rate reactions for complicated enzyme mechanisms from differential equations, following the rules of steady-state kinetics, frequently lead to complex approaches difficult to resolve. In order to also derive equations for such cases without too much mathematical effort, various simplifications were proposed. The method of E.L. King and C. Altman (1956) has been most widely accepted. It is demonstrated here by the example of an *ordered bi-bi* mechanism.

Step 1: A polygon is drawn, the corners represented by the enzyme forms occurring in the mechanism. They are connected by double arrows marked with the corresponding rate constants, multiplied (if occurring) by entering ligands (substrates or products). The release of ligands is not indicated. The reaction schemes must always be completely closed, and all possible pathways have to be considered. For the ordered mechanism the following scheme evolves, whereby the central complexes of substrate and product are combined:

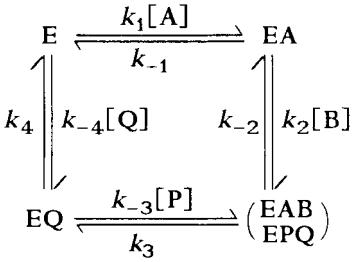

(2.161)

For a *random bi-uni* mechanism (two substrates form one product) the scheme is:

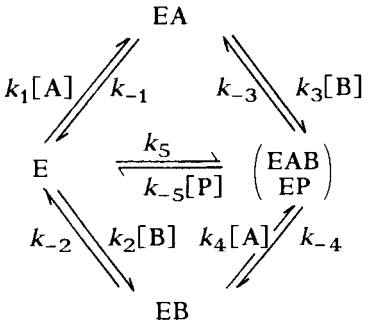

(2.162)

Step 2: All possible patterns are drawn which directly connect all enzyme forms by lines without creating closed patterns. For the *random bi-uni* mechanism there are eight patterns,

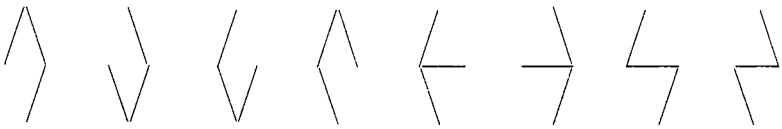

and for the ordered mechanism there are only four:

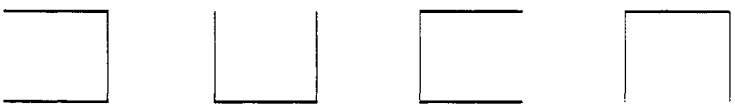

The number of possible patterns is $m!/(n-1)!(m-n+1)!$ for simple mechanisms with only one reaction cycle; n is the number of different enzyme forms and m is the number of connections between the enzyme forms in the original reaction scheme. In case of multiple cycles the combinations forming closed patterns have to be deduced for each cycle. They have to be calculated for each cycle according to $(m-r)!(n-r-1)!(m-n+1)!$, r being the number of connections in a closed cycle. For the *random bi-uni* mechanism there would be altogether $5!/(4-1)!(5-4+1)!=10$ patterns. For two cycles with each three connections $(5-3)!/(4-3-1)!(5-4+1)=1$ must be deduced twice, resulting in eight open patterns.

Step 3: The positions of each enzyme form are marked in sequence in each of the patterns, and the corresponding arrows pointing to each enzyme are drawn in. The relevant captions of rate constants and concentration terms are transferred from the original reaction scheme (2.161). This procedure is shown here for the free enzyme. The other enzyme forms are to be treated similarly. The rate constants and concentration terms of each pattern are combined as product:

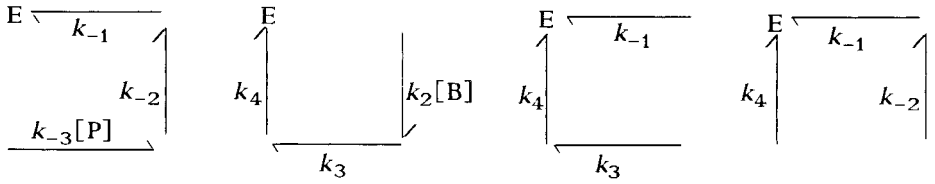

$k_{-1}k_{-2}k_{-3}[P]$ $k_2k_3k_4[B]$ $k_{-1}k_3k_4$ $k_{-1}k_{-2}k_4$.

The expression for the relative amount of each enzyme form is made up of a special nominator term Z and a denominator term N, common to all enzyme forms. The nominator represents the sum of all product terms obtained from the patterns for the respective enzyme form:

$$\frac{[E]}{[E]_0} = \frac{Z_E}{N} = \frac{k_{-1}k_{-2}k_{-3}[P] + k_2k_3k_4[B] + k_{-1}k_3k_4 + k_{-1}k_{-2}k_4}{N} ,$$

$$\frac{[EA]}{[E]_0} = \frac{Z_{EA}}{N} = \frac{k_1k_{-2}k_{-3}[A][P] + k_{-2}k_{-3}k_{-4}[P][Q] + k_1k_3k_4[A] + k_1k_{-2}k_4[A]}{N} ,$$

$$\frac{[EAB]}{[E]_0} = \frac{Z_{EAB}}{N}$$

$$= \frac{k_1k_2k_{-3}[A][B][P] + k_2k_{-3}k_{-4}[B][P][Q] + k_{-1}k_{-3}k_{-4}[P][Q] + k_1k_2k_4[A][B]}{N} ,$$

$$\frac{[EQ]}{[E]_0} = \frac{Z_{EQ}}{N} = \frac{k_1k_2k_3[A][B] + k_2k_3k_{-4}[B][Q] + k_{-1}k_3k_{-4}[Q] + k_{-1}k_{-2}k_{-4}[Q]}{N} .$$

The denominator represents the sum of all nominator terms:

$$\begin{aligned} N &= Z_E + Z_{EA} + Z_{EAB} + Z_{EQ} \\ &= k_{-1}k_{-2}k_{-3}[P] + k_2k_3k_4[B] + k_{-1}k_3k_4 + k_{-1}k_{-2}k_4 + k_1k_{-2}k_{-3}[A][P] + k_{-2}k_{-3}k_{-4}[P][Q] \\ &\quad + k_1k_3k_4[A] + k_1k_{-2}k_4[A] + k_1k_2k_{-3}[A][B][P] + k_2k_{-3}k_{-4}[B][P][Q] + k_{-1}k_{-3}k_{-4}[P][Q] \\ &\quad + k_1k_2k_4[A][B] + k_1k_2k_3[A][B] + k_2k_3k_{-4}[B][Q] + k_{-1}k_{-3}k_{-4}[Q] + k_{-1}k_{-2}k_{-4}[Q] . \end{aligned} \tag{2.163}$$

The rate equation of the reaction in its general form also has N as denominator. Its nominator is the difference of the product of all substrate concentrations and a nominator coefficient Z_1 on the one hand and the product of all product concentrations and a nominator coefficient Z_2 on the other. $Z_1 = [E]_0k_1k_2k_3...$ is the product of all rate constants of the forward reaction with the total enzyme concentration, $Z_2 = [E]_0k_{-1}k_{-2}k_{-3}...$, is the product of all rate constants of the reverse reaction with the enzyme concentration:

$$v = \frac{(Z_1[A][B][C]\ldots - Z_2[P][Q][R]\ldots)}{N} . \tag{2.164}$$

Step 4: The denominator is now transcribed into the coefficient form. All rate constants are arranged according to their concentration terms

$$N = k_{-1}k_4(k_{-2}+k_3) + k_1k_4(k_{-2}+k_3)[\mathrm{A}] + k_2k_3k_4[\mathrm{B}] + k_{-1}k_{-2}k_{-3}[\mathrm{P}] + k_{-1}k_{-4}(k_{-2}+k_3)[\mathrm{Q}] + k_1k_2(k_3+k_4)[\mathrm{A}][\mathrm{B}] + k_1k_{-2}k_{-3}[\mathrm{A}][\mathrm{P}] + k_2k_3k_{-4}[\mathrm{B}][\mathrm{Q}] + k_{-3}k_{-4}(k_{-1}+k_{-2})[\mathrm{P}][\mathrm{Q}] + k_1k_2k_{-3}[\mathrm{A}][\mathrm{B}][\mathrm{P}] + k_2k_{-3}k_{-4}[\mathrm{B}][\mathrm{P}][\mathrm{Q}] \quad (2.165)$$

and the rate constants under the same concentration term are expressed as coefficient *Ko* of the respective concentration term, e.g., $KoAB = k_1k_2(k_3+k_4)$. The complete denominator term in the coefficient form is:

$$N = Ko + KoA[\mathrm{A}] + KoB[\mathrm{B}] + KoP[\mathrm{P}] + KoQ[\mathrm{Q}] + KoAB[\mathrm{A}][\mathrm{B}] + KoAP[\mathrm{A}][\mathrm{P}] + KoBQ[\mathrm{B}][\mathrm{Q}] + KoPQ[\mathrm{P}][\mathrm{Q}] + KoABP[\mathrm{A}][\mathrm{B}][\mathrm{P}] + KoBPQ[\mathrm{B}][\mathrm{P}][\mathrm{Q}] \; . \quad (2.166)$$

Kinetic constants are defined with the aid of the coefficients. The maximum velocity of the forward reaction V_1 is the quotient of the nominator coefficient Z_1 and the coefficient of all substrates. The maximum velocity of the reverse reaction V_2 is the quotient of Z_2 and the coefficient of all products:

$$V_1 = \frac{Z_1}{KoABC\ldots} \; ; \; V_2 = \frac{Z_2}{KoPQR\ldots} \; .$$

The Michaelis constants are ratios of the coefficients of all substrates or products reduced by the variable one to the coefficient of all substrates and products:

$$K_{\mathrm{mA}} = \frac{KoBC\ldots}{KoABC\ldots} \; ; \; K_{\mathrm{mB}} = \frac{KoAC\ldots}{KoABC\ldots} \; ;$$
$$K_{\mathrm{mP}} = \frac{KoQR\ldots}{KoPQR\ldots} \; ; \; K_{\mathrm{mQ}} = \frac{KoPR\ldots}{KoPQR\ldots} \; .$$

K_{e}, the equilibrium constant of the overall reaction, results from the ratio of the nominator coefficients, i.e., the products of the rate constants of the forward reaction to those of the reverse reaction:

$$K_{\mathrm{e}} = \frac{Z_1}{Z_2} = \frac{k_1k_2k_3\ldots}{k_{-1}k_{-2}k_{-3}\ldots} \; .$$

For the *ordered bi-bi* mechanism the following constants are obtained:

$$V_1 = \frac{k_1k_2k_3k_4[\mathrm{E}]_0}{k_1k_2(k_3+k_4)} = \frac{k_3k_4[\mathrm{E}]_0}{k_3+k_4}$$
$$V_2 = \frac{k_{-1}k_{-2}k_{-3}k_{-4}[\mathrm{E}]_0}{k_{-3}k_{-4}(k_{-1}+k_{-2})} = \frac{k_{-1}k_{-2}[\mathrm{E}]_0}{k_{-1}+k_{-2}}$$
$$K_{\mathrm{mA}} = \frac{k_2k_3k_4}{k_1k_2(k_3+k_4)} = \frac{k_3k_4}{k_1(k_3+k_4)}$$
$$K_{\mathrm{mB}} = \frac{k_1k_4(k_{-2}+k_3)}{k_1k_2(k_3+k_4)} = \frac{k_4(k_{-2}+k_3)}{k_2(k_3+k_4)}$$
$$K_{\mathrm{mP}} == \frac{k_{-1}k_{-4}(k_{-2}+k_3)}{k_{-3}k_{-4}(k_{-1}+k_{-2})} = \frac{k_{-1}(k_{-2}+k_3)}{k_{-3}(k_{-1}+k_{-2})}$$
$$K_{\mathrm{mQ}} = \frac{k_{-1}k_{-2}k_{-3}}{k_{-3}k_{-4}(k_{-1}+k_{-2})} = \frac{k_{-1}k_{-2}}{k_{-4}(k_{-1}+k_{-2})}$$
$$K_{\mathrm{e}} = \frac{k_1k_2k_3k_4}{k_{-1}k_{-2}k_{-3}k_{-4}} \ .$$

Step 5: Nominator and denominator of the rate equation converted into the coefficient form are multiplied by the factor $Z_2/(KoABC...KoPQR...)$. The nominator takes the general form:

$$V_1V_2\left([\mathrm{A}][\mathrm{B}][\mathrm{C}]\ldots - \frac{[\mathrm{P}][\mathrm{Q}][\mathrm{R}]\ldots}{K_{\mathrm{e}}}\right) . \tag{2.167}$$

For the denominator, the terms are multiplied in sequence by the constant factor and it is then attempted to replace all coefficients by kinetic constants, following the above definitions. This is shown in Table 2.4. In the second denominator term, e.g., expressions for $K_{\mathrm{mB}} = KoA/KoAB$ and $V_2 = Z_2/KoPQ$ are obtained. Accordingly, K_{mA} and V_2 can be inserted in the third term. In other cases, as in the fourth or fifth term, this can only be achieved by an appropriate extension of the term, as indicated in the second column of Table 2.4. Other terms, as the first, cannot be resolved even by these extensions. In such terms inhibition constants for binding to the free enzyme are hidden. They have not been defined so far as they do not fit into a unified scheme and can better be derived from the actual case. The principal rule also applies here: the variable ligand may not appear in the nominator term while the denominator is made up of the coefficient of all ligands denoted in the nominator plus the variable ligand. Thus, the term *Ko/KoA* in the first term obviously stands for K_{iA}. This assumption is confirmed when replacing the coefficients by their rate constants resulting in the expression k_{-1}/k_1 which actually defines the respective dissociation constant. In term seven the same constant K_{iA} is expressed by different coefficients, *KoP/KoAP*. But here also k_{-1}/k_1 remains after inserting the respective rate constants, proving that for one constant different definitions are possible.

For the *ordered bi-bi* mechanism this gives the rate equation in form of the kinetic constants:

Table 2.4. Transcription of the denominator from Eq. (2.166) from the coefficient form into one of the kinetic constants. The constant factor by which all denominator terms were multiplied, is marked in bold letters in the left column

Denominator terms in the form of coefficients	Attenuation	Denominator terms in the form of constants	Definition of inhibition constants
$\frac{\mathbf{Z_2}\cdot KoA}{\mathbf{KoAB}\cdot\mathbf{KoPQ}}$	KoA	$K_{iA}K_{mB}V_2$	$K_{iA}=\frac{Ko}{KoA}=\frac{k_{-1}}{k_1}$
$\frac{\mathbf{Z_2}\cdot KoA[A]}{\mathbf{KoAB}\cdot\mathbf{KoPQ}}$		$K_{mB}V_2[A]$	
$\frac{\mathbf{Z_2}\cdot KoB[B]}{\mathbf{KoAB}\cdot\mathbf{KoPQ}}$		$K_{mA}V_2[B]$	
$\frac{\mathbf{Z_2}\cdot KoP[P]}{\mathbf{KoAB}\cdot\mathbf{KoPQ}}$	Z_1	$\frac{K_{mQ}V_1[P]}{K_e}$	
$\frac{\mathbf{Z_2}\cdot KoQ[Q]}{\mathbf{KoAB}\cdot\mathbf{KoPQ}}$	Z_1	$\frac{K_{mP}V_1[Q]}{K_e}$	
$\frac{\mathbf{Z_2}\cdot KoAB[A][B]}{\mathbf{KoAB}\cdot\mathbf{KoPQ}}$		$V_2[A][B]$	
$\frac{\mathbf{Z_2}\cdot KoAP[A][P]}{\mathbf{KoAB}\cdot\mathbf{KoPQ}}$	$KoP\ Z_1$	$\frac{K_{mQ}V_1[A][P]}{K_{iA}K_e}$	$K_{iA}=\frac{KoP}{KoAP}=\frac{k_{-1}}{k_1}$
$\frac{\mathbf{Z_2}\cdot KoBQ[B][Q]}{\mathbf{KoAB}\cdot\mathbf{KoPQ}}$	KoB	$\frac{K_{mA}V_2[B][Q]}{K_{iQ}}$	$K_{iQ}=\frac{KoB}{KoBQ}=\frac{k_4}{k_{-4}}$
$\frac{\mathbf{Z_2}\cdot KoPQ[P][Q]}{\mathbf{KoAB}\cdot\mathbf{KoPQ}}$	Z_1	$\frac{V_1[P][Q]}{K_e}$	
$\frac{\mathbf{Z_2}\cdot KoABP[A][B][P]}{\mathbf{KoAB}\cdot\mathbf{CoPQ}}$		$\frac{V_2[A][B][P]}{K_{iP}}$	$K_{iP}=\frac{KoAB}{KoABP}=\frac{k_3+k_4}{k_{-3}}$
$\frac{\mathbf{Z_2}\cdot KoBPQ[B][P][Q]}{\mathbf{KoAB}\cdot\mathbf{CoPQ}}$	Z_1	$\frac{V_1[B][P][Q]}{K_{iB}K_e}$	$K_{iB}=\frac{KoPQ}{KoBPQ}=\frac{k_{-1}+k_{-2}}{k_2}$

$$v=\frac{V_1V_2\left([A][B]-\dfrac{[P][Q]}{K_e}\right)}{K_{iA}K_{mB}V_2+K_{mB}V_2[A]+K_{mA}V_2[B]+\dfrac{K_{mQ}V_1[P]}{K_e}+\dfrac{K_{mP}V_1[Q]}{K_e}+V_2[A][B]+\dfrac{K_{mQ}V_1[A][P]}{K_{iA}K_e}}$$
$$+\frac{K_{mA}V_2[B][Q]}{K_{iQ}}+\frac{V_1[P][Q]}{K_e}+\frac{V_2[A][B][P]}{K_{iP}}+\frac{V_1[B][P][Q]}{K_{iB}K_e}\ . \tag{2.168}$$

This still very complicated equation is reduced to the already known Eq. (2.133) when applying steady-state measurements of initial rates for the forward reaction, assuming [P]=[Q]=0:

$$v=\frac{V_1[A][B]}{K_{iA}K_{mB}+K_{mB}[A]+K_{mA}[B]+[A][B]} \tag{2.133 a}$$

and assuming for the reverse reaction [A]=[B]=0:

$$v=\frac{V_2[P][Q]}{K_{iA}K_{mB}+K_{mQ}[P]+K_{mP}[Q]+[P][Q]}\ . \tag{2.133 b}$$

2.7.2 Simplified Derivations According to the Graph Theory

The King-Altman method represents a considerable simplification compared to the derivation of rate equations after the steady-state rules, but for more complex mechanisms it is still very complicated. Volkenstein and Goldstein (1966) could reduce the King-Altman method by applying the graph theory originally developed for electronic signals. A further reduction, requiring "only a rudimentary understanding of algebra", was suggested by Fromm (1970).

As in the King-Altman method, closed reaction schemes are established for the respective mechanism. Individual enzyme forms are taken as junction points and are numbered consecutively:

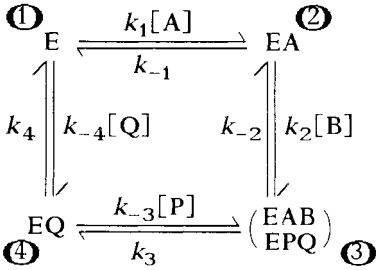

(2.169)

The determinant of one junction, e.g., $1(\approx [E])$ is composed of two parts. The constants or terms of the shortest one-step pathways leading to this junction are taken, hence $2 \rightarrow 1 \approx k_{-1}$ and $4 \rightarrow 1 \approx k_4$ for this example. To those the numbers of junction points not touched by the respective one-step pathways are noted:

$$[E] = (2 \rightarrow 1)(3)(4) + (4 \rightarrow 1)(2)(3) ,$$

and each of these numbers was substituted by expressions of those arrows, which direct away from the respective junction:

$$[E] = k_{-1}(k_{-2} + k_3)(k_{-3}[P] + k_4) + k_4(k_{-1} + k_2[B])(k_3 + k_{-2}) .$$

Multiplying of the terms yield:

$$\begin{aligned}[E] = {} & k_{-1}k_{-2}k_{-3}[P] + k_{-1}k_3k_{-3}[P] + k_{-1}k_{-2}k_4 + k_{-1}k_3k_4 + k_{-1}k_3k_4 + k_2k_3k_4[B] \\ & + k_{-1}k_{-2}k_4 + k_2k_{-2}k_4[B] .\end{aligned}$$

"Forbidden" terms containing rate constants for both forward and reverse reactions of the same step, i.e., $k_{-1}k_3k_{-3}[P]$ and $k_2k_{-2}k_4[B]$, are omitted. For redundant terms ($k_{-1}k_{-2}k_4$, $k_{-1}k_3k_4$) only one expression is left so that the final relationship for [E] is identical to the one in the King–Altman method:

$$[E] = k_{-1}k_{-2}k_{-3}[P] + k_{-1}k_{-2}k_4 + k_{-1}k_3k_4 + k_2k_3k_4[B] .$$

Executing this procedure for all enzyme forms results in a rate equation according to the King-Altman method.

2.7.3 Combination of Equilibrium and Steady-State Assumptions

A further simplification is based on the original assumption of Michaelis and Menten that equilibria are attained much more rapid than by the catalytic turnover (Cha, 1968). More complex mechanisms are divided into several segments in which the individual reaction steps are in rapid equilibrium with each other. These segments are separated by slow reaction steps. A fractional concentration factor f_i gives the ratio of the concentration of a certain enzyme form (E_i) to the sum of the concentrations of all enzyme forms of the respective rapid equilibrium segment:

$$f_i = \frac{[E_i]}{\sum_{i=1}^{n}[E_i]}$$

This procedure is demonstrated by the example of a *ping-pong-bi-bi* mechanism, assuming slow catalytic equilibria compared to rapid binding steps:

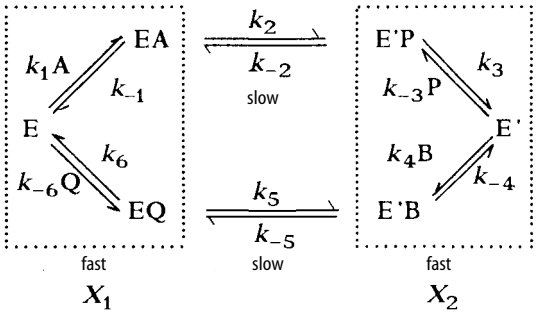

(2.170)

The enzyme forms of both segments $X_1 = [E] + [EA] + [EQ]$ and $X_2 = [E'] + [E'B] + [E'P]$ are in rapid equilibrium with each other. The rate equation according to the general King-Altman form is:

$$v = \frac{(k_2 k_5 f_2 f_5 - k_{-2} k_{-5} f_{-2} f_{-5})[E]_0}{k_2 f_2 + k_{-2} f_{-2} + k_5 f_5 + k_{-5} f_{-5}} \quad . \tag{2.171}$$

The fractional concentration factors for the respective enzyme forms are defined by taking one enzyme form, e.g. E or E′, as reference and setting it as 1. The other enzyme forms are replaced by the concentration variables of the corresponding ligands and the rate and dissociation constants. If the ligand binds to the respective enzyme form, the concentration variable stands on the fraction bar and the dissociation constant below. If it dissociates, the fraction is reversed (hereafter the rate constants are given in place of the dissociation constants):

$$f_{EA} = \frac{[EA]}{X_1} = \frac{\dfrac{k_1[A]}{k_{-1}}}{1 + \dfrac{k_1[A]}{k_{-1}} + \dfrac{k_{-6}[Q]}{k_6}} = \frac{k_1 k_6 [A]}{k_{-1}k_6 + k_1 k_6 [A] + k_{-1}k_{-6}[Q]} ,$$

$$f_{E'P} = \frac{[E'P]}{X_2} = \frac{\dfrac{k_{-3}[P]}{k_3}}{1 + \dfrac{k_4[B]}{k_{-4}} + \dfrac{k_{-3}[P]}{k_3}} = \frac{k_{-3}k_{-4}[P]}{k_3 k_{-4} + k_3 k_4 [A] + k_{-3}k_{-4}[P]} ,$$

$$f_{E'B} = \frac{[E'B]}{X_2} = \frac{\dfrac{k_4[B]}{k_{-4}}}{1 + \dfrac{k_4[B]}{k_{-4}} + \dfrac{k_{-3}[P]}{k_3}} = \frac{k_3 k_4 [B]}{k_3 k_{-4} + k_3 k_4 [A] + k_{-3}k_{-4}[P]} ,$$

$$f_{EQ} = \frac{[EQ]}{X_1} = \frac{\dfrac{k_{-6}[Q]}{k_6}}{1 + \dfrac{k_1[A]}{k_{-1}} + \dfrac{k_{-6}[Q]}{k_6}} = \frac{k_{-1}k_{-6}[Q]}{k_{-1}k_6 + k_1 k_6 [A] + k_{-1}k_{-6}[Q]} .$$

If EQ is taken instead of E as reference and set as 1, the fractional concentration factor f_{EA} is:

$$f_{EA} = \frac{[EA]}{X_1} = \frac{\dfrac{k_1[A]k_6}{k_{-1}k_{-6}[Q]}}{\dfrac{k_6}{k_{-6}[Q]} + \dfrac{k_1[A]k_6}{k_{-1}k_{-6}[Q]}} = \frac{k_1 k_6 [A]}{k_{-1}k_6 + k_1 k_6 [A] + k_{-1}k_{-6}[Q]} ,$$

resulting in the same expression. Replacing the fractional concentration factors in Eq. (2.171) results in the rate equation for the ping-pong mechanism in form of the rate constant. Compared with an equation derived after the King–Altman mechanism, the constants k_2, k_{-2}, k_5 and k_{-5} for the slow step are partially disregarded:

$$v = \frac{(k_1 k_2 k_3 k_4 k_5 k_6 [A][B] + k_{-1}k_{-2}k_{-3}k_{-4}k_{-5}k_{-6}[P][Q])[E]_0}{k_1 k_2 k_3 k_{-4}k_{-6}[A] + k_{-1}k_3 k_4 k_5 k_6 [B] + k_1 k_3 k_4 k_6 (k_2 + k_5)[A][B] + k_{-1}k_{-2}k_{-3}k_{-4}k_6 [P]}$$

$$\overline{+k_{-1}k_3 k_{-4}k_5 k_{-5}k_{-6}[Q] + k_{-1}k_{-3}k_{-4}k_{-6}(k_{-2} + k_{-5})[P][Q]}$$

$$\overline{+k_1 k_{-3}k_{-4}k_6 (k_2 + k_{-2})[A][P] + k_{-1}k_3 k_4 k_{-6}(k_5 + k_{-5})[B][Q]} .$$

2.8 Kinetic Treatment of Allosteric Enzymes

Allosteric enzymes play a central role in metabolism. Along with the essential models – the symmetry and the sequence model – they have already been discussed in the section on *multiple equilibria*, as the cooperativity on which allosteric mechanisms are based, can be led back to equilibrium processes. Nevertheless, allosteric enzymes are often characterised using kinetic methods due to the simpler analysis. Similar (mostly sigmoidal) deviations from the Michaelis-Menten behaviour of substrate as well as influences by allosteric effectors are observed, as already described for ligand binding. The same evaluation methods can be applied, while only the saturation function r or Y is replaced by v. In the Hill plot the ordinate notation $\log (Y/1-Y)$ is replaced by $\log (v/V-v)$. A further treatment of this enzyme class is therefore not necessary and discussion will only be limited to the special phenomenon of *kinetic cooperativity.*

2.8.1 Hysteretic Enzymes

In numerous enzyme reactions as phosphofructokinase and thiamin diphosphate-dependent α-oxo acid dehydrogenase multienzyme complexes (e.g., the pyruvate dehydrogenase complex), reaction runs are observed that cannot be interpreted simply by the steady-state theory. For these enzymes, reaction does not start with a linear initial rate of zero order, rather no turnover is detectable after addition of substrate. Reaction sets in only after a lag period and reaches a linear steady-state rate after a few seconds up to several minutes. Subsequently, it declines as in normal enzyme reactions, due to substrate depletion (Figure 2.30A). In analogy to the respective phenomenon observed in magnetism, for this kind of enzymes C. Frieden created the term *hysteretic enzymes*. Causes for the delayed onset of the reaction may be of different nature. Obviously the enzyme, in interaction with substrate, transforms from an inactive to an active state in a slow process, mostly by conformational changes. As these enzymes do not react immediately, but to back dated processes, they show a kind of enzymatic memory (*mnemonic enzymes*). Hysteresis has a dampening physiological effect. The system does not react immediately to metabolic changes; short, transitory impulses are ignored, and fluctuations are equalised.

The length of the *lag phase* τ is determined by extrapolation of the linear steady-state area to the abscissa or the ordinate as shown in Figure 2.30. More reliably it can be obtained from the gradient of a semi-logarithmic diagram of the turnover rate, reduced by the steady-state rate v_{ss} (determined from tangents on distinct points of the progress curves) against the respective time within the range of the lag phase (Figure 2.30 B). A linear dependence in this plot also serves as control of a pseudo first order process of the lag phase. If the non-linear decline due to substrate depletion sets in early after the lag phase the steady-state area can not be reliably obtained. The progress curve passes a turning point and at this region a steady-state run may be simulated. In this case τ can be obtained from the gradient of a Guggenheim plot (Figure 2.30 C). The difference between two substrate concentrations $[A]_i$ and $[A]_{i+\Delta}$ separated by a constant time interval Δt is plotted logarithmically against time,

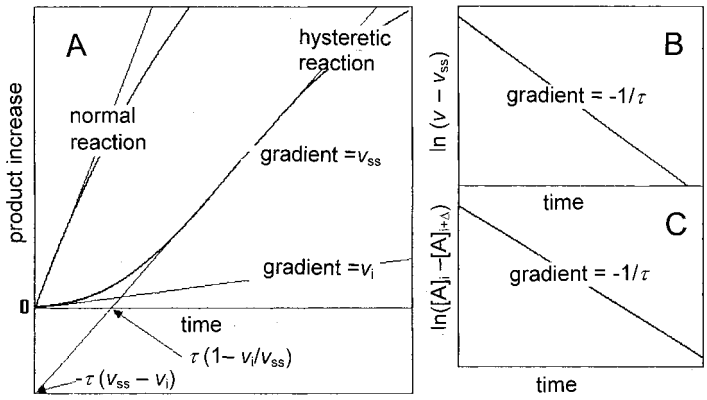

Figure 2.30. Progression of a hysteretic reaction compared to a normal zero order enzyme reaction. (A) Progress curve, the determination of the rate in the initial (v_i) and the steady-state phase (v_{ss}) and the length of the lag phase τ are indicated, (B) semi-logarithmic plot, (C) Guggenheim plot.

the gradient taking the value of $1/\tau$. The relationship of this plot is derived from Eq. (2.3) for a first order reaction

$$[\mathrm{A}]_\mathrm{i} - [\mathrm{A}]_{\mathrm{i}+\Delta} = [\mathrm{A}]_0\, \mathrm{e}^{-t/\tau}(1 - \mathrm{e}^{\Delta t/\tau}) \,, \tag{2.173}$$

$\mathrm{e}^{\Delta t/\tau}$ being constant.

2.8.2 Kinetic Cooperativity, the Slow Transition Model

Slow activation processes in enzymatic reactions can cause deviations from the Michaelis kinetics in the nature of positive or negative cooperativity, without requiring interactions between subunits (*kinetic cooperativity*). In the *slow transition model* (Figure 2.31), a slow transition, as compared with substrate binding and turnover rate, from a low active (E) into a high active enzyme state (E′) is assumed. Sigmoidal saturation behaviour of the substrate is observed in dependence of the turnover rate, provided that both enzyme forms bind substrate and are catalytically active, although with different efficiency. In the absence of substrate the enzyme is present in its inactive form. If only one enzyme form is active and the slow transition of conformation of the enzyme is performed before the binding of ligand (spontaneous transition), a lag phase, but no sigmoidal saturation behaviour may be observed. With kinetic cooperativity, the Hill coefficient can reach a maximum value of 2, as the reaction of substrate is of second order and the substrate reacts in two different places (EA and E′A). In contrast to real cooperativity, sigmoidal saturation curves are only obtained when measuring turnover rates, but not with substrate binding, which exhibits normal hyperbolic behaviour. In order to understand this model it may be imagined that the enzyme converts into the active state after substrate binding. At low substrate levels the enzyme may return into a less active state after each turnover of substrate before

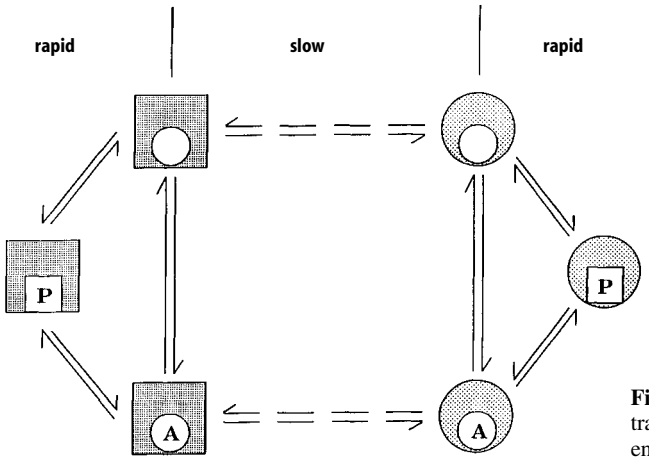

Figure 2.31. Scheme of the slow transition model for a monomeric enzyme.

binding the next substrate molecule. At increasing substrate concentrations there is not enough time left, for an increasing number of enzyme molecules until the next binding of a substrate molecule to revert to the original state. At very high substrate concentrations all enzyme molecules remain in the active form, the enzyme working at its highest efficiency.

In contrast to the allosteric models based on equilibrium – the symmetry model and the sequence model – kinetic cooperativity is also applicable for monomeric systems. This was first detected in monomer ribonuclease. Further examples were found later, i.e., hexokinase and glucokinase. Kinetic cooperativity is not necessarily restricted to monomeric enzymes. Such a mechanism without any interaction among subunits was also established for the bacterial pyruvate dehydrogenase complex, the largest soluble enzyme aggregate of these cells with an assembly of 24 protomers (Bisswanger, 1984).

2.9 Special Enzyme Mechanisms

2.9.1 Kinetics of Immobilised Enzymes

Immobilised enzymes are of increasing significance in biotechnological processes in enzyme reactors, in biosensors, and in medicine. In the cell, membrane-bound enzymes may be regarded as immobilised systems.

Kinetic treatment of an immobilised enzyme system is dependent on its specific structure, and general rules can hardly be defined. Immobilisation of enzymes is frequently achieved by covalent binding to solid surfaces, to a *matrix*, like dextran, agarose, synthetic polymers, glass or ceramics. As long as any effect by the matrix on the reactants, especially on the free diffusion of substrate or product can be excluded, these systems may be treated kinetically like soluble enzymes. The matrix may, however, reject or attract substrates or products and thus affects their concentra-

tion in the vicinity of the immobilised enzyme, either negatively or positively. The (often hydrophobic) surface of the matrix may act as a barrier or boundary layer, impeding the passage of substrate to the catalytic centre. This also applies to enzymes embedded in organelle membranes. Another principle of fixation is embedding the enzymes in a matrix permeable to substrate, e.g. agarose, polyacrylamide, or nylon beads. The enzyme is not modified by covalent fixation and retains its native structure to a large degree. The rules for enzymes in solution apply as long as the concentrations within the particle are equivalent to those of the surrounding solution. This requires free diffusion of all components, like substrates, products or ions (pH changes!). Deviations in the behaviour of the immobilised enzyme will occur if diffusion is affected. If enzymatic transformation of the substrate is faster than its diffusion through the matrix, a depletion of substrate occurs in the area around the enzyme, the extent depending on substrate concentration in the circumfluent medium. In low substrate concentrations, with the enzyme reacting at maximum efficiency, substrate depletion is more pronounced, while being comparatively low near substrate saturation. Conversely, product accumulates with limited diffusion and is prevented from dissociating.

The kinetic models developed from such considerations only regard the interactions between the enzyme and its immediate surroundings on the matrix, especially substrate. Special effects on individual enzymes cannot be considered. Immobilisation of an enzyme by covalent modification of functional groups participating directly or indirectly in the catalytic mechanism can affect the reaction mechanism. Transitions of conformation into the active state or regulatory influences may be impeded or completely repressed by fixation to the matrix. The narrow attachment to the matrix may cause shielding of the active centre.

Because of diffusion hindrance of the substrate, the experimentally determined turnover rate v' of the immobilised enzyme can differ from that of the native enzyme in solution v_{kin}:

$$v' = \eta_e v_{kin} = \eta_e \frac{V[A]}{K_m + [A]} \ . \tag{2.174}$$

The efficiency factor η_e is a function of the substrate concentration, for $\eta_e = 1$ the reaction is kinetically controlled. The reaction of the immobilised enzyme is equal to that of the free enzyme and behaves according to the Michaelis-Menten equation. The reaction becomes increasingly diffusion-controlled the lower the values of this factor are ($\eta_e < 1$). The Michaelis-Menten equation is no longer valid, so that the usual linearisation methods no longer yield straight lines. Eq. (2.174) and the following considerations are based on a one-substrate reaction. As long as all other substrates and cofactors are present in saturating amounts, this treatment can also be applied for multi-substrate reactions.

Generally there exist two kinds of limited diffusion (Figure 2.32). The external diffusion limitation is caused by a boundary layer between the matrix in which the enzyme is embedded and the circumfluent solution. The substrate has to overcome this barrier. In an internal diffusion limitation the matrix affects substrate diffusion.

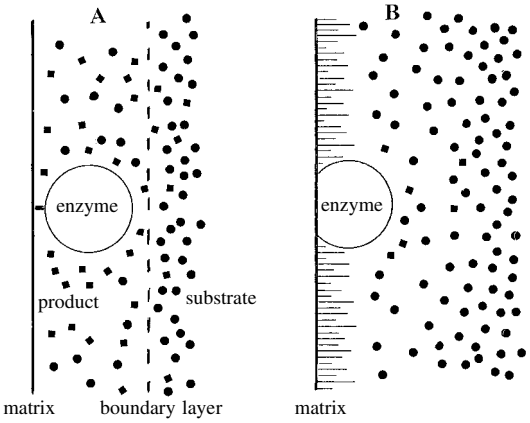

Figure 2.32. Schematic presentation of external (A) and internal (B) diffusion limitation; ● substrate, ■ product.

2.9.1.1 External Diffusion Limitation

Substrate has to pass through a boundary layer to reach the catalytic centre of an enzyme fixed to a solid liquid-impermeable surface. The processes of transport and catalysis take place successively. The flow of substrate J_s from the circumfluent solution with the substrate concentration $[A]_0$ to the active centre on the surface with the substrate concentration [A] is:

$$J_s = h_s([A]_0 - [A]) = \frac{D_s([A]_0 - [A])}{\delta} \quad . \tag{2.175}$$

$h_s = D_s/\delta$ is the transport coefficient and D_s the diffusion coefficient of the substrate, δ is the effective thickness of the boundary layer. D_s and h_s can be determined by methods like radioactive tracer technique or diffusion cells (Rovito et al., 1973) or may be taken from literature (Bird et al., 1960). The flow of substrate towards the active centre and the enzymatic substrate turnover, usually following the Michaelis-Menten relationship, occur successively. Under steady-state conditions both processes take place with equal velocity:

$$h_s([A]_0 - [A]) = \frac{V[A]}{K_m + [A]} \quad . \tag{2.176}$$

For substrate concentration, the non-dimensional term $a = [A]/K_m$ is set:

$$a_0 - a = \frac{Va}{h_s K_m(1 + a)} = \mu \cdot \frac{a}{1 + a} \quad . \tag{2.177}$$

$\mu = V/h_s K_m$ is a non-dimensional substrate module, indicating the ratio between reaction velocities and system transport. The limiting case $K_m \gg [A]$, i.e., at very low substrate concentrations, Eq. (2.177) becomes:

$$h_s([A]_0 - [A]) = \frac{V[A]}{K_m} \ . \tag{2.178}$$

The overall reaction follows first order kinetics. The effective substrate concentration in the area around the active centre is:

$$[A] = \frac{h_s[A]_0}{h_s + \frac{V}{K_m}} \ . \tag{2.179}$$

The experimentally determined turnover rate v' is:

$$v' = \frac{V[A]}{K_m} = \frac{\frac{V}{K_m} h_s[A]_0}{h_s + \frac{V}{K_m}} = \frac{[A]_0}{\frac{1}{h_s} + \frac{K_m}{V}} \ . \tag{2.180}$$

For $h_s \gg V/K_m$ transport is faster than the kinetically controlled enzymatic reaction:

$$v' = v_{kin} = \frac{V[A]_0}{K_m} \ . \tag{2.181}$$

Vice versa, the reaction becomes diffusion-controlled at very slow transportation across the matrix, $h_s \ll V/K_m$:

$$v' = v_{diff} = h_s[A]_0 \ . \tag{2.182}$$

In the limiting case $K_m \ll [A]_0$, i.e., at saturating substrate concentration in the zero order region of the reaction, v' tends to the saturation value V (Eq. (2.176), Figure 2.33 A). In the medium substrate range ($[A] \sim K_m$), depending on their respective size, either v_{kin} or v_{diff} contribute to the larger part of the reaction. A saturation function results, composed of parts of the transport process and the kinetic reaction. It displays, in accordance with the degree of diffusion limitation, an increased apparent K_m value (obtained at half saturation) against the true K_m value of the enzyme reaction. With increasing diffusion limitation the curve in the graphic linearisation methods (e.g., in the double reciprocal plot) deviates from the linear run of the kinetically controlled reaction. A feature of the external diffusion limitation is the fact, that it can be influenced by stirring. Equilibration by diffusion between solution and immobilised enzyme is accelerated.

With a known transport coefficient h_s, the velocity of the kinetically controlled enzyme reaction v_{kin} and the corresponding substrate concentration $[A]_{kin}$ at the active centre on the membrane surface can be determined graphically from the dependence of the measured velocity v' on the substrate concentration of the circumfluent solution (Figure 2.33 B). A straight line with a gradient h_s is drawn through a random point on the abscissa, corresponding to a fixed external substrate concentration $[A]_1$. The intercept of this straight line with the parallel to the abscissa at the point of the

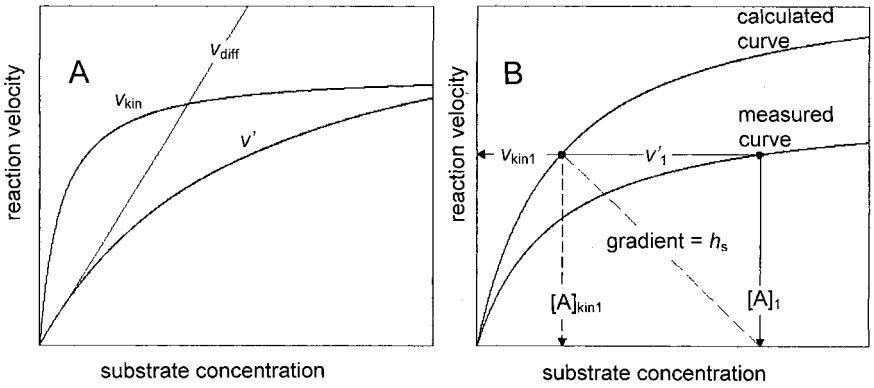

Figure 2.33. Representation of partially competitive inhibition in the double reciprocal plot (A, B) and in the Dixon plot (C, D) with different combinations of inhibitor constants. The inserts show secondary plots of gradients against inhibitor concentrations.

corresponding measured velocity v'_1 has the coordinates $[A]_{kin}$ and v_{kin1}. With this method characteristics of the kinetic reaction are obtained point by point, and the constants by the usual graphic methods.

2.9.1.2 Internal Diffusion Limitation

In contrast to external diffusion, internal diffusion runs parallel to the enzyme-catalysed reaction. Due to substrate depletion, the velocity of the reaction declines with decreasing distance of the immobilised enzyme from the membrane surface, while product formation causes a local accumulation and the formation of a product gradient. The simultaneous processes of diffusion across the membrane and the kinetic reaction behave additively:

$$\frac{\partial[A]}{\partial t} = \left(\frac{\partial[A]}{\partial t}\right)_{diff} + \left(\frac{\partial[A]}{\partial t}\right)_{kin}, \tag{2.183}$$

For the diffusion, Fick's Second Law of Diffusion is applied, and the Michaelis-Menten relationship for the kinetic reaction. V''' is the intrinsic maximum velocity per volume unit of the porous medium or the membrane:

$$\frac{\partial[P]}{\partial t} = D_s\left(\frac{\partial^2[A]}{\partial x^2}\right) - \frac{V'''[A]}{K_m + [A]}. \tag{2.184}$$

In a stationary state is $\delta[A]/\delta t = 0$:

$$D_s\left(\frac{\partial^2[A]}{\partial x^2}\right) = \frac{V'''[A]}{K_m + [A]}. \tag{2.185}$$

The differential equation (2.185) can be resolved by numerical calculation. Non-dimensional terms are introduced for the substrate concentration $\alpha = [A]/K_m$ and for the distance x from the surface, $l = x/L$, L being the thickness of the membrane (for a sphere with the particle radius r, L is substituted by $r/3$) and the l position within the membrane:

$$\frac{d^2\alpha}{dl^2} = \frac{L^2 V'''}{K_m D_s}\left(\frac{\alpha}{1+\alpha}\right) = \Phi_s^2\left(\frac{\alpha}{1+\alpha}\right) . \tag{2.186}$$

Φ_s is the substrate or Thiele module:

$$\Phi_s = L\sqrt{\frac{V'''}{K_m D_s}} . \tag{2.187}$$

The Thiele module contains three factors determining the substrate profile in the membrane: membrane thickness, diffusivity of substrate, and enzyme activity. With increasing Φ_s, the actual substrate concentration in the membrane declines, the steepness of the substrate gradient in the membrane increases. The membrane is depleted of substrate and the enzyme reaction is slowed down. There are deviations in the linearised diagrams. The substrate concentration determined at half-saturation is higher than the K_m value of the free enzyme, same as in the external diffusion limitation. At low values ($\Phi_s \leq 1$) the reaction is mostly kinetically controlled and obeys the Michaelis-Menten kinetics.

For the determination of the kinetic constants of immobilised enzymes it is important to measure within a broad substrate range, as in non-linear dependencies of a narrow range linear regions may appear and may lead to incorrect results. Non-linear curves may be evaluated according to the usual graphic methods, assuming that diffusion limitation will predominate at very low substrate concentrations, and enzyme catalysis at high concentrations. The constants can be obtained from tangents to the extreme regions (see Figure 2.34). These plots are based on the transformation of Eq. (2.174) for the double reciprocal plot:

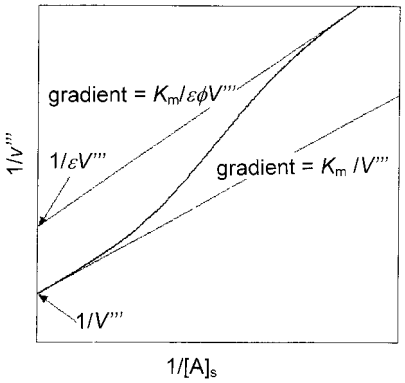

Figure 2.34. Graphic method for the determination of kinetic constants of immobilised enzymes at internal diffusion limitation; ε: effectiveness factor (according to Engasser and Horvath, 1973).

$$\frac{1}{v'''} = \frac{1}{\eta_e V'''} + \frac{K_m}{\eta_e V''' [A]_s} , \tag{2.188}$$

$[A]_s$ is the effective substrate concentration on the surface. Figure 2.34 shows the types of deviations from the normal linear run caused by diffusion limitation. For very low concentrations at $[A]_s$ η_e approximates the efficiency factor η_{e1} for a reaction of first order. The apparent Michaelis constant in this region is $K = K_m/\eta_{e1}$. For high Φ_s values η_{e1} becomes $1/\Phi_s$.

2.9.1.3 Inhibition of Immobilised Enzymes

All effects reducing the reaction rate of an immobilised enzyme counteract substrate depletion around the enzyme. Enzyme inhibition and limited diffusion act antagonistically. If both effects exist simultaneously, they reduce each other; in total they are weaker than should be expected from the sum of the individual effects. Thus inhibition of an immobilised enzyme is relatively smaller than of the native enzyme. Non-linearity of the curves in the linearised plot caused by diffusion limitation is attenuated, but even from non-linearity the type of inhibition remains evident: competitive inhibition only changes the apparent K_m value, but not the maximum velocity, unaffected by limited diffusion. Non-competitive inhibition changes both parameters, which is also apparent in diffusion limitation. For a simple non-competitive inhibition ($K_{ic} = K_{iu} \equiv K_i$, see Eq. (2.65) and Section 2.5.1.2) at external limited diffusion, Eq. (2.176) would be extended to:

$$h_s([A]_0 - [A]) = \frac{V[A]}{(1 + [I]/K_i)(K_m + [A])} . \tag{2.189}$$

Product inhibition is a special case because with diffusion limitation product accumulates in the region of the immobilised enzyme and additionally enforces inhibition. By this diffusion limitation becomes reduced. In total, the immobilised enzyme shows a weaker reaction on changes in product concentration in its vicinity.

All other factors with an effect on enzyme activity also counteract diffusion limitation, e.g., partial inactivation caused by the immobilisation procedure of the enzyme. The degree of inactivation is generally underestimated because of a reduction of diffusion limitation, simulating a more efficient immobilisation. This pretends the impression of apparently improved long-term stability as a consequence of immobilisation.

2.9.1.4 pH and Temperature Behaviour of Immobilised Enzymes

Immobilised enzymes show a altered dependency on pH and ionic strength, particularly if these parameters are altered by the enzyme reaction itself, e.g., consumption or formation of acids (e.g., proteases) or bases (e.g., urease) as substrates or products of the enzyme reaction. Accumulation of such reaction products by diffusion limita-

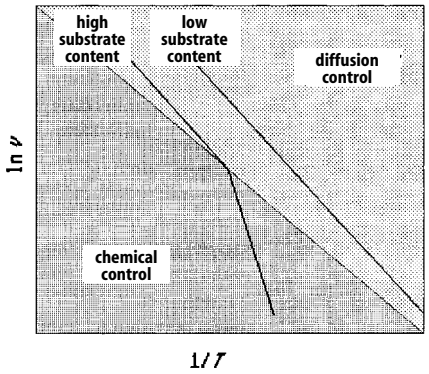

Figure 2.35. Temperature sensitivity of immobilised enzymes.

tion may shift the apparent pH optimum of the enzyme by 1–2 pH values, compared with the free enzyme. Similar shifts of the pH optimum curve occur when the enzyme is fixed to a positively or negatively charged matrix.

In the Arrhenius plot (see Section 2.10.4), immobilised enzymes frequently exhibit inhomogeneities, i.e. transitions between regions of different gradients. This occurs in the lower temperature range when the whole process is chemically controlled, because the enzyme reaction is very slow, and diffusion limitation is not expressed (Figure 2.35). With increasing turnover rate at higher temperatures substrate depletion occurs, the total reaction exhibiting the characteristics of diffusion limitation, resulting in a lower gradient in the Arrhenius plot. At very low substrate concentrations, however, diffusion control covers the whole measurement range, and only a single straight line is obtained.

2.9.2 Polymer Substrates

Enzymes cleaving polymer substrates with numerous identical bonds, such as starch, cellulose, or chitin, do not obey the normal Michaelis-Menten relationship. K_m increases with decreasing degree of polymerisation or molecule mass, while V decreases, i.e., the kinetic constants change during the progress of the enzymatic cleavage reaction. Assuming all reactive bonds to be equal, Chetkarov and Kolev (1984) derived the following relationship:

$$v = \frac{k'_2 \dfrac{M_A - M_{A\infty}}{N_A m_1}\left(1 + \dfrac{M_A}{M_E}\right)[E][A]}{\dfrac{k'_{-1} - k'_2}{k'_1} \cdot \dfrac{a}{(C_b^a)^a} \cdot \dfrac{M_A}{N_A} + [A]} \quad . \tag{2.190}$$

K'_m and k'_2 are the kinetic constants for the reactive bonds, M_A and $M_{A\infty}$ is the substrate molecule mass before and after infinite enzyme reaction. M_E is the molecule mass of the enzyme, m_1 that of the monomer unit of the polymer (e.g., glucose). N_A

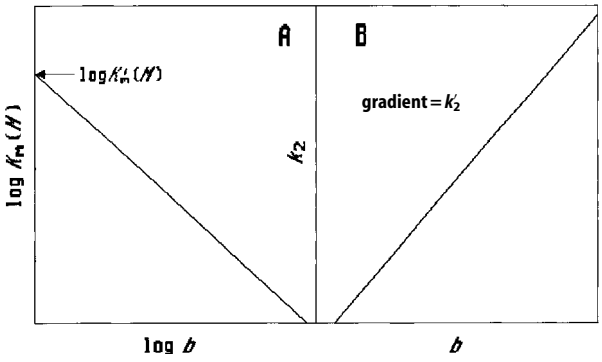

Figure 2.36. Determination of constants K'_m and K'_2 for the reactive bonds of a polymer substrate, plotting (A) the actual measured Michaelis constants K_m, and (B) the maximum velocity k_2 against the number b of the reactive centres of the substrate molecule.

is the Avogadro constant; a is the number of active centres per enzyme molecule, b the number of reactive bonds per substrate molecule, and b_∞ the number of uncleaved bonds after the enzyme reaction. $(C_b^a)^a$ stands for the effective number of possible combinations between the active centres of the enzyme and the reactive bonds of the substrate. For most enzymes $a=1$ and $C_b^1=b$; $a=\sigma_A/\sigma_E$ is the ratio of the effective cross-section of the reactive substrate bond σ_A to the cross-section of the active site σ_E. Eq. (2.190) follows the Michaelis-Menten relationship, assuming $M_A \ll M_E$:

$$V = k_2[E] = k'_2 \frac{M_A - M_{A\infty}}{N_A m_1}[E][A] = k'_2(b - b_\infty)[E][A] \tag{2.191}$$

and

$$K_m(M) = \frac{K_m}{M_A} = \frac{k'_{-1} + k'_2}{k'_1 N_A b^a} = \frac{K'_m(M)}{b^a} \tag{2.192}$$

The corresponding constants can be obtained from plots after Eqs. (2.191) and (2.192), plotting the actually measured Michaelis constant and the maximum velocity, respectively, against the number of reactive centres of the substrate molecule (Figure 2.36).

2.10 pH and Temperature Dependence of Enzymes

2.10.1 pH Optimum Curve and Determination of p*K* Values

Enzyme activity exhibits a significant dependency on the pH value of the medium. With rising pH values, activity increases to a maximum (*pH optimum*) and drops to zero in the alkaline region, which is expressed in a bell-shaped optimum curve (Fig. 2.37 A). The shape of the curve is determined by two effects, varying according to the respective type of enzyme: direct involvement of ionic groups in the catalytic mechanism and participation of charged groups in the stabilisation of the protein structure.

Ionic groups are frequently involved in enzymatic catalysis (e.g., acid-base catalysis), the state of which protonation is essential for the reaction. Thus the active centre of chymotrypsin forms a catalytic triad with the hydroxyl group of serine, the imidazole group of histidine, and the carboxyl group of aspartate. Deviations from the optimum pH value alter the state of protonation of the groups involved and withdraw them from the catalytic process. In a simple diprotic system the pH optimum is formed by a rising titration curve for a residue active in a protonated state, and a decreasing titration curve for the protonation linked inactivation of a second residue. The pK values of the corresponding groups in the enzyme-substrate complex (pK_{EA}) are the midpoints of the titration curve. The point of maximum activity corresponds to the pH optimum of the enzyme (Figure 2.37A). The determination of enzyme activity must always take place under saturating conditions for all substrates and cofactors, i.e., at the apparent maximum velocity (V_{app}, different from the maximum velocity V, extrapolated to $[A] \rightarrow \infty$).

For determination of the pK values according to Dixon and Webb (1974) the logarithm of V_{app} is plotted against the pH value (Figure 2.37 B). At ideal titration conditions the curve rises at both ends with the gradient 1 or –1, respectively. Both gradients extrapolate to a horizontal line drawn through the maximum of the curve, intercepting with it at the position of the pK_{EA} values. If protonation in the active centre of the groups is altered by substrate binding, their pK_E values in the free enzyme differ from the pK_{EA} values of the enzyme-substrate complex. The apparent binding

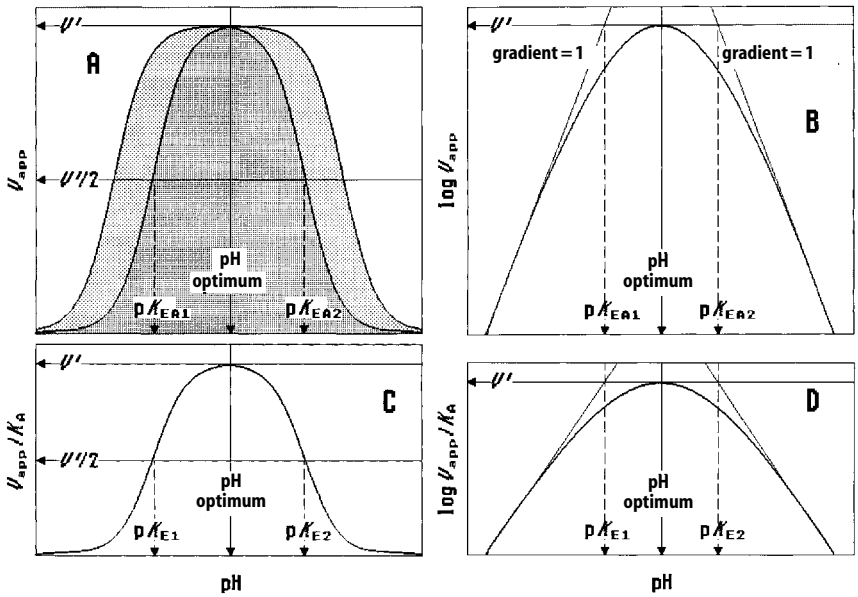

Figure 2.37. pH behaviour of enzymes. (A) Direct plot of the apparent maximum velocity against the pH value. The inner curve shows an ideal pH optimum curve with two titratable groups, while the outer shows a pH stability curve. Method for the determination of pK values of the enzyme-substrate complex (B), and of pK values of the free enzyme (C) and (D) (Dixon and Webb, 1973).

constant of the substrate K_A is then dependent on the state of protonation of the groups and thus on the pH value. The pK_E values of the free enzyme are determined in the same way as the pK_{EA} values by plotting V_{app}/K_A (or V_{app}/K_m) or log V_{app}/K_A, respectively, against the pH value (Figures 2.37 C and D).

Ionisation constants may also be obtained from secondary plots of the Lineweaver–Burk diagram. The dependence of the turnover rate v on substrate concentration is measured at different pH values. Plotting $1/v$ against 1/[A] results in a group of straight lines with a common intercept left of the ordinate. Plotting the gradients of these lines against the reciprocal proton concentration $1/[H^+]$, a straight line intercepting the abscissa at $-1/K_{EA}$ is obtained.

A reliable determination of the pK values from this plot can only be obtained at a difference between pK_1 and pK_2 values of more than 3.5 pH units. With an involvement of more than two ionic groups, or with a different activation behaviour deviating curves result. If only a single group is involved (or the process of protonation is only relevant for enzyme activities within a certain pH range, either acid or basic), only one flank of the optimum curve is obtained. With more than two ionic groups involved, there are superimpositions, detectable only by larger pH differences of the pK values, e.g., by steps in the flanks of the optimum curve. From the pK values of the titration curves it may be concluded which groups were involved in catalysis. However, the pK values of ionic groups of isolated amino acids often differ dramatically from those in the active centre. Their integration into the protein molecule may result in shifts of several pH units.

2.10.2 pH Stability of Enzymes

Due to the polyionic protein nature of enzymes, charged groups not directly involved in catalysis also codetermine the pH behaviour of enzymes. This specifically refers to groups with major functions in conserving the native enzyme structure. In the active centre protonation is a predominantly reversible process, while changes in the charge of structure-supporting residues may cause irreversible damage of the native structure. pH stability curves are applied to distinguish reversible from irreversible pH-dependent processes. The relevant enzyme is pre-incubated at the respective pH value for a certain time, subsequently activity is measured at optimum pH value. Reversible processes may not show any changes in activity, the pH stability curve exhibits a plateau in this region, dropping at both ends as a result of irreversible inactivation, making the curve wider than the pH optimum curve (Figure 2.37A).

Irreversible denaturation may also be detected by time-dependent determination of enzyme activities, incubated at distinct pH values. In reversible processes, activity remains stable, irreversible processes cause a decline in activity, mostly exponentially following a reaction of first order. When studying the pH behaviour of enzymes it must be considered that substrates, coenzymes (e.g., NAD), or indicator enzymes comprised in the test system also exhibit instabilities within certain pH ranges, and may have an effect on the pH optimum. Control pre-incubations with the test components in absence of the enzyme at different pH values must be performed.

2.10.3 Thermal Stability of Enzymes

Similar to chemical reactions the velocity of the enzyme-catalysed reaction increases with temperature by a factor of 2–3 per 10 °C. At higher temperatures the increase is retarded, it passes a maximum, and beyond the maximum the turnover rate declines again (Figure 2.38). Source of this process is the destabilisation and irreversible deactivation of the catalyst, caused by its thermosensitive protein nature. The position of the temperature maximum indicates the temperature stability of the analysed enzyme. For most enzymes, it is between 40 °C and 50 °C, which is somewhat above body temperature. There are also temperature-sensitive enzymes, e.g., alcohol dehydrogenase destabilising already at 30 °C. Enzymes of thermophilic microorganisms from hot volcanic springs sometimes remain active beyond the boiling point of water, although their structure does not significantly differ from normal proteins. The higher temperature sensitivity of most enzymes is not so much an inevitable property of their protein nature, rather the necessity of a high resistance to temperature became dispensable in the course of evolution, with adaptation to moderate living conditions and a constant body temperature.

The temperature maximum is only a qualified indicator of the temperature stability of an enzyme. The maximum temperature is determined by a time-dependent irreversible inactivation and thus depends on the period of time for which the enzyme is exposed to the elevated temperature. If the activity of an enzyme is determined immediately after an increase in temperature, the maximum is higher than it would be, if the enzyme was pre-incubated at this temperature before the test for a longer period of time. This demonstrates that it is not a "temperature optimum" comparable to the pH optimum, as at this point the enzyme is by no means in an optimum state. Therefore, this term should be avoided. For enzyme tests a temperature clearly below the maximum is recommended. At the maximum point and beyond denaturation processes can be observed, and these give insight into the enzyme structure. The enzyme is pre-incubated at a constant temperature. By taking samples at distinct times, the change in enzyme activity is monitored under normal assay conditions. At tempera-

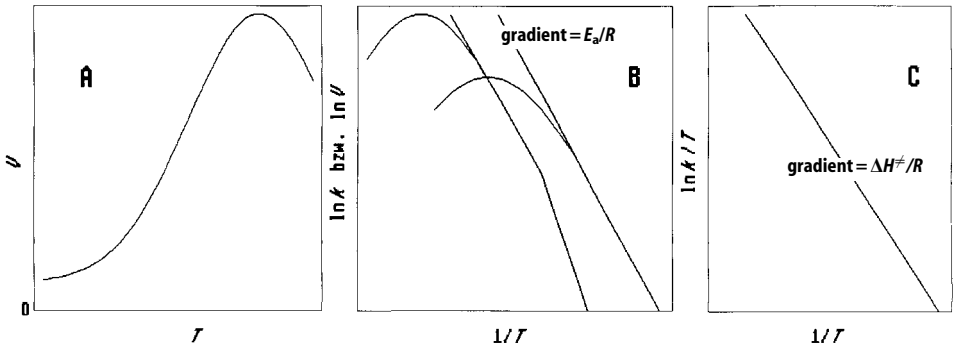

Figure 2.38. Temperature behaviour of enzymes. (A) Direct plot of the apparent maximum velocity against temperature, (B) Arrhenius plot, (C) diagram for the determination of the reaction enthalpy $\Delta H^{\neq}$ of the transition state.

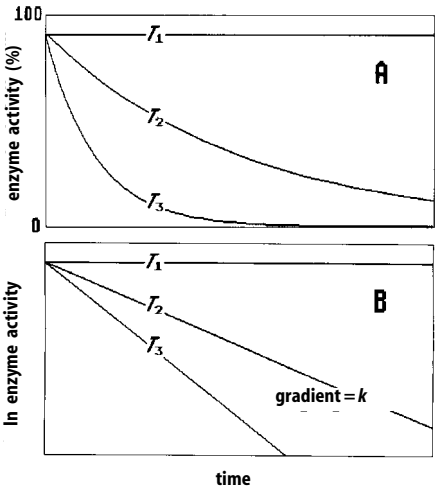

Figure 2.39. Thermostability of enzymes in a direct plot (A), and a semi-logarithmic plot (B). The enzyme is pre-incubated at a distinct temperature below the temperature maximum (T_1), in its range (T_2), and beyond (T_3).

tures within the range of thermic enzyme deactivation, mostly an exponential decline of activity is observed, following first order denaturation kinetics (Figure 2.39 A). Actually, the denaturation process runs over several steps, but normally only one distinct step is responsible for the loss of enzymatic activity. In a semi-logarithmic plot of k_{cat} or v against time, straight lines are obtained the gradients of which yield the rate constants of denaturation (Figure 2.39 B). Denaturation processes can also be studied by other methods, e.g., absorption, fluorescence, and CD spectroscopy or calorimetry. In rare cases the phenomenon of cold inactivation is observed.

2.10.4 Temperature Dependence of Enzyme Reactions

When plotting $\ln k_{cat}$ or $\ln v$ against the reciprocal absolute temperature (K^{-1}, $0\,^{\circ}C = 273.15$ K) in the area below the temperature maximum, i.e., outside the area of thermic denaturation, most enzyme reactions show a linear dependency. This plot is based on the empiric equation by S. Arrhenius (1889)

$$k = A \cdot e^{-E_a/RT} , \tag{2.193}$$

which by logarithmic conversion yields the linear relationship:

$$\ln k = \ln A - \frac{E_a}{RT} \quad \text{or} \quad \log k = \log A - \frac{E_a}{2.3RT} \tag{2.194}$$

E_a is the activation energy of the transition state of enzyme catalysis, which can be derived from the gradient of the Arrhenius plot (Figure 2.38 B). The constant A represents the probability of a reaction to take place and comprises components for the collision frequency and the orientation of the colliding particles. R is the gas constant.

Definite integration of Eq. (2.193) leads to:

$$\log \frac{k_2}{k_1} = \frac{E_a}{2.3R} \left(\frac{T_2 - T_1}{T_1 T_2} \right) . \tag{2.195}$$

With this equation E_a can be determined from the turnover rates at two different temperatures. The rate constants of the reaction k can be replaced by the maximum velocity $V = k\ [E]_0$. Since the dissociation and Michaelis constants also depend on temperature, the studies of the temperature behaviour of enzyme reactions must be undertaken at substrate saturation. In a strict sense the actual V values should be determined for each temperature by extrapolation to $[A] \rightarrow \infty$. The activation energy mostly ranges between 40-50 kJ/mol. It is a complex constant, composed of different partial processes, each possessing its own temperature correlation, so that with steady temperature changes the rate-determining step may change. This may become obvious in the Arrhenius plot in two or more areas of varying gradients. Multi-phase behaviour may also have other reasons, like isoenzymes or conformational transitions of the enzyme or of the membrane with membrane-bound enzymes. Thermostable enzymes which are active over a broad temperature range often show a multi-phase temperature behaviour expressing varying states of stability.

The principle of enzymatic catalysis is based on the theory of H. Eyring (1953). According to this the activation energy is reduced by stabilising the transition state. For conversion into product, the substrate must surmount the energy barrier of the transition state. Only substrate molecules with sufficient energy will be converted. The lower the barrier, the higher the share of molecules able to participate in the reaction. Figure 2.40 shows the energy profile of an enzyme-catalysed reaction, assuming transition states for binding of the reactants from both directions as well as for the effective conversion process. For various enzyme reactions substances were synthesized simulating the transition state (*transition state analogues*). They exhibit binding affinities several orders of magnitude higher than the intrinsic substrate.

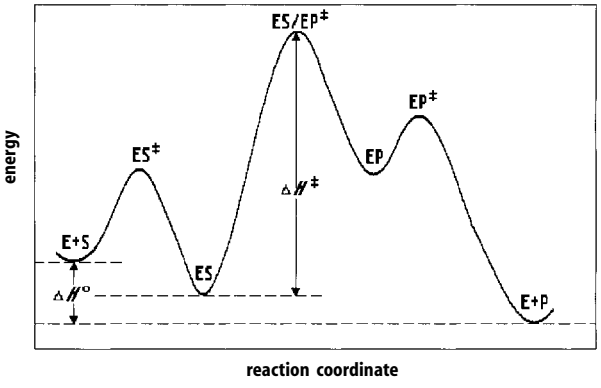

Figure 2.40. Energy profile of an enzyme-catalysed reaction.

Arrhenius developed his equation in analogy to the van't Hoff reaction isobars, describing the dependency of the dissociation constant K_d on temperature at reaction equilibrium:

$$\left(\frac{d \ln K_d}{dT}\right)_P = \frac{\Delta H^0}{RT^2} \ . \tag{2.196}$$

For narrow ranges the standard reaction enthalpy ΔH^0 can assumed to be temperature independent, so that integration

$$\ln K_a = -\frac{\Delta H^0}{RT} + C \tag{2.197}$$

results in a linear relationship of the logarithm of the dissociation constant from the reciprocal absolute temperature. ΔH^0 can be calculated from the gradient. The integration constant C includes the reaction entropy ΔS^0:

$$\ln K_a = -\frac{\Delta H^0}{RT} + \frac{\Delta S^0}{R} \ , \tag{2.198}$$

that can be calculated from the ordinate intercept. Equation (2.196) is obtained from the relationship for the Gibbs free standard energy $\Delta G^0 = \Delta H^0 + T\Delta S^0$, related to the dissociation constant $\Delta G^0 = RT \ln K_d$. For the free energy of the transition state $\Delta G^{\ddagger}$ follows:

$$\Delta G^{\ddagger} = -RT \ln K^{\ddagger} = \Delta H^{\ddagger} - T\Delta S^{\ddagger} . \tag{2.199}$$

From quantum mechanics it follows that the rate constant k for the formation of the transition state relates to the equilibrium constant $K^{\ddagger}$ of the transition state after $k = K^{\ddagger}(RT/N_A h)$, N_A is the Avogadro constant and h Planck's quantum. The following relationship is achieved from Eq. (2.199) for the transition state:

$$\log \frac{k}{T} = -\frac{\Delta H^{\ddagger}}{2.3RT} + \frac{\Delta S^{\ddagger}}{2.3R} + \log \frac{R}{N_A h} \ . \tag{2.200}$$

From this equation $\Delta H^{\ddagger}$ can be calculated from the gradient (Figure 2.38 C), if the dependency of log k/T against $1/T$ is linear. Different from the Arrhenius plot, absolute values must be inserted for k. The Arrhenius activation energy is related to the enthalpy of the transition state by the relationship $E_a = \Delta H^{\ddagger} + RT$.

For experimental practice it must be considered that components of the enzyme test and auxiliary enzymes are also temperature-sensitive and may affect the temperature curve of the test enzyme. It is advisable to pre-incubate the test mixture without enzyme at different temperatures and subsequently measure the enzyme reaction at a constant temperature. If all other components remain stable, a constant turnover rate has to be achieved.

2.11 Isotope Exchange

Isotopes are valuable tools for the study of enzyme reactions. Two frequent applications will be described here: isotope exchange kinetics, providing valuable information especially for multi-substrate reactions, and the kinetic isotope effect, providing information about certain mechanisms of enzyme catalysis.

2.11.1 Isotope Exchange Kinetics

Isotope exchange kinetics can be described under two aspects: the system, consisting of substrate, product and enzyme, may be either in *or* out of equilibrium. Systems in equilibrium allow simple and unique interpretations, and only these will be discussed here. More extensive descriptions are to be found, e.g., in Fromm (1973), Huang (1979), and Purich and Allison (1980).

In the presence of enzyme the system is allowed to attain equilibrium. Substrates and products are already added in their equilibrium concentrations according to the equilibrium constant $K_e = [P][Q]\ldots/[A][B]\ldots$. to speed up the process. The equilibrium constant can be obtained by setting a fixed P/A ratio as shown in Figure 2.41. After adding the enzyme, size and direction of the shifts $\Delta[A]$ or $\Delta[P]$ are determined. The intercept of the resulting curve at $\Delta[A]$ or $\Delta[P] = 0$ equals the position of equilibrium. A particular substrate/product pair, e.g., B/P in a bisubstrate reaction, is varied at several concentration levels, the change lying in the ratio of the equilibrium concentration. The complementary pair A/Q remains constant. A small quantity of a component (e.g., A* as a radioactive isotope), not affecting the equilibrium, is added. $A \leftrightarrow Q$ exchange as the result of changes of the B/P pair is recorded by time-dependent measurement.

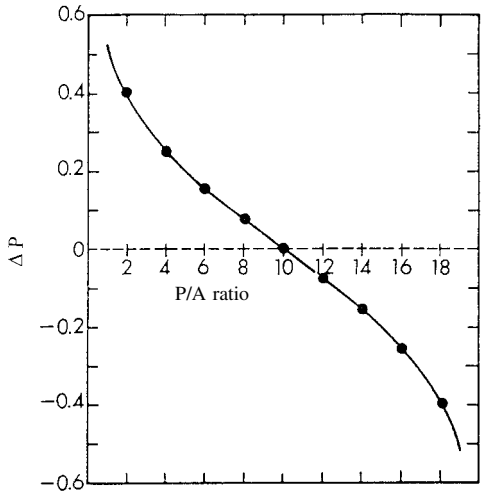

Figure 2.41. Determination of the equilibrium constant of a reaction by approximation of the substrate/product ratio P/A. Enzyme is added to a fixed mixture of A and P and the direction of the change is monitored. Equilibrium is reached at ΔA or $\Delta P = 0$ (Purich and Allison, 1980).

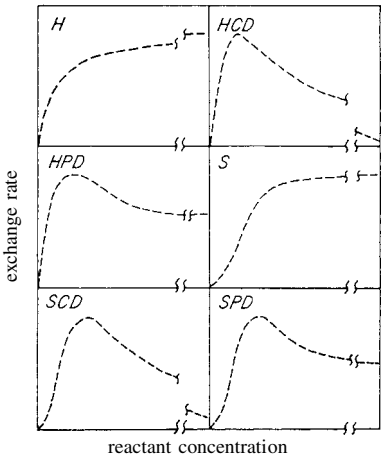

Figure 2.42. Profiles of isotope exchanges for various enzyme reaction mechanisms. H: hyperbolic, HCD: hyperbolic with complete depression, HPD: hyperbolic with partial depression, S: sigmoidal, SCD: sigmoidal with complete depression, SPD: sigmoidal with partial depression (Purich and Allison, 1980).

Table 2.5. Profiles of isotope exchanges in single- and multi-substrate reactions (Purich and Allison, 1980). H: hyperbolic, HCD: hyperbolic with complete depression, L: linear

Mechanism	Exchange	Variable substrate-product pair			
		A-P	B-P	A-Q	B-Q
Uni-uni	A↔P	H			
Ordered *bi-uni*	A↔B	H	HCD		
	B↔P	H	H		
Random *uni-bi*	all	H	H		
Rapid equilibrium					
Ordered *bi-bi*	A↔P	H	HCD	H	HCD
	B↔P	H	H	H	H
	A↔Q	HCD	HCD	H	HCD
	B↔Q	HCD	HCD	H	H
Teorell-Chance *bi-bi*	A↔P	H	H	H	HCD
	B↔P	H	L	H	H
	A↔Q	HCD	H	H	HCD
	B↔Q	HCD	H	H	H
Random *bi-bi*	all	H	H	H	H

Derivation of the rate equations of the exchange reaction R for different multi-substrate reactions is complex (see Huang, 1979; Purich and Allison, 1980) and not very informative, as kinetic constants can hardly be obtained from the isotope exchange itself. Rather the profiles of the exchange rate are indicative of particular reaction types, and it is distinguished between hyperbolic (H), hyperbolic with complete (HCD) and partial depression (HPD), sigmoidal (S), and sigmoidal with complete (SCD) and partial depression (SPD). Depression is defined as a decreasing curve at higher concentrations of the varied substrate/product pair (Figure 2.42, Table 2.5). Sigmoidal curves can also be indicative of cooperative effects.

Especially the A↔Q exchange rate is diagnostic for an obligatory *ordered bi-bi mechanism*, where A precedes binding of B, and P is released before Q (scheme 2.130). A↔Q exchange requires an enzyme species that can bind to the labelled compound A*. This is the case at medium concentrations of the B/P pair. At first the A↔Q exchange rate increases, but at high B/P amounts the enzyme species accessible for A* becomes depleted and the A↔Q exchange rate decreases (Figure 2.42 C, D). A normal hyperbolic exchange profile is achieved for the B↔P exchange by increase of the A/Q pair, as this will create predominance of the enzyme species EA and EQ, required for the combination with B* and P* (Figure 2.42 H).

Because of alternative pathways, where A* can bind either to E or to EB, no decrease of the A↔Q exchange rate is observed at the increase of the B/P pair in the *random bi-bi mechanism*. For symmetry reasons, this statement is valid for all kinds of exchange in this mechanism. If in a random mechanism the conversion of the ternary complexes is rate-limiting, the velocity for each exchange will be identical. Otherwise exchange rates will differ.

A speciality of the *ping-pong mechanism* is that the exchange is already possible with half part of the reaction, e.g., an A↔P exchange can be performed in the absence of the B/Q pair (and *vice versa*):

$$\mathrm{E} + \mathrm{A} \quad \underset{k_{-1}}{\overset{k_1}{\rightleftharpoons}} \quad \mathrm{EA} \quad \underset{k_{-2}}{\overset{k_2}{\rightleftharpoons}} \quad \mathrm{E}' + \mathrm{P}\,, \tag{2.201 a}$$

$$\mathrm{E}' + \mathrm{B} \quad \underset{k_{-3}}{\overset{k_3}{\rightleftharpoons}} \quad \mathrm{E}'\mathrm{B} \quad \underset{k_{-4}}{\overset{k_4}{\rightleftharpoons}} \quad \mathrm{E} + \mathrm{Q}\,. \tag{2.201 b}$$

According to steady-state rules the following equation is valid for the exchange rate of the partial reaction (2.101a) (A* is the marked compound, only the initial reaction is recorded, the reverse reaction of P* to EA* is disregarded):

$$\frac{\mathrm{d}[\mathrm{EA}^*]}{\mathrm{d}t} = k_1[\mathrm{E}][\mathrm{A}^*] - (k_{-1} + k_2)[\mathrm{EA}^*] = 0\,, \tag{2.202}$$

$$[\mathrm{EA}^*] = \frac{k_1[\mathrm{E}][\mathrm{A}^*]}{k_{-1} + k_2}\,. \tag{2.203}$$

The velocity of the exchange reaction is:

$$v^* = k_2[\mathrm{EA}^*]\,. \tag{2.204}$$

Inserting for [EA*] gives:

$$v^* = \frac{k_1 k_2[\mathrm{E}][\mathrm{A}^*]}{k_{-1} + k_2} \tag{2.205}$$

If the exchange takes place in the absence of B and Q, $[\mathrm{E}]_0 = [\mathrm{E}] + [\mathrm{E}'] + [\mathrm{EA}]$:

$$[EA] = \frac{k_1[A][E]}{k_{-1}}\ ,\ [E'] = \frac{k_1 k_2[A][E]}{k_{-1}k_{-2}}\ ,$$
$$[E]_0 = [E]\left(1 + \frac{k_1[A]}{k_{-1}} + \frac{k_1 k_2[A]}{k_{-1}k_{-2}}\right) \tag{2.206}$$

$$v^* = \frac{k_2[E]_0[A^*]}{\dfrac{(k_{-1}+k_2)}{k_1}\left(1 + \dfrac{k_1[A]}{k_{-1}} + \dfrac{k_1 k_2[A]}{k_{-1}k_{-2}[P]}\right)}\ . \tag{2.207}$$

At similar specific radioactivity [A*] and [A] may be set as equal. The reciprocal formula is:

$$\frac{1}{v^*} = \frac{k_{-1}+k_2}{k_1 k_2[E]_0}\left(\frac{1}{[A]} + \frac{k_1}{k_{-1}} + \frac{k_1 k_2}{k_{-1}k_{-2}[P]}\right)\ , \tag{2.208}$$

and in the form of the kinetic constant:

$$\frac{1}{v^*} = \frac{K_{mA}}{V_1[A]} + \frac{K_{mA}}{V_1 K_{iA}}\left(1 + \frac{K_{iP}}{[P]}\right)\ . \tag{2.209}$$

From a plot of $1/v^*$ against 1/[A] at different amounts of [P] parallels are achieved, whose ordinate intercepts, plotted against 1/[P] in a secondary diagram, yield a straight line with the ordinate intercept of a reciprocal maximum exchange velocity: $V^* = k_{-1}k_2[E]_0/(k_{-1}+k_2)$. This differs from the maximum velocity of the forward reaction of the ping-pong mechanism ($V_1 = k_2 k_4\,[E]_0/k_2 + k_4$), the ratio between k_{-1} and k_4 being the determining factor. Are both rate constants equal, than both maximum velocities are also identical. If k_{-1} is larger than k_4, the exchange rate $V^*_{A\leftrightarrow P} > V_1$, and *vice versa*. Beyond this there exist no further relationships between these two terms.

Between the maximum initial and exchange velocities holds the following relationship:

$$\frac{1}{V^*_{A\leftrightarrow P}} + \frac{1}{V^*_{B\leftrightarrow Q}} = \frac{1}{V_1} + \frac{1}{V_2}\ , \tag{2.210}$$

in the form of the rate constants,

$$\frac{k_{-1}+k_2}{k_{-1}k_2} + \frac{k_{-3}+k_4}{k_{-3}k_4} = \frac{k_2+k_4}{k_{-2}k_4} + \frac{k_{-1}+k_{-3}}{k_{-1}k_{-3}} \tag{2.211}$$

i.e., all four parameters must be known in order to evaluate the relationship between exchange rate and initial velocity. This also demonstrates that it is practically not possible to determine kinetic parameters from exchange experiments. The ping-pong mechanism is one of the few exceptions. For the partial reaction of the $A\leftrightarrow P$ exchange in the absence of B and Q the gradient of the straight line in the double reciprocal plot has the value K_{mA}/V_1, and the ordinate intercept $K_{mA}/V_1 K_{iA}(1 + K_{iP}/[P])$.

The ordinate intercepts, plotted against 1/[P], yield K_{mA}/V_1K_{iA} as ordinate, and $-1/K_{iP}$ as abscissa intercepts. Reversely, the constants K_{mB}, K_{iB}, and K_{iQ} are obtained from the $B \leftrightarrow Q$ exchange in the absence of A and P.

Abortive complexes, i.e., non-productive enzyme species, influence and seriously impede the analysis of exchange data. Such abortive complexes can evolve when ligands bind to the enzyme under conditions that prevent the enzyme from performing the catalysis. Binding of pyruvate and NAD^+ by lactate dehydrogenase is an example. Both ligands are already oxidised and hydrogen transfer is not possible.

2.11.2 Isotope Effects

2.11.2.1 Primary Kinetic Isotope Effect

Isotope effects are caused by the fact that the altered mass of the isotope influences the turnover rate of the reaction. In most cases the mass differences are minimal, e.g., only 8% between ^{13}C and ^{12}C. The maximal isotope effects to be observed are $^{13}C/^{12}C = 1.07$, $^{15}N/^{14}N = 1.04$, and $^{18}O/^{16}O = 1.06$. This requires high precision of the respective analytic method, e.g., mass spectroscopy. Mass differences of 100% or 200%, however, exist between deuterium (D) or tritium (T) and hydrogen (H). In reactions where proton transfer is rate-determining, a significant reduction of the reaction rate is to be observed in D_2O. The ratio of the rate constants k_H/k_D ranges between 2 and 15. The effect is even more pronounced in tritium with a relationship of $\log k_H/k_T = 1.44 \log k_H/k_D$. However, only D_2O is available in 100% concentration, so that each molecule reacts in a homogeneous population, while in reactions with T_2O only 1 in 10^{10} molecules exists as ^3H. Macroscopically, a reduction of the turnover rate cannot be realized in this condition, and a different method must be applied to detect the effect. If, e.g., ^3H is released into water in the LDH reaction, ^3H_2O is formed at a non-rate-determining proton transfer ($k_H/k_T = 1$) with the same specific radioactivity as the substrate, at $k_H/k_T = 10$, however, only with 1/10. If 1 mmol lactate is converted into pyruvate, only 100 µmol ^3H_2O is formed. Water can be distinguished from substrate by its volatility. Thus, the reaction discriminates ^3H-marked molecules, so that the specific radioactivity of the remaining substrate molecules increases.

The isotope effect is based on the difference in energy of zero point oscillations. While heavy C atoms are fixed, the frequency of the extended oscillation depends on the mass difference between D and H. The energy of the basic state for C–D binding is lower than that of C–H binding, while both possess the same energy in the transition state. Thus the energy difference between basic and transition state for C–D binding is higher than for C–H binding. The activation energy for the cleavage of C–D bond is 4.8 kJ/mol higher than for C–H binding. This corresponds to an almost 7-fold difference in velocity.

It is generally assumed that at reduction of the velocity by a factor of 2–15 a primary kinetic isotope effect is exhibited, and the cleavage of a C–H bond is rate-determining. Conversely, the absence of an isotope effect indicates that the cleavage of a C–H bond is not rate-limiting, even if it occurs during the total reaction process.

At a reduction of the velocity by less than two, the proton transfer is only partially rate-determining. There either exist two or more comparably slow steps, or a secondary isotope effect may be effective (see Section 2.11.2.3).

2.11.2.2 Influence of the Kinetic Isotope Effect on V and K_m

The isotope effect is manifested in the reduction of proton transfer velocity. Thus, in an enzymatic reaction the maximum velocity is affected, and not so much the Michaelis constant. This can be tested by a double reciprocal plot of $1/v$ against 1/[A], the turnover rate having been measured in dependency of the substrate concentration with hydrogen, as well as in the presence of the isotope. With normal behaviour, straight lines are obtained that display different ordinate intercepts because of different maximum velocities, but show a common abscissa intercept due to the same Michaelis constant. For $V_H/V_D > 1$, V is partially or completely controlled by a single step including a C–H bond cleavage. High V_H/V_D ratios of up to 8 are rarely observed; the V_H/V_D ratio lies mostly between 1.5 and 2.0. These relatively small isotope effects are scarcely determined by a single step. A high energy barrier may be substituted by several small barriers, each step binding partially rate-determining.

In case of $K_m = K_d$ no isotope effect is to be expected for the Michaelis constant, as the physical binding step is not sensitive to isotope exchanges. Because of the different size of D and H there might be a steric isotope effect when the active centre is of limited size. Also, bindings with deuterium are more difficult to polarise than those with hydrogen. If the formation of a transition complex includes removal of a proton, K_m may also be affected.

For the description of the isotope effect the conversion from A into P and the release of product, which both are combined in the simple Michaelis-Menten equation, have to be differentiated:

$$E + A \underset{k_{-1}}{\overset{k_1}{\rightleftharpoons}} EA \underset{k_{-2}}{\overset{k_2}{\rightleftharpoons}} EP \underset{k_{-3}}{\overset{k_3}{\rightleftharpoons}} E + P. \tag{2.212}$$

According to the steady-state rules (under conditions of the initial rate k_{-2} and k_{-3} are not considered) the following equation may be derived

$$v = \frac{\dfrac{k_2 k_3 [E]_0 [A]}{k_2 + k_3}}{\dfrac{(k_{-1} + k_2) k_3}{k_1 (k_2 + k_3)} + [A]} \tag{2.213}$$

where $V = k_2 k_3 [E]_0/(k_2 + k_3)$ and $K_m = (k_{-1} + k_2) k_3/k_1 (k_2 + k_3)$. The influence of the isotope effect depends on the ratio between k_2 and k_3. For $k_2/k_3 < 1$ or $k_2 \ll k_3$ V becomes $V = k_2 [E]_0$, or $V_H/V_D = k_{2(H)}/k_{2(D)}$, respectively. The observed isotope effect approximates the true isotope effect. For $k_2/k_3 > 1$ or $k_2 \gg k_3$, respectively, the release of product becomes rate determining, and because of

$$\frac{V_H}{V_D} = \frac{k_{2(H)}(k_{2(D)} + k_3)}{k_{2(D)}(k_{2(H)} + k_3)} \rightarrow 1$$

an existing isotope effect is suppressed.

The relationship of the kinetic constants according to Eq. (2.213) is:

$$\frac{V}{K_m} = \frac{k_1 k_2 [E]_0}{k_{-1} + k_2} \ . \tag{2.214}$$

Inserting this into the relation of the isotopes gives:

$$\frac{\left(\frac{V}{K_m}\right)_H}{\left(\frac{v}{K_m}\right)_D} = \frac{k_{2(H)}(k_{-1} + k_{2(D)})}{k_{2(D)}(k_{-1} + k_{2(H)})} = \frac{k_{2(H)}}{k_{2(D)}} \left(\frac{1 + \frac{k_{2(D)}}{k_{-1}}}{1 + \frac{k_{2(H)}}{k_{-1}}} \right) . \tag{2.215}$$

The apparent isotope effect is reciprocally dependent on the ratio of k_2/k_{-1}. For $k_2 \ll k_{-1}$, Eq. (2.215) approximates $k_{2(H)}/k_{2(D)}$, the isotope effect is fully expressed. For $k_2 \gg k_{-1}$ the isotope effect is suppressed, as $(k_{2(H)}/k_{2(D)})/(k_{2(D)}/k_{2(H)}) = 1$. Under this condition catalysis is significantly faster than decomposition of the ES complex into E + S, so that the isotope effect cannot manifest itself.

In many enzymatic reactions the effects on V and V/K_m are identical. In these cases K_m is identical for unlabelled and for deuterised substrates. Only if K_m has been altered for the deuterised substrate, the isotope effects on V and V/K_m are different.

2.11.2.3 Other Isotope Effects

A *secondary kinetic isotope effect* occurs if a reaction is affected by an isotope-substituted C–H bond in α-position that itself is not cleaved during the reaction process. The reason for this effect is a change in hybridisation. A basically tetrahedral, sp^3-hybridised carbon atom transforms into a transition state conforming to the carbonium ion, with a planar sp^2 arrangement. The substitution of a C–H bond by a C–D bond reduces the frequency of deformation vibrations. It is easier for the substrate to form the sp^2 intermediate with a C–H bond than with a C–D bond. A ratio of $k_H/k_D = 1.38$ is to be expected; ratios from 1.02–1.40 are observed. The secondary isotope effect is much less pronounced than the primary and is easy to identify. A secondary isotope effect was observed, e.g., for the dehydratisation of malate in the fumarase reaction.

D_2O can also affect the enzyme reaction with its properties as a solvent. The change of proton concentration in D_2O against H_2O and thus the altered ionisation in substrates and enzymes may affect functionality. In D_2O the pH value adjusted by standard buffer is changed: pD = pH + 0.4. Most acids are 3–5 times weaker in D_2O than in water, corresponding to a pK difference of 0.5–0.7. Number and strength of

hydrogen bonds and hydrophobic interactions are also altered. D_2O is 23% more viscous than H_2O, the O–D bond is 0.004 nm shorter than the O–H bond. Thus there are changes in polarisability and in the solvent structure, which may also affect the enzyme structure.

2.12 Application of Statistical Methods in Enzyme Kinetics

2.12.1 General Remarks

The analysis of measurement data and the interpretation of curves in different plots are of great importance in enzyme kinetics. Therefore, the application of statistical methods is indispensable. Within the scope of this book they cannot be extensively treated and it is referred to the relevant literature on statistics. Here only special problems of application of statistical methods in enzyme kinetics will be discussed.

Studies of enzymes often require special procedures complicating the application of statistical rules. In order to reliably interpret the course of curves and to analyse parameters such as equilibrium and Michaelis constants, repeated measurements should principally be performed to ensure the data. However, enzymes in diluted solutions for enzyme tests are often unstable, so that the analysis of connected test series is often a race against time. The following example will demonstrate this. For a thorough analysis of inhibition or multi-substrate mechanisms test series must be performed with one parameter (substrate) varied, and another (cosubstrate, inhibitor) to be kept constant. For 10 concentration values per test series and five constant concentrations of the second parameter, 50 tests are required. Assuming 5 min per test the total time required is more than 4 h for a single analysis. If three repeated tests are undertaken, it takes more than 12 h. If the enzyme loses half of its activity within 20 h, the first measurement value will differ from the last by 14% in single analysis, and even by 35% in triple analysis. Thus the deviation caused by activity loss is much larger than the advantage of statistical safeguarding by repeated measurements. By preparing fresh enzyme dilutions within one test series the original activity will hardly be exactly reproduced, and further tests would not fit into the series. In such cases it is more favourable to establish the results obtained from single measurements by independent test series.

The diagrams used in enzyme kinetics usually serve to confirm or exclude the laws assumed for the system, e.g., the Michaelis-Menten equation. This is done by analysing how far the measured data follow the curve as predicted by the law. Due to error scattering, hardly any of the values will be located exactly on the assumed curves. So it must be decided whether observed deviations are due to error scattering or whether the system obeys any other than the assumed relationship. Normal error scattering should be distributed evenly above and below the assumed function as the average value (*constant absolute error*). This can be tested by *residual plots* where the deviation of each value from the assumed function, calculated by regression methods (e.g., a hyperbolic curve according to the Michaelis-Menten equation), is

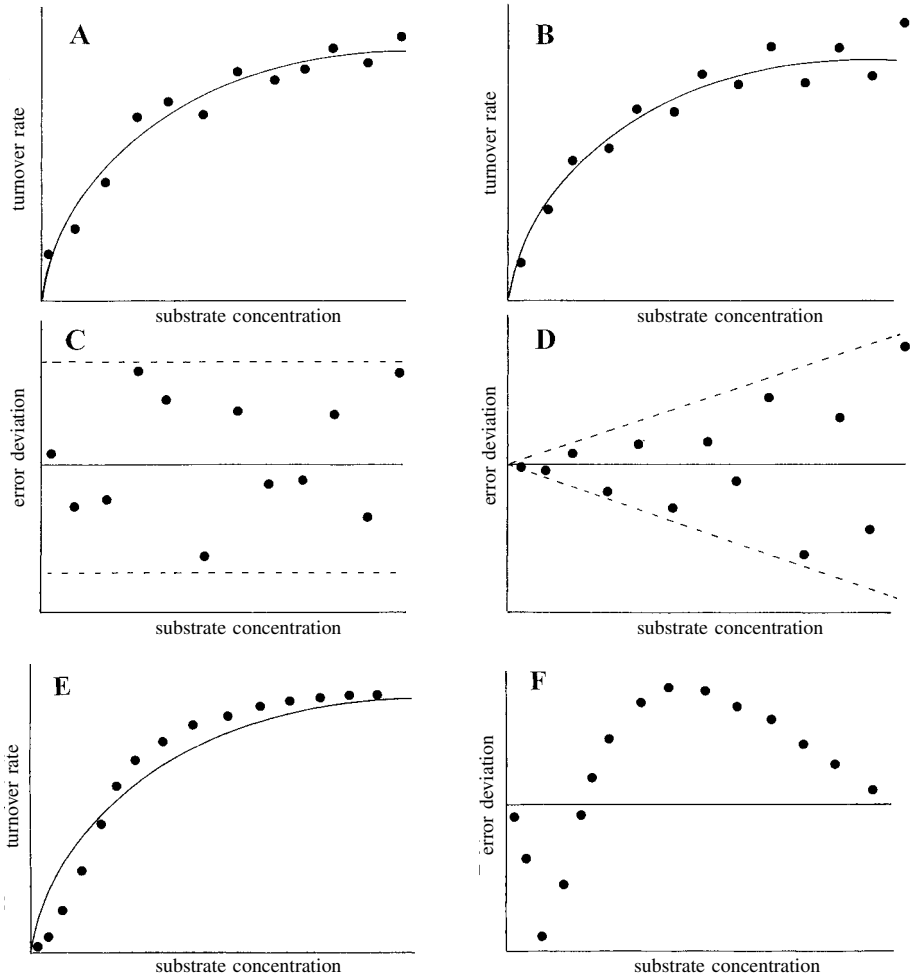

Figure 2.43. Residual plots (C, D, F) from diagrams of the dependency of the turnover rate from substrate concentration (A, B, E). Constant absolute error (σ = constant) (A, C), constant relative error (σ / v = constant) (B, D), adaptation of a sigmoidal saturation function to a hyperbolic curve (E, F).

plotted against the independent variable (e.g., substrate concentration) (Figure 2.43). The points must be distributed evenly around a median line. A *systematic error* is exhibited, if the points drift from the median line to a certain direction. This may be caused by artificial influences on the measurement or by an alternative mechanism. A *relative error* is exhibited, if the values in the residual plot scatter evenly around the median line, but their extent moves into a certain direction (e.g., the error increases with the intensity of the measurement signal). This may still confirm the assumed mechanism, but an appropriate weighting has to be considered for regression analysis. Normal regression methods are based on an even error distribution, i.e., a constant absolute error. Residual plots are especially helpful for non-linear curves,

where systematic deviations are difficult to detect by eye. Appropriate statistical methods, e.g., the *W-test* by Shapiro-Wilks or the *student-* or *t-test* serve to detect runaway data and establish the significance of the measured values. The correlation coefficient indicates the consistency of the data with the assumed curve function.

The application of statistical methods is principally recommended, as it reduces the danger of subjective analysis and interpretation. However, these methods also have their limitations and they should be critically evaluated. In enzyme kinetic measurements, mechanisms, e.g., inhibitions and multi-substrate reactions, are often identified by the patterns of groups of straight lines in linearised plots (common intercepts, parallels). It is rather unlikely that straight lines obtained by regression methods from scattering data within a test series will without exception show the same gradient or meet in exactly the same intercept, and – honestly speaking – such mechanisms will never be established applying statistical rules. It can of course be stipulated to detect parallels or common intercepts for the least deviation of all data by regression analysis, but then the mechanism is already pretended. Figure 2.44 shows two examples of uncritical application of linear regression methods from seminar protocols. The aim of scientific studies should be to obtain data of such quality that the result is also obvious without statistical analysis.

Before applying statistical methods the following criteria should be considered:

1. Is the intended method suitable for the data to be analysed?
2. Can the data be adapted equally well by other relationships?
3. Do the data exhibit deviations in certain directions that cannot be explained by normal error distribution?
4. Can artificial effects be excluded?

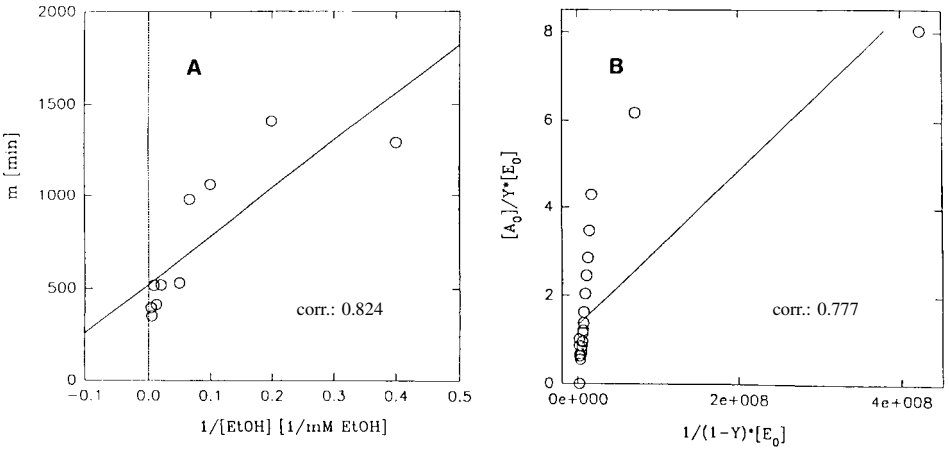

Figure 2.44. Uncritical application of linear regression (from seminar protocols). (A) Secondary plot of a bisubstrate reaction (m, gradient), (B) Stockell plot (corr., correlation coefficient).

2.12.2 Statistical Terms Used in Enzyme Kinetics

Arithmetic mean: The mean value $\overline{x}$ is the sum of all measurements x_i divided by their number n:

$$\overline{x} = \frac{\sum_{i}^{n} = 1x_\mathrm{i}}{n} \ . \tag{2.216}$$

Median: Mean value of a test series with data arrayed according to their size, for a odd number of data: $x_{(\mathrm{n}+1/2)}$, for a even number the mean value of the two mean measurements: $(x_{\mathrm{n}/2} + x_{(\mathrm{n}/2+1)})/2$.

Mode: The most frequently occurring value of a measurement series.

Variance: Mean square sum of errors:

$$\sigma_\mathrm{x}^2 = \frac{\sum_{i=1}^{n}(x_\mathrm{i} - \overline{x})^2}{n} \ . \tag{2.217}$$

Standard deviation: Root mean square deviation, RMS.

$$\sigma_\mathrm{x} = \sqrt{\frac{\sum_{i=1}^{n}(x_\mathrm{i} - \overline{x})^2}{n}} \ . \tag{2.218}$$

Standard deviation of the mean:

$$\sigma_{\overline{\mathrm{x}}} = \frac{\sigma_\mathrm{x}}{\sqrt{n}} \ . \tag{2.219}$$

Linear regression: Adaptation of data to a straight line after the least square error method. Only the error of the dependent variable y is considered (v in enzyme kinetic measurements). For the independent variable x (e.g., substrate concentration) no errors are assumed.

$$y_\mathrm{i} = a + bx_\mathrm{i} \ . \tag{2.220}$$

The ordinate intercept a is:

$$a = \frac{\sum x_\mathrm{i}^2 \sum y_\mathrm{i} - \sum x_i \sum x_\mathrm{i} y_\mathrm{i}}{n \sum x_\mathrm{i}^2 - \left(\sum x_\mathrm{i}\right)^2} \ . \tag{2.221}$$

The gradient or the *regression coefficient b*, respectively, is:

$$b = \frac{n\sum x_i y_i - \sum x_i \sum y_i}{n\sum x_i^2 - \left(\sum x_i\right)^2} \ . \tag{2.222}$$

Standard deviation of the y values:

$$\sigma_y = \sqrt{\frac{1}{n-2}\sum_{i=1}(y_i - a - bx_i)^2} \ . \tag{2.223}$$

Correlation coefficient:

$$r = \frac{\sum(x_i - \overline{x})(y_i - \overline{y})}{\sqrt{\sum(x_i - \overline{x})^2 \sum(y_i - \overline{y})}} \ . \tag{2.224}$$

Non-linear adaptation of the Michaelis-Menten equation according to the least square error method (Cornish-Bowden, 1984):

$$K_m = \frac{\sum \frac{v_i}{[A]_i}\sum v_i^2 - \sum \frac{v_i^2}{[A]_i}\sum v_i}{\sum\left(\frac{v_i}{[A]_i}\right)^2 \sum v_i - \sum \frac{v_i^2}{[A]_i}\sum \frac{v_i}{[A]_i}} \ . \tag{2.225}$$

$$V = \frac{\sum\left(\frac{v_i}{[A]_i}\right)^2 \sum v_i^2 - \sum\left(\frac{v_i^2}{[A]_i}\right)^2}{\sum\left(\frac{v_i}{[A]_i}\right)^2 \sum v_i - \sum \frac{v_i^2}{[A]_i}\sum \frac{v_i}{[A]_i}} \ . \tag{2.226}$$

2.13 References

General Literature on Steady-State Kinetics

Briggs, G.E. & Haldane, J.B.S. (1925) *A note on the kinetics of enzyme action.* Biochemical Journal 19, 338–339.

Brown, A.J. (1902) *Enzyme action.* Journal of the Chemical Society 81, 373–388.

Henri, V. (1902*) Théorie génerale de l'action de quelques diastases*. Comptes rendues de l'Academie des Sciences 135, 916–919.

Michaelis, L. & Menten, M.L. (1913) *Die Kinetik der Invertinwirkung*. Biochemische Zeitschrift 49, 333–369.

Wharton, C.W. (1983) *Some recent advances in enzyme kinetics*. Biochemical Society Transactions 11, 817–825.

Analysis of Enzyme Kinetic Data

Alberty, R.A. & Koerber, B.M. (1957) *Studies of the enzyme fumarase. VII Series solutions of integrated rate equations for irreversible and reversible Michaelis-Menten mechanism*. Journal of the American Chemical Society 79, 6379–6382.

Balcom, J.K. & Fitch, W.M. (1945) *A method for the kinetic analysis of progress curves using horse serum cholin esterase as a model*. The Journal of Biological Chemistry 245, 1637–1647.

Boeker, E.A. (1982) *Initial rates. A new plot*. Biochemical Journal 203, 117–123.

Cornish-Bowden, A. (1975) *The use of the direct linear plot for determining initial velocities*. Biochemical Journal 149, 305–312.

Cornish-Bowden, A. & Eisenthal, R. (1978) *Estimation of Michaelis constant and maximum velocity from the direct linear plot*. Biochimica et Biophysica Acta 523, 268–272.

Dixon, M. (1965) *Graphical determination of equilibrium constants*. Biochemical Journal 94, 760–762.

Eadie, G.S. (1942) *The inhibition of cholinesterase by physostigmine and prostigmine*. The Journal of Biological Chemistry 146, 85–93.

Eisenthal, R. & Cornish-Bowden, A. (1974) *The direct linear plot. A new graphical procedure for estimating enzyme parameters.* Biochemical Journal 139, 715–720.

Foster, R.J. & Niemann, C. (1953) *The evaluation of the kinetic constants of enzyme catalyzed reactions.* Proceedings of the National Academy Sciences of the United States of America 39, 999–1003.

Haldane, J.B.S. & Stern, K.G. (1932) *Allgemeine Chemie der Enzyme*. Steinkopff, Dresden & Leipzig.

Hanes, C.S. (1932) *Studies on plant amylases. The effect of starch concentration upon the velocity of hydrolysis by the amylase of germinated barley.* Biochemical Journal 26, 1406–1421.

Hofstee, B.H.J. (1952) *Specificity of esterases. Identification of two pancreatic aliesterases*. The Journal of Biological Chemistry 199, 357–364.

Jennings, R.R. & Niemann, C. (1954) *The evaluation of the kinetics of enzyme-catalzed reactions by procedures based upon integrated rate equation*. Journal of the American Chemical Society 77, 5432–5433.

Kilroe-Smith, J.A. (1966) *A modified graphical method for determination of equilibrium constants*. Biochemical Journal 100, 334–335.

Lee, H.J. & Wilson, I.B. (1971) *Enzymic parameters: Measurement of V and* K_m. Biochimica and Biophysica Acta 242, 519–522.

Lineweaver, H. & Burk, D. (1934) *The determination of enzyme dissociation constants*. Journal of the American Chemical Society 56, 658–666.

Markus, M., Hess, B., Ottaway, J.H. & Cornish-Bowden, A. (1976) *The analysis of kinetic data in biochemistry. A critical evaluation of methods*. FEBS Letters 63, 225–230.

Nimmo, I.A. & Atkins, G.L. (1978) *An evaluation of methods for determining initial velocities of enzyme-catalysed reactions from progress curves*. Biochemical Society Transactions 6, 548–550.

Orsi, B.A. & Tipton, K.F. (1979) *Kinetic analysis of progress curves.* Methods in Enzymology 63, 159–183.

Rudolph, F.B. & Fromm, H.J. (1979) *Plotting methods of enzyme rate data*. Methods in Enzymology 63, 138–159.
Schwert, G.W. (1969) *Use of integrated rate equations in estimating the kinetic constants of enzyme-catalyzed reactions*. The Journal of Biological Chemistry 244, 1278–1284.
Waley, S.G. (1981) *An easy method for the determination of initial rates*. Biochemical Journal 193, 1009–1012.
Walker, A.C. & Schmidt, C.L.A. (1944) *Studies on histidase*. Archives of Biochemistry 5, 445–467.
Wilkinson, G.N. (1961) *Statistical estimations of enzyme kinetics*. Biochemical Journal 80, 324–332.

Enzyme Inhibition

Dixon, M. (1953) *The determination of the enzyme inhibition constants*. Biochemical Journal 55, 170–171.
Dixon, M. (1972) *The graphical determination of K_m and K_i*. Biochemical Journal 129, 197–202.
Kitz, R. & Wilson, I.B. (1962) *Esters of methanesulfonic acid as irreversible inhibitors of acetylcholinesterase.* The Journal of Biological Chemistry 237, 3245–3249.

Multi-Substrate Reactions

Alberty, R.A. (1959) *The rate equation for an enzymatic reaction*. The Enzymes, Vol. 1, 1st ed. (Boyer, P.D., Lardy, H. & Myrbäck, K. eds.) 143–155.
Cleland, W.W. (1963) *The kinetics of enzyme-catalyzed reactions with two or more substrates or products. I. Nomenclature and rate equations.* Biochimica et Biophysica Acta 67, 104-137. *II. Inhibition: Nomenclature and theory.* Biochimica et Biophysica Acta 67, 173–187. *III. Prediction of initial velocity and inhibition patterns by inspection.* Biochimica et Biophysica Acta 67, 188–196.
Dalziel, K. (1957) *Initial steady-state velocities in the evaluation of enzyme-coenzyme-substrate reaction mechanism.* Acta Chemica Scandinavica 11, 1706–1723.
Fromm, H.J. (1970) *A simplified schematic method for deriving steady-state equations using a modification of the "Theory of Graphs" procedure.* Biochemical and Biophysical Research Communications 40, 692–697.
King, E.L. & Altman, C. (1965) *A schematic method for deriving the rate laws for enzyme-catalyzed reactions.* The Journal of Physical Chemistry 60, 1375–1378.
Volkenstein, M.V. & Goldstein, B.N. (1966) *A new method for solving the problems of the stationary kinetics of enzymological reactions.* Biochimica et Biophysica Acta 115, 471–477.

Kinetic Cooperativity

Bisswanger, H. (1984) *Cooperativity in highly aggregated systems.* The Journal of Biological Chemistry 259, 2457–2465.
Neet, K.H. & Ainslie, G.R. (1980) *Hysteretic enzymes.* Methods in Enzymology 64, 192–226.
Rübsamen, H., Khandker, R. & Witzel, H. (1974) *Sigmoidal kinetics of monomeric ribonuclease I due to ligand-induced shifts of conformation equilibrium.* Hoppe-Seyler's Zeitschrift für Physiologische Chemie 355, 687–708.

Immobilised Enzymes

Goldstein, L. (1976) *Kinetic behavior of immobilized enzyme systems.* Methods in Enzymology 44, 397–443.
Laidler, K.J. & Bunting, P.S. (1980) *The kinetics of immobilized enzyme systems*. Methods in Enzymology 61, 227–248.
Wingard, L.B., Katchalski-Katzir, E. & Goldstein, L. (1976) *Immobilized enzyme principles* in "Applied Biochemistry and Bioengineering". Academic Press, New York.
Engasser, J.-M. & Horvath, C. (1973) *Effect of internal diffusion in heterogeneous enzyme systems: Evaluation of true kinetic parameters and substrate diffusivity.* Journal of Theoretical Biology 42, 137–155.

Polymer Substrates

Chetkarov, M.L. & Kolev, D.N. (1984) *The Michaelis-Menten equation in the case of linear homopolymer substrates with different degrees of polymerization*. Monatshefte für Chemie 115, 1405–1412.

Hiromi, K. (1970) *Interpretation of dependency of rate parameters on the degree of polymerization of substrate in enzyme-catalyzed reactions. Evaluation of subsite affinities of exoenzymes.* Biochemical and Biophysical Research Communications 40, 1–6.

pH and Temperature Behaviour

Arrhenius, S. (1889) *Über die Reaktionsgeschwindigkeit bei der Inversion von Rohrzucker durch Säuren.* Zeitschrift für physikalische Chemie 4, 226–248.

Dixon, M. & Webb, E.C. (1979) *Enzymes,* 3rd ed. Academic Press, New York.

Eyring, H. (1935) *The activated complex in chemical reactions.* The Journal of Chemical Physics 3, 107–115.

Laidler, K.J. & Peterman, B.F. (1979) *Temperature effects in enzyme kinetics.* Methods in Enzymology 63, 234–257.

Tipton, K.F. & Dixon, H.B. (1979) *Effects of pH on enzymes.* Methods in Enzymology 63, 183–234.

Isotope Exchange

Berti, P.J. (1999) *Determining transition states from kinetic isotope effects.* Methods in Enzymology 308, 355–397.

Fromm, H.J. (1975) *Initial rate enzyme kinetics*. Springer-Verlag, Berlin.

Huang, C.Y. (1979) *Derivation of initial velocity and isotope exchange rate equations*. Methods in Enzymology 63, 54–84.

Jencks, W.P. (1969) *Catalysis in chemistry and enzymolog,*. pp. 243–281. McGraw-Hill, New York.

Purich, D.L. & Allison, R.D. (1980) *Isotope exchange methods for elucidating enzymic catalysis.* Methods in Enzymology 64, 3–46.

Richards, J.H. (1970) *Kinetic isotope effects in enzymic reactions.* The Enzymes, 3rd ed. Boyer, P., ed., Vol. 2, 321–333.

Statistics

Cleland, W.W. (1979) *Statistical analysis of enzyme kinetic data*. Methods in Enzymology 63, 103–138.

Cornish-Bowden, A. & Endrenyi, L. (1986) *Robust regression of enzyme kinetics.* Biochemical Journal 234, 21–29.

Cornish-Bowden, A. (1984) *Mathematisches Grundwissen für Biochemiker.* Verlag Chemie, Weinheim.

Kaiser, R.E. & Mühlbauer, J.A. (1983) *Elementare Tests zur Beurteilung von Meßdaten,* 2nd ed. Bibliographisches Institut, Mannheim.

Lehn, J. & Wegmann, H. (1985) *Einführung in die Statistik*. B.G. Teubner, Stuttgart.

Taylor, J.R. (1988) *Fehleranalyse*. VCH, Weinheim.

Zar, J.H. (1984) *Biostatistical analysis,* 2rd ed. Prentice-Hall Inc., Englewood Cliffs, New Jersey, USA.

3 Methods

No strict division can be made between methods for studying binding equilibria and those for enzyme kinetics. Frequently the same method provides information on both fields, this holds especially for optical methods. Techniques for analysing rapid reactions also comprise both kinetic methods, like flow methods, and methods to investigate equilibria, e.g., relaxation methods. These methods also allow the investigation of structural and conformational features of biomolecules. Other methods, like EPR, Raman and IR spectroscopy, can only be applied in enzyme kinetics in a limited way. In this chapter methods are introduced providing information on at least one of the fields treated in this book. Methods providing valuable supplementary information, e.g., the structure and conformation of macromolecules, will also be described. Methods for the study of multiple equilibria are introduced first, followed by enzyme kinetic method and, finally, techniques with a broad range of applications arranged according to instrumental aspects. Enzyme kinetic methods in a stricter sense are mostly enzyme tests as applied in enzyme analytics. They are extensively described in relevant publications (e.g., Bergmeyer, 1983). Therefore, the treatment in this book will be limited to essential features for enzyme kinetics. Aspects of the experimental procedures have already been described in Chapter 2.

3.1 Methods for the Investigation of Multiple Equilibria

Distinct from studies of chemical or enzyme-catalysed reactions investigations of equilibria are complicated by the fact that no stable products, distinct from substrate, are formed, which can be analysed. The enzyme ligand complexes are loose associates, in rapid equilibrium with the free components. Each disturbance, e.g., change of reactant concentrations, temperature, or pH causes an immediate shift in equilibrium and thus in the associate concentration. Isolation of the enzyme ligand complexes by conventional separation methods, e.g., gel filtration, cause inevitable the disaggregation of the complex into the free components. Thus, binding methods must be conceived in a way to enable the quantitative determination of both, the free components and the association complex in an undisturbed equilibrium.

A further problem is to find a measurable signal. Two criteria may be chosen: 1. the considerable size difference between the small free ligand and the bound ligand assuming the size of the macromolecule; 2. spectroscopic changes caused by interactions between ligand and macromolecule. They are mostly minimal and must be enhanced by special procedures. For a given system the most appropriate method must be found. Not every method is equally applicable and yields a detectable signal. To obtain reliable information, frequently a combination of several methods is required.

Enzyme Kinetics: Principles and Methods. Hans Bisswanger

ISBN: 3-527-30343-X

Binding measurements require, in contrast to enzyme kinetic determinations, large quantities of macromolecule or enzyme, since the intensity of the (usually very small) signal depends directly on the macromolecule concentration. The macromolecule may not act as catalyst, but as an equal reaction partner of the ligand, whose concentration should vary around the value of its dissociation constant K_d. If, for example, a macromolecule with a molecular mass of 100 000 and a dissociation constant of $K_d = 1 \cdot 10^{-4}$ M is applied in a concentration of 0.1 mg/ml (i.e., a molar concentration of $1 \cdot 10^{-6}$ M), and the ligand concentration is in the same range, according to the law of mass action:

$$K_d = \frac{[E][A]}{[EA]} = \frac{1 \cdot 10^{-6} \cdot 1 \cdot 10^{-6}}{1 \cdot 10^{-8}} = 1 \cdot 10^{-4} \text{ M} ,$$

only 1% of the ligand ($1 \cdot 10^{-8}$ M) will be bound, and this will be hardly detectable in presence of a 100-fold surplus of the free ligand. An increase of ligand concentration by a factor of 100 ($1 \cdot 10^{-4}$ M) will increase the degree of binding, and half of the macromolecule will be saturated with ligand (since now the ligand concentration corresponds to the dissociation constant), but the ratio of bound to free ligand is actually reduced to 0.5%:

$$K_d = \frac{[E][A]}{[EA]} = \frac{5 \cdot 10^{-7} \cdot 1 \cdot 10^{-4}}{5 \cdot 10^{-7}} = 1 \cdot 10^{-4} \text{ M} .$$

Only an additional, comparable increase of the macromolecule concentration will increase the amount of the aggregation complex to 50% of the free ligand concentration:

$$K_d = \frac{[E][A]}{[EA]} = \frac{1 \cdot 10^{-4} \cdot 1 \cdot 10^{-4}}{1 \cdot 10^{-4}} = 1 \cdot 10^{-4} \text{ M} .$$

To achieve this, however, the total macromolecule concentration has grown to $2 \cdot 10^{-4}$ M $\approx$ 20 mg/ml, i.e., 200 times the quantity originally applied.

3.1.1 Equilibrium Dialysis and General Aspects of Binding Measurements

3.1.1.1 Equilibrium Dialysis

Equilibrium dialysis is a reliable procedure for the determination of binding equilibria. A semi-permeable membrane with a pore diameter permitting passage only for small ligands, divides a test vessel into an *outer* dialysis chamber for the ligand and an *inner* chamber for macromolecule solution (Figure 3.1). The most simple device is a dialysis bag containing the macromolecule solution, diving into the ligand solu-

tion. The ligand diffuses from the outer chamber into the macromolecule solution of the inner chamber until concentration is equal in both chambers. If ligand additionally binds to the macromolecule, the bound part will be withdrawn from the dialysis equilibrium and ligand must be supplemented from the outer chamber until the free ligand concentrations will be equal in both chambers, so that after attainment of the dialysis equilibrium the total ligand concentration in the outer chamber $[A]_o$ is equal to the free ligand concentration [A] in the inner chamber:

$$[A]_o = [A] \ ,$$

while the total ligand concentration in the inner chamber $[A]_i$ is the sum of both the free and the bound ligand $[A]_{bound}$:

$$[A]_i = [A] + [A]_{bound} \ ,$$

Consequently, the amount of bound ligand is the difference in the total ligand concentrations of both chambers:

$$[A]_{bound} = [A]_i - [A]_a \ ,$$

After dialysis the total ligand concentrations can be measured from samples taken from both chambers, and [A] and $[A]_{bound}$ may be calculated. Binding experiments will usually be performed at varying ligand concentrations leaving the macromolecule concentration constant. Ligand concentration should be varied in the range of the dissociation constant (preferentially one order of magnitude below and above the constant).

Equilibrium dialysis has the advantage that [A] and $[A]_{bound}$ can be obtained directly from the equilibrium solutions after the experiment, while in other binding methods they are derived from the difference to the total amount of ligand applied: $[A]_o = [A] + [A]_{bound}$. This prevents errors due to unspecific binding of the ligand to the chamber walls or the membrane. A disadvantage is the fact that $[A]_{bound}$ can not be measured directly, but must be obtained from the difference between the total ligand concentrations of both chambers. Thus, errors in the determination of [A] in the

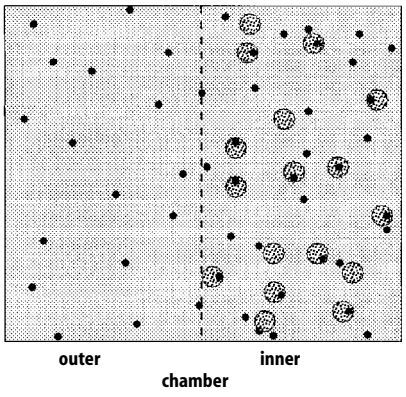

Figure 3.1. Principle of equilibrium dialysis. The small ligand molecules pass freely through the semipermeable membrane and immediately diffuse into both chambers while also binding to the macromolecule that cannot leave the inner chamber.

outer chamber are inevitably transferred to $[A]_{bound}$, causing a considerable inaccuracy of the method and limiting its application mainly to medium binding constants ($K_d \approx 10^{-7}$–10^{-3} M). With weaker binding the minor amount of bound ligand will be lost within the error deviations of the large amount of free ligand [A], while the part of [A] will disappear within the fluctuations of $[A]_{bound}$ in strong binding (Figure 3.2).

Equilibrium dialysis apparatuses are devised to save the precious macromolecular material. Concentrated solutions, but only small volumes are applied (Myer et al., 1962; Englund et al., 1969). This requires the detection of the ligand with very sensitive analytic methods, preferentially radioactive labelling. Therefore, the application of equilibrium dialysis often depends on the availability of ligand in this form. Dialysis chambers are fraised into plastic or Teflon cylinders (Figure 3.3). Width and depth of the holes determine the test volume (e.g., 30 µl). Two such cylinders are pressed proofly together at their holes with a dialysis membrane inserted to form a dialysis cell with two chambers. The chambers are filled or emptied through vertical channels closed by stoppers. For binding experiments with varying ligand concentrations 10–20 cells are re-

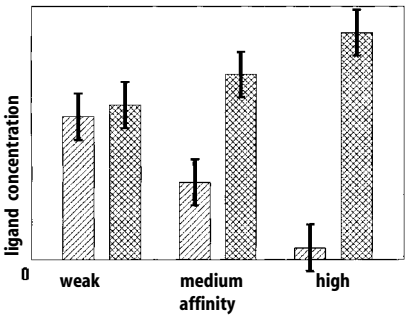

Figure 3.2. Ratio between measurement value and error fluctuation in equilibrium dialysis. The left bars represent measurements from the outer chamber (free ligand), the right bars those from the inner chamber (free and bound ligand). The error limits are shown on top of the bars.

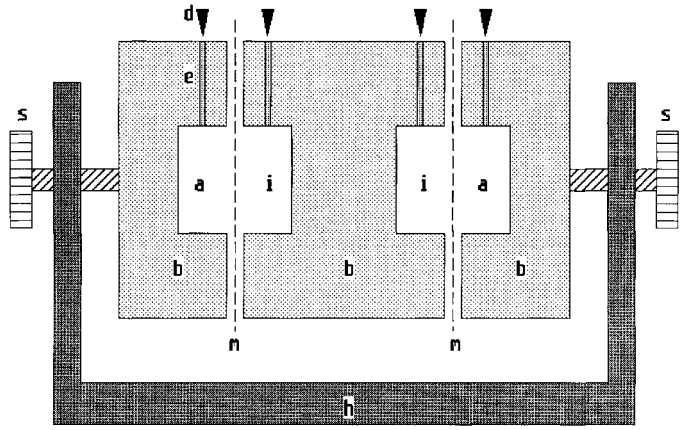

Figure 3.3. Equilibrium dialysis apparatus with twin chambers. a: outer chambers, i: inner chambers, b: dialysis block, d: stopper, e: filling channels, m: dialysis membrane, h: holding device, s: fixing screws. The individual cell may be dimensioned for a volume not higher than 30 μl (after Englund et al. 1969).

quired, fixed in a rotating holder. During the experiment a constant (preferentially physiological) temperature must be maintained (e.g., 37 °C), as the equilibrium constant is temperature-dependent. Therefore, the whole device must be tempered by an incubator or water bath. Ultrafiltration membranes of various materials and different pore diameters or cellulose dialysis bags with an exclusion limit for proteins of about 15 000 (cut open, one-layered) are applied as semi-permeable membranes.

For a dialysis experiment, a constant amount of the macromolecule is filled into one of the dialysis chambers, the other is filled with the ligand solution in varying concentrations. To reduce the time of dialysis it is advisable to fill a mixture of both components into one of the chambers and dialyse it against a buffer solution. If, however, dialysis is stopped too early, incomplete equalisation may erroneously be taken as binding. After attainment of the dialysis equilibrium, aliquots of defined volumes are taken from all chambers and the ligand concentration is analysed, e.g., with a scintillation counter. The Scatchard plot is especially suited for the analysis of the data to determine the binding mechanism, the binding constant and the number of binding sites (Section 1.3.2.1).

3.1.1.2 Control Experiments and Sources of Errors

Dialysis time. Dialysis must be performed long enough to ensure complete equilibration of ligand in the two chambers. This depends on various parameters, e.g., volume, charge, and polarity of the ligand, material and pore diameter of the membrane, dimensions of the chamber, effective membrane surface, movement of the dialysis cells, and temperature. Enzymes are highly sensitive to extended dialysis, especially at higher temperatures, so dialysis should not last longer than absolutely necessary. To determine the optimum dialysis time, one of the chambers is filled with a ligand solution of medium concentration and dialysed against a buffer solution in the other chamber. At given times samples are taken from both chambers and ligand concentration is measured. At the time $t=0$ the ligand chamber contains the total ligand, the other chamber is free of ligand. With progressing dialysis, both values approximate each other in an exponential manner and finally meet at mean concentration (Fig-

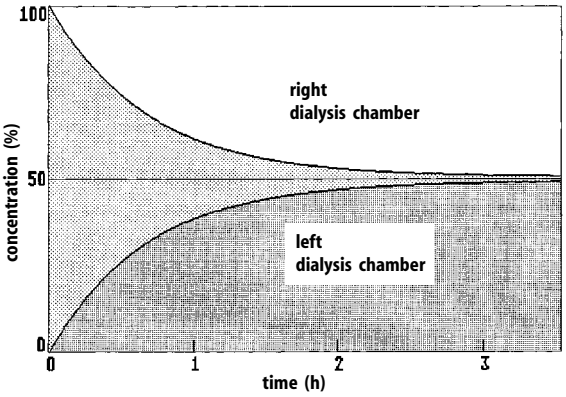

Figure 3.4. Determination of the minimum dialysis time. At the time $t=0$ ligand is present only in the right dialysis chamber (100%) and diffuses in a time-dependent manner into the left chamber. The minimal duration of an equilibrium dialysis experiment corresponds to the time in which concentrations in both chambers approximate each other.

ure 3.4). To ensure complete equilibration, a slightly longer time should be chosen for the dialysis experiment.

Determination of concentrations. The reliability of results depends on the accuracy of the concentration determination of both the ligand and the macromolecule. The concentration must be indicated in molar units, i.e., protein content and molecular mass must be known. It should be noted that protein determination methods are usually adjusted to a standard protein (e.g., serum albumin) from which other proteins may severely differ, so that determination of the absolute content of the special protein is unavoidable.

Stability of reactants. The stability of reactants during experiments has to be ensured by measuring the contents before and after dialysis. Ligand molecules may break down spontaneously, enzyme substrates could enter a catalytic turnover. The latter can be prevented by removing essential factors, cosubstrates, coenzymes, essential metal ions, but with a long period of dialysis and high enzyme concentrations, even traces of such components could trigger a substantial turnover. To avoid such effects, inactivated substrate analogues are employed, but they exhibit a different binding behaviour compared with the native substrate. Loss of ligand, e.g., by adsorption to the membrane and chamber walls, does not interfere much in this method, as the initial concentration $[A]_0$ is not part of the calculation. Only actual concentrations are determined.

Macromolecules may also be subject to changes during the experiment or even denature, affecting or preventing ligand binding. Enzymes can be tested for retaining the native structure by activity tests before and after the experiment. For proteins and other macromolecules their respective concentrations before and after dialysis must be tested at least. This, however, gives no information about the conservation of their functionality during dialysis. The concentration of the macromolecule must strictly be kept constant during the experiment. Partial losses by denaturation or adsorption to chamber walls, if not avoidable, must be considered in the evaluation.

Osmotic pressure and Donnan effect. The semi-permeable dialysis membrane retains the macromolecule in one chamber, so that there is a concentration gradient against the ligand chamber. For compensation, solvent from the ligand chamber flows into the macromolecule chamber. Osmotic pressure is building up, the flexible dialysis membrane arches outward, and the macromolecule solution will be diluted. This effect can be corrected by determining the macromolecule concentration before and after the experiment, but in most cases it is minimal because of the relatively small quantities of macromolecule.

Much more disturbing are the effects of distribution of ions in equilibrium, discovered by W. Gibbs in 1876 and formulated by G.F. Donnan in 1911 (Donnan effect, Gibbs-Donnan equilibrium). It stipulates that the chemical potentials of cations and anions of the inner (μ^{i}_{KA}) and the outer (μ^{o}_{KA}) chamber must be equal:

$$\mu^{i}_{KA} = \mu^{o}_{KA} \,. \tag{3.1}$$

Proteins and other macromolecules carry a large number of charges on their surface. Positive and negative charges compensate each other, but there remains a surplus charge not neutralised by the macromolecule. This charge has no counterpart in the ligand chamber, and freely penetrating ions diffuse unevenly within the two chambers in order to establish the equilibrium according to Eq. (3.1). If the ligand itself is charged it is also subject to this uneven distribution. If the charge of the ligand and the surplus charge of the macromolecule have the same sign, ligand is expelled from the inner chamber, the share of specific binding is apparently decreased. Charges with different signs will attract themselves, the ligand will accumulate in the macromolecule chamber and binding will apparently be enhanced. Thus, the Donnan effect can significantly distort the results of a dialysis equilibrium experiment. The chemical potentials of anions ($[A_i]$, $[A_o]$) and cations ($[K_i]$, $[K_o]$ in the inner and outer chamber follow the relationship:

$$\mu^{i}_{KA} = \mu^{0i}_{KA} + RT \ln[A_i][K_i] \,, \tag{3.2}$$

$$\mu^{o}_{KA} = \mu^{0o}_{KA} + RT \ln[A_o][K_o] \,. \tag{3.3}$$

The standard potentials may be regarded as identical. When inserted in Eq. (3.1) the following equation results:

$$[K_i][A_i] = [K_o][A_o] \,;\; \frac{[K_i]}{[K_o]} = \frac{[A_i]}{[A_o]} \,. \tag{3.4}$$

The ratio of anions and cations between the two chambers is equal. Based on electron neutrality, the sum of positive charges must be equal to the sum of negative charges:

$$z[E_i] + [K_i] = [A_i] \quad \text{and} \quad [K_o] = [A_o] \,,$$

The number z of the surplus charge of the macromolecule E_i is assumed to be positive. By inserting Eq. (3.4) follows:

$$[K_o]^2 = [K_i]([K_i] + z[E_i]) \,, \tag{3.5 a}$$

$$[A_o]^2 = [A_i]([A_i] - z[E_i]) \,. \tag{3.5 b}$$

The difference in cations and anions in the two chambers is:

$$[K_i] - [K_o] = \frac{-z[E_i][K_i]}{[K_i] + [K_o]} \,, \tag{3.6 a}$$

$$[A_i] - [A_o] = \frac{z[E_i][A_i]}{[A_i] + [A_o]} \,. \tag{3.6 b}$$

For a negative surplus charge the sign of both equations would be reversed.

Table 3.1. Dialysis of a sodium chloride solution with different concentrations (Na_o^+) against serum albumin with negative surplus charges. The surplus charges $z[E]_0$ are neutralised with sodium ions, accordingly before dialysis is $Na_i^+ = z[E]_0$. Indicated are relative values

Relative Na^+ concentration				Apparent binding (%)
Before dialysis		After dialysis		
Na_i^+	Na_a^+	Na_i^+	Na_o^+	
1.0	0.01	1.000098	0.0099	99.0
1.0	1.0	1.333	0.667	66.7
0.01	1.0	0.508	0.502	1.2

Table 3.1 shows the consequences of the Donnan effect on serum albumin with a negative surplus charge, neutralised by sodium ions. It is dialysed against a sodium chloride solution in varying concentrations. At a 100-fold surplus of the serum albumin surplus charges over the sodium in the outer chamber, nearly all cations are found in the protein chamber after dialysis. The serum albumin appears completely "saturated" with ligand. Even on addition of equal quantities of salt against the surplus charges, two thirds of ligand appear to be bound, and even at a 100-fold surplus of salt more than 1% of ligand still accumulates in the protein chamber. This demonstrates that the Donnan effect depends on the relative number of charges and can be diminished by high salt concentrations.

3.1.2 Continuous Equilibrium Dialysis

This method does not require the long periods of dialysis of the normal equilibrium dialysis but can be performed within 10–20 min. Furthermore, only one dialysis cell and thus only a fraction of the macromolecule is required to establish a binding curve. The method is based on the principle that the penetration rate of a substance through the membrane is directly proportional to its concentration. The system should not reach dialysis equilibrium, only the quantity of ligand penetrating the membrane per time unit is determined. The two chambers of the dialysis cells are arranged one above the other so that the membrane becomes fixed between both in a horizontal manner. A magnetic stirrer in each chamber provides homogeneous mixing. The upper chamber, open at the top, contains macromolecule and ligand, the lower one is filled with buffer solution up to the membrane. During dialysis buffer solution is continuously pumped through the lower chamber via side channels, flowing past the dialysis membrane at a constant rate. The eluting solution is collected in fractions in which the continuous passage of ligand through the membrane during the dialysis process can be analysed.

Initially only a small quantity of radioactively labelled ligand is added to macromolecule in the upper chamber, so that only a minor part of the free binding sites will be saturated. Only the portion of the free ligand passes through the membrane. After addition of the ligand it takes about 1 min to achieve a constant penetration

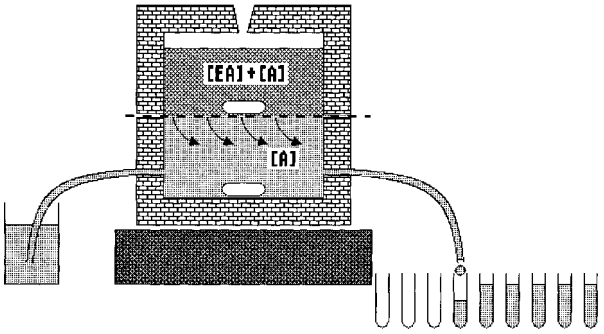

Figure 3.5. Continuous equilibrium dialysis. From a vessel buffer solution flows continually along a dialysis membrane and washes the free ligand penetrating from the upper macromolecule chamber into a fraction collector.

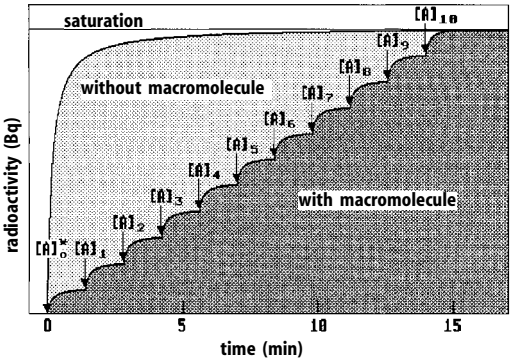

Figure 3.6. Time course of a continuous equilibrium dialysis. At the time $t = 0$ radioactively cabelled ligand is added in low concentration. Without binding a macromolecule, the upper curve evolves. At a surplus of macromolecule, the larger part of ligand binds and only a small step remains for the free ligand. After reaching the step level, defined quantities of unmarked ligand are added which increasingly remove the labelled ligand from its binding sites on the macromolecule until the original step plateau of ligand is reached in absence of macromolecule.

rate, the radioactivity beyond the membrane increases rapidly within this time, until a constant plateau is reached (Figure 3.6). The height of the plateau is proportional to the free ligand concentration in the upper chamber.

At that time another small sample of unlabelled ligand is added to the upper chamber. It equilibrates with the labelled ligand and partially displaces it from its binding sites on the macromolecule. This results in a larger ratio of labelled ligand in free form and a higher plateau is achieved. This procedure is continued with further small additions of unlabelled ligand, and the plateau rises at each addition. This continues until practically all labelled ligand has been displaced from its binding sites and the macromolecule is saturated with unlabelled ligand. This is achieved by adding a large surplus of unlabelled ligand as the final step of the experiment. A plateau of the same height is obtained, when the initial amount of labelled ligand is added to the upper chamber in the absence of the macromolecule. Such an experiment is done to calibrate the plateau height with the free ligand concentration. The radioactivity of the plateau value at this stage corresponds 100% to ligand in its free form. Radioactivity of the different plateau

values in the binding experiment, divided by the maximum value of the control, provide the ratio of bound ligand. With a period of 1–2 min to reach the plateau, 10 measurements can be carried out in nearly 10 min. The total amount of labelled ligand in the upper chamber is assumed to remain constant during the whole experiment, any loss by passage through the membrane is neglected. On achieving complete equilibrium after about 2 h, about 1% of the originally added ligand will be lost at each step, i.e., about 10% during the whole experiment.

3.1.3 Ultrafiltration

This method is mainly employed for concentration and separation of macromolecules in solution. Depending on the respective sample volumes and separation ranges various devices are commercially available. Solutions are forced through ultrafiltration membranes either by high pressure, vacuum, centrifugal power or simply by free diffusion. The membranes possess defined pore diameters, retaining molecules according to their size. Due to the broad exclusion limits of the pores and the varying shapes of molecules separation is not very sharp. About 5% of serum albumin (M_r=66,000) will pass a membrane with an exclusion limit of 30 000. For complete separation the difference between the exclusion limit of the membrane and the true molecule size should be considerably large. A special problem of ultrafiltration is that the particles to be concentrated are pressed to the membrane and form a firmly attached layer, plugging the membrane and blocking the filtration procedure. To remove the macromolecules from this layer is hardly successful.

Various ultrafiltration methods can be employed for the determination of binding equilibria. The principle is that only free ligand from a solution in equilibrium passes the membrane, the macromolecule with the bound ligand remaining beyond the membrane. Essential concentration of the macromolecule during the procedure, however, should be avoided, as it is taken as constant throughout the experiment. Only a small portion of the solution is pressed through the membrane to determine the free ligand in the filtrate. Determination of the bound ligand from the remaining solution above the membrane is problematic because of the concentration effect. Usually this value is obtained from the difference between added and free ligand, although unspecific adsorptions of ligand to membrane and walls may misrepresent the result. Ultrafiltration is less exact than equilibrium dialysis, but it is a rapid method, requiring only a few minutes and is, therefore, suited for sensitive and unstable materials.

The simplest form of ultrafiltration is the application of an equilibrated solution onto a filter funnel equipped with an ultrafiltration membrane, mounted on a suction flask connected to a vacuum (Figure 3.7 A). The solution of the penetrating free ligand is taken off either below the filtration plate or from the vacuum vessel. Only a fraction of the total solution should be filtered. More critical is the method of complete suction of the equilibrium solution through the filter. This will be removed without washing, and the radioactivity of the labelled bound ligand is directly measured in the wet filter in comparison to a control experiment with ligands in the absence of macromolecule (Suter and Rosenbusch, 1974). It cannot be excluded that concentration will affect the equilibrium. A modification of this method especially

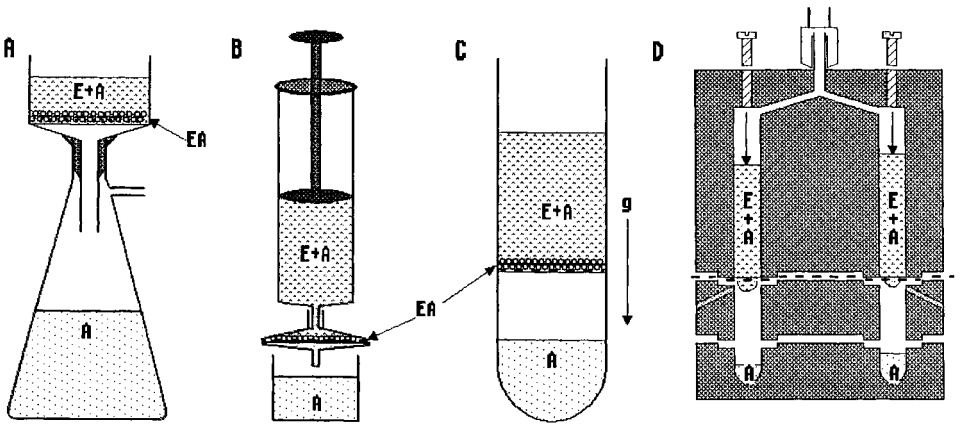

Figure 3.7. Ultrafiltration equipment. (A) Filter attachment on a suction flask, (B) filter attachment for a syringe, (C) centrifuge tube with filtration membrane, (D) ultrafiltration apparatus after Paulus (1969). Compressed air is pumped through a central aperture into the tubes filled with various equilibrium mixtures, and solution with free ligand is pressed through the membrane.

for small volumes are commercially available filtration kits to be mounted on syringes. They possess, however, a relatively large dead volume. With filter units using the gravitational force of a laboratory centrifuge several samples with various ligand concentrations can be run simultaneously (Figure 3.7 C).

In 1969 H. Paulus developed a special equipment for the study of ligand binding. Several ultrafiltration cells in the shape of concentrically arranged vertical holes are drilled in a perspex cylinder (Figure 3.7 D). A second shorter cylinder with identically arranged holes is attached from the bottom, fixing a stable ultrafiltration or dialysis membrane between both. The penetrating solution is collected in small holes in a perspex plate fixed at the bottom of the apparatus. The holes of the upper cylinder are tightly locked by screws. In the middle of this cylinder a connecting piece for compressed air is installed. This is connected with each hole by radial channels. Transversal channels in the lower cylinder permit withdrawal of samples of the penetrating solution during the ultrafiltration procedure. Experiments are performed by filling macromolecule solution with varying ligand concentrations into the holes of the upper cylinder. These are tightly screwed, and pressure of ca. 275 kPa is applied via the central connection piece from a nitrogen or compressed air cylinder. A defined aliquot of the filtrate is withdrawn with a syringe from the bottom of the membrane or from the holes of the lower perspex plate and analysed. Concentration of the solution above the membrane should be kept low. The macromolecule solution necessary for the experiment is determined by the hole dimensions and may be as low as 100 µl per cell.

3.1.4 Gel Filtration

This method, performed mostly in the form of column chromatography, is used as a preparative method for the purification of macromolecules from homogenates, for desalting and rebuffering of macromolecule solutions, and for determination of molecular masses (molecular sieve chromatography). The gel beads, mostly consisting of dextran, agarose or polyacrylamide, possess pores of defined width. Due to this feature two compartments are created in the chromatography reservoir: an outer volume V_o around the beads and an inner volume V_i of the beads which is only accessible for molecules small enough to penetrate the pores. These molecules have access to the total volume $V_t = V_o + V_i$, while for larger molecules only to the outer volume is available. When eluting a gel filtration column, large molecules have to pass a smaller volume and move faster than small molecules, so that molecule mixtures are separated according to size. The same holds for small ligands, which are retarded and, due to the rapid reversible equilibrium will be stripped off from the macromolecule during the passage through a long gel filtration column. Therefore, binding measurements applying this method must be devised in a manner to separate the ligand-macromolecule complex from the free ligand without disturbing the equilibrium.

3.1.4.1 The Batch Method

A simple arrangement, requiring no special tools, serves to determine binding equilibria. A small volume of swollen gel is put into a cup or beaker (Figure 3.8). First V_o and V_i must be determined. A distinct amount of the macromolecule is mixed with the gel and the gel allowed to sediment. From the supernatant solution the macromolecule concentration is determined and, taking the total amount of the macromolecule and the volume of the gel suspension, V_o can be calculated. In a similar way, adding the ligand, the total accessible volume V_t and thus also V_i are obtained. In the binding experiment a mixture of macromolecule and ligand is added to the gel and the total ligand concentration will be determined in the supernatant. Accordingly, as it

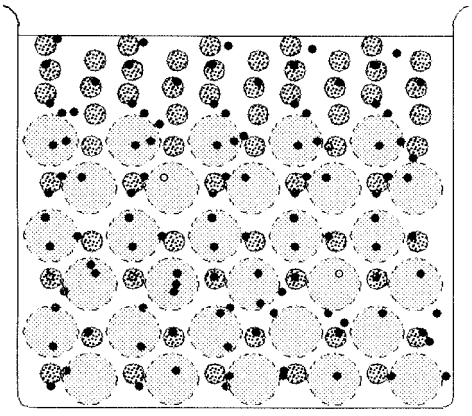

Figure 3.8. Batch method for the determination of ligand binding. Only the low molecular weight ligand, but not the macromolecule can permeate the pores of the gel particle.

binds to the macromolecule, the ligand concentration in the supernatant will exceed the original value found in the absence of the macromolecule. Principally this method is equal to equilibrium dialysis, the outer volume corresponding to the macromolecule chamber and inner volume to the ligand chamber. It is, however, not very precise.

3.1.4.2 Elution of Broad Zones

Contrary to normal chromatography, in this method described by Ackers in 1975 the mixture of macromolecule and ligand is applied to a gel filtration column in such a large volume that during their passage both components cannot be completely separated. In the eluting solution three zones can be differentiated: the macromolecule that has lost its ligand moving ahead, followed by the macromolecule still binding its ligand and, finally, the ligand released during the passage. Its concentration corresponds just to the free ligand concentration [A] in the equilibrium mixture. This applies as long as the three zones are in direct contact and are not separated from each other. $[A]_{bound}$ can be calculated from [A] and the known amount $[A]_0$ of the ligand applied.

3.1.4.3 The Method of Hummel and Dreyer

In this method the whole gel filtration column must be equilibrated with the ligand solution of a defined concentration [A]. It is photometrically controlled that the eluate has the same concentration as the applied solution (Figure 3.9). Now a small volume of a macromolecule solution [E], also containing ligand in the same concentration [A] as in the equilibration solution, is applied, followed by further elution with the original ligand solution. During the whole procedure the ligand concentration [A] in the solutions must be kept constant. The macromolecule will bind part of the ligand withdrawing it from the surrounding solution. Although the total amount of li-

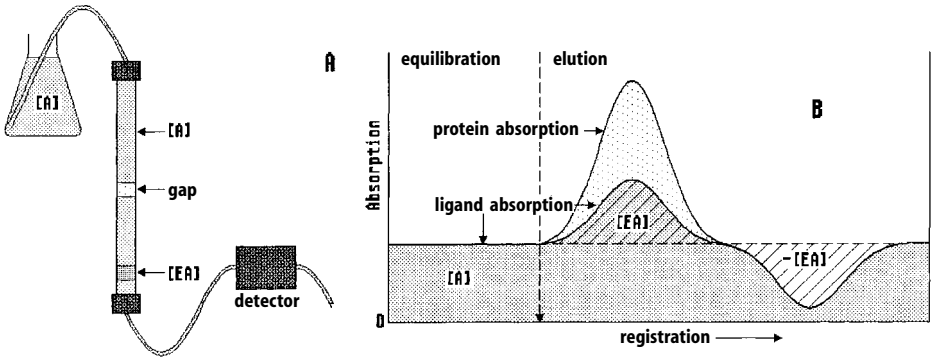

Figure 3.9. Column chromatrographic method for ligand binding after Hummel and Dreyer (1962). (A) Experimental arrangement, (B) elution profile.

gand is not altered, the free ligand concentration will be diminished. Passage of the macromolecule with its bound ligand through the column is faster than that of the free ligand and creates a gap correlating exactly to the amount of ligand withdrawn for binding to the macromolecule. Inversely, the macromolecule with its bound ligand moves into the equilibrated ligand solution causing a maximum over the constant level. The macromolecule will equilibrate with the surrounding ligand solution [A] that its concentration corresponds to the free ligand. The bound part $[A]_{bound}$ is obtained by integration of the maximum or of the gap. The latter is more reliable, as the macromolecule may also contribute to maximum. This method has the advantage that free and bound ligand can be measured directly. No radioactive markers are necessary, however, larger amounts of substance are required.

3.1.4.4 The Brumbaugh and Ackers Method

This method is more accurate than the other methods mentioned above. However, expensive experimental equipment is required. This method can be regarded as a combination of the batch method and the Hummel-Dreyer method. The detection is also achieved photometrically, but here not the eluate, but the whole column is analysed, which instead of a cuvette is placed into the light path of a photometer (Figure 3.10). Therefore, it must consist of UV-permeable quartz glass. A motor drives the column stepwise through the light path. The column may virtually be divided into a large number (e.g., 100) of identical volume elements, each defined by the cross section of the column and the height of the light path. Each volume element may be regarded as a vessel used in the batch method (resp. an equilibrium dialysis cell) with an inner volume V_i and an outer Volume V_o. These volumes are determined in preliminary tests by separate equilibration with ligand and macromolecule solutions and measuring the absorption within each volume element. The small ligand A distributes between both compartments according to the relationship:

$$\zeta_A = V_o + \sigma_A V_i \; . \tag{3.7}$$

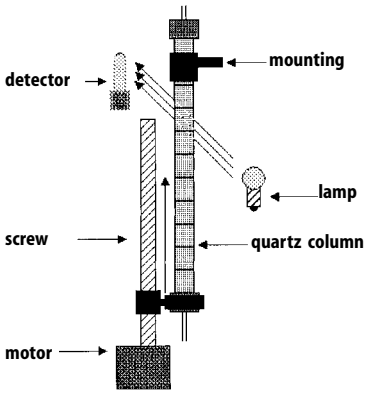

Figure 3.10. Column chromatrographic method for ligand binding after Brumbaugh and Ackers (1974). The column packed with the equilibrium mixture is gradually moved through the light beam of a photometer by motor power.

ζ_A is the cross sectional distribution and σ the distribution coefficient, ranging from 0 to 1, depending on the gel material and the size of the compound. For free diffusion of ligand into the gel pores $\sigma_A = 1$ and Eq. (3.7) becomes $\zeta_A = V_o + V_i$, at total exclusion of the macromolecule $\sigma_A = 0$ and $\zeta_A = V_o$. After equilibration of the column with a macromolecule-ligand mixture the binding ratio is obtained by determining the deviations from the distribution of the free components. Due to the high number of volume elements to be measured a lot of data accumulates, conferring high statistic reliability.

3.1.5 Ultracentrifugation Methods

3.1.5.1 Preparative Ultracentrifugation

Preparative ultracentrifuges, part of the basic equipment in any biochemical laboratory, provide a gentle method for investigation of binding equilibria without any additional equipment. Macromolecules, together with their bound ligands, migrate faster in the gravity field of the centrifuge than the small free ligands, which will essentially remain at the meniscus in its original equilibrium concentration. This can be determined from aliquots taken from the meniscus after centrifugation. Sedimentation of the ligand itself and mixing after centrifugation must be excluded.

The application of this method to a small volume (170 μL per centrifuge tube) air-driven ultracentrifuge (Airfuge®, Beckman) was described by Alberts and Krishan (1979). The macromolecule is sedimented to the bottom of the centrifuge vessel. This can be done within a few minutes. It is assumed that the bound ligand in the pellet is still in undisturbed equilibrium with the supernatant-free ligand. Scintillation measurement of the centrifuge tube with the pellet yields the portion of bound ligand. The free ligand is obtained from the supernatant.

3.1.5.2 Centrifugation Method of Chanutin et al. (1942)

This rapid and more precise method can be performed with low amounts of substance in small-volume ultracentrifuges. The method is based on a transformation of the binding equation (1.23):

$$[A]_{bound} = [A]_0 - [A] = \frac{n[E]_0[A]}{K_d + [A]} ,$$

$$[A]_0 = \frac{n[E]_0[A]}{K_d + [A]} + [A] . \qquad (3.8)$$

Assuming [A] = constant, the total ligand concentration $[A]_0$ becomes a linear function of the macromolecule concentration $[E]_0$. Plotting $[A]_0$ against $[E]_0$ yields a straight line, the ordinate intercept is [A], the free ligand concentration (Figure 3.11B). These straight lines are experimentally obtained by spinning several tubes with macromole-

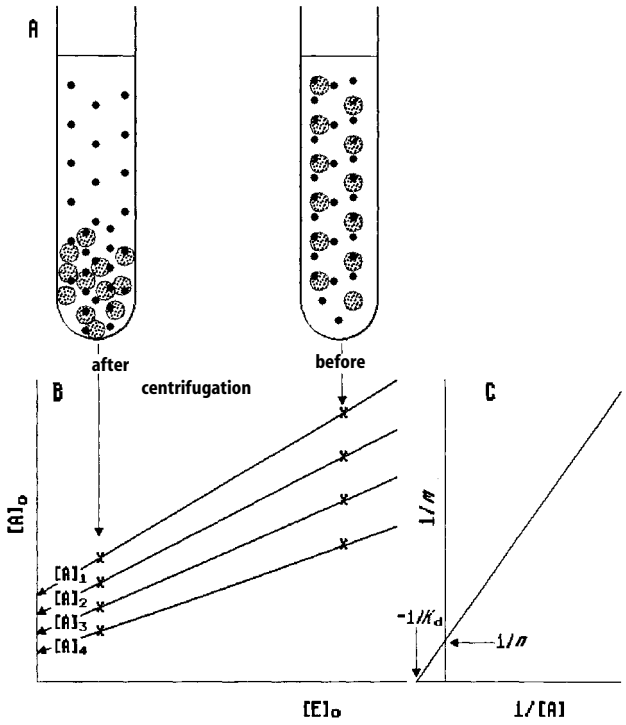

Figure 3.11. Ultracentrifugation method after Chanutin et al. (1942). (A) Centrifuge tube before (right) and after (left) centrifugation. In (B) the values for $[A]_0$ and $[E]_0$ are plotted from both tubes and linked by straight lines. Their gradients result in the straight line in (C) and gives in the constants by extrapolation.

cule-ligand mixtures for a given time, the ligand concentrations varying and the macromolecule concentrations being constant in the different tubes. Subsequently samples are removed from different parts of the tubes and ligand and macromolecule concentrations are analysed. For each tube a straight line with a respective [A] value is obtained. It is irrelevant from which part of the tube the samples are taken after centrifugation, as long as sedimentation has taken place and the values differ from each other. If there are enough tubes with different ligand concentrations it may already be sufficient to analyse one sample of the equilibrium mixture before centrifugation and the meniscus fraction after centrifugation (Figure 3.11A). This is justified although in this case the straight lines will be defined only by two points, as the proper evaluation is performed with a secondary plot. According to Eq. (3.8) the reciprocal gradient *Sl* of the straight lines yields a linear function:

$$Sl = \frac{n[\mathrm{A}]}{K_\mathrm{d} + [\mathrm{A}]} \; ; \quad \frac{1}{Sl} = \frac{K_\mathrm{d}}{n[\mathrm{A}]} + \frac{1}{n} \; . \tag{3.9}$$

Plotting 1/*Sl,* the reciprocal gradient, against 1/[A] yields a linear function with the reciprocal values for n and K_d as ordinate and abscissa intercepts, respectively (Figure 3.11C). A similar method where the distribution of components is measured during centrifugation by direct absorption measurement in the analytical ultracentrifuge was described by Steinberg and Schachman (1966).

3.1.5.3 Sucrose Gradient Centrifugation after Draper and Hippel

Ultracentrifugation in fixed angle rotors with tubes distinctly declined to the rotor axis (Figure 3.12A) has two serious disadvantages. The gravity field caused by the centrifugal force directs perpendicularly from the rotor axis and does not point straightway through the tube from the meniscus to the bottom. Thus the particles sediment to the opposite tube wall, migrating a far shorter distance than the tube size. From the wall they will slip to the bottom. Furthermore, the macromolecules will not migrate through the tube in sharply condensed bands, rather will they broaden due to convulsions and shaking during centrifugation, acceleration and slowing down of the rotor and removal of the tubes. Thus preparative ultracentrifugation in fixed angle rotors is mainly suited for the separation of particles in sediments of the supernatant solution. Differential ultracentrifugation for the separation of different macromolecules according to size is not possible.

These disadvantages can be circumvented by applying swinging bucket rotors (Figure 3.12B) and density gradients. At the starting phase of centrifugation the swinging buckets turn perpendicularly to the rotor axis so that the particles migrate through the whole bucket to the bottom. The density gradient counteracts the broadening of bands. There are two basic kinds of density gradient centrifugations. In true density gradient centrifugation (*isopycnic centrifugation*) a gradient of increasing density is formed from the meniscus to the bottom during centrifugation, because the particles of a dense medium, e.g., cesium chloride, sediment in the gravity field. As the diffusion of particles counteracts sedimentation, an equilibrium between sedimentation and diffusion causes the formation of a stable gradient in the gravity field. Macromolecules like proteins and nucleic acids will accumulate in sharp bands at the position of their own density. Separation is not according to particle size (which can be estimated from the width of the bands), but according to density. Macromolecules of the same type, e.g., proteins, RNA, single-chain or double-chain DNA, accumulate at the same positions.

Ultracentrifugation in sucrose gradients and similar media, such as glycerol, is not a density gradient centrifugation in its true sense, but a *zonal* (or rate zonal) centrifugation, as the particles actually travel according to their size. The increasing density gradient prevents the widening of bands, as they run against an increasingly dense medium. After a correspondingly long centrifugation the bands would finally sediment at the tube bottom. The gradient will not be formed during centrifugation, but has to be prepared before in a gradient mixer (Figure 3.12C). The sucrose concentration constantly increases from the meniscus (e.g., 5%) to bottom of the tube (e.g., 20%). If handled carefully such gradients remain stable for several days. Immediately before centrifugation the macromolecule solution is overlayered on top of the gradient. Length and speed of centrifugation depend on the sedimentation velocity of the particles. For a satisfactory separation the particle bands should make use of the whole gradient without sedimenting to the bottom of the tube. After centrifugation the solution is withdrawn either by pricking the tube bottom with a syringe or by inserting a capillary from above through the gradient to the tube bottom. Fractions of equal volume are collected. The number of drops is a relative measure of the migra-

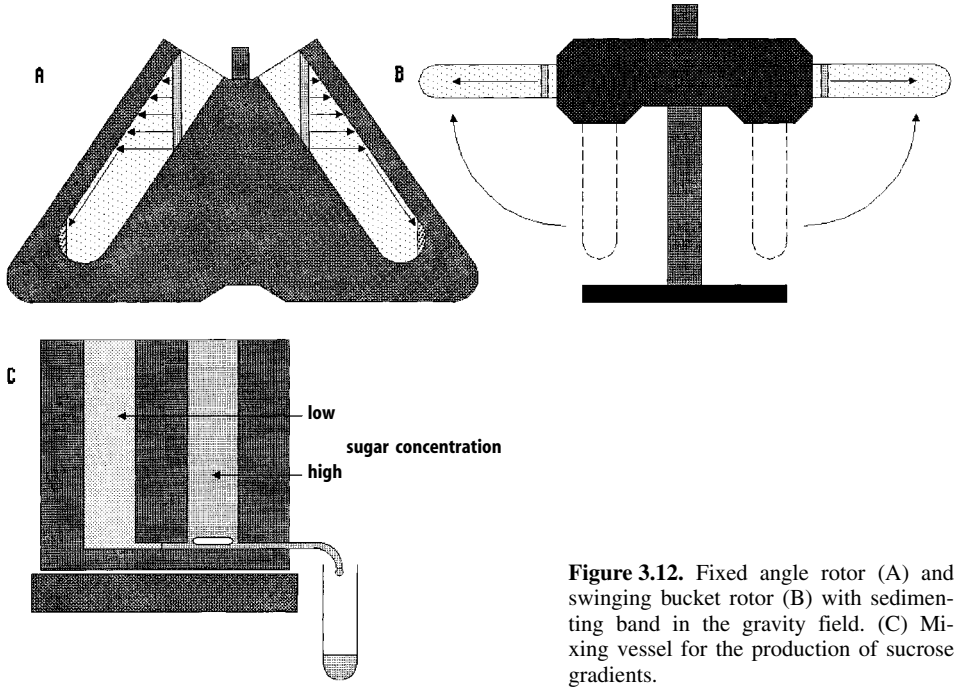

Figure 3.12. Fixed angle rotor (A) and swinging bucket rotor (B) with sedimenting band in the gravity field. (C) Mixing vessel for the production of sucrose gradients.

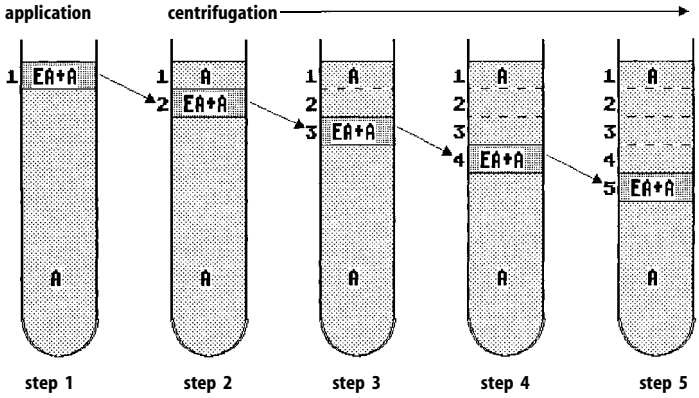

Figure 3.13. Sucrose gradient centrifugation for binding measurements (Draper and Hippel, 1979).

tion distance from which the approximate sedimentation coefficient and the relative molecule mass of macromolecules may be determined (Martin and Ames, 1961).

Differential separation can advantageously be applied for the determination of binding equilibria. The methods discussed so far require a large size difference between ligand and macromolecule, while this method allows the study of binding processes between molecules of similar size, e.g., association between macromolecules and subunit-

subunit interactions. As described above, a linear sucrose gradient is overlayered with a defined volume of a ligand-macromolecule mixture. The component sedimenting more rapidly (i.e., the macromolecule) must be present in a large surplus (at least 10-fold) over the low molecular weight component. Subsequent ultracentrifugation is performed until the band of the macromolecule has migrated an n-fold distance of its own thickness (Figure 3.13). After centrifugation the gradient is fractionated and ligand concentration is analysed in dependence of the migration distance.

At the start of centrifugation, i.e., at step one, the portion of bound ligand will be $[A]_{bound}$ corresponding to the rules of the general binding equation (1.23). This equation, however, will be transformed, as the free macromolecule [E] is regarded variable in place of the ligand concentration [A], and $[A]_0$ is regarded constant. As the total volume of [E] in relation to [A] is very large, [E] is approximated to $[E]_0$, $[E] = [E]_0$:

$$([A]_{bound})_1 = \frac{[E]_0[A]_0}{K_d + [E]_0} \ . \tag{3.10}$$

When, in a second step, the macromolecule band migrates just the distance d of the band thickness into the gradient due to the centrifugation, it takes the bound ligand along, while free ligand is left at the starting position. Because of rapid equilibration the ligand bound, during the first step, is now the total ligand which distributes between free and bound ligand:

$$([A]_{bound})_2 = \frac{[E]_0([A]_{bound})_1}{K_d + [E]_0} = \left(\frac{[E]_0}{K_d + [E]_0}\right)^2 [A]_0$$

Correspondingly, for the third step of translocation of the macromolecule by two distances d

$$([A]_{bound})_3 = \frac{[E]_0([A]_{bound})_2}{K_d + [E]_0} = \left(\frac{[E]_0}{K_d + [E]_0}\right)^3 [A]_0$$

and, in general for step i:

$$([A]_{bound})_i = \left(\frac{[E]_0}{K_d + [E]_0}\right)^i [A]_0 \ .$$

$$K_d = \frac{[E]_0}{\sqrt[i]{\frac{([A]_{bound})_i}{[A]_0}}} - [E]_0 \ . \tag{3.11}$$

At the end of centrifugation the gradient is fractionated and the migration distance of the macromolecule band from the meniscus l is determined. The quotient of this distance and the band thickness is $l/d = i$. The dissociation constant is obtained from the

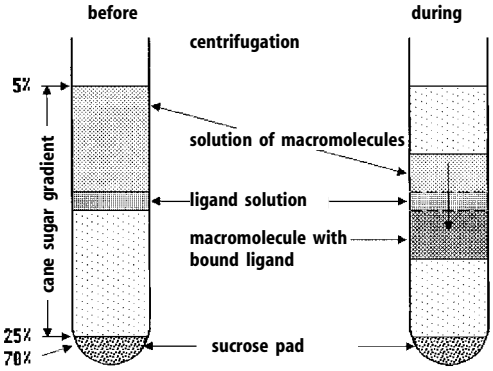

Figure 3.14. Sucrose gradient centrifugation for binding measurements (Yamamoto and Alberts, 1974).

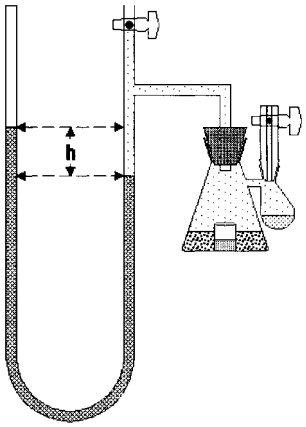

Figure 3.15. Warburg manometer for the measurement of gas-releasing or gas-consuming enzymatic reactions.

portion of bound ligand in the macromolecule band and the applied concentrations of both components.

In the method of Yamamoto and Alberts (1974) the ligand is already inserted as a narrow band at about 12% sucrose during the formation of the gradient. The upper part of the gradient (from 5–11.5%) contains the macromolecule (Figure 3.14). During centrifugation the macromolecule sediments through the narrow ligand band, carrying a portion of bound ligand. After fractionation the amount of bound ligand is analysed.

3.2 Electrochemical Methods

Electrochemical methods are especially suited for enzyme kinetic studies, as the time dependence of the reaction can be monitored continuously. The resulting progress curves serve to obtain the initial velocity or they are treated according to the integrated Michaelis-Menten equation (Section 2.3.1.5).

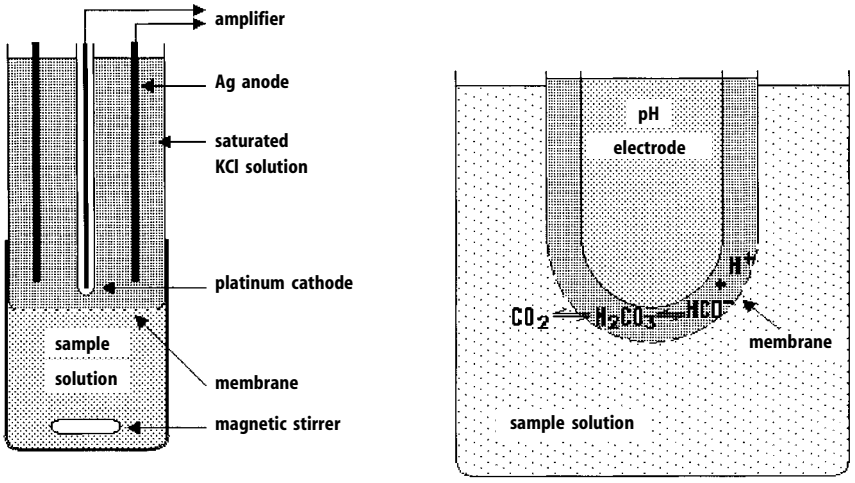

Figure 3.16. Schemes of an oxygen electrode (A) and a CO_2 electrode (B).

Formation or consumption of gases in enzymatic reactions are mostly measured with an oxygen or CO_2 electrode, but it should be mentioned that the *manometric* apparatus developed by Otto Warburg (Figure 3.15) may also be used. A reaction vessel is constructed in such a way that the substrate solution is held in a lateral flask. A central round compartment on the bottom of the vessel contains a stop solution, the surrounding outer compartment contains the enzyme solution. The whole arrangement must be gasproof and is connected to a manometer. By tilting the apparatus, substrate solution is poured into the enzyme solution to start the reaction. During the reaction the vessels must be kept at constant temperature in a water bath and are slightly shaken. The reaction is terminated by pouring the stop solution from the inner compartment into the outer compartment and the gas is expelled from the aqueous solution. The volume of gas produced or consumed can be read from the liquid column of the manometer.

3.2.1 The Oxygen Electrode

Oxygen plays an important role in numerous biological processes such as the respiratory chain. It is involved in the reactions of oxygenases, hydroxylases and oxidases, and it binds to transport proteins such as haemoglobin and myoglobin. The oxygen electrode developed by L.C. Clark in 1953 (Figure 3.16A) greatly facilitated the study of oxygen-dependent processes. A platinum wire fixed in the centre of a glass tube serves as the cathode. Besides this there is a silver-silver chloride anode. Both electrodes are surrounded by a saturated potassium chloride solution. They carry a constant voltage of 0.5–0.8 V. The whole arrangement is separated from the sample solution by a teflon or polyethylene membrane. The sample compartment must have an airtight connection to the electrode. It will be filled through a tight stopper with a

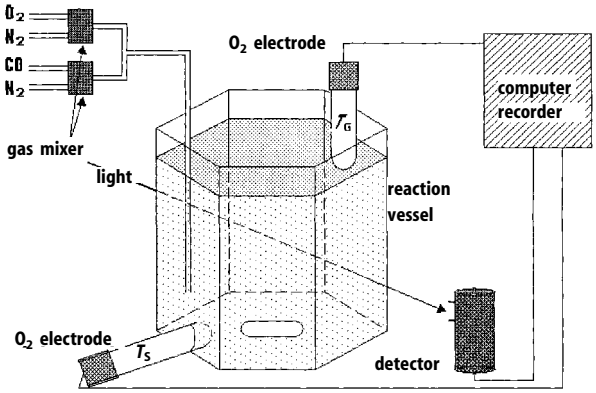

Figure 3.17. Apparatus for the kinetic observation of oxygen-dependent reactions with the aid of oxygen electrodes for measurements in solution and in the gaseous phase.

microsyringe. For better exchange the sample solution is stirred with a magnetic stirrer. Dissolved oxygen diffuses through the membrane and is reduced at the cathode:

$$\begin{array}{lrcl} \text{cathode} & 4\,H^+ + 4\,e^- + O_2 & \rightarrow & 2\,H_2O \\ \text{anode} & 4\,Ag + 4\,Cl^- & \rightarrow & 4\,AgCl + 4e^- \\ \hline & 4\,H^+ + 4\,Ag + 4\,Cl^- + O_2 & \rightarrow & 4\,AgCl + 2\,H_2O. \end{array}$$

The current produced is proportional to the oxygen concentration in the solution. Due to the membrane the oxygen electrode has a delayed response time. In the cathode compartment oxygen accumulates with a half-life of about 2 min. This impedes the response especially at transitions from high to low oxygen concentrations. A shorter response time can be achieved with open electrodes lacking a membrane, although there is the danger of poisoning by components of the solution. The electrode must be calibrated before measurement. 0% oxygen is achieved by expelling the gas in a nitrogen stream or by addition of sodium dithionite to the buffered solution. 100% is achieved by air saturated water.

Figure 3.17 shows an apparatus for the kinetic monitoring of oxygen-dependent reactions (Degn et al. 1980). The reaction vessel is a photometric cuvette, allowing simultaneous monitoring of changes in absorption during the reaction. A gas stream with defined oxygen content passes over the reagent solution. For faster exchange of gaseous oxygen with the solution it is intensively stirred. Therefore, a hexagonal cuvette, or, if no photometric measurement is performed, a round vessel is used. An oxygen electrode is inserted through a hole in the lower part of the vessel. A second electrode measures the oxygen content from above in the gaseous phase. A multichannel pen recorder monitors the signals of both electrodes and of the photometer. The kinetics of the reactions can be directly evaluated with a software programme. The turnover rate of the system v_r at a linear increase of oxygen content of the gaseous phase is measured and plotted directly or in a linearised form. It is assumed that in equilibrium v_r is equal to the velocity v_t of the oxygen transport from the gaseous

phase into the liquid; v_t is proportional to the difference between the oxygen pressures in the gaseous phase T_G and the solution T_S:

$$v_r = v_t = K(T_G - T_S) \ . \tag{3.12}$$

At given conditions K is a factor dependent on temperature, stirring speed and the ratio between surface and volume of the reaction solution. At a linear increase of oxygen content in the gaseous phase a steady state is not achieved for the oxygen exchange between the gaseous phase and the solution, i.e., $dT_S/dt \neq 0$:

$$v_r = v_t = K(T_G - T_S) - \frac{dT_S}{dt} \ . \tag{3.13}$$

K is obtained by determining T_S after alteration of T_G from an assay without an oxygen-reactive system (v_r=0):

$$\frac{T_S}{dt} = K(T_G - T_S) \ . \tag{3.14}$$

3.2.2 The CO_2 Electrode

The system of the CO_2 electrode is completely different from that of the oxygen electrode. It is based on pH measurement with a glass electrode. The CO_2 electrode is covered by a membrane of rubber coated cellophane or silicon rubber and is immersed into the sample solution (Figure 3.16B). Dissolved carbon dioxide diffuses into the space between the membrane and the gas electrode and becomes hydrated to carbonic acid. The resulting change of pH is proportional by a factor S to the CO_2 content of the solution:

$$\Delta pH = S \, \Delta \log pCO_2 \ .$$

This demonstrates that CO_2 determinations are sensitive to pH changes. The pH of the solution must be strictly controlled. The CO_2 electrode is calibrated with a standard hydrogen carbonate solution, or by different CO_2 partial pressures.

3.2.3 Potentiometry, Oxidation-Reduction Potentials

Oxidation-reduction systems (redox pairs) occurring in biological systems, e.g., the respiratory chain and enzyme reactions, can be studied by potentiometric measurement. An electrode (e.g., a platinum electrode) in a redox solution is electrically charged and exhibits a potential difference against a reference electrode to be measured with a potentiometer. Redox potentials are characteristic values for defined redox systems. They are adjusted to a standard hydrogen electrode, a platinum electrode surrounded by hydrogen gas under atmospheric pressure, immersed into a solu-

tion of 1.228 M HCl. Its potential is defined as 0. Naturally occurring redox pairs are NAD^+/NADH, $NADP^+$/NADPH, FAD/$FADH_2$, and cytochrome Fe^{3+}/Fe^{2+}. A redox pair may either be oxidised or reduced with oxidising or reducing reagents. A potentiometric titration curve is obtained when the potential difference is measured against the degree of oxidation or reduction.

Redox processes can also be demonstrated with redox indicators. They change in colour with the redox state and may function as electron donors or acceptors in enzymatic redox reactions. Frequently applied electron acceptors are ferricyanide, 2,6-dichlorophenolindophenol, methylene blue, phenazine methosulfate, and tetrazolium salts which are often used for histochemical enzyme assays. These dyes serve as probes for photometric monitoring the progress of the redox reaction.

3.2.4 The pH-Stat

In many enzyme reactions protons are either released or bound, as in dehydrogenases:

reduced substrate + $NAD(P)^+ \longleftrightarrow$ oxidised product + NAD(P)H + H^+,

oxidases, hydrolases, esterases, and proteases (by their esterase activity, proteolytic cleavage does not release protons). The enzyme reaction could be followed measuring the pH changes with a pH electrode. However, the pH change itself affects enzyme activity. In order to keep the pH constant during the reaction, enzyme reactions are usually measured in buffered solutions. This, however, eliminates the possibility of monitoring the reaction by pH measurement. If the reaction is performed in non-buffered solution and the pH is kept constant by adding acid or base, their consumption being a direct measure of the enzyme reaction. This is achieved by an auto-titrator or pH-stat (Figure 3.18). It consists of a pH electrode, e.g., a glass electrode with a calomel reference electrode, a pH meter and a control unit. At any change of pH an impulse is sent to the drive of an automatic burette that will run until the adjusted

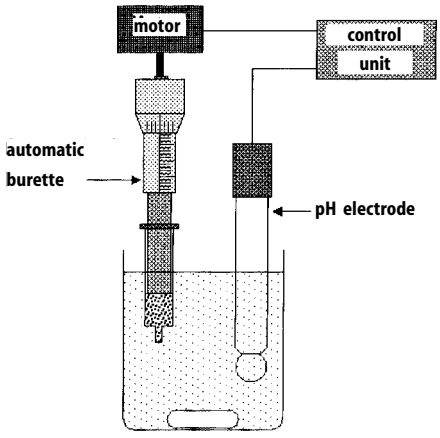

Figure 3.18. Scheme of a pH-stat.

pH level is regained. The sensitivity of this equipment is defined by the degree of dilution of the acid or base in the burette which, however, is limited by the fact that the sample volume should not change significantly during the enzyme reaction. Titration is achieved either by alternating additions and pauses (this, however, affects sensitivity and includes the danger of over-titration) or by proportional control, supporting a quick response of the system. The reagent solution must be evenly stirred. Influences from outside, e.g., CO_2 or electrostatic interactions with other instruments or synthetic fibres (clothing of the experimenter) must be avoided. pH-stats are available in different versions (automatic sampling with intermediate washing and sample preparation, simultaneous maintenance of constant substrate concentration with a second burette, system control and electronic data processing).

In another pH-stat system the pH change is not compensated by titration, but by an electrolysis stream producing acids or bases at the electrodes. This has the advantage that the reaction volume remains constant. The pH is controlled by spectrophotometry with pH indicators (Karcher and Pardue, 1971).

pH-stat measurements often are more sensitive than photometric tests. It is also possible to investigate highly absorbing homogenates and light scattering suspensions, like membrane-bound or immobilised enzymes. The pH-stat procedure is, however, circumstantial to handle and has a relatively slow response period.

3.2.5 Polarography

When two electrodes with a small negative potential difference are immersed into an electro-reducible substance, a small residual current flows between the electrodes. At a continuous increase of the potential a point is finally reached, at which the substance is reduced at the cathode. The current starts to increase and this increase continues at a further rise of the potential until reduction of the substance at the cathode is limited by diffusion. From this point any rise of the potential does not cause a further increase of the current. A sigmoidal current-voltage curve, a polarogram, re-

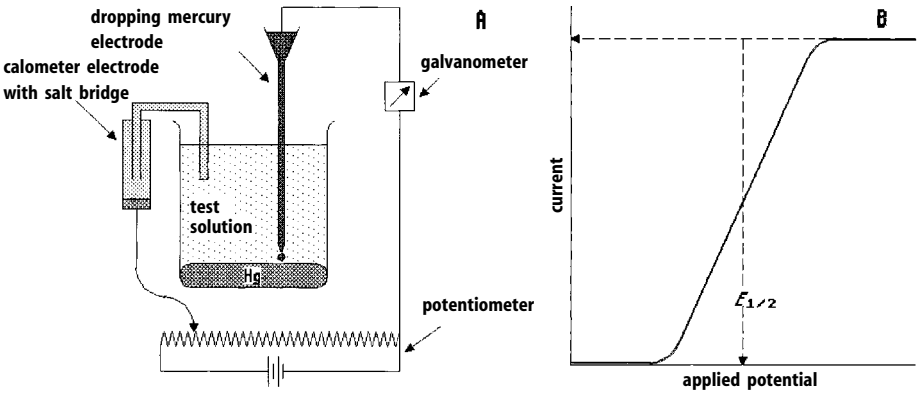

Figure 3.19. Schematic sketch of a polarographic measurement with a dropping mercury electrode (A) and polarogram for the determination of the half-wave potential $E_{1/2}$ (B).

sults. Its point of inflection, the half-wave potential $E_{1/2}$, is a characteristic, concentration-independent value of the respective substance (Figure 3.19B). The height of the curve, the limiting current, is a measure of the substance concentrations and may be used for its determination. Electro-oxidisable substances with positive potential will be oxidised at the anode and yield a corresponding, but opposing signal.

Polarography is an extremely sensitive method working with dissolved solutions and small sample volumes (Figure 3.19A). A dropping mercury electrode is used for the study of reductions. Mercury drops from a reservoir through a capillary into the solution. The reservoir level is adjusted to release 10–20 drops per min. The continuous renewal of the surface prevents poisoning of the electrode, e.g., by proteins. The mercury layer forming at the bottom of the vessel may serve as the anode. Frequently, instead, a calomel electrode is used, connected to the sample solution by a salt bridge. The voltage applied is potentiometrically changed and the current produced is measured with a galvanometer. For oxidations, a rotating platinum electrode or a carbon electrode is used as the anode.

When product or substrate of an enzyme reaction generates a polarographic signal, the enzymatic turnover may be recorded time-dependent at a constant potential. A progress curve is obtained. The intensity of the current is a measure of the turnover. Polarographic measurement may be applied for oxygen reactions (with an oxygen electrode), for thiol compounds (e.g., of coenzyme A-dependent reactions), for carbonyl compounds, e.g., pyruvate and NAD^+ or NADH. Contrary to photometric procedures, measuring may also be performed in turbid and highly absorbent samples.

3.3 Calorimetry

Calorimetry is one of the oldest biological methods. In 1780 Lavoisier and Laplace already studied respiration in animals with the aid of calorimetry. Nevertheless, this method has found little acceptance in biochemistry so far. Most chemical and biological processes are accompanied by the release or the uptake of heat from the environment. Development of heat is directly related to the reaction process. Therefore, calorimetry represents a method with a broad potential of applications and has the advantage of directly studying systems without external influences or modifications. There also are no special requirements of purity. Changes in the range of mJ may be detected with microcalorimeters, thus micromolar concentrations are accessible.

Two calorimetric principles are mainly applied. With *adiabatic calorimeters* there is no heat exchange with the environment. The heat quantity released or taken up by the system $Q=\varepsilon\Delta T$ is detected by the relative change of temperature, to which it is proportional by way of the calibrating constant ε. The calorimetry chambers are protected by an air or vacuum mantle (*isoperibolic calorimeters*). This can, however, not completely prevent a certain heat exchange, especially for a longer time period. Heat exchange with the environment is prevented by a heatable adiabatic metal sheet within the outer mantle that automatically adjusts to the inner temperature in the calorimetric chamber (Figure 3.20A). With this device it is, however, not possible to measure at constant temperature.

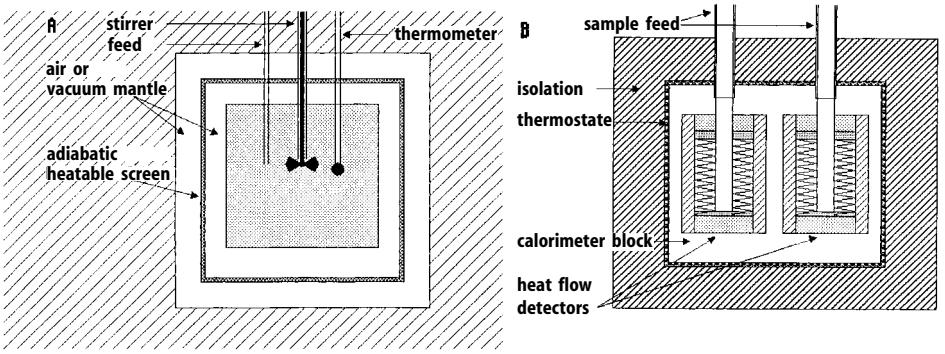

Figure 3.20. Schemes of an adiabatic isoperibolic calorimeter (A) and of a heat-conducting (thermal) calorimeter with twin arrangement (B).

With *heat conducting calorimeters*, heat is directly transferred from the reaction chamber into an outer thermal reservoir, heat flow is controlled by a thermocouple fixed between the two compartments (Figure 3.20B). This equipment is comparatively slow and is best suited for slow processes. In *isothermic calorimeters* endothermal and exothermal effects are compensated by heating or cooling in the measuring cell, and the impulses required for compensation are chronologically registered. In the *scanning calorimeter* both the reference and the sample cell are kept at an identical temperature, and the heat quantity required for compensation in the sample cell is registered.

Manipulations, e.g., initiating a reaction by adding substrate or stirring, affect calorimetric measurements. For compensation and for the equalisation of unspecific heat exchanges with the environment, twin calorimeters equipped with two identical chambers are installed. Sample and reference chamber are equally treated, the reaction, however, occurs only in the sample chamber. To monitor changes in absorption or optical density in the measuring cell, calorimeters are additionally equipped with photometric systems. *Flow calorimeters* with mixing or flow cells are recommended for enzyme reactions. In a zero order reaction under steady-state conditions the heat quantity released per time unit is constant and inclination from the base line is proportional to the turnover rate.

Ligand binding to macromolecules may also be calorimetrically detected. In separate experiments the part of ligand dilution heat and, if necessary, of the macromolecule is determined and subtracted from the values measured for binding. By calorimetric titration of the macromolecule with the ligand the binding constant K_d and the enthalpy of the binding ΔH are obtained. The calorimetrically measured heat quantity Q yields a linear dependency on ligand concentration [A] in the double reciprocal plot for a simple binding process:

$$\frac{1}{Q} = \frac{1}{Q_m} + \frac{K_d}{Q_m[A]} \ . \tag{3.15}$$

Q_m, the heat quantity at saturation, is proportional to the binding enthalpy: $Q_m = \Delta H [A]_{eq}$. $[A]_{eq}$ is the molar amount of bound ligand at full saturation. Aggregations of proteins and subunits, protonations of amino acid residues, hydrations, conformational changes and denaturation processes may be recorded in a similar fashion by calorimetric measurements.

3.4 Spectroscopic Methods

Spectroscopic methods, especially absorption spectroscopy, are widely used for studies of enzyme kinetics, enzyme tests, ligand binding, conformational changes, catalytic mechanisms, etc. Easy handling and continuous monitoring of time-dependent processes like enzyme reactions, make these methods attractive. At any time intervention into ongoing reactions is possible, e.g., by additions or modifications. High-quality absorption spectrophotometers are not very expensive and of versatile use, e.g., for the detection of a wide variety of biologically relevant substances, such as proteins, nucleic acids, lipids, and low molecular weight metabolites. A survey of the most relevant photometric methods for enzyme studies and their special applications will be presented here. All these methods are based on irradiation of a sample solution by a light beam to observe the alterations caused by the sample (absorption, ORD, CD) or the light emitted by the sample (fluorescence, Raman effect).

A photon may interact with a molecule in various ways. Figure 3.21 shows the term scheme of the states of an electron. It exists in a lower energy state S_0 and a higher energy or excited state S_1. The energy difference between the two is 340 kJ/mol. Each state has different vibrational states the energy differences of which are about 40 kJ/mol and rotational states that differ less than 4 kJ. At normal temperatures, the molecules preferably remain at the lowest vibrational state of S_0, but various rotational levels may be adopted. Absorption of a photon of a distinct frequency induces the molecule to transform into the excited state S_1, where various vibrational and rotational states can be occupied. From this an absorption spectrum consisting of many adjacent sharp bands should be expected. However, influences by their environment – especially in solution – and by other factors cause broadening of the bands, so that they merge into one or few broad absorption bands characteristic for the respective molecule.

The molecule cannot remain in the excited state S_1. In most cases the excited state becomes deactivated in a radiationless process and the excitation energy is transmitted to the environment as heat. This occurs in collisions with molecules of the same species or with other molecules in the solution. Certain compounds, as dissolved molecular oxygen, are particularly effective. These deactivation processes of the excited state together are designated as *external conversions*. Deactivation within the molecule occurs by energy shifts to internal oscillations (*internal conversion*). Finally, the excited singlet state may be transferred by a forbidden radiationless spin exchange into a low energy triplet state T_1 (*intersystem crossing*). This possesses a long lifetime within a range from milliseconds to few seconds and *phosphorescence* light will be emitted. Due to its extremely long lifetime, this state will in solution usually be completely deactivated by internal or external conversions. Therefore, it may only be observed in solid phase and at low temperatures.

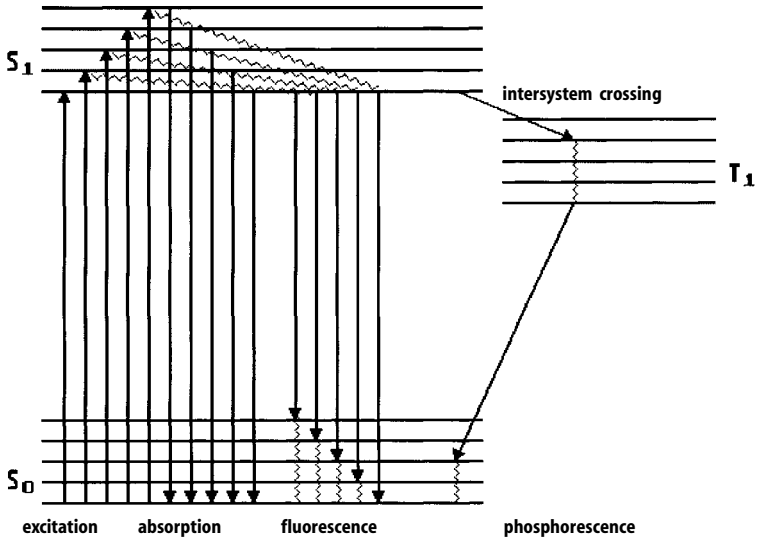

Figure 3.21. Term scheme of the energy content of an electron. Taking up energy by photon irradiation, the electron transits from the ground state S_0 into the excited state S_1. From there it either returns directly to the ground state (absorption), or, when remaining for a longer period at the lower vibrational level of the S_1 state, it returns to the ground state under emission of fluorescent light, i.e., it follows an intersystem crossing into a less energetic triplet state T_1. The lines above the states correlate with the vibrational levels.

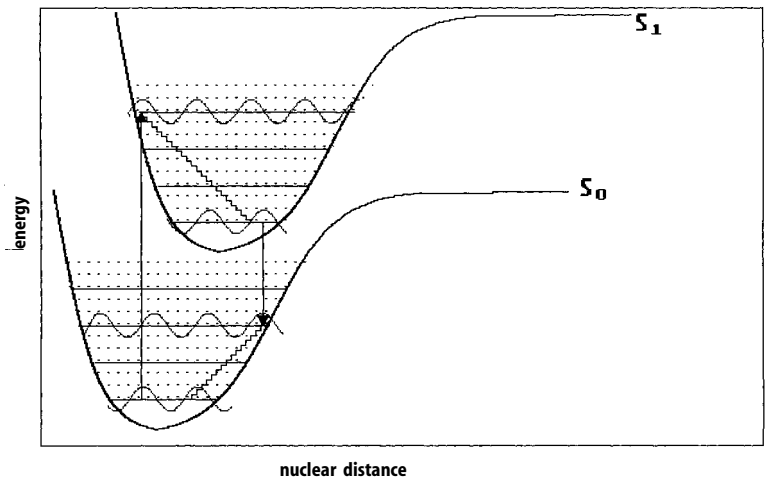

Figure 3.22. Franck-Condon principle for a two-atom molecule. The transition of the electron takes place in resonance from the ground state S_0 to a level of the excited state oscillating with the same phase.

When the excited electron in the S_1 state is not immediately deactivated after excitation, it changes radiationless to the lowest vibrational level (Figure 3.21). The duration of the respective processes is decisive. Excitation of the molecule is so rapid ($\approx 10^{-15}$ s) that the nuclei cannot adapt so quickly to the excited state because of their inertia. They will initially retain the nucleic distance of the low energy state S_0 (*Franck-Condon principle*). The transition occurs vertically (Figure 3.22) over several vibrational levels to the state of highest probability for a nucleic distance closest to the original state. From there the electron quickly (10^{-12} s) moves to the lowest vibrational level where it rests with on average for a few ns. Finally, the excited electron reverts to the low energy state S_0 emitting light of less energy, i.e., longer wavelengths (*fluorescence*). This process competes with the deactivation processes described above. If these deactivation processes are more rapid than the emission, fluorescence is either weakened or completely quenched, and only absorption may be observed.

3.4.1 Absorption Spectroscopy

3.4.1.1 The Lambert-Beer Law

Absorption measurement is based on the Lambert-Beer law describing the attenuation of light intensity I_0 of a given wavelength λ after passage through the solution of an absorbing compound with the molar concentration c:

$$I = I_0 e^{-\varepsilon dc} . \tag{3.16}$$

d is the length of the light path in the solution and ε the molar absorption coefficient ($1 \cdot \text{mol}^{-1}\ \text{cm}^{-1}$). I/I_0 is termed *transmittance* or permeability usually indicated in percent. Unhindered passage of light, $I=I_0$, equals a transmittance of 1 or 100%. 0% transmittance is total impermeability, e.g., a closed optical path. These boundary values serve for the calibration of photometers for a given wavelength. According to Eq. (3.16), light intensity exponentially decreases with the concentration of the absorbing substance. A linear dependency exists on the negative logarithm of the transmittance:

$$A = -\log(I/I_0) = \varepsilon dc . \tag{3.17}$$

A is the measure of absorption. The previous terms extinction or optical density are no longer valid (actually the quotient I_0/I represents optical density or opacity).

3.4.1.2 Spectral Properties of Enzymes and Ligands

Principally all biological compounds exhibit absorption and are, therefore, accessible for this method, although the absorption maxima of many substances, e.g., carbonyls

or peptide bonds, are located in the hardly accessible far UV region where overlapping spectra from many contributions make interpretations difficult. For numerous investigations, e.g., enzyme kinetics, ligand binding, or conformational changes, however, not the absolute absorption is of importance, but the spectral change. Photometric recording of the conversion of substrate into product becomes easier, the greater the difference of the spectra of the reactants. NAD^+ and $NADP^+$ are an ideal example. After reduction into NADH and NADPH (+ H^+) a new absorption band emerges in the easily accessible region at 340 nm, so that reactions they participate in as cosubstrates are easily measured by way of the appearance or disappearance of this band. This *optical test* not only provides access to the dehydrogenases directly dependent on these compounds, but also to enzymes whose product is a substrate of a dehydrogenase and also to enzymes which accept the product of a dehydrogenase as substrate. Their reactions may be coupled with those of dehydrogenases as indicator enzymes and substrate consumption or product increase of the enzyme tested may be determined by way of the NAD turnover (*coupled assays*). Up to three reactions may be coupled in this way. Coupled assays are helpful for the determination of enzyme activity, but not recommended for enzyme kinetic studies, as it cannot be excluded that the indicator reaction will be limiting and affect the test reaction when certain parameters are changed.

Most substrate/product pairs in enzyme reactions do not show such marked spectral differences as NAD^+/NADH. There are minimal spectral shifts or differences in intensity, sometimes there are no detectable changes at all, as in many isomerisations. Ligand binding and conformational changes in proteins mostly exhibit minimal spectral alterations that may be recorded only with highly sensitive photometers, e.g., dual beam and dual wavelength photometers (see below).

While for enzyme kinetic measurements the absorption properties of substrates and products are of relevance, binding measurements and studies in conformation concentrate on the spectral properties of proteins and their possible cofactors. As the proteins are composed of the 20 proteinogenic amino acids, their spectra exhibit an identical form. The contribution of peptide binding is in the far UV region ($\sim$190 nm), as well as that of amino and carboxyl groups. Anorganic ions also absorb there, e.g., Cl^- (181 nm) and OH^- (187 nm), as does oxygen in gaseous or dissolved form. For measurements in this region the optical system of the photometer has to be gassed with nitrogen. Dissolved air must be removed from solutions in vacuum. However, this region is hardly accessible with conventional equipment as lamps are only of weak intensity.

Between 190 nm and 210 nm, secondary structural elements of proteins like α-helix, β-sheets and random coils, contribute to the absorption. The α-helix band has the least intensity, however, it shows a characteristic shoulder between 200 nm and 210 nm (Figure 3.23). The ratio of secondary structures and also conformational changes in such structures can be studied from these absorptions. In this region also the three aromatic amino acids exhibit pronounced maxima, phenylalanine with the shortest wavelengths and the highest intensity (<190 nm with a shoulder at 206 nm). Tyrosine shows the weakest maximum with the longest wavelengths (220 nm), the tryptophan spectrum is located in the middle (Figure 3.24). Histidine shows a band, methionine a shoulder at 210 nm. Cysteine absorbs between 200 nm and 210 nm,

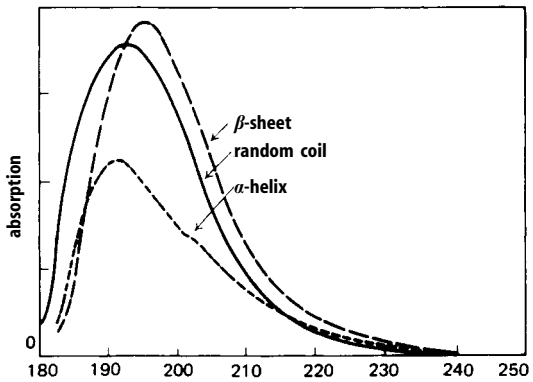

Figure 3.23. UV spectra of secondary structural elements of proteins (Rosenheck and Doty, 1961).

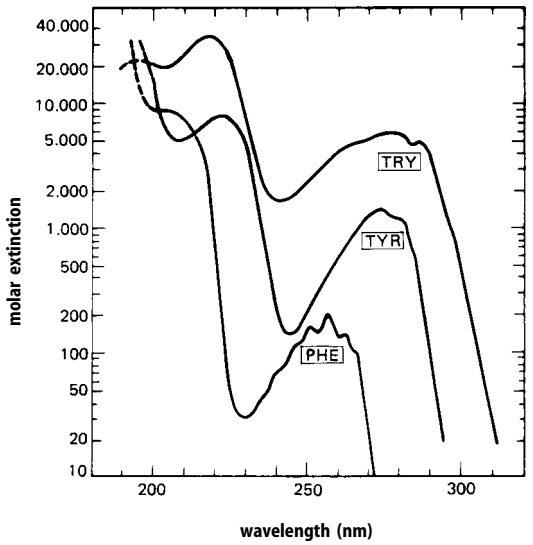

Figure 3.24. UV spectra of aromatic amino acids (Wettlaufer, 1962).

upon deprotonation of the thiol group the intensity increases, and an additional band is formed between 230 nm and 240 nm. The remaining amino acids exhibit absorptions in the region below 200 nm, mainly originating from the carboxyl group. Between 190 nm and 220 nm many factors contribute to the protein spectrum, resulting in a strong absorption band in this area.

To study specific effects out this variety of spectral contributions is difficult. The second absorption band located in the longer wavelength region between 260 nm and 300 nm is much better suited. This band is significantly weaker but is formed solely from absorption contributions of the three aromatic amino acids (Figure 3.24). Phenylalanine shows here the weakest absorption at shorter wavelengths. Its maximum at 257 nm is eight times weaker than that of tyrosine and 35 times weaker than that of trytophan (Table 3.2). Phenylalanine is therefore only detectable in protein spectra in the absence of the other two aromatic amino acids. Characteristic for the phenylalanine

Table 3.2. Spectral features of amino acids and coenzymes in aqueous solution. ε: molar absorption coefficient, Φ_F: quantum yield (in part after Fasman, 1989)

Compound	Absorption maxima		Emission maxima	
	λ_{max} (nm)	ε ($l \cdot mol^{-1}cm^{-1}$)	λ_{max} (nm)	Φ_F (%)
Phenylalanine	206	9300	282	4
	242	86		
	257	197		
	267	91		
Tyrosine	224	8800	303	21
	274.6	1420		
Tryptophan	219	35000	350	20
	280	5600		
Histidine	211	5860		
Cysteine	250	360		
Cystine	248	350		
Adenine	259	14900	321	0.026
Coenzyme A	260	16000		
FAD	260	46200	536	2.5
	375	9300		
	438	14600		
	445	11300		
FMN	450	12200	536	24
NAD, NADP	260	18000		
NADH, NADPH	260	14100	470	1.9
	340	6220		
Pyridoxal phosphate	295	6700	392	
	388	6500		
Thiamin diphosphate	235	10100		
	267	9200		
p-Aminobenzoic acid	305		360	
ANS	350		515	0.4
ANS in ethanol			470	37
TNS	317		500	0.08
TNS in ethanol			429	52
DANSYL amide	320		580	5.5
DANSYL protein-bound			468	84
Fluoresceine	495		518	92
Rhodamine B	575		630	80

spectrum in this region is a pronounced fine structure of several small maxima, which may appear at the short-wave flank of the tyrosine and tryptophan absorption, especially in solid phase at low temperatures. The tyrosine absorption at 274 nm is usually superimposed by strong tryptophan absorption at 280 nm. Thus, native proteins, containing all aromatic amino acids, show the characteristics of the tryptophan spectrum with a maximum at 280 nm in this region. The intensity of this band serves as a measure of protein concentration. The absorption maximum of tyrosine is intensified and shifts at ionisation of the phenolic hydroxyl group in alkaline environment by about 20 nm towards longer wavelengths at 295 nm. Therefore, tyrosine can be quantitatively determined by alkaline titration.

From the known amino acid composition of a given protein its spectrum may be derived by superimposing the individual amino acid spectra. Such calculated spectra, however, deviate considerably from the measured ones, especially the intensity of the bands is weaker than expected from the sum of the individual amino acid contributions. This is due to the fact that amino acid residues are shielded within the folded proteins. By partial unfolding of the protein molecule by urea, guanidine and other detergents, these residues become exposed and the spectral bands increase. By successive denaturation information on the protein structure can be obtained. Conformational changes of proteins, accompanied by hiding or exposing of aromatic amino acid residues, may cause spectral alterations. Changes in the polarity in the vicinity of distinct amino acid residues lead to spectral shifts. A decrease in polarity causes a red shift in the absorption maxima of aromatic amino acids, due to the difference energy levels of ground and excited state. Complex bonds, e.g., charge-transfer complexes or metal complexes, also cause spectral alterations.

The determination of ligand binding of proteins by spectroscopic titration with difference spectroscopy is based on such effects. The interactions of the binding ligand with the protein causes either directly an alteration of the protein or the ligand spectrum, or the binding is revealed by an induced conformational change.

3.4.1.3 Structure of Spectrophotometers

The Göttingen physicists Julius Elster and Hans Geitel, who described the first vacuum photo cell in 1891 initiated the development of photometers. The main parts of a photometer are the light source, a monochromator for the spectral splitting of light and a photocell or a photo multiplier for measuring light intensity. Equipment for the display and recording of the measurement signal is also part of the unit (Figure 3.25).

Light source. An ideal light source for spectral photometers should cover the total spectral region with a constant light intensity, a continuum. Such light sources, however, do not exist, all available lamps show distinct characteristics with an intensity maximum within a distinct wavelength range. It is not possible to completely cover both the UV and the visible spectral region with a single lamp. Commercial spectrophotometers are therefore equipped with a hydrogen or deuterium lamp for the UV region from 190–340 nm and a tungsten or a halogen lamp for the visible region from 320–900 nm. A pivoting mirror directs the light of the respective lamp through the sample. Simple instruments omit the UV lamp. For measurements at constant wavelengths *filter photometers* with a mercury lamp emitting distinct lines (line spectrum) are often sufficient. They are of high stability and suited for various enzyme tests and protein determinations. The line of the respective wavelength is collimated by interference or liquid filters so that no monochromator is required.

Monochromator. Most photometers perform spectral light resolution with the aid of diffraction gratings. Compared to glass or quartz prisms previously used, they have the disadvantage of a larger degree of light dispersion and thus yield monochromatic light of minor spectral purity. The advantage of gratings lies in the registration of

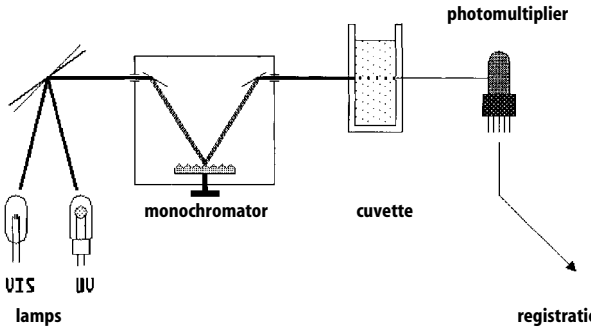

Figure 3.25. Set-up of a spectrophotometer.

spectra. The monochromatic light is collimated through the exit slit at constant rotation of the grating and directed into the sample solution. For gratings, the degree of rotation is proportional to the wavelength. Rotation is effected by a stepping motor, its progression serving as a direct signal for the wavelength scale of the spectrum. Prisms, however, do not exhibit a linear light dispersion, thus complicating the registration of continuous spectra. Spectral purity of gratings, i.e., their quality, depends on the number and shape of the grooves. A high burr between the furrows leads to light dispersion. Flattening may prevent this, the grating is blazed to a given wavelength and incidence angle. Dispersion-free holographic concave gratings produced by laser-holographic methods are frequently used. To obtain light of the highest optical purity, two monochromators are connected in series one behind the other. The width of the entrance and exit slits of the monochromator determines the sharpness of the spectral cutout. The measure is the *bandwidth* of the incident light, i.e., the spectral width at half intensity. The gain in optical purity at narrow spatial collimation, however, goes along with a loss in light intensity and thus in sensitivity. The slit width must correlate with the quality of the grating; narrowing the slit cannot compensate bad spectral resolution from a simple grating.

Cuvettes. To eliminate reflections and dispersion, rectangular cuvettes with ground surfaces are used. They usually have a thickness of 1 cm. For the visible spectral range (340–800 nm) glass or plastic cuvettes are used, which are, however, impermeable for UV light. For this range cuvettes of quartz glass have to be applied.

Photomultipliers. Light intensity is measured after penetration of the sample cuvette in a photocell or a photomultiplier. Photo cathodes normally applied for the release of electrons from alkaline material have an optimal response only within a given spectral range. Besides the light source, all other optical materials, e.g., diffraction gratings, mirrors and collective lenses, also exhibit characteristics dependent on wavelength. These effects superimpose the spectrum of an absorbing sample, which suffers significant distortion. To obtain authentic spectra, photometers possess corrective functions. The photomultiplier signal is adjusted to a constant level, dependent on wavelength, by resistor strips. With computer-controlled equipment corrections are executed with software programmes. Photomultipliers always retain a certain level of dark current even

in total absence of light, causing a constant background noise that affects the sensitivity of the unit.

Diode array photometers are based on a multi-channel photodetector instead of a photomultiplier. A large number of photo diodes are linearly arrayed. The whole polychromatic light of the lamp is directed through the cuvette. Spectral resolvation occurs in the grating monochromator behind the cuvette and the complete spectrum is projected onto the multi-channel photo detector and recorded as a whole. Spectra may be recorded within milliseconds with this method. This technique is applied in rapid scanning-stopped flow units that are able to measure several hundred spectra per second.

Recording. For recording the current induced in the photomultiplier is transmitted to a laboratory recorder at a voltage proportional to the recorder. The transmission signal is transformed into an absorption signal by a transmission-absorption transformer according to the Lambert-Beer law. Even smallest absorption differences are detectable by amplification, limited, however, by the noise of the unit. The quality of instruments is determined by the signal-noise ratio, indicating the weakest possible measuring signal still recognisable over the background noise. For kinetic measurements, time-dependent recordings are applied, wavelength-dependent measurements for spectral studies. Computer-controlled instruments display the primary data on a screen; they can be saved and documented by printer. Computer control permits direct processing and calculation of data. Sections may be cut out, slopes calculated by regressive methods (e.g., the determination of reaction velocities) and data sets (spectra) subtracted from each other.

3.4.1.4 Double Beam Spectrophotometer

Ordinary photometers are based on the *single beam technique*; there is only one cuvette in the light beam. Reference or blank values are measured separately and are deducted from the sample values either by calculation or suppression of the blank to zero. This also applies for spontaneous reactions, e.g., due to instability of a substance, occurring in the sample solution apart from the genuine enzyme reaction. For such cases the *double beam technique* represents a significant improvement (Figure 3.26). Passing the monochromator the beam meets a rapidly rotating diaphragm with a reflecting mirror, alternatively totally reflecting the beam or allowing it to pass completely. The alternating beams are directed on mirror-symmetric pathways through a sample and a reference cuvette, respectively. After penetrating the cuvettes, both beams are conducted over a second diaphragm, identical to the first one and rotating at the same frequency, so that they are rejoined and reach the photomultiplier over a united pathway. In connection with the rotating diaphragm the photomultiplier discriminates between the two beams and the difference between sample and reference intensity is displayed as measuring signal. In another construction the beam is split into two beams of each half intensity by a beam splitter and sent through the two cuvettes on parallel pathways. The rotating diaphragm is not necessary, but each beam must be detected separately with a own photomultiplier.

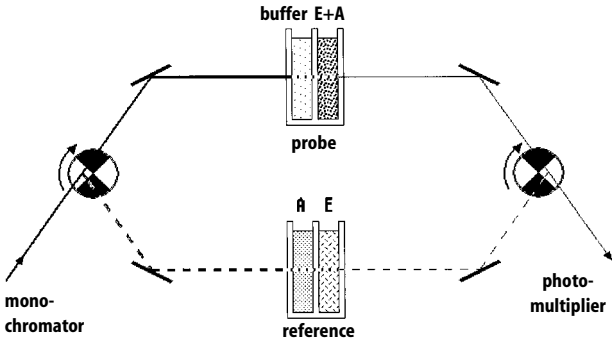

Figure 3.26. Set-up of a dual beam spectrophotometer with tandem cuvettes for difference spectroscopy.

Both beams in a double-beam photometer register the same absorption spectrum, the sample beam with a positive, the reference beam with a negative sign. If sample and reference cuvette both contain the same absorbing substance in identical concentration, both measuring effects compensate each other, the photometer will record a base line. This allows the detection of very small differences between two samples at high absorption. At high absorption, however, even faint deviations, like small differences in concentration, badly adjusted light beams or differences in the thickness of the cuvettes will produce considerable effects and may simulate spectral differences between both cuvettes.

3.4.1.5 Difference Spectroscopy

The double-beam method is especially suited for the study of spectral shifts caused by interactions of different components by difference spectroscopy; this is to be demonstrated here by the example of macromolecule-ligand binding. To apply this technique binding must cause a spectral shift, either of the protein or the ligand spectrum, or of both. Because of its macromolecular structure a shift in the protein spectrum is more probable. Spectral shifts are caused either by direct interactions between ligand and groups on the binding site of the macromolecule or by ligand-induced conformational changes. The effect must be specific, not e.g., changes in pH or ion strength caused by the ligand solution. To detect spectral shifts, the absolute spectra both of macromolecule and ligand have to be compensated. The double-beam arrangement will compensate the absorption of one component, e.g., the protein, which is the same in the sample and the reference cuvette and remains constant during the experiment. The ligand, however, as the variable component is added to the protein only in the sample cuvette and so its own absorption will not be compensated. This is achieved by *tandem cuvettes*, which are divided into two chambers of equal size by a transparent window (Figure 3.26). For binding measurements, macromolecule solution in identical concentration is filled into each one chamber of the sample and the reference cuvette. The two remaining chambers are filled with buffer solution. As the absorption of both cuvettes compensate each other, a base line will be expected. Deviations at this stage indicate differences in concentration and should be corrected. To study the binding process the ligand will be added in var-

ious aliquots to the macromolecule solution of the sample cuvette. The same additions are done to the buffer chamber of the reference cuvette to compensate for ligand absorption. As repetitive ligand additions will dilute the macromolecule solution in the sample cuvette, the macromolecule solution in the reference cuvette must similarly be diluted by additions of the same volumes of buffer. Because of the minimal spectral shifts to be detected in highly absorbing solutions, this technique is very sensitive to concentration differences. Ligand additions should therefore be small in volume, and no solution should be spilled from the chambers when stirring or mixing the solutions. A small magnetic stirrer at the bottom of the cuvette is recommended. To evaluate the binding process ligand is added to the macromolecule in many small aliquots until saturation is reached (*spectroscopic titration*). Initially, the spectral shift grows proportionally to the addition of ligand and approaches a plateau value at saturation of the binding sites. The evaluation of spectroscopic titration is described in Section 1.3.2.2.

Difference spectra, if caused only by a spectral shift without intensity change, has the shape of the first derivation of the absorption spectrum. The smallest changes will be observed at the maxima of the absorption spectrum, while the shift of the flanks result in maxima or minima of the difference spectrum. Aromatic amino acids exhibit a bathochrome shift towards longer wavelengths, at transition from a polar to a less polar environment, due to energy differences between ground and excited state in different polarity (Figure 3.27). This occurs when such residues are shielded by ligand binding or they turn from the surface to the inside of the protein. Changes of this kind may be demonstrated by *solvent-dependent difference spectra*. The polarity of the solvent water in the sample cuvette is gradually reduced against the one in the reference cuvette by adding less polar solvents, e.g., glycerine, glucose, ethyleneglycol or polyethyleneglycol. Residues at the protein surface get into contact with the increasingly non-polar environment, while the environment inside does not change, so that information about distinct residues may be obtained. A more detailed analysis can be obtained by applying solvents of varying molecular size. The low molecular ethyleneglycol may penetrate into regions of the protein molecule that are not accessible to high molecular polyethylene glycol. Differences between the both solvents of comparable polarity are indications of narrow folds and pockets, e.g., active or regulatory centres, at the surface. Complete unfolding of the protein structure and gradual exposure of individual residues from the inside of the molecule can be followed by addition of urea, detergents or chaotropic substances. Enthalpic and entropic processes of protein folding can be studied by *temperature-dependent difference spectra,* where the temperature in the sample cuvette is gradually raised while that in the reference cuvette remain constant.

Protonation processes of distinct residues (e.g., tyrosyl and thiol residues) are investigated by *pH-dependent difference spectra.* Spectral changes can also be caused by alterations of charges in the vicinity of chromophores, splitting and formation of ionic bonds and hydrogen bridges, and conformational changes caused by such effects. Reversible aggregation processes of subunits of the macromolecule may be studied with the aid of *concentration-dependent difference spectra*. Decrease or increase of the macromolecule concentration in the sample cuvette shifts the aggregation equilibrium relative to the unchanged one in the reference cuvette. To compensate for the concentration differences between both cuvettes their pass length is cor-

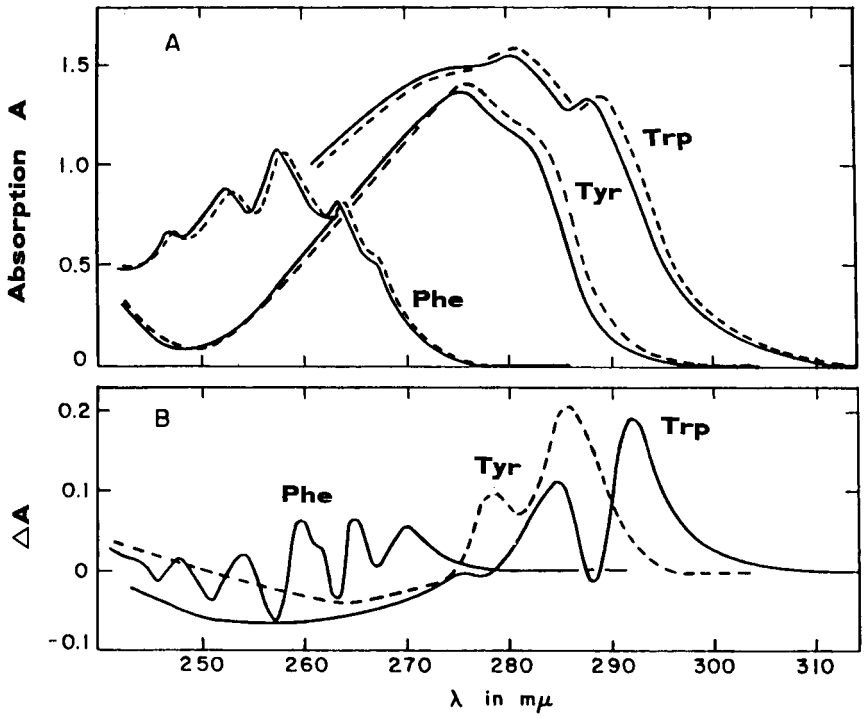

Figure 3.27. Spectral shifts and difference spectra of the aromatic amino acids phenylalanine, tyrosine, and tryptophan at transition from the aqueous phase into 20% dimethylsulfoxide. (A) Absorption spectra (shift in dashed lines), (B) difference spectra (Herskovits, 1969).

respondingly adapted, a tenfold dilution of the sample solution is compensated by a tenfold thickness of the sample cuvette.

When the macromolecule itself does not display any significant spectral changes, the effect may be enhanced by introducing chromophore groups at defined positions, e.g., the thiol or amino groups. If proflavin is added to chymotrypsin binding of ligand or substrate can be followed by the subsequent removal of the chromophore.

3.4.1.6 The Double Wavelength Spectrophotometer

In 1954 B. Chance developed the double wavelength photometer for measurements in turbid and strongly scattering solutions, e.g., membrane-bound cytochromes of the respiratory chain in mitochondria suspensions. A monochromator with two separately adjustable gratings create two light beams of different wavelengths: a sample and a reference beam (Figure 3.28). With a rotating mirror disc both beams pass alternatively through the cuvette on the same path. The photomultiplier signals of both beams are separately detected and recorded as a difference signal.

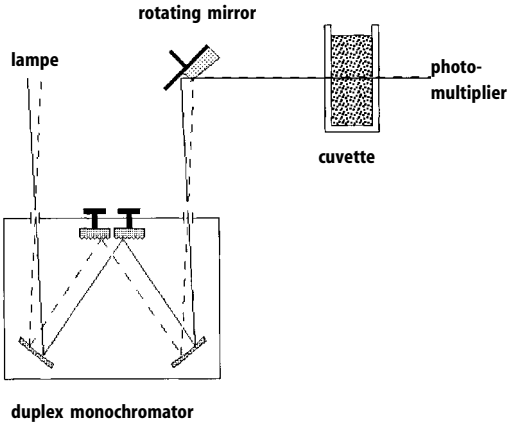

Figure 3.28. Construction scheme of a dual wavelength photometer.

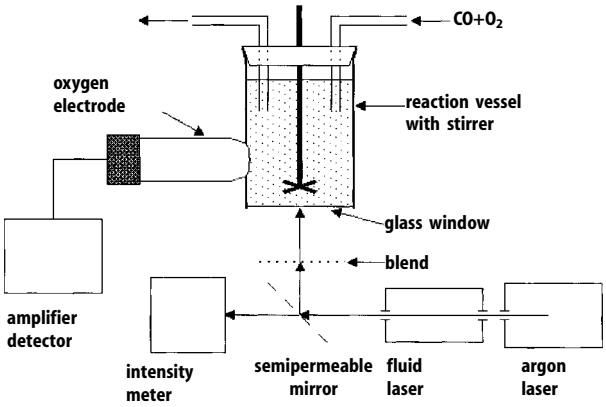

Figure 3.29. Scheme of an apparatus for measuring photochemical action spectra.

This method can also be applied for the detection of very small spectral changes in binding studies or enzyme kinetic measurements. The sample beam is adjusted to the wavelength of the largest absorption change, frequently the flank of the absorption band, the reference beam is fixed to an isosbestic point of constant absorption, often located near the absorption maximum. The latter corrects fluctuations in the cuvette. This technique allows the measurement of effects with maximal absorption changes of 0.005. Commercial instruments usually combine double beam and double wavelength optics.

3.4.1.7 Photochemical Action Spectra

Otto Warburg discovered that haemoglobin inactivated by CO may be regenerated by light exposure. Castor and Chance (1955) developed a specific apparatus for measuring such photochemical action spectra, which are suitable for the study of the reactive state of pigments like cytochromes, phytochromes and chlorophylls (Figure 3.29). A cell sus-

pension or a cell extract is exposed to a fixed $CO:O_2$ ratio. By irradiation with a lamp the interaction of the pigment with a component of the system is altered, e.g., CO becomes released and oxygen can bind. An oxygen electrode detects the change of oxygen concentration in the solution. Application of liquid colour lasers enhance the emission intensity at narrow spectral bandwidths.

3.4.2 Bioluminescence

Bioluminescence is an extremely sensitive technique for the determination of ATP, FMN and NAD(P)H, widely used in enzyme analytics. Enzyme reactions dependent on these compounds may be analysed and linked with further enzyme reactions. Two bioluminescence systems are commercially available. In glow-worm luciferase (*Photinus pyralis*) ATP reacts with the cofactor luciferin emitting light of 562 nm. Luciferase from the bacterium *Photobacterium fischeri* is FMN-dependent and reacts with NADH and NADPH. As the detection of the substrate to be studied (e.g., ATP) is itself based on an enzyme reaction, bioluminescence measurements always are coupled tests with the disadvantages already mentioned for the determination of initial velocities for enzyme kinetic studies. In the initial phase of the reaction (e.g., by adding ATP), the intensity of the emitted light reaches a maximum value after about three seconds, subsequently declining again because of product inhibition. Maximum light intensity is proportional to ATP concentration. Greater precision is achieved by integration of the curve over a defined time period.

The instrumental requirements for luminescence measurements are comparatively small. Luminometers consist of a sensitive photomultiplier, an amplifier and a digital meter. Test combinations with the respective components are commercially available.

3.4.3 Fluorescence

3.4.3.1 Quantum Yield

The measure for the intensity of fluorescence light emitted by a component is the quantum yield Φ_F. It represents the ratio of photons emitted (q_e) to photons absorbed (q_a) by the compound. The quantum yield depends on the rate of all processes competing for the energies of the excited state (see Section 3.4):

$$\Phi_F = \frac{q_e}{q_a} = \frac{k_e}{k_e + k_{ic} + k_{is} + \sum k_{ec}} \; ; \tag{3.18}$$

k_e, k_{ic}, and k_{is} are the rate constants of the emission, the internal conversion and the radiationless intersystem crossing, respectively. $\sum k_{ec}$ is the sum of all external conversions. Thus a compound will only emit fluorescent light, if the competing processes are slower than the lifetime of the excited state. $\sum k_{ec}$ is determined by external factors at the vicinity of the chromophore and can be influenced from the outside, while k_{ic} and k_{is} are determined by the constitution of the molecule.

The quantum yield is, like the absorption coefficient, a substance constant. It may adopt values of 0–1, respectively 0–100%. At a quantum yield of 1, respectively 100%, the total light absorbed by the chromophore is emitted as fluorescent radiation, at 0% there is no fluorescence. To determine the quantum yield, fluorescence intensity of the respective compound must be measured and the absorbed photons are analysed under identical conditions either in a highly scattering solution, or, in the place of a cuvette, by a totally reflecting magnesium oxide screen. For compounds with similar spectral properties their quantum yields behave nearly in the same way as their maximum fluorescence intensities, so that the quantum yield of an unknown sample may be determined by comparison with a standard compound. Quantum yield is highly temperature-sensitive, it decreases at higher temperatures because of the increase of deactivating collisions.

3.4.3.2 Perturbations of Fluorescence Measurements

Processes subsumed under *external conversions* are generally termed *fluorescence quenching*, mainly due to collisions of molecule in excited state, causing deactivation of the excited state. Molecular oxygen dissolved in solutions is especially effective and has to be removed by degassing with inert nitrogen. Impurities in the solvent or the components are frequently responsible for fluorescence quenching, therefore, all components must be of highest purity. At higher concentrations deactivate chromophores themselves. Occasionally two molecules in the excited state enter into resonance and form dimers (*excimers*). Because of this *concentration quenching* fluorescence intensity is only proportional to the amount of the chromophore in highly diluted solutions. At higher concentrations, a deviation from linearity up to the total disappearance of fluorescence may be observed. Fluorescence measurements should therefore be limited to diluted solutions.

Reabsorption of emitted light (*inner filter effect*) also causes fluorescence quenching. This effect is to be observed when the solution contains substances with an absorption spectrum overlapping the one of the emitted light. The extent of this effect depends on the concentration of the absorbing substance and on the length of the path the emitted light has to cover in the solution; it may be identified by varying the size of the cuvettes.

A perturbation generally occurring in fluorescence measurements is light scattering, pretending an emission maximum just at the excitation wavelength. This may have various causes, Rayleigh- or Tyndall scattering (see Section 3.4.5.2) in colloidal solutions, and reflections from impurities or fingerprints on cuvette walls, or in the cuvette room by incomplete elimination of entering light, scattering at floating particles and air bubbles in the solution. Light scattering is identified by altering the excitation wavelength, the scatter peak will move in the same sense. To minimise light scattering, highest purity of samples and solutions, and cleanliness of cuvettes have to be observed.

Also the *Raman effect* appears as a perturbation especially in weak fluorescence. Photons interact with vibration and rotation levels of the molecule without exciting them, but delivering or taking over a distinct amount of vibration energy v', the fre-

quency ν_R of the emitted photons is either above or below the excitation frequency ν_0: $\nu_R = \nu_0 \pm \nu'$. At some distance from the exciting wavelength, longer-waved *Stokes* and shorter-waved *anti-Stokes* lines are to be observed. Raman lines differ from fluorescence bands by their relative sharpness and the tendency to shift along with the exciting wavelength. They appear in the solvent also in the absence of the chromophore. The Rayleigh bands found at the excitation wavelength are caused by photons, which adsorb for a short time at the (solvent) molecule and are scattered in all directions without exchange of energy.

3.4.3.3 Fluorophores (Fluorescent Compounds)

Equation 3.18 demonstrates that without the knowledge of the molecular constitution of a compound it is impossible to predict whether and with which intensity it will emit fluorescent light. Fluorescence is to be found in compounds with conjugated double bonds, in aromatic and heterocyclic ring systems, also in lanthanides (europium, gadolinium, and terbium in the trivalent oxidation state). This can be applied by replacing naturally bound metal ions by fluorescent ions. From the organic compound classes mentioned very few show actually measurable emissions. Emission is also dependent on the state of the compound, e.g., the ionisation state or the polarity of the environment. The indol ring of tryptophan exhibits a strong fluorescence with maximum intensity between pH 9–11 where the carboxyl group is deprotonated and the amino group is uncharged. In the hybrid ion form between pH 4–8 emissions are weaker (Figure 3.30). In the acid region below pH 2, as well as in the alkaline region above pH 12, the indol fluorescence is quenched, firstly by the protonated carboxyl group, secondly by interactions with hydroxyl ions. NAD^+ respectively $NADP^+$, emit only in their reduced forms as NAPH or NADPH (see Table 3.2). The very sensitive fluorimetric dehydrogenase tests make use of this property.

A frequent phenomenon is a hypsochrome shift (blue shift) of the emission maximum of a chromophore, often linked with an increase in intensity, at the transition from a polar into non-polar environment. A prominent example is the strongly lipo-

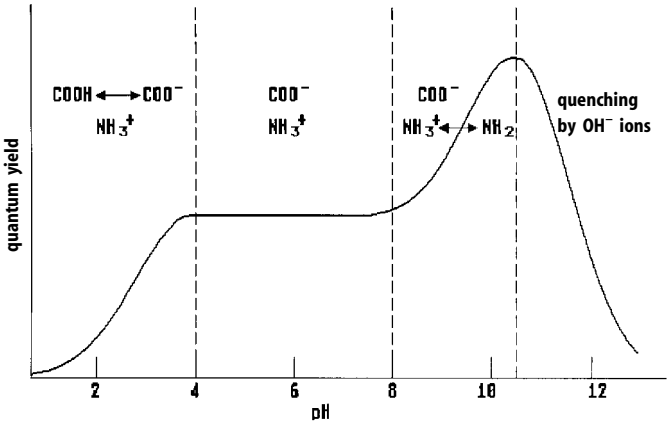

Figure 3.30. Dependence of the quantum yield of tryptophan on the pH value of the solvent (after Brand and Witholt, 1967).

phile compound 1-anilino-naphthalene-8-sulfonate (ANS, Figure 3.31). In water it exhibits only a weak fluorescence, which rises considerably at transition into increasingly non-polar solvents, e.g., alcohols of growing chain lengths, simultaneously shifting the emission maximum by 20–30 nm towards shorter wavelengths (Figure 3.32). Blue shifts are to be observed when the dipole moment of the chromophore is higher in the excited state than in the ground state. Interactions occur with the polar molecules of the solvent. On return to the ground state a smaller amount of energy is released than in non-polar solvents, due to the loss of solvation energy. On account of its lipophile character, ANS binds with high affinity to non-polar regions of proteins, frequently to binding centres. This is accompanied by a high increase in fluorescence intensity. Upon binding of ANS to the porphyrine binding pocket of apomyoglobin the quantum yield is rised from 0.4 to 98%. Such effects can also be observed with other artificial chromophores, e.g., toluidine naphthalene-6-sulfonate (Figure 3.31), and with naturally occurring chromophores, e.g., aromatic amino acids, especially tryptophan. Tryptophan dissolved in water shows an emission maximum at 350 nm, which shifts to 330–340 nm when the amino acid is buried within the relatively apolar inner core of a protein.

This sensitive interaction of fluorophores with their environment makes fluorescence spectroscopy such a valuable tool for enzyme studies. Structural changes in the protein molecule, interactions with other components, ligand binding, protein aggregation, membrane association, etc., may be measured with high sensitivity. The fact that only few compounds emit fluorescent light is more an advantage of the method, the observed effects remain specific and are hardly covered by many other signals as in absorption spectroscopy. First choice is the naturally occurring chromophore, like tryptophan, which does not require modification of the macromolecule.

In proteins, only the three aromatic amino acids exhibit fluorescence emissions. Phenylalanine shows the weakest emissions, while tryptophan and tyrosine are comparable in their quantum yield (Table 3.2). This, however, applies only to free amino acids. In protein compounds, tryptophan has the highest fluorescence intensity, due to partial quenching of the tyrosine fluorescence. In the excited state the pK value of the phenolic hydroxyl group decreases, the resulting phenolate has a very low quantum yield. Tryptophan can always be identified in proteins by its fluorescence; the non-appearance of tryptophan fluorescence is a sure indicator for the absence of this amino acid. The weaker tyrosine fluorescence becomes visible only in the absence of tryptophan, at best it will be detectable at the short wavelength flank of the tryptophan band. Phenylalanine is detectable only in the absence of other aromatic amino acids. So practically each protein possesses its own chromophore, whose spectral characteristics will supply valuable information for the study of conformations and bindings.

Of the other naturally occurring compounds NAD(P)H, flavins, pyridoxal phosphate, steroids (cholesterol, bile acids, and steroid hormones), and the components of folic acid, pteridine and p-amino benzoate, as well as anthranilate, exhibit a noticeable fluorescence (Table 3.2). Purines and pyrimidines and their nucleotides, on the other hand (e.g., adenosine phosphates and the nucleic acids), show all very low quantum yields. With proper modifications various non-emitting compounds may be transmitted into chromophores, e.g., the adenosine compounds AMP, ADP, ATP, NAD, NADP, and coenzyme A by inserting a N-6-etheno group (ε-group) at the pyri-

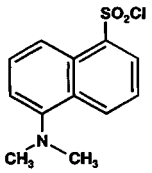

5-dimethylaminonaphthalene-1-sulfonylchloride (DANSYL chloride)

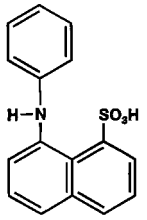

1-anilinonaphthalene-8-sulfonic acid (ANS)

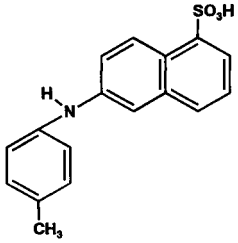

2-toluidinonaphthalene-6-sulfonic acid (TNS)

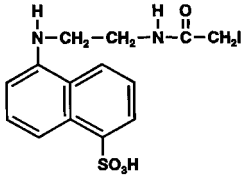

N-(iodoacetaminoethyl)-1-naphthyl-5-sulfonic acid (1,5-I-AEDANS)

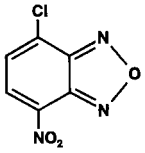

7-chloro-4-nitrobenzo-furazan (NBD-chloride)

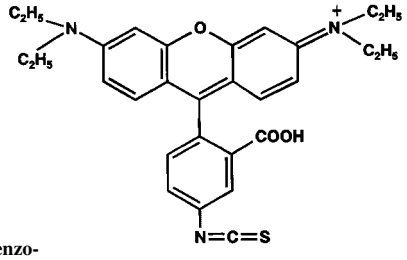

rhodamine B-isothiocyanate

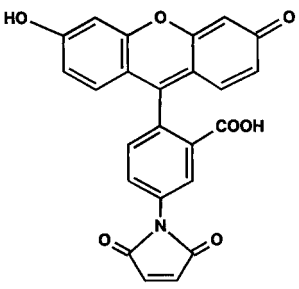

fluorescein maleimide

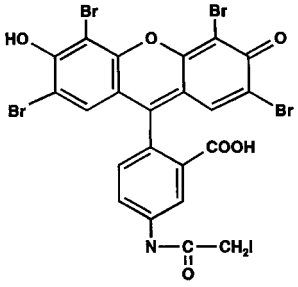

eosin iodoacetamide

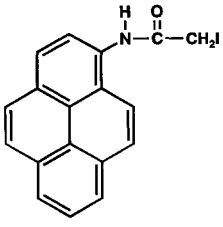

pyrene iodoacetamide

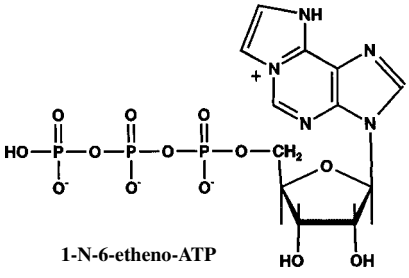

1-N-6-etheno-ATP

Figure 3.31. Structures of important fluorescent dyes.

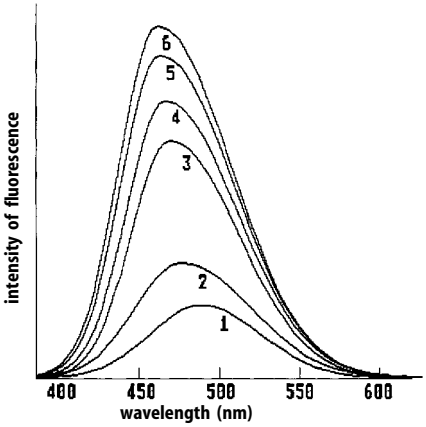

Figure 3.32. Blue shift and intensity increase of the fluorescence spectrum of anilinonaphthalene sulfonate at decreasing polarity of the solvent: (1) ethylene glycol, (2) methanol, (3) ethanol, (4) *n*-propanol, (5) *n*-butanol, (6) *n*-octanol (after Stryer, 1968).

midine ring (Figure 3.31). They partially retain their biological activity. A fluorescent analogue of thiamin and its derivates is thiochrome.

When the natural fluorescence of proteins and their cofactors is not sufficient, chromophores may be introduced. Apart from the compounds already mentioned, e.g., ANS and TNS, forming non-covalent bonds to hydrophobic regions of the protein, chromophores with group-specific reactive residues will form covalent bonds to the protein. Such groupings are iodoacetamide, maleimide, aziridine or disulfide for thiol groups, isothiocyanate, succinimide, or sulfonyl chloride, respectively fluoride, for amino groups, hydrazine and amine for aldehyde and ketone groups. Azides are groups activated by photo processes. With their support chromophores irradiated with light of a wavelength of 300–350 nm are covalently bound to the target molecule. Frequently employed chromophores are fluoresceine, rhodamine, NBD chloride (7-chloro-4-nitrobenzofurazan) and the 5-dimethylaminonaphthalene-1-sulfonyl-(DNS-, DANSYL-) residue (Figure 3.31).

3.4.3.4 Structure of Spectrofluorimeters

The structure of spectrofluorimeters (Figure 3.33) is similar to that of spectrophotometers. However, a more powerful light source is required. Usually a xenon high-pressure arc lamp is used for the whole spectral range, but its intensity is weak in the far UV region. To equalise fluctuations in the lamp, e.g., movements of the light arc, ratio systems are employed, with a beam-splitter directing a fixed part of the light beam into a reference photomultiplier placed before the cuvette. The instrument indicates as signal the ratio of the intensities of the sample and the reference beam.

The essential difference between absorption and fluorescence photometers is that the latter ones detect the weak light emitted by the sample in all directions, instead of the intense permeating lamplight. The permeating light must completely be eliminated by light traps, preventing scattering, while the emission light is measured at right angle to the incoming light to avoid reflections. For this glass (or quartz) cuvettes with all its

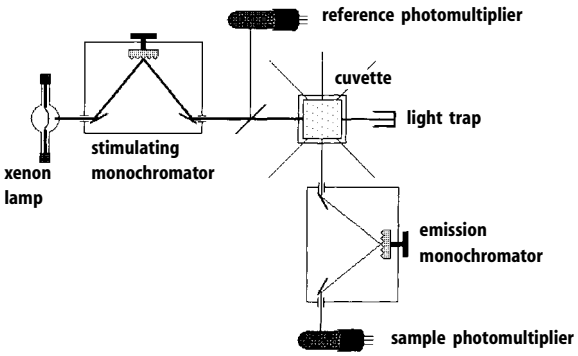

Figure 3.33. Construction scheme of a spectrofluorimeter.

windows polished are employed. The emitted light passes through a second monochromator before reaching the photomultiplier. This is much more sensitive than those used in absorption photometers as it is not exposed to the full lamplight, but only the small share of the light emitted by the sample. Because of this, fluorescence measurements are much more sensitive than absorption measurements. For the blank without the emitting sample the photomultiplier receives no light and may be greatly amplified to detect traces of the chromophore, while in absorption spectroscopy the highest light intensity occurs with the blank in the absence of the absorbing compound. Thus, small absorptions of dilute solutions might be overlaid by fluctuations of the lamp and the fully activated photomultiplier. Accordingly photomultipliers in fluorimeters are highly sensitive and may be damaged by high light intensity, e.g., strong scattering of the sample, incoming daylight or room lightning.

With two separate monochromators two different types of spectra may be recorded by spectrofluorimeters. The *excitation* monochromator, placed in front of the cuvette, performs excitation spectra of the chromophore, which are measured in the wavelength region below a fixed emission wavelength (fluorescence light is of lower energy than the excitation). Since a chromophore will only emit light in such an extent as it absorbs light, excitation and absorption spectra of a chromophore should be identical. Frequently both these spectra are quite different, due to the fact that they are superimposed by the wavelength dependencies of the lamp and other optical parts (as already described for spectrophotometers). To obtain authentic spectra a corrective function is needed, which is usually realized, with more or less precision, in spectrophotometers, while fluorimeters frequently produce uncorrected spectra.

With the *fluorescence* or *emission* monochromator, placed behind the cuvette, emission spectra at wavelengths higher than the constant excitation wavelength can be recorded. They exhibit the fluorescence characteristic of the chromophore. As excitation wavelength usually the largest absorption maximum is chosen, to gain the highest quantum yield. With a single chromophore, also other wavelengths may be chosen for excitation, as long as there is a detectable absorption, like smaller excitation maxima or flanks. This causes a loss of intensity, but the shape of the spectrum is retained. It is recommended in the case of interferences from scatter or Raman peaks. A variation of the excitation wavelength is anyway suggested as a control of the fluorescence phe-

nomenon, changes the shape of the spectrum is an indication for other effects, like impurities, presence of different chromophores, Raman or scatter peaks.

Phosphorescence can also be measured with spectrofluorimeters. A rotating diaphragm allows alternately the excitation or the emission beam to pass. In the moment the excitation becomes switched off the longer-lasting luminescence will remain while the short-term fluorescence disappears immediately.

3.4.3.5 Radiationless Energy Transfer

A peculiarity of fluorescence is the phenomenon of radiationless transfer of excitation energy from one singlet state to a second one. A certain chromophore (*donor*) is excited while a second, non-excited chromophore (*acceptor*) emits light. This effect occurs when the emission spectrum of the donor overlaps with the absorption spectrum of the acceptor (Figure 3.34) and the distance between both chromophores is less than 8 nm. According to the theory of Theodor Förster (1948) the rate of the energy transfer is:

$$k_T = 8.71 \cdot 10^{-23} \cdot k_e r^{-6} J \cdot n^{-4} x^2 \ (s^{-1}) \tag{3.19}$$

and its efficiency E:

$$E = \frac{r^{-6}}{r^{-6} + R_0^{-6}} \tag{3.20}$$

is reciprocally proportional to the sixth power of the distance r of both chromophores from each other. R_0 is the distance at 50% transfer efficiency:

$$R_0 = 978.5 \cdot (J \cdot n^{-4} \kappa^2 \Phi_D)^{-6} \,(\text{nm})\,. \tag{3.21}$$

J is the integral of the spectral overlap of donor fluorescence and acceptor absorption, n is the refraction index of the solvent, Φ_D is the donor quantum yield, and k_e the rate constant of the emission, κ is an orientation factor of the dipole moments of both chromophores towards each other:

$$\kappa = \cos\gamma - 3\cos\alpha\cos\beta\ ; \tag{3.22}$$

α and β are the inclinations of the dipoles to the joint axis and γ is the angle formed by the dipoles with themselves. κ may adopt values between 0 (vertical orientation) and 4 (parallel orientation), and requires detailed knowledge of the molecular arrangement of both chromophores. This can be hardly known without detailed structural data, but frequently it may be assumed that the chromophores are relatively mobile on the macromolecule surface and will not remain in a fixed orientation. In such cases a medium value of 2/3 can be taken for κ.

Distances between two chromophores fixed on the same macromolecule in aqueous solution may be measured with the Förster equation, which otherwise can only be done using X-ray structure analysis on protein crystals. When successfully insert-

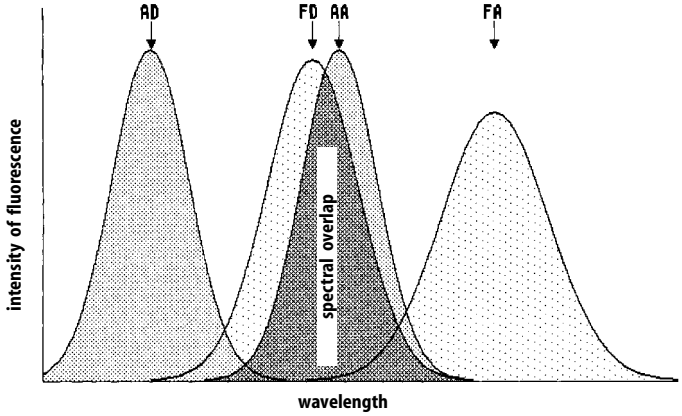

Figure 3.34. Radiationless fluorescence energy transfer. The fluorescence spectrum of a donor chromophore (FD) almost overlaps the excited spectrum of an acceptor chromophore (AA). At excitation of the donor (AD, excitation spectrum of the donor), the fluorescence spectrum of the non-excited acceptor (FA) is to be observed.

ing a pair of chromophores with suitable overlaps at defined locations of a macromolecule, e.g., at active or regulatory centres, their distance from each other may be determined. Either analogues of the original ligands or fluorophores fixed covalently to defined amino acids may be employed as chromophores. This technique could demonstrate that the three catalytic centres of the pyruvate dehydrogenase complex are more than 4 nm distant from each other. This finding ruled out the previous assumption of a 1.4 nm swinging lysyl-lipoyl arm which should be able to reach all centres from its attachment point. It turned out that the swinging arm is fixed to a mobile peptide domain. Employing the same method the assembly of the same enzyme complex from its subunits could be followed. For the bifunctional allosteric enzyme aspartokinase:homoserine dehydrogenase the distance of the two catalytic centres was determined to be 2.9 nm. A change in conformation induced by binding of the allosteric inhibitor threonine causes the two centres to move apart by 0.7 nm. The distance of the two tRNA binding sites for ribosomes could also be determined. These examples demonstrate the wide variety of applications for this technique. Ligand binding can be measured, the ligand, taking one (donor or acceptor) part, a chromophore fixed in the neighbourhood the other, or by affecting the interactions of a pair of chromophores placed in the vicinity of the binding site.

An energy transfer effect is identified by fluorescence quenching of the excited donor or, even better, by the emission of the non-excited acceptor. Energy transfer may also occur with a non-fluorescent acceptor when its absorption spectrum overlaps with the donor emission. In this case only fluorescence quenching of the donor is to be observed. The radiationless energy transfer must be distinguished from a simple reabsorption of fluorescence light described in Section 3.4.3.2, which is significantly weaker and only occurs in higher concentrations.

3.4.3.6 Fluorescence Polarisation

Linearly polarised light can only excite chromophores the dipoles of which are directed towards the polarisation plane, but not perpendicular to it. Only the part of the molecules properly oriented will be excited and in turn emit light (*photoselection*). However, due to molecular motion the original orientation will be changed during the lifetime of the excited state, leading to a partial depolarisation of fluorescent light. According to the Perrin equation the decrease of the polarisation P depends on the molar volume of the chromophore V (ml/mol), the absolute temperature T, the solvent viscosity n and the lifetime of the excited state τ_0:

$$\frac{1}{P} = \frac{1}{P_0} + \left(\frac{1}{P_0} - \frac{1}{3}\right) \frac{R\tau_0}{V} \cdot \frac{T}{\eta} \ . \tag{3.23}$$

P_0 is the polarisation of immobile molecules ($T = 0$ K) and R the gas constant. A linear dependency of $1/P$ against T/η results when polarisation of the emitted light is measured by variation of temperature or solvent viscosity (or both). The straight line intercepts the ordinate at $1/P_0$, so that the gradient only contains τ_0 and V as unknowns. This method permits to determine the volume of a chromophore if τ_0 is known (or *vice versa*, the lifetime of the excited state if V is known), the mobile element determining the volume. If a small chromophore is attached to a large protein molecule, the latter dictates mobility, including hydrate shell and shape (spheric, elliptic, etc). With the molecule mass known, information on the shape of the molecule may be obtained. If the chromophore is freely mobile on the surface of the molecule, slow movements of the protein and rapid movement of the chromophore may be observed simultaneously. In the Perrin plot two overlapping straight lines appear. In this way the required information for the orientation factor κ in the Förster equation can be obtained.

Fluorescence polarisation is measured with spectrofluorimeters collecting the emission in two symmetrical beam paths perpendicular to the incoming irradiation through two emission monochromators and photomultipliers. In the exciting beam path a polarisation filter is placed for the production of linearly polarised light. In the two emission beam lines analysator filters are placed, one of them oriented in parallel, the other right-angled to the polarisation plane of excitation (Figure 3.35). As measurement value the instruments record the fluorescence polarisation P as the ratio between the difference and the sum of fluorescence intensities in parallel (F_{II}) and vertical (F_{II}) direction:

$$P = \frac{F_{II} - F_{\perp}}{F_{II} + F_{\perp}} \ . \tag{3.24}$$

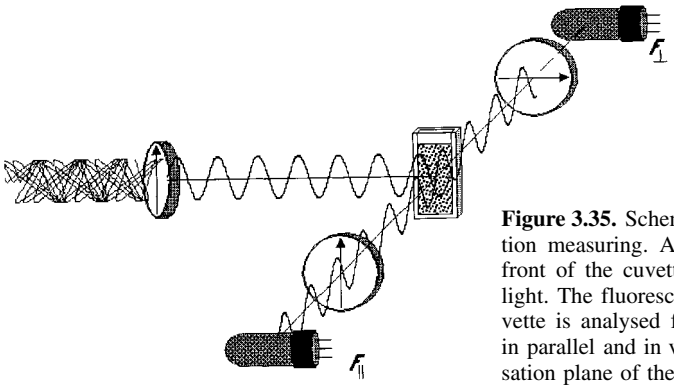

Figure 3.35. Scheme of a fluorescence polarisation measuring. A vertical polarisation filter in front of the cuvette produces linearly polarised light. The fluorescent light emitted from the cuvette is analysed for the part of polarised light in parallel and in vertical direction to the polarisation plane of the incoming irradiation.

3.4.3.7 Pulse Fluorimetry

Pulse fluorimetry, a further development of fluorescence polarisation, is basically a fast measuring method (*cf.* Chapter 3.5). The chromophore is excited by a flashlight shorter than the lifetime τ_0 of the excited state. After extinction of the flashlight decline of fluorescence is followed over the given time period (Figure 3.36A). Fluorescence intensity S_0 at the moment of excitation ($t=0$) decreased exponentially over time t:

$$S_t = S_0 e^{-t/t_0} \ . \tag{3.25}$$

In a half-logarithmic plot of ln S_t against t, τ_0 is obtained from the gradient of the resulting straight line. With excitation by linearly polarised light, the time-dependent course of fluorescence intensity may be registered separately, i.e., in parallel ($F_{II,t}$) and at right-angled ($F_{\perp,t}$) to the polarisation plane. Measurand is the anisotropy A_t:

$$A_t = A_0 e^{-t/\tau_{ri}} = \frac{F_{II,t} - F_{\perp,t}}{F_{II,t} + 2F_{\perp,t}} \ . \tag{3.26}$$

The denominator is composed of the fluorescence intensities of the three spacial directions: x parallel, y and z, at identical intensity, each at right angles to the excitation. It correlates to the total fluorescence S_t. A_0 is the anisotropy at the time of excitation, τ_{ri} is the rotation relaxation time of the chromophore. Its reciprocal value is a linear combination of the rotation diffusion constant D_i (i = 1,2,3) of the three main rotational axes of a particle:

$$D_i = \frac{k_B T \gamma_i}{6\eta V} \ . \tag{3.27}$$

V is the hydrodynamic volume of the particle, k_B the Boltzmann constant, η the solvent viscosity, T the absolute temperature and γ_i a function of the axial ratio of an ellipsoid. τ_{ri} results from the gradient of a half-logarithmic plot of A_t against t. From

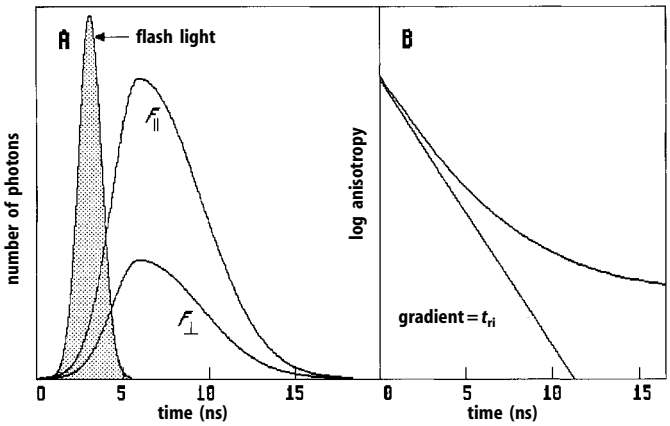

Figure 3.36. Pulse fluorimetry. (A) Time course of fluorescence intensities in parallel ($F_{||}$) and perpendicular ($F_{\perp}$) to the polarisation plane of irradiation after excitation with a short flashlight. (B) Semi-logarithmic plot of the time-dependent change of anisotropy upon overlay of two motions with differing velocities.

the number and magnitude of the relaxation time periods conclusions may be drawn on the size of the molecule (Figure 3.36B). With a spherical shape ($D_1 = D_2 = D_3$) a linear dependency is obtained with a uniform rotation relaxation time:

$$\tau_{ri} = \frac{1}{6D} = \frac{\eta V}{k_B T} \ . \tag{3.28}$$

Two different relaxation times result at free mobility of a chromophore bound to a macromolecule.

A rapid sequence of very short flashlights ($\approx$ 1 ns) from a flash lamp, a laser or a Kerr cell excites the sample solution. A photon counter performs a time-dependent registration of the emitted photons. The Kerr cell contains a highly dipolar liquid (nitrobenzene, acetonitrile, benzonitrile). The molecules are aligned by an external field in such a way that an incoming linearly polarised light beam is turned by 90°. A polarisation filter is then placed in such a way that the beam may not pass. By switching of the external field for a short period of time (only a few ns) the molecules in the Kerr cell disorientate, the light beam regains its original polarisation plane and can pass the filter.

3.4.4 Circular Dichroism and Optical Rotation Dispersion

Asymmetrical structures possess the property of optical rotation. They deflect the plane of polarised light. Except for glycine, all amino acid residues in proteins possess at least one optically active centre due to the asymmetrical α carbon atom. Such centres are, however, not of interest here, as they remain unchanged during enzyme reactions or binding processes and are not suited as measuring signals. Structural ele-

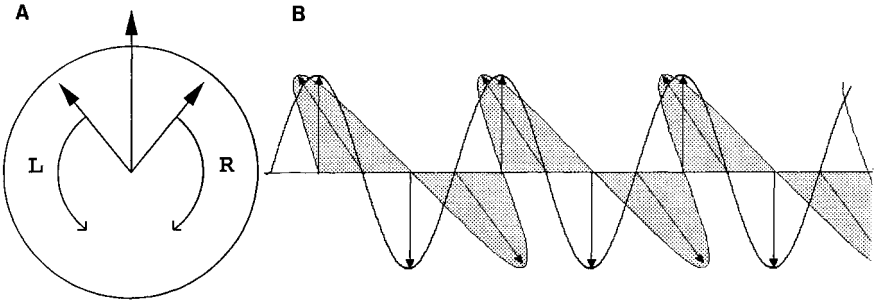

Figure 3.37. (A) Linearly polarised light develops by superposition of equal parts of right(R)- and left(L)-handed circularly polarised light. (B) Circularly polarised light develops from two phase-shifted perpendicularly oriented parts of linearly polarised light (after van Holde, 1985).

ments as they occur also in active centres, e.g., α-helix and β-sheet, exhibit asymmetrical properties that may be influenced by catalytic and regulatory processes.

Optical rotation may be measured in two different ways. *Optical rotation dispersion* (ORD) registers the difference in refraction indices, *circular dichroism* (CD) records absorbance differences between right- and left-handed circularly polarised light. Circularly polarised light can be regarded as the sum of two linearly polarised components with a phase difference of 90°, while linearly polarised light is composed of two opposite circularly polarised beams (Figure 3.37).

The ORD method measures the dependence of the refraction angle of linearly polarised light from the wavelength:

$$\Phi = \frac{180 \cdot d \cdot (n_L - n_R)}{\lambda} \quad . \tag{3.29}$$

Φ (degree) is the optical rotation, d is the path length of the beam in the cuvette, λ the wavelength, n_L and n_R the refraction indices for left- and right-handed circular light. In protein and nucleic acid solutions with a chromophore concentration of $\approx 10^{-4}$ M the polarised light rotates at 0.01–0.1 deg/cm. Precise instruments still register refractions of 10^{-4} deg.

For the CD method applies:

$$\Theta = \frac{2.303 \cdot 180 \cdot (A_L - A_R)}{4\pi} \quad . \tag{3.30}$$

A_L–A_R is the absorption difference of right- and left-handed polarised light. Ellipticity θ (°) is defined as an arc tangent of the ratio of the small axis to the big axis. The difference is about 0.03–0.3% of total absorption. For comparison of different samples molar rotation $[\Phi]$:

$$[\Phi] = \frac{100 \cdot \Phi}{cd} = \frac{[a]M_r}{100} \tag{3.31 a}$$

or molar ellipticity $[\Theta]$:

$$[\Theta] = \frac{100 \cdot \Theta}{cd} = \frac{[\Psi]M_r}{100} = 3.300 \cdot (\varepsilon_L - \varepsilon_R) \qquad (3.31\,b)$$

is indicated. c is the sample concentration, $[\alpha]$ the specific rotation, $[\psi]$ the specific ellipticity, M_r the relative molecule mass of the sample, ε_L and ε_R the absorption coefficients for left- and right-handed circular light.

The CD spectrum of a compound may be obtained in the region of its absorption spectra, beyond the absorption becomes $[\theta] = 0$. It exhibits the shape of the absorption

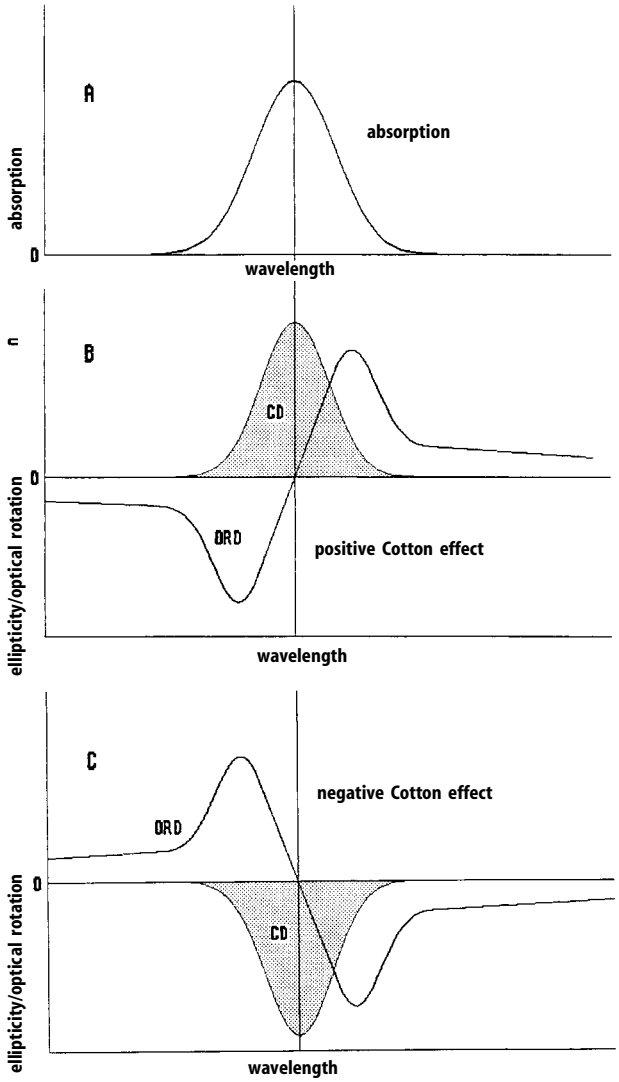

Figure 3.38. Schematic illustration of absorption (A), ORD and CD spectra of an asymmetrical compound with positive (B) and negative (C) Cotton effect.

spectrum, however, depending on the molecule structure, either with a positive or negative Cotton effect and differing intensity (Figure 3.38). ORD spectra appear as the first derivation of CD spectra, but at higher or lower wavelengths they are reaching far beyond the absorption region. With a positive Cotton effect originating from low wavelengths first a minimum and then a maximum is passed. With a negative Cotton effect, the maximum appears before the minimum. In both cases the turning point correlates with the maximum or the minimum, respectively, of the CD spectrum.

With the aid of the *Drude equation*

$$[\Phi]_\lambda = \frac{k}{\lambda^2 - \lambda_0^2} \tag{3.32}$$

the ORD spectrum, reaching far beyond the absorption band, was in the past, when instruments for the far UV region were not yet available, frequently used to conclude from measurements of accessible wavelengths λ on the optical rotation of the wavelength λ_0 of the turning point of the ORD spectrum; k is a constant.

ORD and CD spectroscopy are closely related. This is further demonstrated by the fact that they may be converted into each other by the *Krönig-Kramers* transformation

$$[\Theta(\lambda)] = -\frac{2\lambda}{\pi} \int_0^\infty \frac{[\Phi(\lambda')]\lambda'}{\lambda^2 - \lambda'^2} \mathrm{d}\lambda' \,, \tag{3.33}$$

so that basically only one of the methods have to be employed, while no additional information will come from the other method. In spite of the greater technical input, CD spectroscopy is usually preferred. It yields less complicated spectra which is of advantage especially in cases of atypical behaviour or of overlapping effects. The far reaching ORD spectra furthermore exacerbates analysis in case of overlapping effects.

CD spectra are widely used for the characterisation of secondary elements of protein structure. As shown in Figure 3.39, α-helix and β-sheet on one hand and coil structure on the other show opposite CD spectra. The α-helix is characterised by *exciton splitting* into a double band between 210 nm and 220 nm caused by the formation of excimers. This allows conclusions on the relative distribution of these structural elements in proteins. Conformational changes of such structural elements, induced by substrate or effector binding, may also be observed.

Disulfide bridges and the side chains of aromatic amino acids (Figure 3.40) also exhibit optical activities within protein structures. Similar to the absorption spectra, these amino acid residues show the most outstanding effects in the far UV region between 200–240 nm, but these spectra are superimposed by those of the secondary structures. At 210 nm also histidine exhibits a CD spectrum. Characteristic for these amino acids is the near UV region between 250 and 300 nm, where especially tryptophan shows a prominent CD spectrum. Tyrosine has only a weaker negative band, while phenylalanine demonstrates a less intensive but characteristic structure. CD spectroscopy is the best suited method for analysis of aromatic amino acids in proteins. Also prosthetic groups and coenzymes, e.g., porphyrins and NADH, yield CD spectra.

For the study of regulatory or kinetic mechanisms, spectral changes as a consequence of the respective process are of greater interest than the spectra themselves.

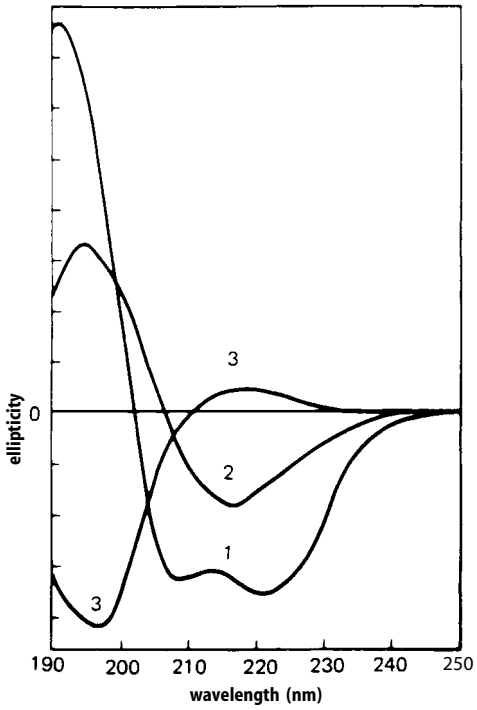

Figure 3.39. CD spectra of the secondary structure elements of proteins. (1) α-helix, (2) β-sheet, (3) random coil (after Greenfield and Fasman, 1969).

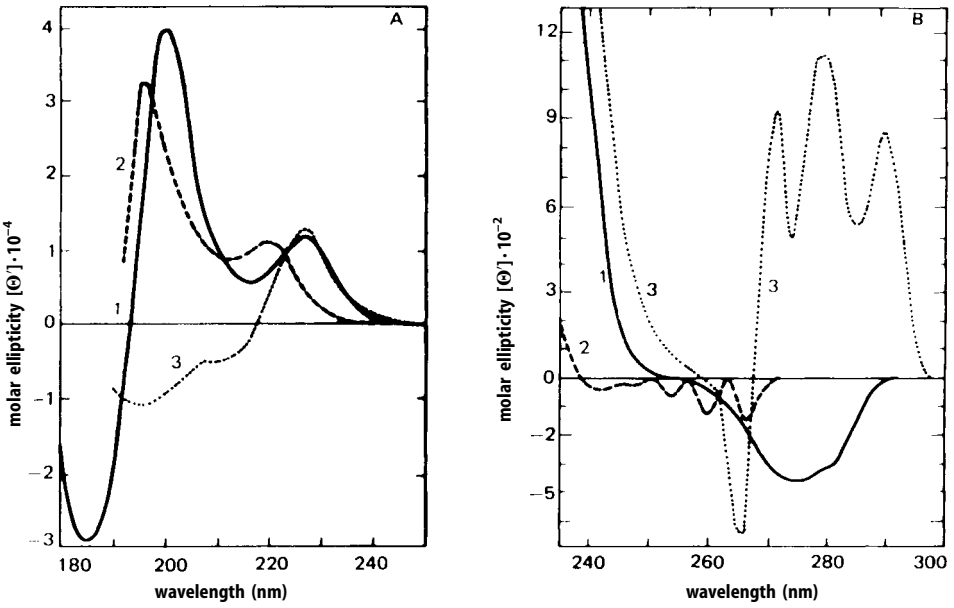

Figure 3.40. CD spectra of aromatic amino acid derivatives in the far (A) and near (B) UV region. (1) N-acetyl-*L*-tyrosineamide, (2) phenylalanineamide, (3) N-acetyl-*L*-tryptophanineamide (after Shikari, 1969).

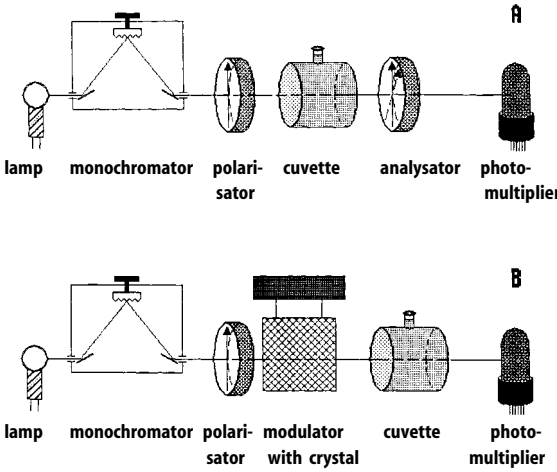

Figure 3.41. Construction scheme of an ORD (A) and a CD spectrometer (B).

Apart from the analysis of conformational changes, the CD method has the advantage that even optically inactive ligands may produce CD signals by their interactions with the asymmetrical structures of the protein molecule, so that such specific signals represent a direct measure of ligand binding.

The structure of an ORD apparatus resembles that of an absorption photometer (Figure 3.41A). Light is spectrally resolved by a monochromator, passes the sample cell and is detected on a photomultiplier. Specific for the ORD unit is a polarisation crystal positioned in front of the sample cell, producing plane-polarised light. Contrary to the rectangular absorption and fluorescence cuvettes, cylindrical cells are used. The light passing the cell penetrates an analysator filter which is applied to measure the deflection angle. In a CD instrument, monochromatic light is also plane-polarised by a polarisator (Figure 3.41B). It then passes through a birefringent quartz plate set at an angle of 45° to the plane of polarisation, splitting the light into two components of equal intensity but different refraction indices, oriented at right angles to each other. The thickness of the plate is chosen to delay the slower beam by a quarter-wave on exit (electro-optic modulator, lambda quarter plate). Applying an electric field the refraction indices of both beams and the orientation of the rotation may be reversed.

3.4.5 Infrared and Raman Spectroscopy

Infrared (IR) and Raman spectroscopy detect transitions between vibration levels of molecules. On account of their different frequencies, information may be gathered about the nature of the vibration (torsion, translation, valence, or deformation vibration), about the participating atoms as binding partners (C–O, C–N, and C–H), and about the nature of bonds (single, double, or triple bonds). This allows conclusions on the molecular structure. For macromolecules (i.e., proteins), however, this may lead to highly complex results. IR and Raman spectroscopy basically supply the same information, similar to absorption and fluorescence spectroscopy. IR spectroscopy analyses

absorptions at the frequency of molecular vibration, Raman spectroscopy measures the dispersion of photons modified by the amount of vibration energy. For vibration spectra, the wave number $\upsilon = 2\pi/\lambda$ (cm^{-1}), also termed "Kayser", is normally applied.

3.4.5.1 IR Spectroscopy

The clearest IR signals are obtained from groups that are either asymmetrical or may be polarised. Liquid substances are directly measured. Solid compounds are embedded in nujol or other materials or pressed in potassium bromide. Water and dissolved salts, e.g., buffer substances, may cause strong absorptions, and therefore largely restrict the application of the IR method for enzymes. It is necessary to operate outside the absorbance region of water. By using heavy water (D_2O), the spectrum may be shifted in such a way that the spectral region initially overlaid by water may become accessible. A significant improvement allowing a wider application also for studies of proteins and enzymes in aqueous solution was found by combining IR with Fourier transformation (FT-IR spectroscopy), thus reducing the originally very long measuring time of 10–20 min to a few seconds. Light source is a Nernst stick out of a mixture of zirconium and yttrium oxide or a sintered silicon carbide stick (globar). The light is directed through a monochromator and into the cuvette. For detection, heating by the incoming IR irradiation is measured with a thermoelement. With a bolometer, the temperature-dependent alteration in the resistance of platinum wires or semiconductors is determined. With the pneumatic Golay cell, heating of a gas is registered after the light was directed onto a blackened metal plate.

3.4.5.2 Raman Spectroscopy

In Raman spectroscopy, molecules are excited by photons (UV or visible light) with higher energy than necessary for vibrations. They either transmit a certain amount of energy as vibration energy to the molecule and loose energy themselves (*Stokes lines*), or they take this amount of energy from the molecule and enhance their own energy (*anti-Stokes lines*). The excitation band, the so-called *Rayleigh scattering*, caused by elastic scattering of the photons at the molecules, has by far the highest intensity, the longer-waved Stokes lines possess a higher intensity than the short-waved anti-Stokes lines. Excitation normally occurs at wavelengths not overlapping with the absorption band of the compound. With the resonance Raman method, however, the excitation wavelength concurs with the absorption band, enhancing the vibrations coupled with electronic transitions, producing very specific vibration bands. Raman spectroscopy is affected by the fluorescence phenomenon in the same way as fluorescence spectroscopy in turn is interfered with by the Raman effect. The frequency of the Raman bands is quoted as the difference between the excitation frequency and the respective Raman band. The method detects even weak interactions as hydrogen bonds and is, therefore, well suited for the study of catalytic mechanisms. In aqueous solution Raman spectroscopy becomes accessible by excitation with intensive long-waved, monochromatic, laser light, as the Nd:YAG laser (1064 nm), a yttrium-alumi-

nium garnet doped with neodymium. As in fluorescence spectroscopy, scattering radiation of the sample is measured at right angles to the excitation. Pulse lasers allow very rapid processes to be measured with precision.

3.4.5.3 Applications

IR and Raman spectroscopy are mostly applied in structural studies of proteins, for the analysis of secondary structures (α-helix, β-sheets), conformational changes, ligand binding, prosthetic groups, and metals. These methods were used, e.g., for the study of interactions of oxygen and carbon monoxide with haemoglobin. Groups containing sulphur show strong Raman scattering because of the high polarisation potential of sulphur, and the formation and cleavage of disulfide bridges may be studied. With IR spectroscopy R and T states of haemoglobin could be differentiated by ligand-induced alterations of thiol spectra. Metal proteins exhibit intensive effects, especially in resonance Raman spectroscopy, e.g., porphyrin haem proteins (cytochrome, haemoglobin), proteins with Fe-S complexes (components of the respiratory chain, ferredoxin), and copper proteins. Various enzyme reactions and enzyme catalytic mechanisms were studied with FT-IR and Raman spectroscopy, e.g., the cleavage of fructose biphosphate by aldolase into glyceraldehyde phosphate and dihydroxyacetone phosphate, and the appearance of the acyl-intermediate in the proteolytic mechanisms of chymotrypsin and papain. For direct observation of enzyme reactions in enzyme kinetic studies, however, both of these methods are not well suited.

3.4.6 Electron Spin Resonance Spectroscopy

The discussion of IR and Raman spectroscopy has already dealt with methods that are to be counted as only peripheral for the subject of this book. This is all the more true for electron spin resonance spectroscopy (ESR, also EPR for electron paramagnetic resonance) which should, nevertheless, be mentioned here for the valuable information it provides on structure and binding, since the spin-labelling technique is accessible to all proteins. The extensive instrumental requirement oppose, however, a wide application. For details and related methods, especially NMR spectroscopy, text books of physical chemistry are recommended.

ESR spectroscopy allows the study of molecules with paramagnetic properties, i.e., with unpaired electrons. Unpaired electrons have a spin quantum number $S = 1/2$, correlating to a magnetic moment of $m_s = \pm 1/2$. In a magnetic field they either move parallel ($m_s = +1/2$) or anti-parallel ($m_s = -1/2$) to the field axis z. An oscillating magnetic field at right angle to the field axis induces transitions between the two spin states, when the field frequency lies in the region of the Larmor frequency of the spinning electron. The energy content E_m of an electron spin in the magnetic field H is:

$$E_m = g\mu_B m_s H \; ; \tag{3.34}$$

μ_B is the Bohr magneton ($9.273 \cdot 10^{-24}$ JT^{-1}), H the field strength, g is called g factor (see below). The difference of the energy contents of two electrons α and β with the magnetic moment $m_s = +1/2$, respectively $m_s = -1/2$ is:

$$\Delta E = E_\alpha - E_\beta = g\mu_B H \ . \tag{3.35}$$

Resonance stands for

$$h\nu = g\mu_B H \ . \tag{3.36}$$

h is Planck's constant and ν the microwave frequency. In ESR spectroscopy molecules with unpaired electrons are studied that enter into resonance with a monochromatic radiation.

Local permanent fields H_{loc} in the environment of the unpaired electron, especially the magnetic moment of the nucleus, overlap with the external magnetic field H and lead to a *hyperfine splitting*, a special property of ESR spectra. If an electron is located around a nucleus with a nuclear spin I, then H_{loc} may adopt along the external field axis $2I+1$ values, according to the $2I+1$ values of the magnetic moment of the nucleus m_I:

$$H_{loc} = H + a \cdot m_I \ ; \tag{3.37}$$

a is the hyperfine coupling constant. For a hydrogen atom ($I = 1/2$), half of the radicals of the sample is $m_I = +1/2$. They enter into resonance, when the external field meets the conditions

$$h\nu = g\mu_B (H + 1/2a)$$

respectively

$$H = (h\nu / g\mu_B) - 1/2a \ . \tag{3.38 a}$$

The other half with $m_I = -1/2$ meets the resonance conditions at:

$$H = (h\nu / g\mu_B) + 1/2a \ . \tag{3.38 b}$$

Instead of one line, the spectrum now exhibits two lines with each half of the original intensity, separated by the coupling constant a and centred around a field defined by the g factor.

If the radical contains a nitrogen atom ($I = 1$), it will split into three lines ($m_I = -1$, 0, 1), as the nitrogen nucleus has three possible spin orientations, each of which will be taken by one third of the radicals (Figure 3.42A).

Most commercial instruments use a magnetic field of 0.3 Tesla (1 Tesla = 10^4 Gauss), corresponding to a resonance with an electromagnetic field with a frequency of 10^{10} Hz (10 GHz) and a wavelength of 3 cm ("X-band", microwave region). The magnetic field is varied, and by measuring the absorption of the microwave radiation from a microwave generator (klystron), the ESR spectrum is recorded with a microwave detector. It is represented as the first derivation of the absorption spectrum.

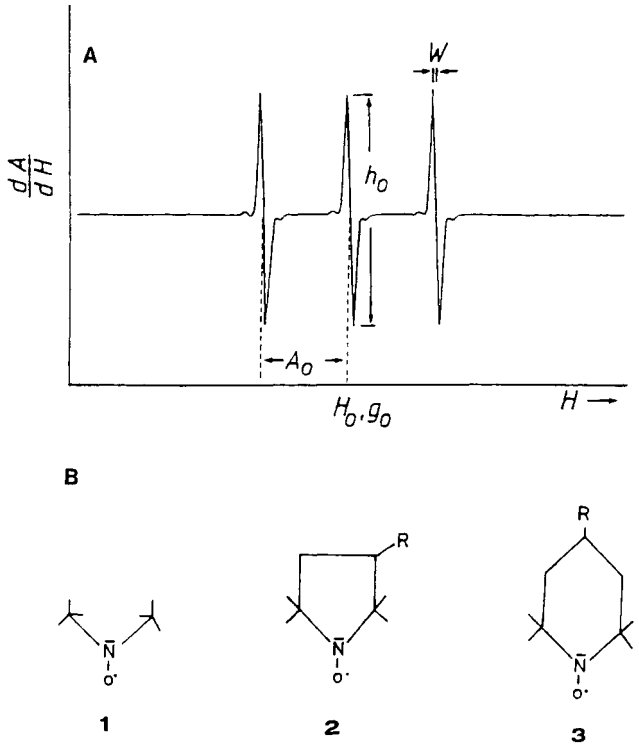

Figure 3.42. ESR spectrum of a nitroxyl radical (A). A_0 is the anisotrope coupling constant, g_0 the isotrope g factor, W the width of line, h_0 the amplitude, H the magnetic field strength (after Graupe, 1982). (B) Structures of stable nitroxyl radicals. (1) Di-*tert*.-butyl-nitroxyl, (2) tetramethylpyrolidine-nitroxyl (proxyl), (3) tetramethylpiperidine-nitroxyl (tempo).

ESR spectra are characterised by the shape of their lines, the g factor and the coupling constant a. The latter results from the distance of the spectral lines and is a measure of the interaction of the electron with the local field of the nucleus. The g factor is to be obtained from the centre of the spectrum (Figure 3.42A). It is a measure for the total moment of spin and orbital moment interacting with the external magnetic field. The g factor for an electron is $g_e = 2.0023$. The deviation of the g factor determined by the ESR spectroscopy from this value, $g = (1-\sigma)g_e$, depends on the ability of the magnetic field to influence the local electron stream of the radical. This interaction is dependent on the orientation of the magnetic field vector to the molecular axes. In anisotropic alignments (in a single crystal) the shape of the spectrum depends on the angle of the crystal to the magnetic field. In an isotropic distribution in solution a uniform spectrum is obtained. By restricting mobility, e.g., by binding a radical to a macromolecule, the spectral lines will be broadened and become asymmetrical. This property allows the direct observation of the binding of paramagnetic ligands or to study the influence of bound radicals.

The transition metals Cr^{3+}, Mn^{2+}, Co^{2+}, Cu^{2+}, and the lanthanides are naturally occurring paramagnetic compounds. For pyruvate-formiate lyase an enzyme could be

analysed, forming a stable paramagnetic intermediate. Stable radicals may be synthesised, and similar to fluorescence chromophores, fixed covalently to the protein by side chain-reactive groups, e.g., maleimide or isothiocyanate (*spin-label*). Mostly nitroxyl radicals shielded by tertiary butyl groups are used in the form of stable tetramethylpiperidine- or tetramethylpyrolidine-1-oxyls (Figure 3.42B).

3.5 Measurement of Fast Reactions

In recent years a great number of methods for measuring fast reactions have been developed, one of the fastest being pulse fluorimetry already described in Section 3.4.3.7, with a time resolution in the nanosecond region. The various methods may be reduced to a common scheme. Characteristic for the special method is a module which serves to initiate the fast reaction. The construction principle of this module determines the time range and the type of the reaction to be analysed by the method (Figure 3.43). The selection of an appropriate method is important not only for the time resolution, but also for the applicability for a certain type of reaction. The principle of *flow methods* is based on rapid mixing of reactants. They are especially suited to analyse fast enzymatic reactions for the investigation of the catalytic mechanism. With a time resolution in the range of milliseconds they are comparatively slow within the scale of fast reactions. With *relaxation methods* reactions 1000-fold faster may be measured. They are based on short-term disturbance of equilibrium so that no reaction turnover, but only reactions in equilibrium are to be observed, e.g., ligand binding, isomerisations, or spontaneous and induced conformational changes in macromolecules. Even more rapid irradiation methods require the sensitivity of the system to light impulses. For the characterisation of a defined process it is often necessary to combine different methods and experimental approaches in a suitable manner.

In all these methods the reaction process has to be detected after initiation. The type of reaction rather than time resolution is important here, so that different fast

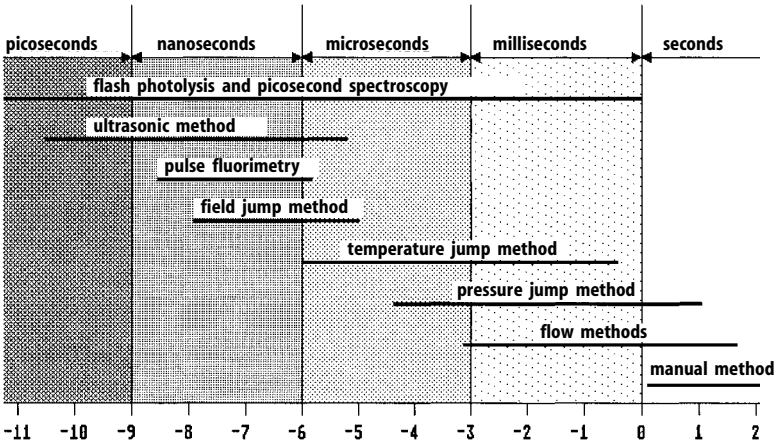

Figure 3.43. Time resolution of methods for the measurement of rapid reactions.

methods employ similar modes of detection. Optical methods are especially suited for enzyme reactions, absorption photometry being the universal and simplest method most widely used, but also fluorescence, CD, ESR and NMR spectrometry are combined with fast methods. Measuring of light scattering, electrical conductivity or determination of oxygen are applied. As most of these methods have already been discussed, only the relevant adaptation to the rapid method will be described here.

The third essential module of fast methods serves the rapid registration/recording of measuring signals. Previously, mostly storage oscillographs were used which now are being replaced by computer-controlled rapid memories. These are able to directly evaluate and process measuring data.

3.5.1 Flow Methods

3.5.1.1 The Continuous Flow Method

This technique was the first method for the observation of fast reactions. Already in 1905 Raschig succeeded to observe a reaction in the gaseous phase for up to 25 ms with a simple instrument. In 1923 H. Hartridge and F.J.R. Roughton developed a continuous flow apparatus for the study of carbon monoxide binding to haemoglobin. The fundamentals of this method still are valid today (Figure 3.44A). Two components – an enzyme and a substrate solution – are filled into reaction syringes. With continuous motor drive advance, these syringes press the solutions simultaneously into a mixing chamber and the reaction starts. The reactant solution flows continuously through an observation tube where the reaction process is monitored, either optically (by photometry or fluorimetry), or with a thermo element. In an optical device the tube serves as a cuvette and must be constructed accordingly (quartz glass for UV measurements).

The time coordinate of the reaction process is converted into a one of space in the observation tube in this method. The reaction progresses in time from the point of mixing, while the reaction mix flows along the observation tube at a constant rate. The growing distance from the mixing chamber is proportional to the age of the reaction:

$$\text{Age (s)} = \frac{\text{Volume observation} - \text{mixing point (cm}^3\text{)}}{\text{Flow rate (ml/s)}} = \frac{\text{Flow distance (cm)}}{\text{Flow (cm/s)}}.$$

At continuous flow, the reactant mixture always has the same age at a fixed observation point. At a flow rate of 10 m/s the reaction 1 cm behind the mixing chamber will be 1 ms old. Each point of the reaction coordinate can, therefore, be basically measured time independent, i.e., short time periods may be observed over longer periods of time and the signals can be made reliable by averaging of times. This advantage has to be paid for with a large consumption of substance, as flow has to be kept constant during measurement. Observing a single point for 1 s requires 200 ml flow through a tube of 5 mm diameter. As several measuring points at different distances from the mixing chamber are necessary for recording the time progress of the reac-

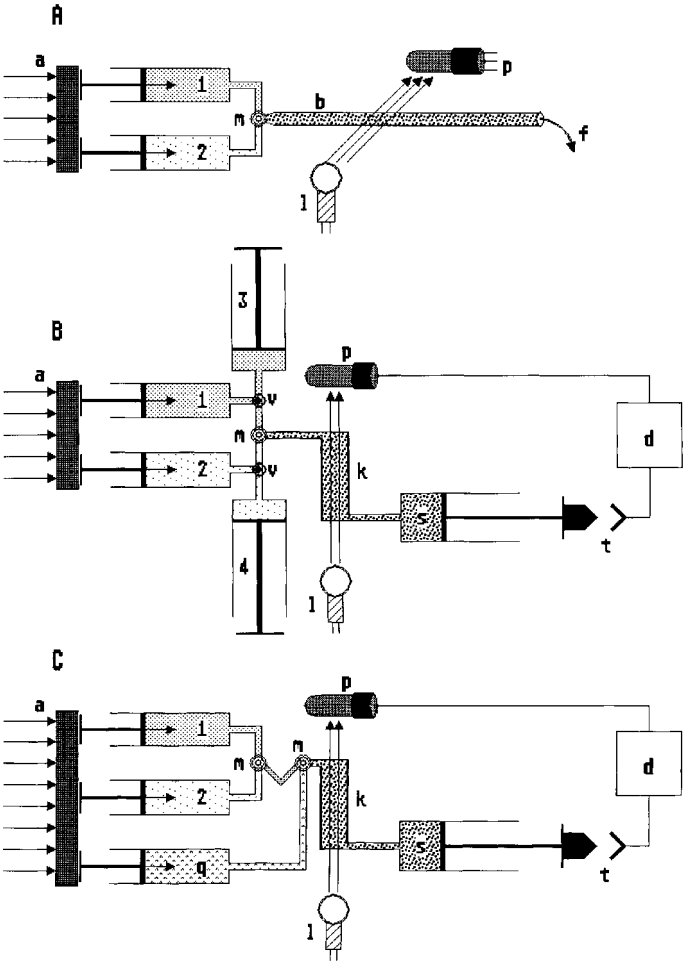

Figure 3.44. Schematic representations of flow apparatuses: (A) Continuous-flow apparatus, (B) stopped-flow apparatus, (C) multi-mixing apparatus. (1, 2) Reaction syringes, (3, 4) reserve syringes, (a) drive, (b) observation tube, (d) detector, (f) runout, (k) cuvette, (l) lamp, (m) mixing chamber, (p) photomultiplier, (q) third reaction syringe (with quenching liquid), (s) stop-syringe, (t) trigger, (v) three-way valve.

tion, several litres of the reactant solution would be required. For haemoglobin studied by Hartridge and Roughton this was not a problem, and this apparatus could be developed even at a time, where fast recording was not possible. However, for the study of enzyme reactions, such volumes are not realistic. The breakthrough of fast kinetics came with the development of the storage oscillograph and finally of rapid data memories and the higher sensitivity of photometers, so that time and volume of reactions could be significantly reduced. A reduction of the tube diameter to 1 mm allowed to reduce substance requirements to 10 ml for a measurement.

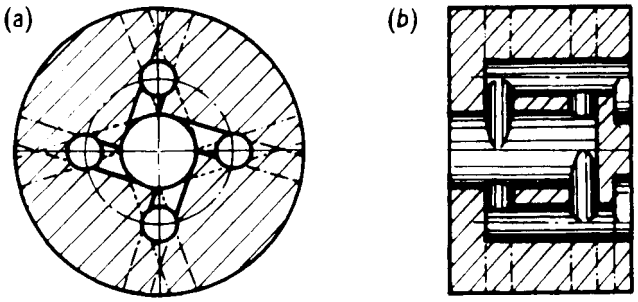

Figure 3.45. Cross section of a mixing chamber for flow apparatuses. (a) Front view, (b) side view (after Gibson and Milnes, 1964; with permission from the publisher).

A further advantage of the continuous-flow method is the short dead time, i.e., the time between initiation of the reaction and the onset of detection. It determines the time resolution of the apparatus. The first measuring point in the continuous-flow method is located directly behind the mixing chamber at the entrance of the observation tube, so that the path to be covered unobserved by the solution is extremely short. Good instruments reach dead times of 0.2 ms. The dead time also depends on the flow rate and may be further reduced by increasing the flow rate. However, homogeneous mixing of the reactant solution becomes more difficult at higher flow rates. Inhomogeneous solutions form streaks and cause perturbations in sensitive measurements of the reaction process. A homogeneous mixing within milliseconds requires perfect construction of the mixing chamber. From various nozzles the reactant solutions are sprayed into the mixing chamber in counter current flow, causing strong turbulences (Figure 3.45). Too high flow rates produce friction effects in the narrow nozzles and thus heating of the reactant solution influences the reaction process and leads to streaking.

A modification for reducing the reaction volume is the *pulse-flow method* developed by B. Chance. Solution is pressed into the tube with short continuous shots. A further application is a combination of the continuous-flow method with scanning of ESR spectra (Yamazaki, 1960).

3.5.1.2 The Stopped-Flow Method

Fast methods were more widely used for enzyme reactions only after B. Chance developed the stopped-flow apparatus in 1943. Contrary to the continuous-flow method, the reaction syringes are not continuously emptied into the mixing chamber and directed into the observation tube, but with a rapid shot. The reaction process is followed in the observation tube after the flow has stopped (Figure 3.44B). Usually the observation chamber is a photometric cell, arranged in such a way, that the optical beam for absorption measurements is perpendicular to direction of flow. In fluorimetric measurements fluorescent light is detected perpendicularly to the excitation. The reactant solution must pass the whole path through the cell before the onset of registration, which significantly increases the dead time. With custom-made instruments, dead times < 1 ms may be achieved. Commercial devices have resolutions of < 5 ms. A reduction of dead time, however, at the expense of sensitivity, is achieved by reducing the path length of the cell (e.g., to 0.2 mm). As already discussed for the continuous-flow method, homogeneous

mixing is essential. By mixing a dye with water homogeneity may be tested. Incomplete mixing reveals from a drift of the signal after stopped-flow. Since temperature differences in the flow system cause streaking, all components of the apparatus coming into contact with the solutions have to be controlled by a thermostat.

The impulse for emptying of the drive syringes is either released hydraulically or by a gas pressure-driven piston which simultaneously pushes both reaction syringes via a drive block. In another system, the reactant solutions are directly put under high gas pressure and the flow is released by opening an electromagnetic valve. The two reaction syringes normally have the same volume so that both reactants are dissolved at a ratio of 1:1 after mixing. By using syringes with different volumes, a different mixing ratio may be achieved if, e.g., the enzyme solution should not be dissolved (*generative flow apparatus*; B. Chance, 1974). The reaction syringes may be refilled from reservoir syringes placed at the sides and repeat measurements may be made. As the apparatus disperses air bubbles into fine opaque fog, it is not recommended to empty and refill the apparatus after each shot. After the end of the reaction the solution in the cell will be replaced by the solutions of the next shot and pressed into the stop syringe. This causes the plunger to move back and trigger the recording (*end-stop system*). The stop syringe has to be emptied after each shot. In another construction scheme the driving block, and thus the flow, is stopped by a resistor located near the reaction syringes (*front-stop system*). This allows a more simple construction because the observation cell is not exposed to high pressures. To avoid release of gas bubbles in the observation chamber due to relaxation of the solution, a limited counter-pressure is produced by a constriction between the cell and the terminal reservoir.

The data collected with the optical system are either displayed in an oscillograph and photographed or stored in a digital data memory. They may then be projected on a screen, recorded on a printer, and processed in a connected computer (data calculation, adaptation of curves, etc.).

P. Strittmatter (1964) developed an easy-to build but effective stopped-flow apparatus (Figure 3.46). The mixing chamber is a plunger of synthetic material, fitted exactly into a photometric cuvette, which in turn is fixed to a photometer. The reactant solutions from the reaction syringes are pressed via tubes into the plunger by a motor drive and leave it after exiting from the mixing chamber through an opening at the bottom of the plunger. The reactant mixture pressed into the cuvette pushes the plunger upwards and opens the light path for the photometric measurement. This instrument achieves dead times of only a few milliseconds. Photometers available in the laboratory may be employed, however, they must be adapted for registration of the rapid measuring signal. If microcuvettes are used, only some tenths of a millilitre of sample solution are required.

UV-Vis absorption spectrophotometers are the most frequently used detection systems for stopped-flow instruments. Based on the small changes in absorbance to be registered within a short period of time, the instrument must operate with a much higher sensitivity than normal spectrophotometers. The lamp current must be stabilised. An enhancement of sensitivity by reducing the background noise may be achieved by a higher light intensity (larger slit), but at the expense of a deterioration in resolution. A *double beam device*, as shown in Figure 3.47, further enhances the sensitivity of the instrument.

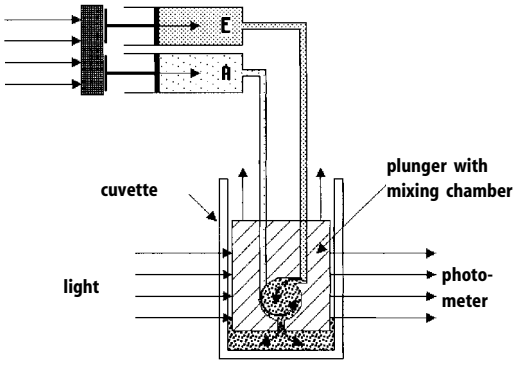

Figure 3.46. Stopped-flow apparatus after Strittmatter (1964).

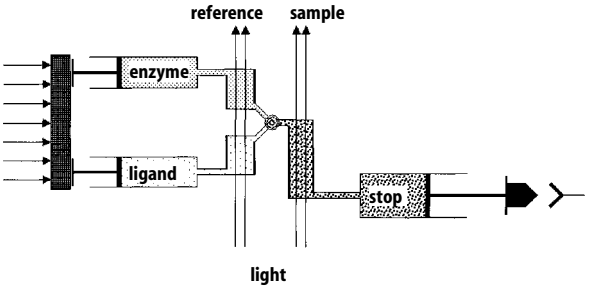

Figure 3.47. Dual beam-stopped-flow apparatus.

The reactant solutions pass through cells, each half of the thickness of the sample cell, before entering the mixing chamber. A reference beam passes through the two reference cuvettes and measures the absorptions of separate reaction components, which are deduced from the absorption signal of the sample cell, so that the difference of the reactants before and during the reaction is recorded. Especially for minimal absorption differences and for measurings in turbid solutions the *double wavelength principle* is applied, where the reference beam follows the same path through the sample cell, but at a different wavelength than the sample beam. As with the double wavelength photometer (see Section 3.4.1.6), the reference beam is adapted to the wavelength of the isosbestic point or that of the turbidity beyond the absorption maximum of the reactant. This device may also be employed to observe the time-related absorption changes in the sample cell at two different wavelengths simultaneously. *Rapid-scan stopped-flow* units allow the time-resolved observation of spectra. Light from the light source is sent directly through the sample cell and becomes spectrally dispersed after passing the cell. A multi-channel photo detector (diode array detector) scans the complete spectral region within a few milliseconds. In one second more than 100 spectra may be registered (Hollaway and White, 1975).

For *fluorescence measurements*, excitation is effected with D_2 or halogen lamps also used for absorption measurements – or even better, a xenon lamp – and the emitted light collected perpendicularly after passage through an emission filter or a monochromator. Fluorescence polarisation requires two photomultipliers in perpendicular position to the

linearly polarised excitation beam and polarisation filters oriented in perpendicular position to each other for the two emission beams (see Section 3.4.3.6). For the measurement of conformational changes in enzymes stopped-flow units equipped with *circular dichroism* optics with a mercury or xenon arc lamp as light source are used (Bayley and Anson, 1975). *NMR stopped-flow units* are suited for the observation of conformational changes, but they require higher reactant concentrations and possess a poorer time resolution (more than 10 ms) (Grimaldi and Sykes, 1975). For the study of association-dissociation processes in macromolecules, the *light scattering stopped-flow apparatus* is employed, using light from a laser or other sources including X-ray radiation from a synchrotron (Flaming and Parkhurst, 1977; Moody et al., 1980). Light-sensitive reactions may be initiated by short irradiation with a flashlight or laser. Combining this method with a stopped-flow apparatus, reactants may be rapidly mixed and the reaction activated by flashlights, e.g., the reaction of oxygen with cytochrome oxidase blocked by CO. CO becomes released after irradiation and vacates the binding sites for oxygen (see flash photolysis, Section 3.5.3). Stopped-flow units are also combined with the *temperature-jump method* (Section 3.5.2.1). Temperature changes induced by enzyme reactions may be measured with a *calorimeter stopped-flow apparatus*, a thin thermo element or a thermistor serving as sensor. The response time is near 50 ms (Nakamura, 1978). Reaction-dependent changes in the concentration of protons are to be measured with a *pH stopped-flow apparatus* with a glass electrode.

A modification of the stopped-flow method is the *multi-mixing system* (Figure 3.44C). The two reactants pass a defined distance after mixing, while already reacting unobserved. Another reactant from a third reaction syringe is fed to this reaction mixture via a second mixing chamber. The (photometric) observation only starts at this point. By changing the flow rate or the path length between the two mixing chambers, reaction times of the first two reactants may be altered. A simplification of this method is the *quenched-flow technique* with a third reaction syringe containing a quench solution which immediately stopps the reaction of the first two reactants, e.g., by pH changes or denaturation of the enzyme with perchloric acid or trichloroacetic acid, it may also contain an indicator. The turnover is subsequently analysed chemically. The apparatus requires no device for fast registration (Fersht and Jakes, 1975). Bray (1961) used isopentane cooled in liquid nitrogen as quenching liquid. The reactant solution is shot into it and freezes immediately. This *rapid-freezing* method is especially suited for ESR measurings with free radicals or paramagnetic metals.

3.5.1.3 Measurement of Enzyme Reactions by Flow Methods

The stopped-flow technique is the most appropriate method for the observation of fast enzymatic turnovers. Reactions may be analysed that cannot be recorded with normal photometric methods, e.g., the true initial velocity at low substrate concentrations that is already running out before onset of measuring by manual mixing. It is especially suited for studies of pre-steady-state reactions, i.e., processes running before the steady-state phase. They start with the mostly diffusion-controlled binding of substrate to the enzyme. Although in principle a rapid process, as a second-order reaction it may become observable by a proper choice of reactant concentrations. This

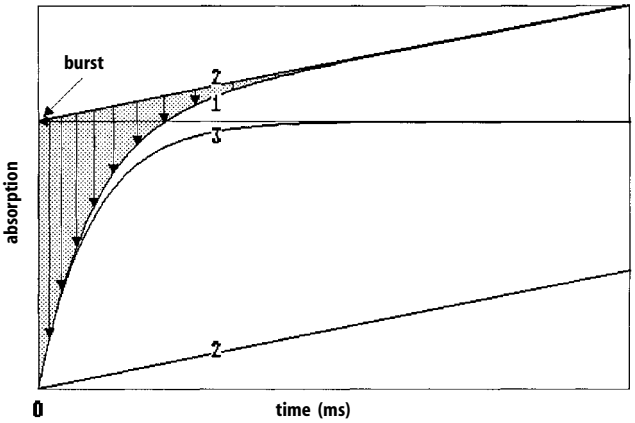

Figure 3.48. Progression of a burst reaction with (1) and without (3) subsequent steady-state phase; (2) is the extrapolated steady-state phase. The vertical arrows show the time-related absorbance change of the pre-steady-state reaction.

process is often followed by isomerisation of the enzyme into an active conformation. Finally the substrate molecule passes through a transition state at the enzyme and becomes converted into product in the catalytic process. The reaction step actually observed with the apparatus depends on the existence of a detectable signal. As in conventional enzyme kinetics, substrate degradation or product formation may be observed. So-called *burst-kinetics* are to be observed in these cases, due to a fast increase before the linear steady-state phase is reached (Figure 3.48). The burst π results from the rapid interaction of substrate with the still unoccupied enzyme immediately after mixing and initiates the first reaction cycle. Substrate in its binding to the enzyme is not hindered by already bound substrate or product molecules that would contribute to a delay of the total reaction in the steady-state phase. The amplitude of the burst indicates the amount of product molecules formed in the first reaction cycle. By extrapolating the steady-state phase to the ordinate at the time $t=0$, and at substrate saturation, the number of active centres participating in this process is obtained. In a double-reciprocal plot of $1/\sqrt{\pi}$ against $1/[A]_0$ the concentration of the active centres at infinite substrate concentration is obtained from the ordinate intercept (Bender *et al.* 1965). For the evaluation of the pre-steady-state process, e.g., the analysis of the reaction order or the possible resolution of several overlapping processes, the steady-state phase has to be deduced from the total curve.

Compared with ordinary steady-state measurements, enzyme concentration has to be increased considerably in order to obtain detectable effects within this short period. This allows measuring of the processes directly at the enzyme, e.g., by observing protein absorbance or fluorescence. Pre-steady-state reactions may be observed without superposition of the signal of product formation. However, the changes to be expected in protein absorbance will be relatively small. Larger effects are obtained, if the protein possesses chromophore, prosthetic groups as flavines or haem. With the stopped-flow method interactions of the enzyme with cofactors, metal ions, inhibitors, allosteric effectors, etc. may be studied. Reactions releasing or binding protons, as in dehydrogenases, may also be observed in unbuffered or weakly buffered solutions with suitable pH indicators. The pK_a value of the indicator should be as near as possible to that of the reactant mixture.

A special application is the *pH jump-stopped-flow method*. The enzyme is filled into a reaction syringe in weakly buffered solution, while the second syringe contains a buffer set at another pH value. When mixed, the enzyme experiences a sudden jump into the other pH environment and changes of the enzyme molecule itself as well as interactions with ligands at changed protonation of certain groups are to be observed. Jumps in ionic strength and in reactant concentrations are produced in a similar way, or solvents are added under change of polarity.

3.5.1.4 Determination of Dead Time

The time between the start of a reaction in the mixing chamber and registration of the measuring signal by the detection system – the *dead time* – determines the time resolvation of fast kinetic equipment and is an important criterion for quality. Dead times are experimentally determined with dye reactions running as pseudo-first order reactions because of the surplus of one reactant. Their exponential run may be linearised in a half-logarithmic plot. The straight line obtained is extrapolated to a blank value containing the dye in the corresponding concentration before start of the reaction. The difference between this point and the start of registration on the time axis correlates to the dead time (Figure 3.49).

Reduction of 2,6-dichlorophenolindophenol by ascorbic acid or alkaline hydrolysis of 2,4-dinitrophenyl acetate into 2,4-dinitrophenol serve as indicator reactions. The chemiluminescent reaction of luminol (3-aminophthalhydracine) with hydrogen peroxide and potassium hexacyanoferrate in alkaline solution which does not require a light source is also applicable for absorption and fluorescence optics. The high increase in fluorescence of anilinonaphthalene-sulfonate (ANS) when binding to serum albumin makes it especially suitable for fluorimetric detectors.

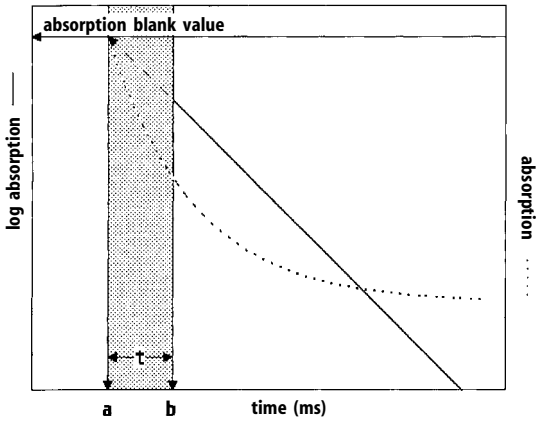

Figure 3.49. Determination of dead time *t* of a stopped-flow apparatus with the aid of a reaction of pseudo-first order (· · · · · ·) by half-logarithmic linearisation (——) and extrapolation (– – – –) to the absorption of the blank value; (**a**) reaction start in the mixing chamber, (**b**) start of registration.

3.5.2 Relaxation Methods

The term *relaxation,* first used by J.C. Maxwell for the return of a molecular system to its thermic equilibrium, determines a group of methods for the observation of the processes of restoring the equilibrium after a short perturbation. According to the van't Hoff reaction isobar, the thermodynamic equilibrium constant K is dependent on the absolute temperature T

$$\left(\frac{\partial \ln K}{\partial T}\right)_P = \frac{\Delta H^0}{RT^2} \ . \tag{3.39}$$

A correlating dependency refers to the pressure P:

$$\left(\frac{\partial \ln K}{\partial P}\right)_T = \frac{\Delta V^0}{RT} \tag{3.40}$$

and to the electric field strength E:

$$\left(\frac{\partial \ln K}{\partial E}\right)_{T,P} = \frac{\Delta M}{RT} \ . \tag{3.41}$$

ΔH^0 is the standard reaction enthalpy at a temperature T, ΔV^0 is the change in volume per formula turnover of the reaction under standard conditions, R is the gas constant. The difference of partial molar polarisations between products and substrates ΔM represents the change in charges of the reactants induced by the reaction. For each of these dependencies a separate technique was developed (originally by Manfred Eigen and his coworkers in Göttingen, Germany) by which the time-resolvation could be raised by several magnitudes compared to the flow methods. In all these techniques the reaction system is in equilibrium at the start. Because of inertia, the system is not able to react immediately to the short perturbation, i.e., change in temperature, pressure or field strength. The apparatus monitors the adaptation of the system to the altered conditions. It is not possible to measure enzymatic turnovers directly, but the shifts of enzyme reactions in equilibrium may be studied. Ligand binding, conformational changes, association equilibria, etc., may be observed. The shifts in equilibrium are comparatively small and the signals are weak and require great precision in the detection.

3.5.2.1 The Temperature Jump Method

Of all relaxation methods, the temperature jump method (T jump) has the widest range of application, especially in enzymatic studies. The reaction mix in the observation chamber is heated by a sudden temperature shock and observed with optical and polarographic techniques (Figure 3.50). The temperature jump is mostly triggered by discharging a high voltage condenser over a spark gap. The electric surge dis-

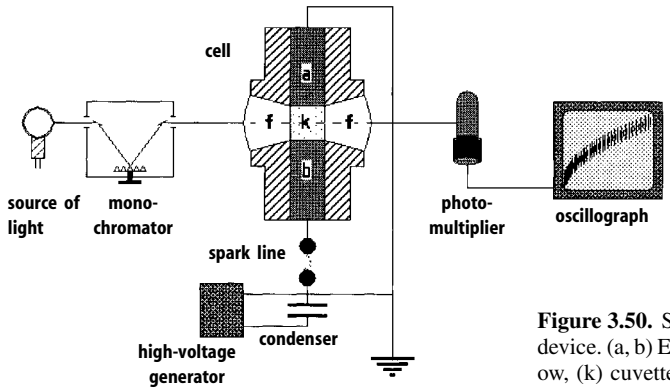

Figure 3.50. Scheme of a temperature jump device. (a, b) Electrodes, (f) observation window, (k) cuvette.

charges over gold or platinum electrodes through the solution in the observation cell and is then grounded. Ion friction in the electric field induces a rapid temperature increase (Joule heating).

The degree of temperature rise may be fixed according to the relationship

$$\Delta T = \frac{CU^2}{8.36 c_p \rho V}$$

by the voltage U (normally between 10 000 and 100 000 V) and the capacitance C (0.01–0.1 μF). It is mostly between 5–10 °C. V is the reaction volume, c_p the specific heat and ρ the density of the solution. ΔT is dependent on the resistance which is highest in the solution. To limit the temperature increase, especially in enzyme solutions, the resistance R must be kept as low as possible in the observation cell. Following $R \sim d/QL$, this may be achieved by a narrow distance of the electrodes d, a broad electrode diameter Q and a high conductivity L. To enhance conductivity, the solution must contain a high concentration of electrolytes (0.1–0.2 M KNO_3 which is relatively inert towards the electrodes). The duration of the temperature jump depends on resistance and capacity and may be reduced by lowering these factors. However, times below 1 μs cannot be achieved, as a shock wave is created that interferes with the measurement and releases gas bubbles in aqueous solutions. On account of mass inertia, the rise in temperature is faster than thermic relaxation. This induces an increase in pressure by 5 MPa for a temperature difference of 10 °C in aqueous solution, that then relaxes in a shock wave. Although the application of a 5 m coaxial cable instead of a condenser could achieve a pulse duration of 50 ns (Hoffmann, 1971), this effect limits the method to a range of 1 μs. The effect is slightest when measurements are carried out at 4 °C.

Apart from the method based on Joule heating, irradiation by microwaves or laser light are employed, especially for measurements at low ionic strength or in non-aqueous solutions. By absorbance of microwaves of a frequency of 10^{10} s^{-1} from a microwave generator in aqueous solution, warming of 1 °C in 1 μs is achieved. This relatively minor effect as well as the high price of the microwave generator prohibits a wider use of this method. Shocks from a neodymium laser with a wavelength in-

creased by liquid nitrogen from 1060 nm to 1410 nm may achieve a warming of several °C within 25 ns, as water exhibits a strong absorbance in this region. This method is thus more rapid than the shock wave appearing in the region of microseconds. However, heating-up of the measurement solution with a light path of more than 1 mm is inhomogeneous, as light absorbance in the aqueous phase rises exponentially with the length of the light path. Therefore, only small volumes may be analysed.

A *T* jump apparatus employs basically the same detection techniques as are used for the stopped-flow method. Because of the weak measurement signals the demands on the sensitivity of the equipment are equally high. Absorption spectroscopy is the method most frequently applied, fluorescence and fluorescence polarisation measurements are also used, and, to a small degree, the determination of optical rotation which, however, requires a longer beam path. Equipment for the observation of light scattering and electrical conductivity has also been developed, but the latter method is not applicable for the method based on Joule heating.

Combining the *T* jump method with a stopped-flow apparatus increases the range of applications of this technique. The fact that it may be used only for reactions in equilibrium requires the reactants to be available in comparable quantities to make a shift in equilibrium accessible, i.e., reactions with an equilibrium clearly preferring one side will hardly be detected. This applies to many quasi-irreversible enzyme reactions. With the *stopped-flow temperature jump method,* the reactants of such a reaction are rapidly mixed and immediately exposed to the temperature jump. Time resolution of the *T* jump method is faster by three magnitudes of 10 than that of the stopped-flow method, so that an enzyme reaction running in the millisecond range does not affect the *T* jump measurement. Figure 3.51 shows the scheme of such an apparatus. A combined observation cell with electrodes is built into a regular stopped-flow apparatus linked to the equipment of a *T* jump apparatus.

As the dead time for the stopped flow apparatus, the characteristic factor for time resolution for the *T* jump equipment is the time required to reach 90% of the maximum temperature level. It can be determined by protonation reactions with a pH indicator.

T jump apparatuses are employed for the study of enzyme reactions, ligand binding, conformational changes in enzymes, spontaneous or ligand-induced transitions of allosteric enzymes, catalytic mechanisms or aggregation processes. The observed signal may often be composed of several individual processes with different time constants, e.g.,

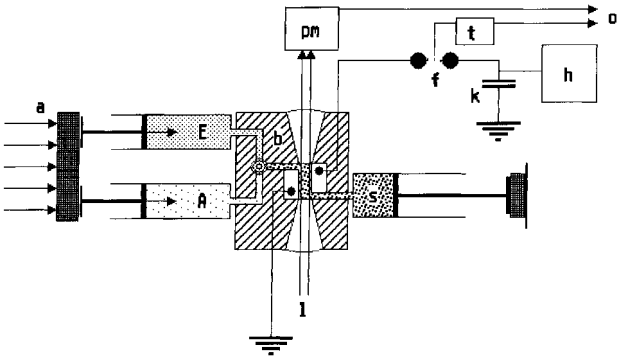

Figure 3.51. Scheme of a stopped-flow temperature jump device. (A, E) Reaction syringes, (a) drive, (b) cuvette block, (f) spark line, (l) lamp, (h) high-voltage generator, (k) condensator, (pm) photomultiplier, (o) oscillograph, detector, (s) stop syringe, (t) trigger.

binding of a ligand followed by an isomerisation reaction of the enzyme. Reactions yielding too weak signals may be linked with another reaction showing a strong signal. In this way, the temperature-dependent pH shift of a rapidly reacting buffer system may be coupled with another proton-dependent process, e.g., a dehydrogenase reaction. The *T* jump apparatus is thus turned into a pH jump apparatus.

3.5.2.2 The Pressure Jump Method

Various pressure jump systems (*P* jump) for the generation of short-term pressure differences in solution have been described. In the equipment developed by Strehlow and Becker (1959) (Figure 3.52) the sample is inserted into the cell of an special autoclave, closed by a flexible Teflon membrane and surrounded by a pressure conducting medium (water, paraffin). This is covered with an elastic polyethylene membrane and the remaining space in the autoclave is filled with compressed gas of 5.5 MPa. One opening of the autoclave has been previously closed with a conductive, pressure-resistant membrane out of copper beryllium bronze. A magnetic trigger releases the locking device of a metal needle fixed above the membrane. This needle punches the membrane and simultaneously starts recording. The membrane tears under high pressure and pressure in the solution relaxes. The time resolution of this method (20–100 μs) is significantly lower than that of the *T* jump method. It is limited by the duration of tearing of the membrane and by the velocity of propagation of the shock wave front in the solution. An improved model of the apparatus (Knoche, 1974) omits the gas chamber. The paraffin solution is directly put under rising pressure until the membrane locking the autoclave bursts.

Another equipment consists of a long tube, divided into two cells by an aluminium disc. Both cells are filled with water, one at normal pressure, the other at high pressure. The sample chamber is located below the low-pressure compartment and separated from it by a rubber membrane. Pressure in the high pressure compartment is raised until the separating disc breaks and pressure is transmitted to the sample solution in the form

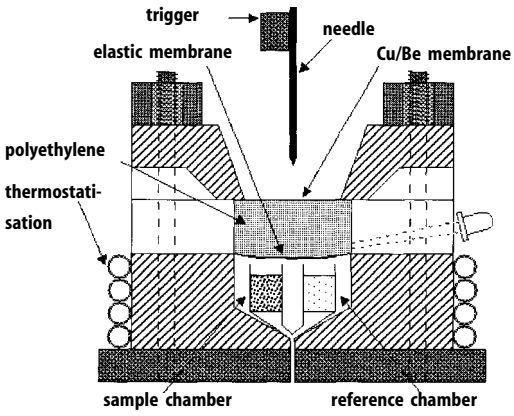

Figure 3.52. Set-up of a pressure jump apparatus.

of a shock wave. The extent of high pressure is determined by the tear strength of the separating disc. Pressures of up to 100 MPa are achieved (Knoche, 1974).

The equipment of Macgregor *et al.* (1985) employs an observation cell locked by an arrangement of piezoelectric crystals. The crystals expand and contract cyclically, induced by a high-voltage switch-on/switch-off cycle. The sample solution is under a stationary pressure of ca. 10 MPa that is increased by the repetitive pressure jumps for 500 kPa.

The ultrasonic method is also based on the principle of periodic pressure changes of sound waves in solution. This is only briefly mentioned here, as it is of minor importance for the study of enzymes. The perturbation is not a sudden jump but a rapidly oscillating sinus wave. When the frequency of this wave approaches the range of the rate constant (respectively the reciprocal relaxation time, see Section 3.5.4) of the reactant solution, the system oscillates in resonance with the sound wave. The concentration change of the system for regaining its equilibrium follows with a reduced amplitude and delays the sound wave front. This yields the rate constant of the reaction. In the dispersion method the sound velocity and in the absorption method the absorption coefficient as a function of frequency are determined. The ultrasonic frequency is varied from 0.05–100 MHz. Reactions down into the nanosecond range may be observed in aqueous solutions. However, for such measurements large volumes in high concentrations (10 mM) are required.

The measurement signals of the p jump method are registered by conductivity measurement or observed optically. The transparent parts of the observation cell are equipped with pressure-resistant sapphire windows.

The possibilities to apply the pressure jump method for biological systems, especially in enzyme studies, are limited. As demonstrated in Eq. (3.40), the pressure-dependent change of the equilibrium constant is proportional to the volume change of the system, i.e., only such reactions are accessible that exhibit a pronounced change in volume. Biological macromolecules are highly pressure-resistant, despite their complex structure. Organisms from deep sea regions normally live under pressures of up to 100 MPa without suffering any damage. For the dependence of the rate constant on pressure the following relation applies, in analogy to Eq. (3.40):

$$\left(\frac{\partial \ln k}{\partial P}\right)_T = \frac{\Delta V^{\ddagger}}{RT} \ . \tag{3.43}$$

$\Delta V^{\ddagger}$ is the difference between the volumes of transition and initial states (activation volume). At the increase of pressure, equilibrium shifts according to the Le Chatelier-Braun principle in the direction of a decrease in volume. Relatively large changes in volume and a good pressure dependence are exhibited by protonation reactions and ionic and hydrophobic interactions, while the release and formation of hydrogen bridges results in only insignificant changes in volume. Proteins, by nature of their quasi-crystalline structure, are highly resistant against pressure. The denaturation of a protein progresses in many individual steps, partially accompanied by either volume increases or decreases that more or less compensate each other over the total process. The resulting change in volume is comparatively insignificant, so that pressure-dependent denaturation may hardly be achieved. Generally, proteins have a negative re-

action volume, they are destabilised by pressure, while DNA is stabilised on account of its positive reaction volume.

3.5.2.3 The Electric Field Method

The electric field method (*E* jump) is even less applicable to biological systems than the *P* jump method. It is described here only for the sake of completeness. The equipment is similar to the *T* jump apparatus. The sample solution is subjected to a high-voltage pulse instead of an electric surge. At a tension of 100 000 V water would boil within seconds. The electric field is, therefore, built up over a rectangular impulse of only a few nano- to microseconds and discharged again. Instead of a condenser, a coaxial cable of 0.3–1 km length is charged by a high-voltage generator. A condenser in the shape of two electrodes attached to the observation cell is charged over a spark gap and rapidly discharges again. The sample is exposed to a high-voltage electric field for a short time. Protonation reactions may be studied with this method. Furthermore, relaxation times of a haemoglobin-oxygen mixture could successfully be determined, and helix-coil transitions in proteins could be observed.

3.5.3 Flash Photolysis, Pico- and Femtoseconds Spectroscopy

Flash photolysis, first developed by Norrish and Porter (1949) only for reactions in the gaseous phase and later transferred to reactions in solutions, serves to study unstable compounds with half life times of less than 1 s. This method was applied to observe processes in photosynthesis and vision, porphyrin-metal complexes, binding of O_2 and CO to haemoglobin and myoglobin. The release of ATP from a photosensitive ATP derivative by UV irradiation with a laser pulse is a good example for the observation of an enzyme reaction by flash photolysis. The principle of flash photolysis is based on activating a component of the reaction system by a short, very intensive flashlight and then observe the reaction thus initiated. The molecules have to be photosensitive and are transformed into free radicals or into a triplet state. This limits the range of applications to systems possessing such compounds or where such compounds may be inserted.

For the generation of flashes discharge flash lamps are used with argon, krypton or xenon fillings. They may achieve time resolutions of a few milliseconds. The picosecond range becomes accessible with pulse lasers. Figure 3.53A shows the scheme of an apparatus where flashes are generated by discharging a condenser. The lamp is aligned in parallel to a quartz cylinder with the reactant solution. For optimal irradiation the unit is encased in a cylinder covered on the inside with a reflector screen of magnesium oxide. The progress of the reaction within the cylinder is measured by a photometric device attached lengthwise to the cylinder. The photometric lamp is also a flash lamp, emitting a flash somewhat delayed to that of the photolysis flash (*flash spectroscopy*). The whole wavelength range is registered simultaneously. For the observation of the time-dependent progress of the reaction at a certain wavelength (*kinetic spectrophotometry*) a continuous light source is employed.

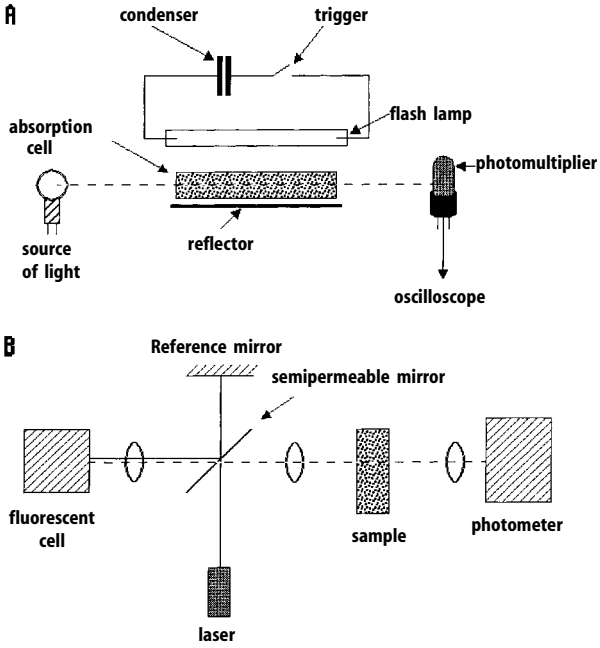

Figure 3.53. Set-up of a flash photolysis apparatus with flash lamp (A) and laser (B).

Introduction of lasers made the nano- and picosecond range accessible for flash photolysis. With pulsed solid-phase lasers with rubies (694 nm), Nd^{3+} in glass or yttrium-aluminium garnet (YAG, 1063 nm) pulses of 10–30 ns duration are obtained. Mode locking of the laser yields pulses in the region of 30–100 fs. By modulating the laser light wavelengths of 347 (ruby), 532, 355, and 266 nm (Nd:YAG) are accessible. Dye lasers pumped up with flash lamps are also used. They have a significantly lower light intensity, but a larger wavelength range and are also less expensive. Their pulse duration lies mostly >100 ns. To obtain the necessary excitation energy for the molecules, light impulses have to be enhanced. In the UV region, excimer lasers are employed, utilising the formation of dimers in the excited state between an inert gas and a halogen, e.g., ArCl (308 nm) and XeCl (248 nm). They have a pulse duration of 20 ns. For flash spectroscopy, the light pulse is split into two beams, one for excitation of the sample, the other as spectroscopic light pulse. For a time delay it deflected by a reflection mirror and finally directed into a fluorescent solution, that in turn emits a continuous light within a defined spectral range (Figure 3.53B). A spectral continuum is also obtained by focussing the light pulse into a water- or water-alcohol-filled cell. For kinetic spectrophotometry in the nanosecond range, the light intensity of the photometric lamp must be very high to eliminate interferences by scattering light and the photolysis flash. To avoid fatigue of the photomultiplier, measuring is done by very short pulses with a flash lamp or a pulsed xenon arc lamp.

A modification of flash analysis is *pulse radiolysis*, employing electron pulses of 1–100 ns from a microwave linear electron accelerator (LINAC) instead of light impulses. Different from photoexcitation, where a defined compound in solution is spe-

cifically excited and the solvent is permeable for radiation, the electron energy in diluted solutions is almost completely released to the solvent. Electron irradiation induces the formation of radicals, ionisation and excitation of molecules into permitted (singlet-singlet) and forbidden (singlet-triplet) transitions. In water, H_3O^+, OH^-, $H^\bullet$, H_2, and H_2O_2 are formed, and also hydroxyl radicals ($OH^\bullet$) with oxidating and hydrated electrons (e^-_{aq}) with reducing properties, whose reactivities have been studied by this method. Pulse radiolysis, rather than dealing with the direct effects of the electron pulse on the compounds to be studied, observes their reactions with such reactive particles. In this way, the reduction of methaemoglobin by hydrated electrons and the subsequent binding of oxygen could be studied.

3.5.4 Evaluation of Rapid Kinetic Reactions (Transient Kinetics)

From experiments with rapid methods, especially relaxation methods, relaxation curves are obtained (Figure 3.54A). The system asymptotically approaches the equilibrium forced upon it by the new conditions (elevated temperature, relaxed pressure). The maximum achievable change should be Δ_0, the shift from the original equilibrium at a random time t is Δ_t. A characteristic factor is the relaxation time τ, i.e., the time at which 63.2% of the maximum deviation Δ_0 are reached (Figure 3.54 A):

$$\Delta_t = \Delta_0 e^{-(t/\tau)} . \tag{3.44}$$

For $t = \tau$ read:

$$\Delta_t = \Delta_0 e^{-1} = \Delta_0 \cdot 0.368 .$$

The relaxation time may be obtained from the intercepts of a source tangent with the horizontal straight line for the initial and final states, or from the slope of a half-logarithmic plot of the deviation Δ_t against time (Figure 3.54 B):

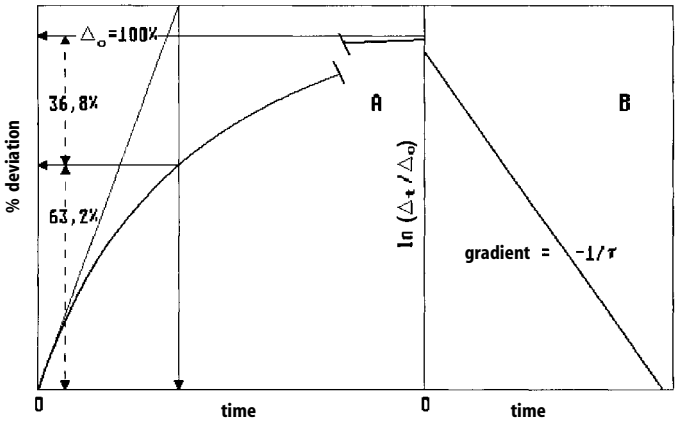

Figure 3.54. Determination of relaxation time τ from a relaxation curve (A). (B) Half-logarithmic plot: Δ_0 is the maximum deviation, Δ_t the deviation from time t.

$$\ln \frac{\Delta_t}{\Delta_0} = -\frac{t}{\tau} \,. \tag{3.45}$$

Relaxation time is a complex factor composed of the rate constants and concentration terms of the components of the respective reaction. Here the relaxation time for a bimolecular reaction as in ordinary binding equilibria is to be deducted:

$$E + A \underset{k_{-1}}{\overset{k_{+1}}{\rightleftharpoons}} EA \,. \tag{1.18}$$

By perturbation of the equilibrium the concentrations of the reactants are changed ([A], etc.) by the amount δ into $[\overline{A}]$, etc.:

$$[E] = [\overline{E}] + \delta_E \,;\; [A] = [\overline{A}] + \delta_A \,;\; [EA] = [\overline{EA}] - \delta_{EA} \,. \tag{3.46}$$

The total volumes of the reactants remain unchanged by perturbation:

$$[A]_0 = [A] + [EA] = [\overline{A}] + [\overline{EA}] \,, \tag{3.47 a}$$

$$[E]_0 = [E] + [EA] = [\overline{E}] + [\overline{EA}] \,. \tag{3.47 b}$$

Follows

$$[\overline{A}] + \delta_A + [\overline{EA}] - \delta_{EA} = [\overline{A}] + [\overline{EA}]$$
$$[E]_0 + \delta_E + [\overline{EA}] - \delta_{EA} = [\overline{E}] + [\overline{EA}]$$

and therefore

$$\delta_A = \delta_E = -\delta_{EA} = \delta \,. \tag{3.48}$$

The differential equation for the change in time of the reactants according to reaction Eq. (1.18):

$$-\frac{d[A]}{dt} = k_{+1}[A][E] - k_{-1}[EA]$$

may be converted by insertion of Eqs. (3.46) and (3.48) into

$$-\frac{d([\overline{A}] + \delta)}{dt} = k_{+1}([\overline{A}] + \delta)([\overline{E}] + \delta) - k_{-1}([\overline{EA}] - \delta)$$
$$-\frac{d[\overline{A}]}{dt} - \frac{d\delta}{dt} = k_{+1}[\overline{A}][\overline{E}] - k_{-1}[\overline{EA}] + \{k_{+1}([\overline{A}] + [\overline{E}]) + k_{-1}\}\delta + k_{+1}\delta^2 \,. \tag{3.49}$$

In equilibrium, the concentrations are time-independent factors, also after perturbation:

$$-\frac{\mathrm{d}[\overline{\mathrm{A}}]}{\mathrm{d}t} = k_{+1}[\overline{\mathrm{A}}][\overline{\mathrm{E}}] - k_{-1}[\overline{\mathrm{EA}}] = 0\,. \tag{3.50}$$

Thus the first two terms of the left part of Eq. (3.49) are to be omitted. For small changes the square term may be disregarded:

$$-\frac{\mathrm{d}\delta}{\mathrm{d}t} = \{k_{+1}([\overline{\mathrm{A}}] + [\overline{\mathrm{E}}]) + k_{-1}\}\delta = \frac{\delta}{\tau}\,. \tag{3.51}$$

The bracket term, containing only constant factors as the concentration terms can be also regarded as constant in equilibrium, is replaced by $1/\tau$. By integration after the time t for a given concentration change Δ

$$\int_{\Delta_0}^{\Delta_t} \frac{\mathrm{d}\delta}{\delta} = -\int_0^t \frac{\mathrm{d}t}{\tau} \tag{3.52}$$

Equations (3.44) and (3.45) are obtained. Following Eq. (3.51), the relaxation time for the present reaction mechanism is:

$$\frac{1}{\tau} = k_{+1}([\overline{\mathrm{A}}] + [\overline{\mathrm{E}}]) + k_{-1}\,.$$

The rate constants can be calculated by the determination of relaxation times at different concentrations of $[\overline{\mathrm{A}}]$ and $[\overline{\mathrm{E}}]$. From a plot of $1/\tau$ against $[\overline{\mathrm{A}}] + [\overline{\mathrm{E}}]$, k_{+1} may be obtained from the gradient, k_{-1} from the ordinate intercept, and $K_\mathrm{d} = k_{-1}/k_{+1}$ from the abscissa intercept. However, concentration values on the abscissa refer to the conditions *after* perturbation, i.e., high temperature that may be obtained from Eq. (3.47), with K_d known. Correspondingly, the constants calculated from these data are valid for conditions after perturbation.

According to Eq. (3.44) the relaxation curve is an exponential function, but only as long as the square term from Eq. (3.49) may be disregarded, i.e., only for small changes. Otherwise deviations from the linear progression as in Figure 3.54 would occur. Non-linearity may, however, also result from superimposition of different processes. To differentiate between both possibilities, the extent of the perturbation, i.e., the temperature jump, may be reduced. If the non-linear characteristics remains, several relaxation times may actually superimpose each other. For n states of the reactants n–1 relaxation times are to be expected. If they differ by more than one order of magnitude they can be decoupled by a variation of the time axis. Otherwise they may be separate by calculation.

The scheme for the derivation of the relaxation time for a bimolecular reaction may also be applied to other reaction mechanisms. Table 3.3 shows a compilation of various frequently occurring mechanisms. The constants are obtained by corresponding plots, as shown in Figure 3.54 for the bimolecular mechanisms.

Table 3.3. Significance of relaxation times τ in different reaction mechanisms (after Hiromi, 1979)

Reaction mechanism	Reciprocal relaxation time ($1/\tau$)	Remarks
$A \underset{k_{-1}}{\overset{k_1}{\leftrightarrow}} P$	$k_{+1} + k_{-1}$	
$nA \underset{k_{-1}}{\overset{k_1}{\leftrightarrow}} P_n$	$n^2 k_{+1}[\overline{A}]^{n-1} + k_{-1}$	
$A + B \underset{k_{-1}}{\overset{k_1}{\leftrightarrow}} P$	$k_{+1}([\overline{A}] + [\overline{B}]) + k_{-1}$	
$A + B \underset{k_{-1}}{\overset{k_1}{\leftrightarrow}} P$	$k_{+1}[\overline{B}] + k_{-1}$	B in surplus
$A + E \underset{k_{-1}}{\overset{k_1}{\leftrightarrow}} P + E$	$(k_{+1} + k_{-1})[\overline{E}]$	E is catalyst
$A + B \underset{k_{-1}}{\overset{k_1}{\leftrightarrow}} P + Q$	$k_{+1}([\overline{A}] + [\overline{B}]) + k_{-1}([\overline{P}] + [\overline{Q}])$	
$A + B \underset{k_{-1}}{\overset{k_1}{\leftrightarrow}} 2P$	$k_{+1}([\overline{A}] + [\overline{B}]) + 4k_{-1}[\overline{P}]$	
$A + B + C \underset{k_{-1}}{\overset{k_1}{\leftrightarrow}} P$	$k_{+1}([\overline{A}][\overline{B}] + [\overline{A}][\overline{C}] + [\overline{B}][\overline{C}]) + k_{-1}$	

3.6 References

General Methods and Enzyme Analytics

Bergmeyer, H.U. (1983) *Methods of enzymatic analysis.* Verlag Chemie, Weinheim.

Clark, J.M. & Switzer, R.L. (1977) *Experimental biochemistry.* W.H. Freeman, San Francisco.

Eisenthal, R. & Danson, J. (1992) *Enzyme assays. A practical approach.* IRL Press, Oxford.

Umbreit, W.W., Burris, R.H. & Stauffer, J.F. (1972) *Manometric and biochemical techniques,* 5th edn. Burgess Publ. Co., Minneapolis.

Williams, B.L. & Wilson, K. (1975) *Principles and techniques of practical biochemistry.* Edward Arnold Publ., London.

Methods to Determine Multiple Equilibria

Ackers, K.G. (1975) *Molecular sieve methods of analysis.* The Proteins, 3rd edn. 1, 1–94.

Alberts, R.W. & Krishnan, N. (1979) *Application of the miniature ultracentrifuge in receptor-binding assays.* Analytical Biochemistry 96, 396–402.

Brumbaugh, E.E. & Ackers, K.G. (1974) *Molecular sieve studies of interacting protein systems. Direct optical scanning method for ligand-macromolecule binding studies.* Analytical Biochemistry 41, 543–559.

Chanutin, A., Ludewig, S. & Masket, A.V. (1942) *Studies on the calcium-protein relationship with the aid of the ultracentrifuge.* The Journal of Biological Chemistry 143, 737–751.

Colowick, S.P. & Womack, F.C. (1969) *Binding of diffusible molecules by macromolecules: Rapid measurements by rate of dialysis.* The Journal of Biological Chemistry 244, 774–777.

Draper, D.E. & Hippel, P.H. (1979) *Measurement of macromolecule binding constants by a sucrose gradient band.* Biochemistry 18, 753–760.

Englund, P.E., Huberman, J.A., Jovin, T.M. & Kornberg, A. (1969) *Enzymatic synthesis of deoxyribonucleic acid. Binding of triphosphates to deoxyribonucleic acid polymerase.* The Journal of Biological Chemistry 244, 3038–3044.

Hummel, J.P., & Dreyer, W.J. (1962) *Measuring of protein-binding by gel filtration.* Biochimica et Biophysica Acta 63, 530–532.

Martin, R.G. & Ames, B.N. (1961) *A method for determining the sedimentation behavior of enzymes. Application of protein mixtures.* The Journal of Biological Chemistry 236, 1372–1379.

Myer, Y.P. & Schellman, J.A. (1962) *The interaction of ribonuclease with purine and pyrimidine phosphates. Binding of adenosine-5′-monophosphate to ribonuclease.* Biochimica et Biophysica Acta 55, 361–373.
Paulus, H. (1969) *A rapid and sensitive method for measuring the binding of radioactive ligands to proteins.* Analytical Biochemistry 32, 91–100.
Steinberg, I.Z. & Schachman, H.K. (1966) *Ultracentrifugation studies with absorption optics. Analysis of interacting systems involving macromolecules and small molecules.* Biochemistry 5, 3728–3747.
Suter, P. & Rosenbusch, J. (1976) *Determination of ligand binding: Partial and full saturation of aspartate transcarbamylase. Applicability of a filter assay to weakly binding ligands.* The Journal of Biological Chemistry 251, 5986–5991.
Yamamoto, K.R. & Alberts, B. (1974) *On the specificity of the binding of estradiol receptor protein to deoxyribonucleic acid.* The Journal of Biological Chemistry 249, 7076–7086.

Electrochemical Methods

Beechey, R.B. & Ribbons, D.W. (1972) *Oxygen electrode measurements.* Methods in Microbiology 6B, 25–53.
Clark, L.C. Jr., Wolf, R., Granger, D. & Taylor, Z. (1953) *Continuous recording of blood oxygen tensions by polarography.* Journal of Applied Physiology 6, 189–193.
Degn, H., Lundsgaard, J.S., Peterson, L.C. & Ormick, A. (1980) *Polarographic measurements of steady-state kinetics of oxygen uptake by biochemical samples.* Methods of Biochemical Analysis 26, 47–77.
Lessler, M.A. (1982) *Adaptation to polarographic oxygen sensors for biochemical assays.* Methods of Biochemical Analysis 28, 175–199.
Lessler, M.A. & Bierley, G.P. (1969) *Oxygen electrode measurements in biochemical analysis.* Methods of Biochemical Analysis 17, 1–29.
Nicolls, D.G. & Garland, P.B. (1972) *Electrode measurements of carbon dioxide.* Methods in Microbiology 6B, 55–63.
Weitzman, P.D.J. (1969) *Polarographic assay for malate synthase and citrate synthase.* Methods in Enzymology 13, 365–368.

Calorimetric Methods

Freire, E. & van Ospold, W.W. (1990) *Calorimetrically determined dynamics of complex unfolding transitions in proteins.* Annual Reviews of Biophysics and Biophysical Chemistry 19, 159–188.
Hemminger, W. & Höhne, G. (1979) *Grundlagen der Kalorimetrie.* Verlag Chemie, Weinheim.
Spink, C. & Wadsö, I. (1976) *Calorimetry as an analytical tool in biochemistry and biology.* Methods of Biochemical Analysis 23, 1–159.
Jolicoeur, C. (1981) *Thermodynamic flow methods in biochemistry, calorimetry, densitometry and dilatometry.* Methods of Biochemical Analysis 21, 171–287.

Spectroscopic Methods

Adler, A.J., Greenfield, N.J. & Fassman, G.D. (1973) *Circular dichroism and optical rotation dispersion of proteins and polypeptides.* Methods in Enzymology 27, 675–735.
Brand, L. & Witholt, B. (1961) *Fluorescence measurements.* Methods in Enzymology 11, 776–856.
Brand, L. & Gohlke, J.R. (1972) *Fluorescence probes for structure.* Annual reviews of Biochemistry 41, 843–868.
Castor, L.N. & Chance, B. (1955) *Photochemical action spectra of carbon monoxide-inhibited respiration.* The Journal of Biological Chemistry 217, 453–465.
Chance, B. (1991) *Optical methods.* Annual Reviews of Biophysics and Biophysical Chemistry 20, 1–28.
Donovan, J.W. (1973) *Ultraviolet difference spectroscopy – New techniques and applications.* Methods in Enzymology 27, 497–525.

Eftink, M.R. (1989) *Fluorescence techniques for studying protein structure.* Methods of Biochemical Analysis 35, 127–205.

Dewey, T.G. (1991) *Biophysical and biochemical aspects of fluorescence spectroscopy.* Plenum Publ., New York.

Fasman, G.D. (1989) *Practical handbook of biochemistry and molecular biology.* CRC Press, Boca Raton.

Förster, T. (1948) *Zwischenmolekulare Energiewanderung und Fluoreszenz.* Annalen der Physik 437, 6th Series, Vol. 2, S. 55–75.

Galla, H.-J. (1988) *Spektroskopische Methoden in der Biochemie.* Thieme-Verlag, Stuttgart.

Graupe, K. (1982) *Struktur-Funktionsbeziehung im Pyruvatdehydrogenase-Multienzymkomplex aus Escherichia coli.* Doktorarbeit, Universität Tübingen.

Graupe, K., Abusaud, M., Karfunkel, H. & Bisswanger, H. (1982) *Reassociation of the pyruvate dehydrogenase complex from Escherichia coli: Kinetic measurements and binding studies by resonance energy transfer.* Biochemistry 21, 1386–1394.

Greenfield, N.J. & Fasman, G.D. (1969) *Computed circular dichroism spectra for the evaluation of protein conformation.* Biochemistry 8, 4108–4116.

Guibault, G.G. (1990) *Practical fluorescence.* Marcel Dekker, New York.

Günzler, Böck (1983) *IR-Spektroskopie*. Verlag Chemie, Weinheim.

Harris, D.A. & Bashford, C.L. (1987) *Spectrophotometry & spectrofluorimetry.* IRL Press, Oxford.

Herskovits, T.T. (1967) *Difference spectroscopy.* Methods in Enzymology 11, 748–775.

Johnson, W.C. (1985) *Circular dichroism and its empirical application to biopolymers.* Methods of Biochemical Analysis 31, 61–163.

Lloyd, D. & Scott, R.I. (1983) *Photochemical action spectra of CO-liganded terminal oxidases using a liquid dye laser.* Analytical Biochemistry 128, 21–24.

Mendelsohn, R. (1978) *Application of infrared and Raman spectroscopy to studies of protein conformation*. In: Kornberg, H.L. (ed.) *Techniques in protein and enzyme biochemistry.* B109, 1–28. Elsevier/North Holland, County Clare.

Perrin, F. (1926) *Polarisation de la Lumière de Fluorescence. Vie Moyenne des Molécules dans l'Etat excité.* Le Journal de Physique, Serie VI, 7, 390–401.

Rosenheck, K. & Doty, P. (1961) *Far ultraviolet absorption spectra of polypeptide and protein solutions and their dependence on configuration.* Proceedings of the National Academy of Sciences USA 47, 1775–1785.

Seitz, W.R. & Neary, M.P. (1969) *Recent advances in bioluminescence and chemoluminescence assay.* Methods of Biochemical Analysis 23, 161–188.

Shikari, M. (1969) Sci. Pop. Coll. Gen. Educ. Univ. Tokyo, 19, 151.

Strehler, B.L. (1968) *Bioluminescence assay: Principles and practice.* Methods of Biochemical Analysis 16, 99–179.

Stryer, L. (1968) *Fluorescence spectroscopy of proteins.* Science 162, 526–533.

Stryer, L. (1978) *Fluorescence energy transfer as a spectroscopic ruler.* Annual Reviews of Biochemistry 47, 819–846.

Urry, D.W. (1985) *Absorption, circular dichroism and optical rotary dispersion of polypeptides, proteins, prosthetic groups and biomembranes.* In: Neuberger, A. & Van Deenen, L.L.M. (eds) *Modern Physical Methods in Biochemistry.* New Comprehensive Biochemistry 11A, 275–346, Elsevier, Amsterdam.

Van Holde, K.E. (1985) *Physical Biochemistry.* Prentice Hall, Englewood Cliffs.

Warburg, O. & Negelein, E. (1929) *Über das Absorptionsspektrum des Atmungsferments.* Biochemische Zeitschrift 214, 64–100.

Wettlaufer, D.B. (1962) *Ultraviolet spectra of proteins and amino acids.* Advances in Protein Chemistry 17, 303–390.

Wharton, C.W. (1986) *Infra-red and Raman spectroscopic studies of enzyme structure and function*. Biochemical Journal 233, 25–36.

Measurement of Rapid Kinetic Reactions

Bender, M.L., Kézdy, F.J. & Feder, J. (1965) *The kinetics of the trypsin-catalyzed hydrolysis of p-nitrophenyl-α-N-benzyloxycarbonyl-L-lysinate hydrochloride*. Journal of the American Chemical Society 87, 4953-4954.

Bernasconi, C.F. (1976) *Relaxation kinetics*. Academic Press, New York.

Bayley, P.M. & Anson, M. (1975) *Stopped-flow circular dichroism: A fast-kinetic system*. Biopolymers 13, 401–405.

Bray, R.C. (1961) *Sudden freezing as a technique for the study of rapid reactions.* Biochemical Journal 81, 189–193.

Chan, S.S. & Austin, R.H. (1984) *Laser Photolysis in Biochemistry.* Methods of Biochemical Analysis 30, 105–139.

Chance, B., Eisenhardt, R.M., Gibson, Q.H. & Lonberg-Holm, K.K. (1964) *Rapid mixing and sampling techniques in biochemistry.* Academic Press, New York.

Chance, B. (1974) *Rapid-Flow-Methods*. In: Weissberger, A. (ed.) *"Techniques of chemistry"*. Vol. VI, Part II. S. 5–62. J. Wiley & Sons, New York.

Dorfman, L.M. (1974) *Pulse radiolyse.* In: Weissberger, A. (ed.) *"Techniques of chemistry"*. Vol. VI, Part II, S. 363–419. J. Wiley & Sons, New York.

Eigen, M. & De Mayer, L. (1974) *Theoretical basis of relaxation spectroscopy.* In: Weissberger, A. (ed.) *"Techniques of chemistry.*" Vol. VI, Part II, S. 63–146. J. Wiley & Sons, New York.

Eigen, M. & De Mayer, L. (1963) *Relaxation methods.* In: Friess, S.L., Lewis, E.S. & Weissberger, A. (eds.), *"Techniques of organic chemistry."* Vol. VIII, Part II, S. 895–1054. John Wiley & Sons, New York.

Erman, J.E. & Hammes, G.G. (1966) *Versatile stopped-flow temperature jump apparatus*. The Review of Scientific Instruments 37, 746–750.

Fersht, A.R. & Jakes, R. (1975) *Demonstration of two reaction pathways for the amino acylation of tRNA. Application of the pulsed quenched flow technique.* Biochemistry 14, 3350–3356.

Flamig, D.P. & Parkhurst, L.J. (1977) *Kinetics of the alkaline tetramer-dimer dissociation in liganded human hemoglobin: A laser light scattering stopped-flow study.* Proceedings of the National Academy of Sciences USA 74, 3814–3816.

Gibson, Q.H. & Milnes, L. (1964) *Apparatus for rapid and sensitive photometry.* Biochemical Journal 91, 161–171.

Grimaldi, J.J. & Sykes, B.D. (1975) *Concanavalin A: A stopped-flow nuclear magnetic resonance study of conformational changes induced by Mn^{++}, Ca^{++}, and α-methyl-D-mannoside*. The Journal of the Biological Chemistry 250, 1618–1624.

Gutfreund, H. (1969) *Rapid mixing: Continuous flow*. Methods in Enzymology 16, 229–249.

Hartridge, H. & Roughton, F.J.W. (1923) *The velocity with which carbon monoxide displaces oxygen from combination with haemoglobin*. Proceedings of the Royal Society of London, Series B, 94, 336–367.

Hilinski, E.F. & Rentzepis, P.M. (1983) *Biological applications of picosecond spectroscopy.* Nature 302, 481–487.

Hiromi, K. (1979) *Kinetics of fast enzyme reactions.* J. Wiley & Sons, New York.

Hoffmann, G.W. (1971) *A nanosecond temperature-jump apparatus.* Review of Scientific Instruments 42, 1643–1647.

Hoffmann, H., Yeager, E. & Stuehr, J. (1968) *Laser temperature-jump apparatus for relaxation studies in electrolytic solutions*. The Review of Scientific Instruments 39, 649–653.

Hollaway, M.R. & White, H.A. (1975) *A double beam rapid-scanning stopped-flow spectrometer.* Biochemical Journal 149, 221–231.

Knoche, W. (1974) *Pressure-jump methods*. In: Weissberger, A. (ed.) "*Techniques of chemistry.*" Vol. VI, Part II, S. 187–210. J. Wiley & Sons, New York.

Kustin, K. (1969) *Fast reactions*. Methods in Enzymology Vol. 16. Academic Press, New York.

Macgregor, R.B., Clegg, R.M. & Jovin, T.M. (1985) *Pressure-jump study of the kinetics of ethidium bromide binding to DNA*. Biochemistry 24, 5503–5510.

Martin, J.L. & Vos, M.H. (1992) *Femtosecond biology.* Annual Reviews of Biophysics and Biomolecular Structure 21, 199–222.

Moody, M.F., Vachette, P., Foote, A.M., Tardieu, A., Koch, M.H.J. & Bordas, J. (1980) *Stopped-flow x-ray scattering: The dissociation of aspartate transcarbamylase*. Proceedings of the National Academy of Sciences USA 77, 4040–4043.

Norrish, R.G.W. & Porter, G. (1949) *Chemical reactions produced by very high light intensities.* Nature 164, 658.

Porter, G. & West, M.A. (1974) *Flash photolysis.* In: Weissberger, A. (ed.) "*Techniques of chemistry.*" Vol. VI, Partl II, S. 367–462. J. Wiley & Sons, New York.

Roughton, F.J.W. & Chance, B. (1963) *Rapid reactions.* In: Friess, S.L., Lewis, E.S. & Weissberger, A. (eds), *"Techniques of organic chemistry."* Vol. VIII, Part II, S. 703–792. John Wiley & Sons, New York.

Stehlow, H. & Becker, M. (1959) *Ein Drucksprungverfahren zur Messung der Geschwindigkeit von Ionenreaktionen*. Zeitschrift für Elektrochemie 63, 457–461.

Strittmatter, P. (1964) In: Chance, B., Eisenhardt, R.M., Gibson, Q.H. & Lonberg-Holm, K.K. (eds.) *Rapid mixing and sampling techniques in biochemistry.* S. 76. Academic Press, New York.

The program *EKI3.exe* was designated to work under Win95/98 NT operation systems. Files with *.eki* extension are data samples. For all kinetic diagrams the regression analysis of G.N. Wilkinson (1961) Biochemical Journal 80, 324–332 was applied, so coincident values are obtained. By activating the representative symbols in the menu a worksheet to enter the data can be created, values of constants (equation parameters K_m, V) may be changed, points, curves and error bars can be added or removed.

The co-ordinates of the diagrams can be moved by pressing the left mouse key, the zoom-function allows stretching and compressing the diagrams in x and y direction.

For most diagrams regression analysis for distinct regions within a test series sequence can be executed. After pressing left mouse key at the number of the respective test series right above in the diagram appears an asterisk. Now pressing the right mouse key the region within the curve to calculate the regression analysis can be marked. Thereafter, a line will be drawn, the slope of which is indicated above to the right.

The first line in the worksheet is to enter parameters which may differ between distinct series of data, like inhibitor or cosubstrate concentrations in inhibition or bisubstrate studies, which are necessary to create secondary plots. For calculation of the co-ordinates for the Stockell plot of binding data from optical titrations the actual enzyme concentration must be entered. A constant factor can be applied to change all or part of the data within the worksheet.

Data samples:

Enzymkinetik1.*eki*	Michaelis-Menten kinetics
Enzymkinetik2.*eki*	competitive inhibition
Enzymkinetik3.*eki*	non-competitive inhibition
Enzymkinetik4.*eki*	uncompetitive inhibition
Enzymkinetik5.*eki*	sigmoidal saturation kinetics
Enzymkinetik6.*eki*	temperature dependency
Enzymkinetik7.*eki*	binding data from optical titrations

The program was designated by Dmitriy Degtiarev, Moscow (Email: mitek@motor.ru)

Index

Enzyme Kinetics: Principles and Methods. Hans Bisswanger

ISBN: 3-527-30343-X

WILEY-VCH

Hans Bisswanger

Enzyme Kinetics
Principles and Methods

Enzyme Kinetics – Principles and Methods is a user-friendly and comprehensive treatise indispensable for biochemists, biologists, medical scientists, and chemists working with enzymes, from advanced students to experts in academia and industry. Theory and practice are well-balanced, with emphasis on the relation to the biological system. Theoretical aspects are presented in a way which is also comprehensible for the beginner. An extensive methodological part provides the expert with valuable support in planning and performing laboratory experiments.

The book contains a central part on classical enzyme kinetics. This is preceded by an introduction into the theory of binding equilibria and followed by a presentation of methods for both binding studies and enzyme kinetics including fast reactions.

Special feature: A CD-ROM with EKI-3, the elaborate and easy-to-use version of the enzyme kinetics practical course!

ISBN 3-527-30343-X

9 783527 303434

www.wiley-vch.de